Design and assessment of SMES and battery hybrid energy storage for microgrid applications

Sun, Qixing

Award date:
2019

Awarding institution:
University of Bath

Design and assessment of SMES and battery hybrid energy storage for microgrid applications

Qixing Sun

A thesis submitted for the degree of Doctor of Philosophy (PhD)

Department of Electrical and Electronic Engineering

University of Bath

2019

Abstract

The major challenges of microgrid systems are driven by energy shortages and environmental concerns, which encourage energy storage systems be integrated into microgrids. With the implementation of energy storage systems, microgrids become more stable and more effective. This research propose to hybridize superconducting magnetic energy storage (SMES) with battery to build a hybrid energy storage system (HESS) for microgrid applications. The SMES-battery HESS is a good choice to compensate for the highly fluctuating power demand in microgrids and extent battery service lifetime. However, the SMES-battery HESS applied in microgrids is a newly proposed concept. Challenges remain on the HESS control method, system design, energy management method and HESS sizing optimisation. Therefore, the achievement of this PhD research project is the development of a SMES-battery HESS for microgrid applications. The accomplishments are list below:

- The SMES magnet structure design has been completed in this thesis. The newly developed method is able to design the SMES with a requested energy capacity, which is vital for SMES-battery HESS applications. Moreover, the weak point area in the SMES magnet has been located. That can be used to prevent SMES quench.
- To achieve a high power capacity in the SMES magnet in the HESS for microgrid applications, a feasibility study using Roebel cable to build the SMES magnet has been investigated.
- A new fuzzy logic energy management method has been proposed to deal with the power unbalance inherent in microgrids. The proposed method is able to allocate the power output of the HESS for high fluctuating power demands.
- A novel two-stage energy management method with PI-droop control is developed, which is able to improve the battery performance when a microgrid is disconnected from main grid.
- The SMES-battery HESS experimental platform was built to test the proposed method's achievability.

By investigating a HESS for microgrid applications, a HESS topology and SMES structure design has been proposed. Furthermore, a control methodology for the HESS in the microgrid

application has been established. The experimental results validate the HESS achievability. This prototype SMES-battery HESS is the first step towards the implementation of future commercialised SMES-battery HESS for microgrids.

Acknowledgement

Firstly, I would like to express my sincere and deepest gratitude to my supervisor Professor Weijia Yuan, for his guidance, encouragement and support throughout my research. He leads me to learn how to do the independent research. I want to thank Dr. Xiaoze Pei for her instructions with my paper and PhD thesis. Also, I would like to thank Dr. Min Zhang for her generous advice and support.

I would like to thanks my colleagues in the applied superconductivity group in the department of electrical and electronic engineering. Happy memories have been shared with my colleagues at the University of Bath. I want to thank Dr. Huiming Zhang, Dr. Zhenyu Zhang, Dr. Fei Liang, Dr. Jianwei Li, Dr. Yawei Wang, Dr. Xiaojian Li, Hamoud Alafnan, Mariam Elshiekh, Zixuan Zhu, Muhammad Zulfiqar Ali, Sriharsha Venuturumilli, Zhidun Zeng, Fangjing Weng, Jiawen Xi. The friendship and support have been the most valuable asset during my PhD study process. I want to thank Pengfei Yao from Tsinghua University for his experimental support.

Last but not least, I am grateful to my parents who always love me unconditionally and give me enormous encouragements through all my study and life. Thanks to my wife Dong Xing for being by my side all the time.

List of publications

[1] Sun Q, Xing D, Yang Q, et al. A new design of fuzzy logic control for SMES and battery hybrid storage system[J]. Energy Procedia, 2017, 105: 4575-4580.

[2] Xing D, Patel J, Sun Q, et al. AC loss comparison between multifilament and nonstriated YBCO coils designed for HTS propulsion motors[J]. IEEE Transactions on Applied Superconductivity, 2017, 27(4): 1-5.

[3] Li J, Yang Q, Yao P, et al. A novel use of the hybrid energy storage system for primary frequency control in a microgrid[J]. Energy Procedia, 2016, 103: 82-87.

Contents

List of Figures

List of Tables

Nomenclature

T_c	Critical temperature
J_c	Critical current density
H_c	Critical magnetic field
I_c	Superconductor critical current
D	Duty cycle
E	Energy capacity
C	Capacitance
L	Inductance
t	Time
V	Voltage
I	Current
B	Magnetic field
θ	Angle between magnetic field and superconductor tape surface
L_{TRANS}	Roebel cable transposition length
W_R	Roebel cable stand width
W_x	Roebel cable crossover width
W_c	Roebel cable stand edge clearance
Φ	Roebel cable Roebel angle
L_{ISG}	Roebel cable inter-strand gap
R	Roebel cable cut-out fillet radius

y_o	Fuzzy logic output
K_p	Proportional term in PI controller
K_i	Integral term in PI controller
E_{smes_max}	SMES maximum energy capacity
E_{smes}	Energy remained in the SMES
P_{bat_out}	Battery power output
V_{bat}	Battery terminal voltage
I_{out_max}	Battery maximum output current
I_{out_lim}	Battery maximum output current limitation
E(I)	Voltage drop across the superconductor when the operating current is I
E_c	Voltage drop criterion

List of Abbreviation

HESS	Hybrid energy storage system
DC	Direct current
AC	Alternating current
SMES	Superconducting magnet energy storage
SOC	State of charge
BESS	Battery energy storage system
LTS	Low temperature superconductor
HTS	High temperature superconductor
FEM	Finite element method
ESS	Energy storage system
EV	Electrical vehicle
REBCO	Rear earth-based barium-copper-oxide
KVL	Kirchhoff's voltage law
HESS	Hybrid energy storage system
SOC	State of charge
PV	Photovoltaics
VSC	Voltage source converter
PI	Proportional integral
DSP	Digital signal processor
ADC	Analog-digital converter

BSCCO	Bismuth strontium calcium copper oxide
YBCO	Yttrium barium copper oxide
MgB_2	Magnesium diboride
NVB	Negative very small
NB	Negative big
NS	Negative small
ZE	Zero
PS	Positive small
PB	Positive big
PVB	Positive very big

Chapter 1 Introduction

1.1Thesis background

Microgrids are becoming more and more popular in power systems. Microgrids have advantages such as improved local energy delivery efficiency and increased system reliability. Microgrids are mostly composed of power generation parts, energy storage systems, and loads. With the concern of negative environmental impact, more renewable power generation systems are being implemented into microgrids to replace fossil fuel power generation [1, 2]. Compared with fossil fuel power generation, renewable power generation has the feature of intermittency and variability. That makes renewable power generation not able to provide stable power output. Therefore, with the increasing growth of renewable power generation, electricity security becomes more important. Adding energy storage systems to the power system is one good solution to enhance voltage regulation of microgrids [3, 4, 5, 6].

The energy storage system is the technology that can convert the electricity into other kinds of energy and able to feed the electricity back to the system when needed [7, 8]. A number of researches have focused on using energy storage systems to solve the power balancing

problem [9, 10], power system frequency regulation [11], voltage stabilisation [12], etc. Different types of energy storage systems have been designed and tested for power system applications [7, 13, 14, 15, 16]. According to the previous studies, the battery energy storage system is the most popular energy storage system because it has high efficiency, high energy capacity, relatively high power capacity and low economic cost. Therefore, the battery energy storage system is commonly used in power systems.

However, batteries have a short service lifetime, which is caused by the limited number of discharge/charge cycles [17, 18, 19]. Moreover, battery service lifetime decreases when dealing with short-term fluctuating power demands and transient high currents [20]. Furthermore, if the transient power demand for a battery is higher than the battery's maximum discharging rate, the battery is not able to compensate for the power demand. To solve this problem, a fast responding energy storage device is proposed to be hybridised with a battery to form a hybrid energy storage system (HESS). A supercapacitor and SMES are the two mainly used fast-responding devices. A number of researches have investigated the supercapacitor-battery HESS [21, 22, 23, 24, 25] and SMES-battery HESS [26, 27, 28]. Compared with the supercapacitor, the SMES has higher power density, a lower self-discharging rate and is more environmentally friendly. The biggest obstacle of the SMES is that the cost is too high. However, some recent studies have shown the positive aspects of cost-benefit analysis about the SMES [29, 30]. The active combination of a SMES with a battery to build a HESS increases the storage system's maximum power handling capacity, maximum energy capacity and extends the HESS service lifetime. Moreover, the energy management method, control method and electrical circuit topology are essential for the HESS application to achieve the required performance.

A good SMES magnet structure design can enhance the performance of a HESS. Furthermore, a well-designed SMES magnet can support not only high power output but is also able to reduce the probability of a SMES quenching [31, 32]. Different researches have shown their design results for SMES magnets. However, the SMES design process and method has not been discussed in detail.

For SMES-battery HESS applications, different SMES sizes are required for various applications. It is important to design the SMES magnet structure for the required energy/power capacity.

Therefore, a SMES magnet design method needs to be developed, which is able to design the SMES magnet structure for the requested capacity. The control method needs to be investigated to enhance the performance and to extend the system service lifetime. Moreover, the experimental platform should be established to test the HESS applied microgrid performance and verify the control method reliability.

1.2 Research motivation

The cost of superconducting energy storage systems is decreasing. The superconducting energy storage (SMES) system is composed of three majority parts: the SMES magnet, a cooling system and an external power electronics control circuit. The cost of the SMES magnet is approximately 90% of the total cost [33]. In this research, the SMES magnet is constructed from high temperature superconducting coils. Moreover, with manufacturing process improvements, the cost of high-temperature superconducting materials has dramatically decreased. The price of yttrium barium copper oxide (YBCO) second generation type high-temperature superconductor has decreased from $100 per meter in 2012 to $50 per meter in 2018 [34]. The cost of MgB_2 high-temperature superconductor is only $10 per meter [34]. Moreover, the price is still decreasing. Therefore, the overall cost of SMES systems is decreasing, which can stimulate the growth of SMES applications. Hence, it is necessary to study the features and the applications for SMESs.

With the significant changes in electrical power generation in recent years, more and more environmentally friendly power generation systems are being coupled to the power system, which is called renewable power generation. Many countries and regions have set targets to encourage more renewable power generation systems to be connected to the grid. A report from the British National Grid shows that renewable power generation will supply 15% of the total electrical power consumed in the UK by 2020 [35]. The European Union set a target to 20% for renewable power generation [36].

China is aiming to make renewable power generation reach 15% also by 2020 [37]. However, compared with fossil fuel power generation, renewable power generation has higher

uncertainty of power output and higher power output fluctuation. Hence, the high penetration of renewable power generation into microgrids and the power system is increasing the challenges of power system reliability. Research has shown that energy storage is one solution to solve these problems [38, 39, 40, 41]. Energy storage systems can absorb the energy when the renewable power generation systems generate more power than the requested power demand, and can supply the power system demand when the renewable power generation has low power output. Moreover, with the appropriate control of the energy storage system, the power fluctuating in the power system can also be compensated for by the energy storage system. There are several kinds of energy storage systems, which are available for power system applications. Different energy storage devices have different characteristics. By combining different types of energy storage systems, hybrid energy storage systems can utilise the advantages of different energy storage systems for power system applications.

Microgrids consist of distributed power generation systems, energy storage systems (mostly battery energy storage systems) and residential loads. Microgrids can work both in grid-connected mode and isolated mode. When a microgrid is working in the grid-connected mode, the microgrid works like a distribution network in the power system. However, when the microgrid is working in isolation mode, the microgrid disconnects from the main grid and uses the energy storage system and distributed power generators to supply the load power demand in the system.

Microgrids have the advantages of improving the local energy delivery, high system reliability and are able to save money for local users [42, 43]. Therefore, microgrids have great potential for application in power systems. Microgrids rely on the energy storage system to support reliable power to the local loads. Thus, energy storage performance management is the most critical part for microgrid applications. Different papers have presented about energy storage systems to compensate for the power demand fluctuating during a microgrid working in isolation mode [37, 41, 44, 45]. However, these researches have not studied the energy storage performance when a microgrid switches from the grid-connected mode to isolation mode.

When a microgrid switches to the isolation mode, the unbalanced power in the microgrid needs to be supplied by the energy storage system. To support that amount of high power requirement, the battery energy storage system needs to increase its power output in a short period of time [46, 47]. Therefore, the use of a fast responding energy storage device to compensate part of the HESS power demand in first few second to extend the battery energy storage system's response time is one solution to slow the battery system attenuation. A study of SMES-battery HESS used to deal with microgrid mode changes has been conducted in this thesis. By adding the SMES to the system, the new method shows a significant improvement in the battery output performance.

1.3 Challenges and contributions of the thesis

The SMES magnet is one of the most important parts in the SMES system, which affects the SMES system's performance. However, there is no commercially available SMES magnets on the market. Moreover, different sizes of SMESs need be designed based on the SMES system's application. The working conditions of each SMES also affect its performance. Therefore, for different SMES applications, the SMES magnet design is the first step. Additionally, a good design of the SMES magnet can not only increase the SMES system's working stability but also increase the SMES energy capacity. Different papers have discussed SMES magnet design methods and give the SMES magnet structure details for their requested energy capacity. Therefore, for SMES system applications, a self-made SMES magnet design algorithm needs to be developed to design the SMES magnet structure. The developed algorithm needs to be able to design the SMES magnet structure for the requested SMES energy capacity.

Superconductor quenches in the SMES magnet is another problem for SMES applications. A superconductor quench can cause the quench point to have a relatively higher resistivity. Joule heating will be produced due to the current which passes through the quenching point. The joule heat accumulates and can cause the SMES to overheat and damage the superconducting material. Once a superconductor is damaged, the SMES magnet is not able to work and will expensive to repair. Therefore, it is important to accurately detect a quench

as it happens. In this thesis, the most susceptible quench area in the solenoid SMES magnet design has been located. This can help the quench detection system to more quickly detect the quench by adding more quench detection points in that area.

For microgrid applications, it would be better to have the energy storage system with better performance such as higher energy capacity, higher reliability or higher power capacity. Therefore, different winding methods [48, 49, 50] and different magnet structures [51, 52, 53] to build SMES magnet are considered to enhance SMES performance. In this thesis, a feasibility study of using Roebel cable to wind SMES magnet has been investigated. The new SMES design method aims to improve the SMES maximum power capacity and response speed. Therefore, one highlight of this thesis is that the results of the feasibility study are given by considering the mechanical stability, electrical stability, energy capacity, power capacity and manufacturing difficulties.

The power management strategy is vital for the SMES-battery HESS for microgrid applications. Without a suitable control strategy, the SMES has no use in the power system. The power management strategy should consider the characteristics of the SMES and the battery. The final target of the energy management strategy is not only to deliver the requested power demand from the HESS but also to extend the HESS service lifetime. As discussed previously, renewable power generation has an unstable power output, which increases the power system's power demand unbalancing.

Therefore, in this thesis, one highlight is that an energy management methodology has been developed based on a fuzzy logic controller for microgrid applications. The new proposed energy management method uses a non-linear controller to allocate the power for the SMES and the battery in a HESS. The proposed method has better performance in preventing the SMES from fully charging/discharging, which is able to prevent the battery system suffering a high fluctuating power demand. Moreover, the proposed method is able to control the battery power output with a better performance than the commonly used method.

The microgrid decoupling process is another challenge for the HESS in microgrid applications. When a microgrid switches to isolation mode, the unbalanced power between local loads and local generations needs to be supported by the hybrid energy storage system. There are not many published papers on the short time response for the HESS when the microgrid switches

mode. The primary challenge is that at the time when the microgrid switches mode, most of the loads need to be supported by the energy storage system. This means a large amount of power demand for the HESS suddenly appears, which is a heavy burden for the battery system. Moreover, the battery system needs time to increase the power output from zero to the requested power output. During the time the battery system's power output increases, the battery system is not able to adequately support the load power demand. Otherwise, the HESS needs to sacrifice battery service lifetime to achieve an extremely high discharging rate. Therefore, the SMES is proposed in this thesis to be integrated with a battery energy storage system to build a HESS for microgrid applications. One more challenge for the HESS is the control method. The control method of the HESS needs to consider the characteristics of the SMES low energy capacity and battery low power capacity. More than that, the most critical target of the control method is to stabilise the system's voltage in any circumstances.

Therefore, a novel control method for the SMES-battery is developed to deal with the microgrid decoupling process. The new control method is able to control the battery power output to a better performance. The new proposed method can enhance the battery performance during the process. A case study is carried out to introduce the detailed implementation of the control method for the SMES-battery HESS.

There are many theoretical studies about SMES and battery HESS control methodologies [19, 54], sizing design [55] algorithm and energy management methods [54, 56]. However, for the author's best knowledge, none of the published papers show the SMES-battery HESS experimental performance. The experimental performance is fundamental to validate the SMES-battery HESS applications. Moreover, the experimental platform can be used to test the proposed control method's working performance. Reliable experimental performance of the proposed control method and proposed circuit topology can help the SMES-battery HESS applications be commercialised.

One highlight in this thesis is that the SMES-battery HESS experimental platform has been established and tested at the University of Bath. Moreover, the designed control methodology is implemented in a programmable microcontroller. Various control methods can be used in the microcontroller to test the control method's reliability and performance. According to the experimental results, a novel HESS charging method has been developed.

The new charging method can help to stable the power system's voltage level when the HESS is charged.

Sizing optimization is another challenge when designing SMES-battery HESSs. However, sizing optimization will not be studied in this research. The capacity of the SMES presented in this research is determined by the author's experience and previous research. The batteries size is able to satisfying long-term power demand in microgrids.

1.4 PhD thesis structure

Chapter 2 reviews different superconducting materials and different energy storage systems. After the literature review of the commercialised superconducting materials, the YBCO high temperature superconducting material is selected to build the SMES magnet because the YBCO material has a good performance under high background magnetic field and a relatively high working temperature. Moreover, a literature review of microgrids has been investigated with their advantages and challenges. Different types of energy storage devices have been studied and the advantages of using SMES-battery hybrid energy storage systems for microgrid applications have been discussed.

Chapter 3 discusses the design of the SMES magnet in the HESS. The SMES design is used to help the SMES magnet manufacturing, which will be applied in the SMES-battery HESS. Moreover, the weak point area in the solenoid SMES magnet has been located in the SMES magnet study, which can help the quench protection for the solenoid SMES magnet.

Chapter 4 proposed using Roebel cable to wind the SMES magnet to enhance the SMES magnet power capacity, which is used to improve the SMES-battery HESS overall power capacity. The feasibility study has been conducted using a different winding structure to build the SMES magnet. In this study, Roebel cable is used to wind the pancake coil in the SMES magnet. By using the Roebel cable in the SMES magnet, the SMES magnet is able to achieve higher power output capacity than a conventional winding method.

Chapter 5 presents a new fuzzy logic energy management methodology for the SMES-battery HESS to compensate for the power demand fluctuations in microgrids. The energy management method is used to control the power sharing between the SMES and battery. The new proposed energy management method shows good performance on decreasing the battery power output fluctuating. A case study is presented and used to test the performance of the proposed fuzzy logic energy management method.

Chapter 6 introduces a new control method for the SMES-battery HESS for the microgrid decoupling process. The proposed two-stage method with PI-droop controller shows good performance on stabilising the load voltage and extends battery service lifetime. The case study compares the proposed method with the filtration method, which indicates that the proposed method has better performance. By combining the fuzzy logic control method discussed in chapter 5 and the two-stage method in chapter 6, the whole set of the control method for the HESS to deal with the microgrid daily operation requirement has been established.

In chapter 7, to validate the SMES-battery HESS reliability and achievability, a HESS experimental platform was built. The self-made SMES magnet is designed by the magnet design method, which was discussed in chapter 3. The HESS platform design has been discussed in detail and the circuit topology is presented in chapter 7. The control algorithm in chapter 6 is applied in the experimental platform to test the control method's reliability. The experimental results are discussed at the end of chapter 7, which matches the simulation results in chapter 6.

In the conclusions in chapter 8, the SMES-battery HESS for microgrid applications has been achieved. The system control circuit topology has been designed and tested. The control method for the SMES-battery HESS response of the microgrid daily operation has been designed and validated by the experiments. The SMES design process has been developed to help establish the SMES magnet in a HESS for microgrid applications.

1.5 Graphical abstract of the thesis

The graphical abstract, as shown below, also indicates the contributions of this thesis. To study the SMES-battery HESS for microgrid applications, a SMES magnet must be built. There is no commercially available SMES magnets on the market. Therefore, the SMES magnet must be designed. In this study, the SMES energy capacity design has been researched. The study helps to design the SMES magnet structure with the required SMES energy capacity. A feasibility study of the Roebel cable SMES has been done, which aimed to develop a high power capacity SMES magnet for the HESS. The high power capacity of the SMES is its benefit to increase the HESS maximum output power capacity when dealing with highly fluctuating power demands.

The HESS needs an appropriate control algorithm for different scenarios in microgrid applications such as the microgrid grid connected mode, islanded mode and microgrid grid decoupling process. The microgrid in the grid connected mode acts as one distribution network, which does not need an energy storage in the system. For the microgrid working in islanded mode, the new proposed fuzzy logic control algorithm and conventional filtration methods have been investigated. A novel two-stage energy management control method is proposed to control the HESS to deal with the microgrid decoupling process.

Moreover, the HESS circuit topology needs to be selected to build a HESS experimental platform, which will be introduced in chapter 7. By connecting the SMES and battery to the designed HESS circuit topology, the experimental rig has been established. The experimental platform verification for the HESS is discussed in chapter 7.

By integrating fuzzy logic control and two-stage control, the whole control algorithm of the SMES-battery HESS for microgrid applications is established. Finally, applying the proposed control method in the experimental platform with the designed SMES magnet tells the whole story about the assessment of the SMES and battery HESS for microgrid applications.

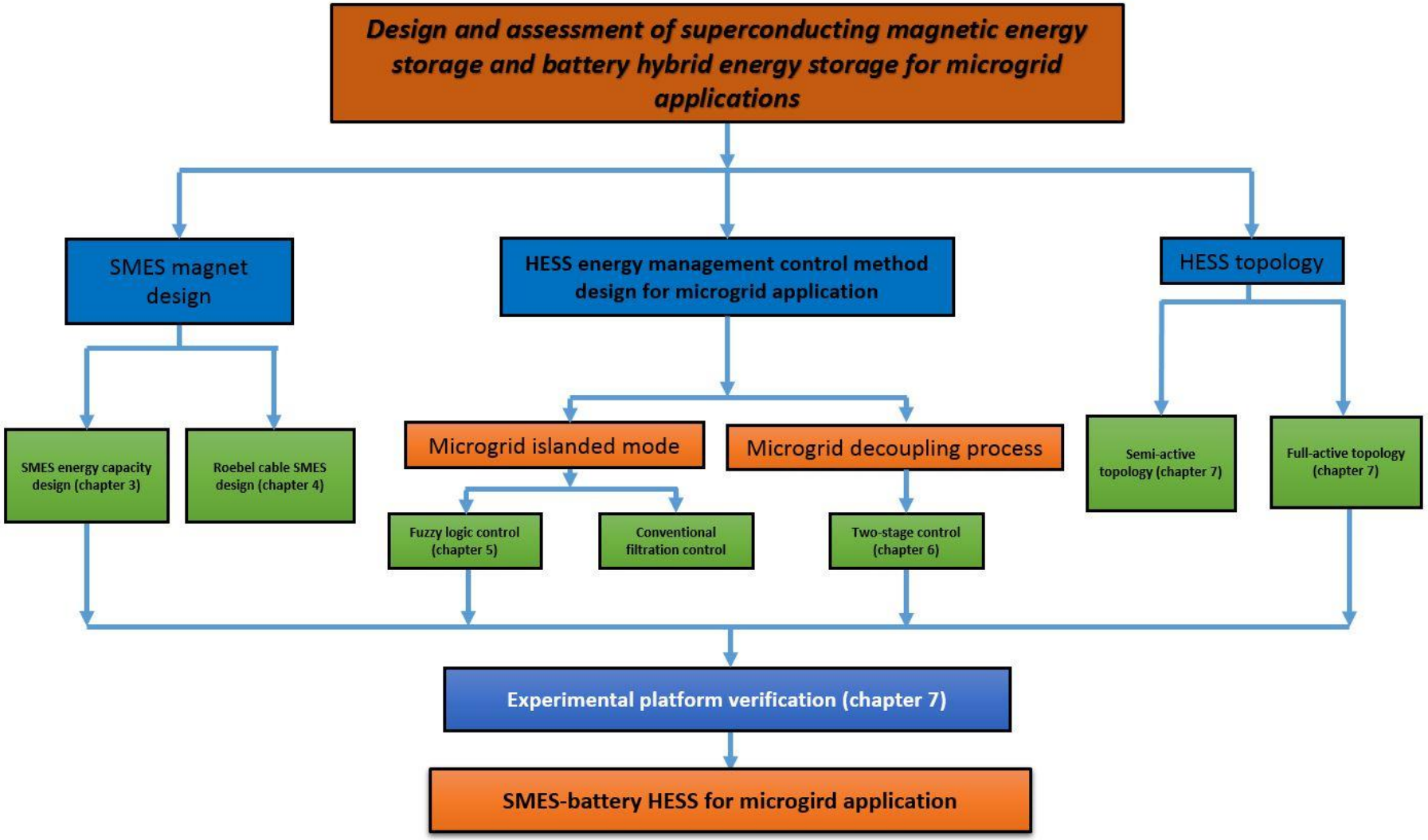
Design and assessment of superconducting magnetic energy storage and battery hybrid energy storage for microgrid applications
SMES magnet design
HESS energy management control method design for microgrid application
HESS topology
SMES energy capacity design (chapter 3)
Roebel cable SMES design (chapter 4)
Microgrid islanded mode
Microgrid decoupling process
Semi-active topology (chapter 7)
Full-active topology (chapter 7)
Fuzzy logic control (chapter 5)
Conventional filtration control
Two-stage control (chapter 6)
Experimental platform verification (chapter 7)
SMES-battery HESS for microgird application

Chapter 2 Literature review

In this chapter, literature about the superconducting materials and different energy storage systems has been reviewed. The SMES magnet design is based on the characteristics of superconducting materials which requires the theoretical study of different superconductors. Different energy storage systems have been studied, and the advantages of the SMES-battery HESS were described. Moreover, the advantages and challenges of the microgrid in the power system have been investigated in this chapter.

2.1 Superconducting materials

Superconducting materials have many potential applications due to having zero resistance at the superconductivity state [57]. This section introduces the characteristics of superconductors. Furthermore, this section briefly introduces three high-temperature superconducting materials which have generated a significant interest from academia and industry [58, 59, 60].

2.1.1 Introduction of superconductor

Superconductors are materials that can conduct electricity with zero resistance, which means that there would be no energy released from the material when transmitting energy. Superconducting material was first discovered in 1911 by Heike Kamerlingh Onnes [61]. For normal conductors, such as copper and silver, the electrical resistance gradually decreases when the temperature of the material decreases. However, such materials cannot achieve zero resistance due to impurities and other defects. In a superconductor, as shown in Figure 2-1, the resistance drops to zero when the material reaches its critical temperature.

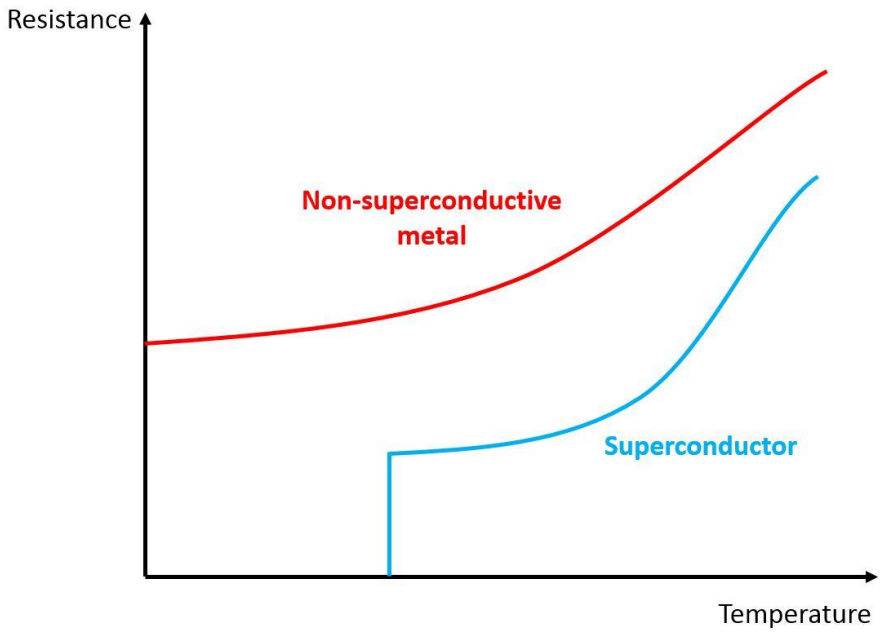

Figure 2-1 Resistance of superconductor and normal conductor

All superconducting materials at superconductive state are affected by three factors, which are current density in the material, background magnetic field, and the operating temperature. As shown in Figure 2-2, the grey area denotes the superconducting region. The superconductor has superconductivity only if the conductor's current density, temperature and magnetic field within this area. T_c (critical temperature), J_c (critical current density), and

H_c (critical magnetic field) denote the maximum limits of a superconductor's superconductive state [62, 63].

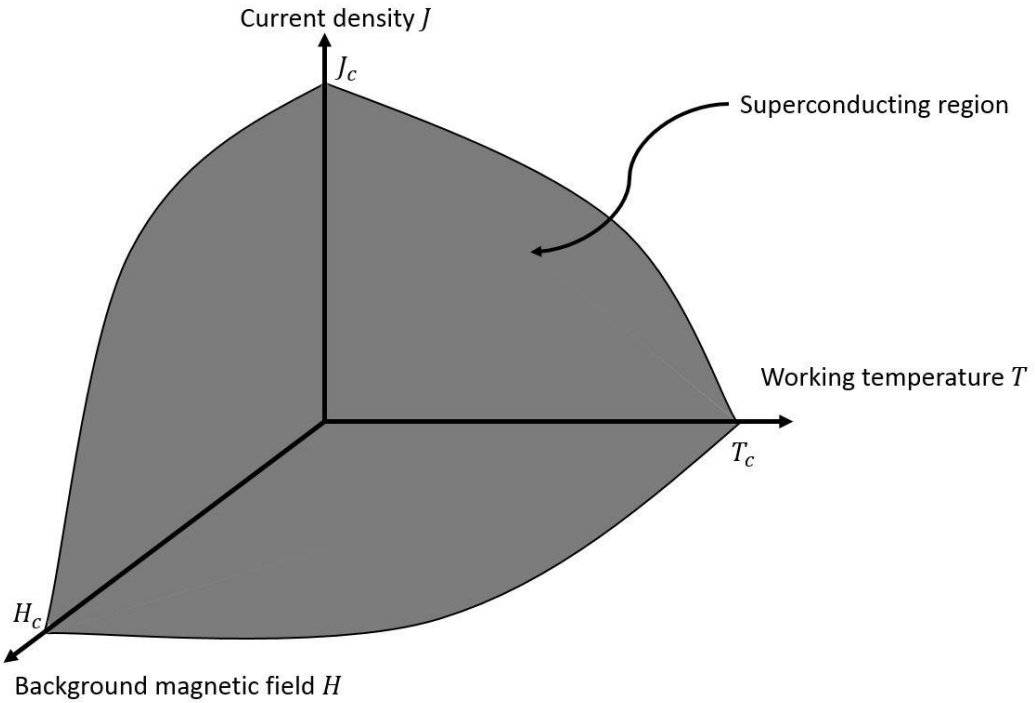

Figure 2-2 Superconductivity defined by operating temperature, magnetic field and current density

2.1.2 V-I curve of superconductor

The voltage drop (V) along the superconductor wire as the current (I) go through can be characterized by the V-I curve. The critical current for the superconductor wire is defined as the current when the voltage drop per centimetre is 1 μV [64]. The general V-I curve is shown in Figure 2-3, with the voltage drop per centimetre changing according to the applied current.

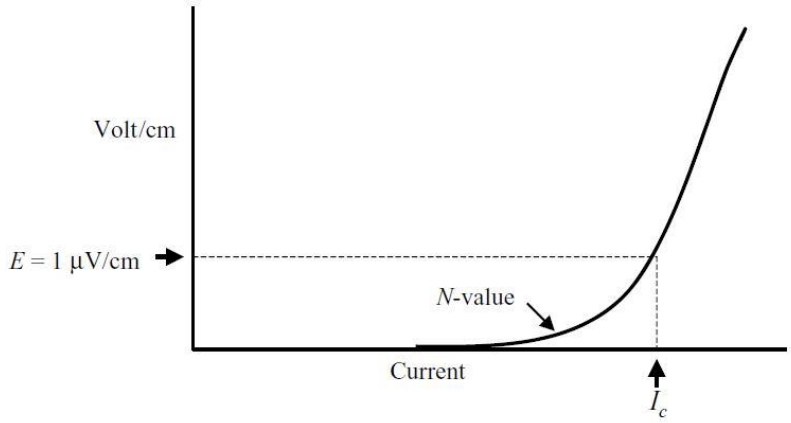

Figure 2-3 V-I curve of superconductor

The V-I curve of the superconducting wire can be summarized as E-J power low shown in Eq. 2-1 [64]

$$E(I) = E_c(\frac{I}{I_c})^N \qquad 2\text{-}1$$

$\mathrm{E(I)}$ is the voltage drop across the superconductor, $\mathrm{E_c}$ is voltage drop criterion which usually is 1 μ V/cm, I is the current in the conductor, $\mathrm{I_c}$ is the critical current, and N is the exponent. The higher the N-value of a superconductor is, the sharper the V-I curve would be. Good quality superconductors have high N values. This means that superconductors which have high N-values will generate lower losses than low N-value superconductors when transmitting the same amount of current.

2.1.3 Low temperature superconductors and high temperature superconductors

Low temperature superconductors (LTS) are superconductors with critical temperature lower than 30 K (lower than -240 °C) such as niobium-titanium (NbTi) and niobium–tin (Nb_3Sn). High temperature superconductors (HTS) are those whose critical temperatures are higher than 30

K, such as bismuth strontium calcium copper oxide (BSCCO), YBCO and MgB_2. In this research, the high temperature superconductor will be used due to its relatively low requirement for the operating temperature which also reduces the cooling equipment cost.

2.1.4 BSCCO-2223 superconductor

BSCCO [65, 66] is a family number of the high-temperature superconductors, BSCCO-2223 has the best performance in BSCCO type superconductor. The critical temperature of the BSCCO-2223 HTS is about 110 K, and the critical current density at 77 K (boiling point of liquid nitrogen) is about 100 A for a 4-mm-wide tape. The manufacturing process of BSCCO-2223 tapes is robust and well implemented, with lengths of about one kilometre being achievable. But BSCCO-type superconductors do not have good performance under high background magnetic field. The critical current of BSCCO-2223 superconductor under different external fields is shown in Figure 2-4.

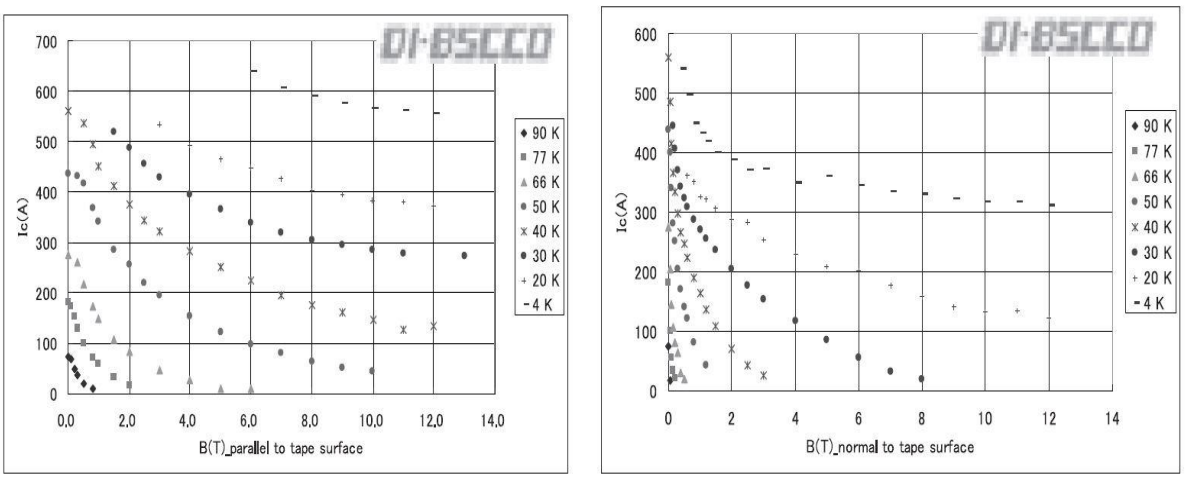

Figure 2-4 Critical current of 4mm wide tape at different temperatures when the external magnetic field is parallel and perpendicular to the conductor's flat side [66]

2.1.5 MgB_2 superconductor

The critical temperature of magnesium diboride (MgB_2) is 40 K [67]. As the performance of MgB_2 from 30 K to 40 K is not good (low critical current), this kind of material mostly used at temperatures under 25 K. The price of the MgB_2 superconductor is much cheaper than other HTS materials as the elements needed to process MgB_2 are easy to get. However, the operating temperature of MgB_2 is much lower than BSCCO and YBCO which limit its applications. Figure 2-5 shows the critical current density of different types of MgB_2 wires at 20 K.

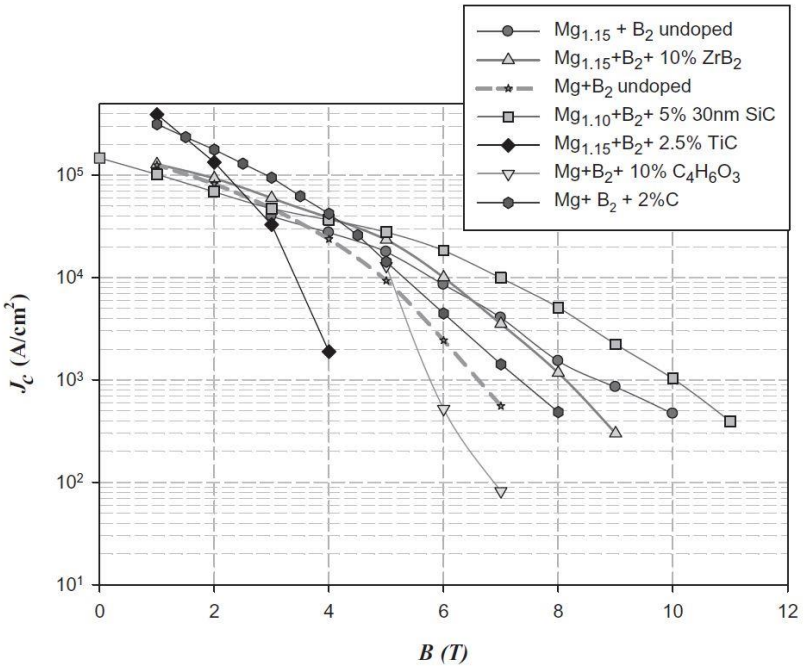

Figure 2-5 Critical current of different types of MgB_2 at 20 K [67]

2.1.6 YBCO superconductor

YBCO-type high temperature superconductors have high critical current density and good performance under high external magnetic field [68, 69, 70]. Furthermore, it has better

working performance than BSCCO-type superconductors at 77 K. Therefore, YBCO is the most popular type of high temperature superconductors for research and industrial applications. Figure 2-6 compares the critical current densities of YBCO and BSCCO-2223 type superconductors under different external magnetic fields.

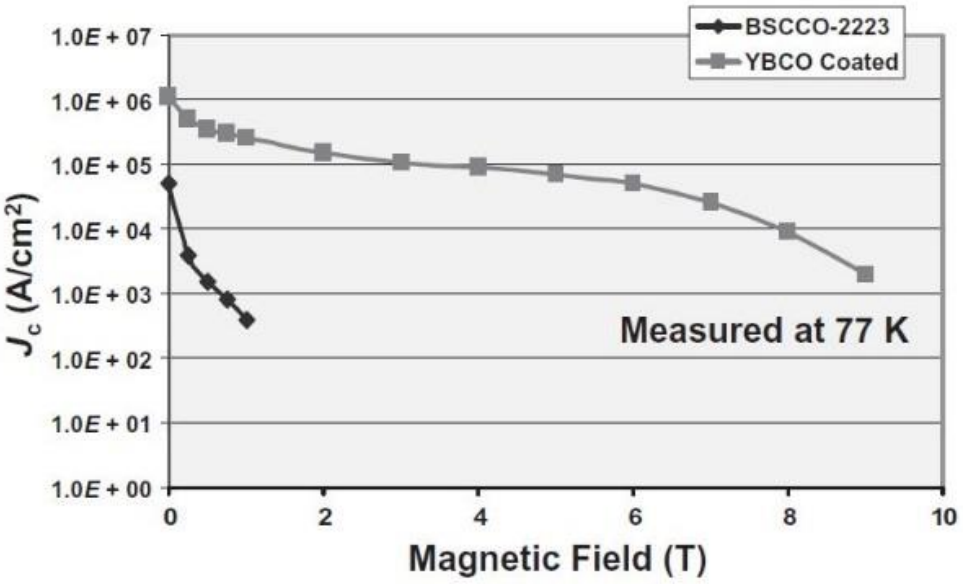

Figure 2-6 Performance comparison between BSCCO and YBCO superconductor [68]

Because the SMES magnet works at high external magnet field, YBCO type superconductor is a good choice to build the SMES magnet.

YBCO HTS tapes are commercially available and excellent performance under the high magnetic field, and are manufactured as multi-layer superconductor tapes as shown in Figure 2-7. Superconducting tape suppliers are able to manufacture tapes that are over 1000 meters in length, which is beneficial for large-scale magnet manufacturing [71, 72].

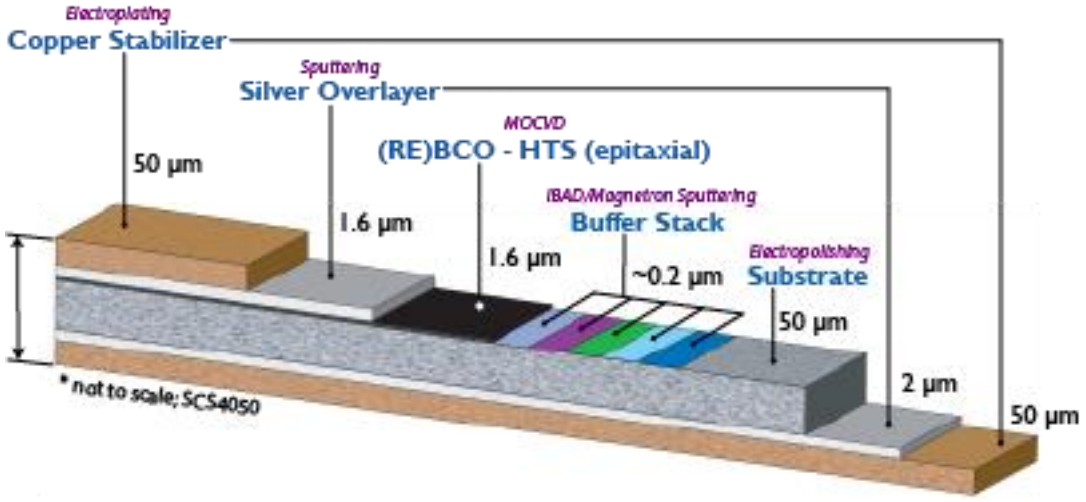

Figure 2-7 YBCO HTS tape

The YBCO layer in the YBCO superconducting tape is about 1µm, with the total thickness of the tape being about 0.1 mm. The copper stabilizer and substrate in the tape can be used to enhance the tape's mechanical properties. The YBCO HTS tape fabricated by SuperPower is able to withstand 700 MPa pressure without current capacity degradation [73].

For magnet design research, the HTS electrical properties are the primary consideration. In this section, the critical current (I_c) and the YBCO material's angle dependency are discussed in the following parts. The HTS electrical performance in the SMES magnet determines the SMES current rating which also determine the energy capacity of the SMES magnet.

The critical current of a superconductor is determined by the background magnetic field and operating temperature [74]. For a background magnetic field that is applied perpendicularly to the YBCO HTS tape, the critical current for the 12 mm wide tape is shown in Figure 2-8.

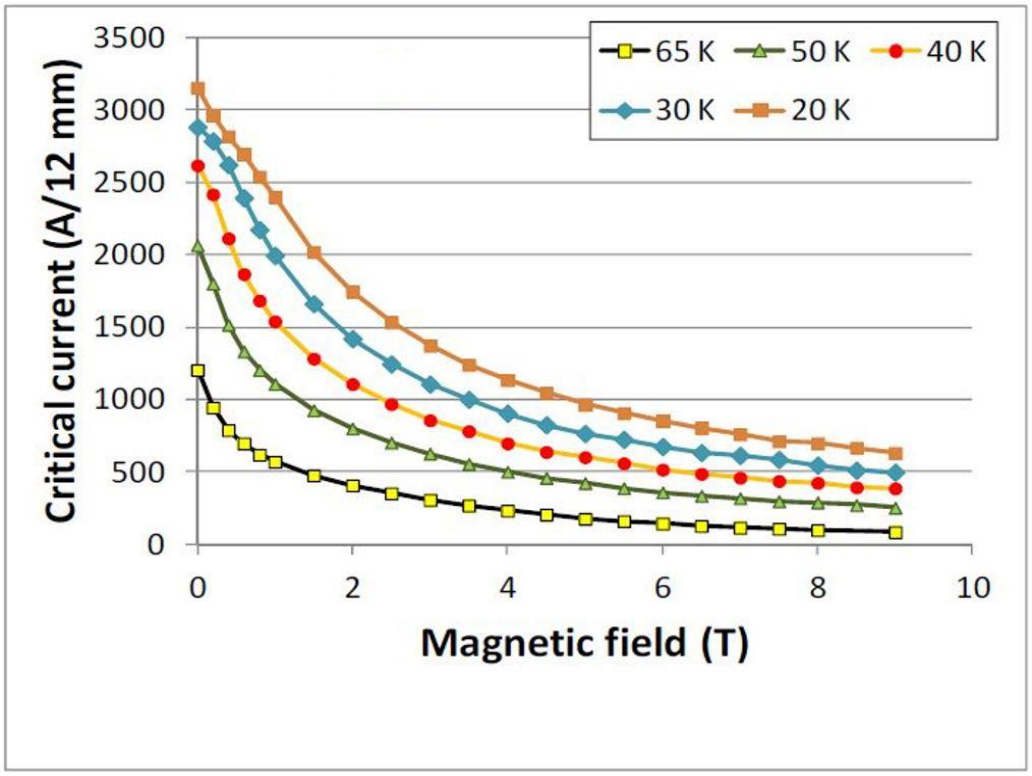

Figure 2-8 Superpower J_cB (perpendicular)

Figure 2-9 shows the critical current of the 12 mm wide YBCO HTS tape when the background magnetic field is applied parallel to the tape.

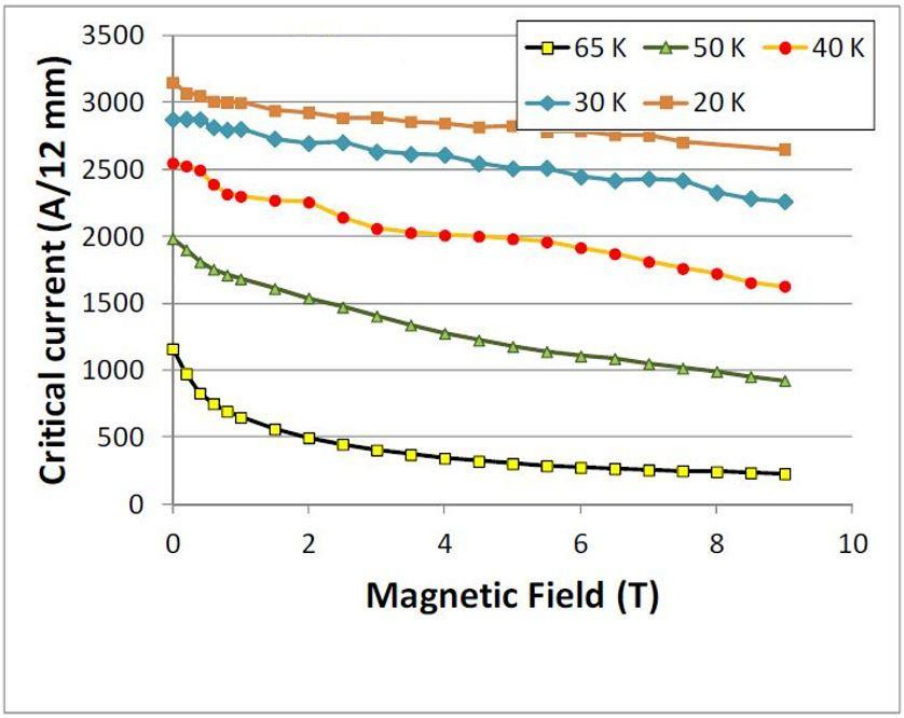

Figure 2-9 Superpower J_cB (parallel)

In the SMES magnet, the magnetic field is dependent upon its structure, and the magnetic field is not evenly distributed. Furthermore, the magnetic field penetrates into the YBCO HTS tape from different angles. Therefore, the angle dependency of the HTS critical current needs to be considered when designing the SMES magnet.

B. Ramshaw et al. [75] studied the angle dependency of the YBCO HTS tape made by SuperPower. The results are shown in Figure 2-10. The results show that the lowest critical current for the YBCO HTS tape is when the magnetic field is applied perpendicularly to the HTS tape. And when the magnetic field is applied parallel to the tape, the critical current has a small amount of attenuation. Moreover, the angle dependency of the HTS has a non-linear relationship with the critical current. These factors, in addition to the uneven distribution of the magnetic field across the SMES magnet and the application of the field from different angles onto the HTS tape, increase the difficulty of designing the SMES magnet.

When comparing YBCO, BSCCO and MgB_2 HTS materials, the YBCO-type superconducting material was found to have better performance under a high background magnetic field, and was thus proposed for use in building SMES magnets in this project.

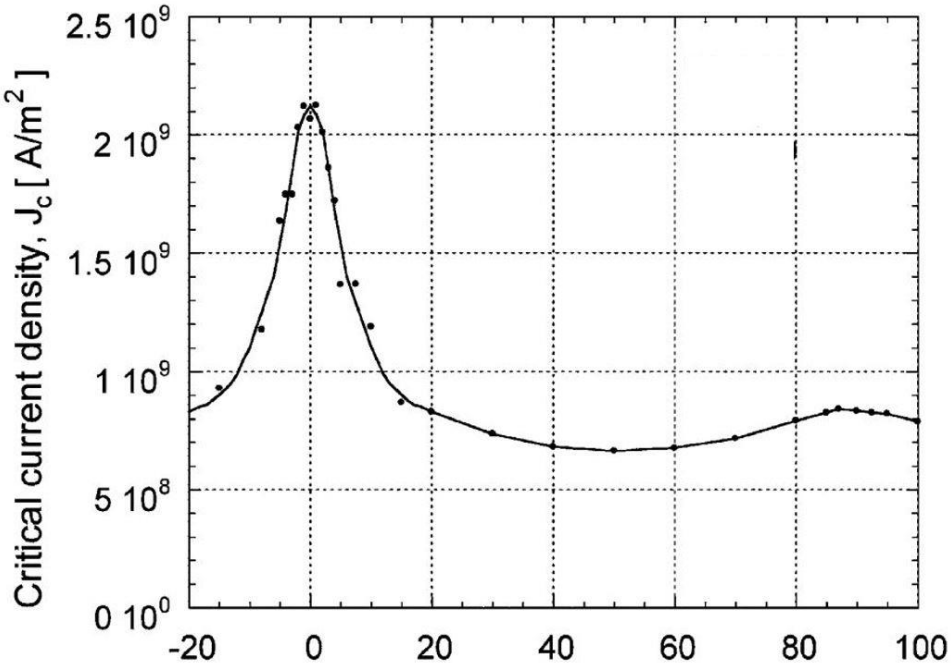

Figure 2-10 Superpower YBCO tape angle dependency under 75 K [75]

2.2 Energy storage systems

An energy storage system (ESSs) is one tool used to store electricity by transferring the electrical energy to other forms of energy, such as chemical energy, potential energy, magnetic energy, etc. which can be stored and retrieved back as electrical power when needed [7, 76, 77]. The history of energy storage is very long. During the early 20th century, the lead-acid accumulator was first proposed to offer direct current electricity storage. In 1929, the first pumped hydroelectric energy storage system was built to store electricity with a high energy capacity. In recent years, with advances in renewable generation and higher quality requirements of storing and supplying electricity, ESSs began receiving more attention. Although battery energy storage and pumped hydro-energy storage systems are the main storage systems used within conventional power systems, a wide range of other energy storage devices are currently available [78]. Figure 2-11 shows different types of technologically mature energy storage systems which are currently being used in electrical power applications.

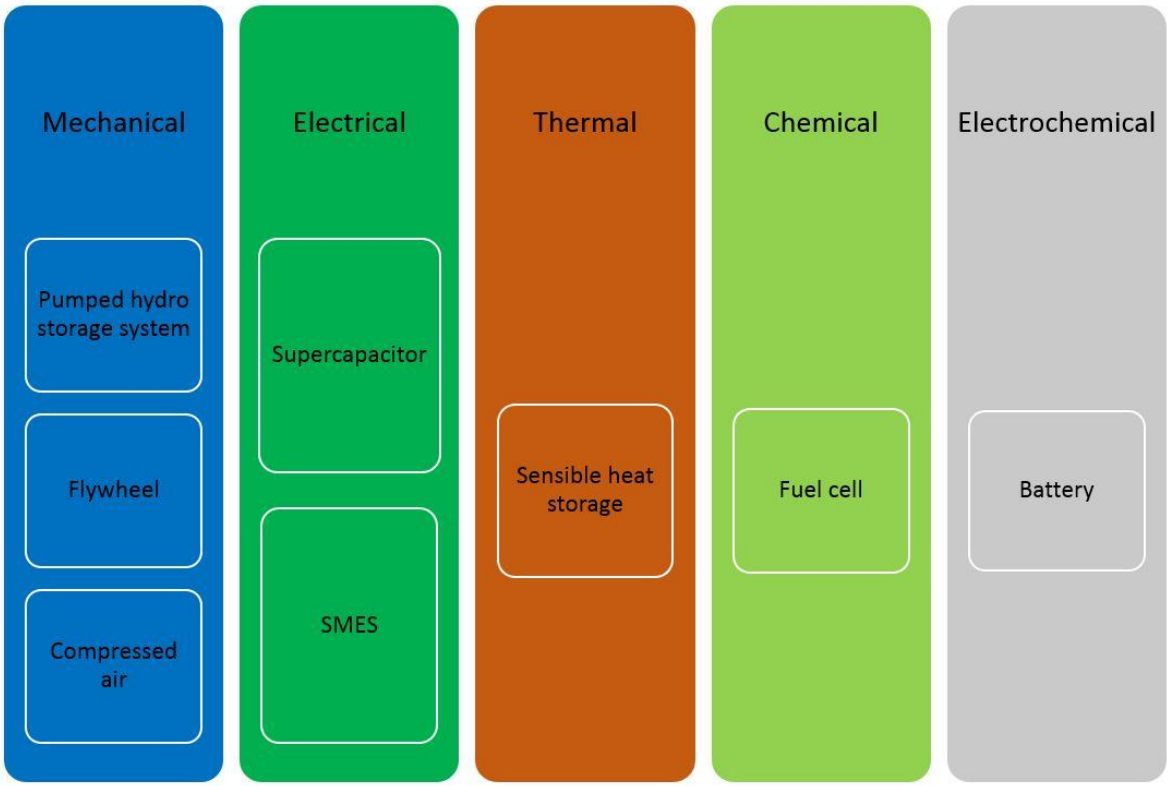

Figure 2-11 Energy storage technologies in electrical power applications

Section 2.3.1 to 2.3.5 reviews some of the most commonly used energy storage systems. The characteristics of different ESSs are evaluated, and their advantages and disadvantages are analysed.

2.2.1 Battery energy storage system

The battery energy storage system is one of the most commonly used energy storage technologies in recent years [76]. The battery energy storage system is composed of number of battery cells, with each cell formed of a positive electrode and a negative electrode placed together in a sealed container. When the battery gets charged/discharged, the electrolyte can exchange ions between the electrodes to deliver electrical energy.

A. Lead-acid batteries

The lead-acid battery was first developed in 1859, and since then the lead-acid battery is one of the most commonly used energy storage devices. Features of lead-acid batteries include:

- The cost of battery energy storage system is relatively cheap (300-600 $/kWh [78]; 50-100 $/kWh [79]; 210-270 €/kWh [80]; 185 €/kWh [81])
- Relatively high efficiency(75%-80% [80])
- High reliability [82]
- Low self-discharge(less than 0.1% [83])
- Need maintenance during the operation which causes higher expense.
- Short life cycle(500–1000 cycles [78]; 200-300 [41]; 500 [84]; 1200–1800 [80])
- Low power density(180 W/kg [79])
- High requirement for the working environment due to the battery needs to work in dry and warm place.

B. Lithium-ion battery

The lithium-ion battery was developed in the 1960s and was commercialized in 1991 by Sony. Since then, the lithium-ion battery has also become one of the most commonly used batteries,

particularly due to its uses normally applied in small devices such as mobile phone, watches and laptops. Moreover, it is also used in electric vehicles (EVs) [85]. In recent years, we have witnessed a booming development of EVs which resulted in dramatic increases in capacity, efficiency, and other properties for Li-ion batteries. The main characteristics of the Li-ion battery are listed below:

- High energy density(80–150 Wh/kg [79]; 100–150 Wh/kg [86];120–200 Wh/kg [87])
- High power density(500-2000 W/kg [79]
- Low self-discharge(1% [88])
- Long life cycles(more than 1500 cycles [79])
- High efficiency(90%-100% [79])
- High cost(900-1300 $/kWh [79])

The lithium-ion battery has the advantage of high power density and high energy density. However, the high unit cost limits its application in large scale application such as in power systems applications.

The comparison of different battery energy storage systems is shown in Figure 2-12.

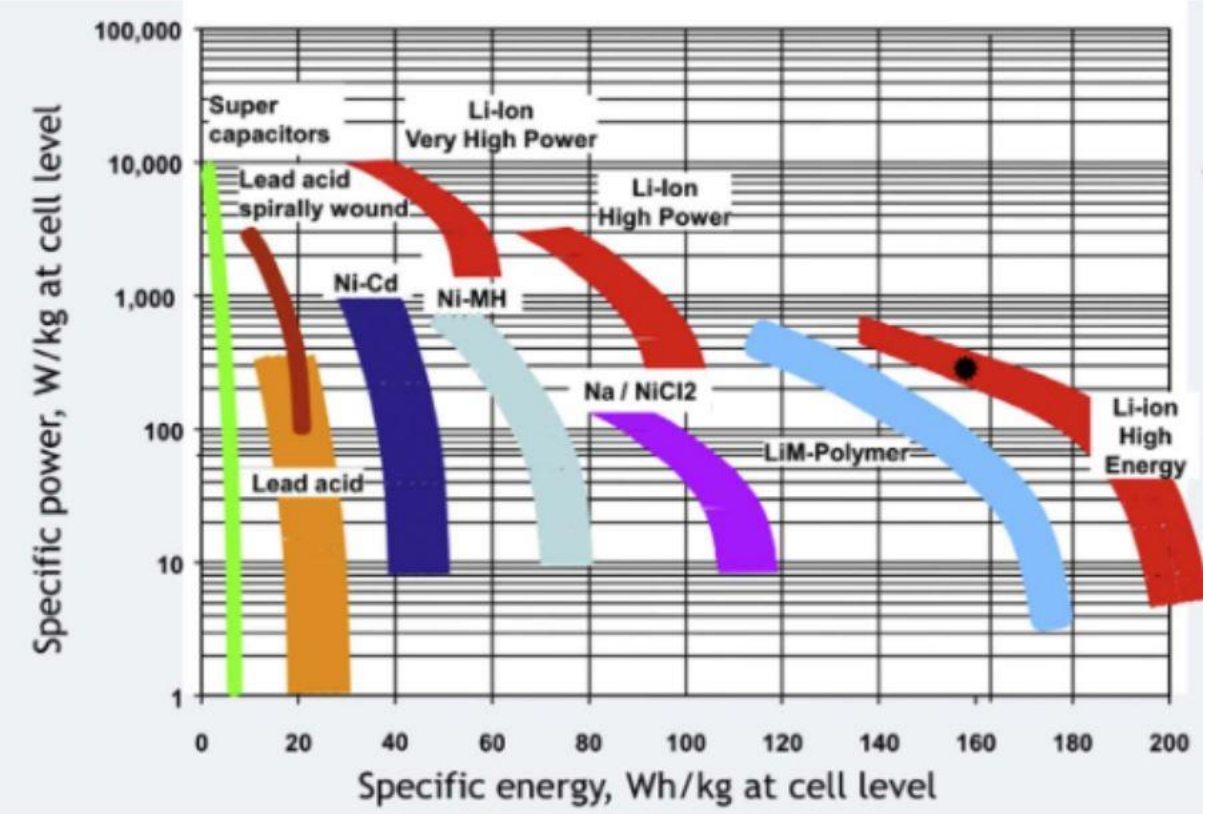

Figure 2-12 Specific energy power of the main battery technologies [89]

Li-ion batteries have higher energy capacity and power capacity than lead acid batteries. However, Li-ion batteries need to sacrifice energy capacity in return for a higher power capacity. Therefore, the design of the battery energy storage solution applied in the microgrid needs to consider both the energy and power capacity demands. If a high energy capacity battery been chosen for the power system, it would be difficult for the battery to compensate for a high power demand. On the other hand, if a high power capacity battery was chosen, it may not withstand the long-term power demand of the power system. Therefore, it would be better if the high power capacity battery is hybridized with a high energy capacity energy storage device or the high energy capacity battery hybridize with a high power capacity energy storage device.

2.2.2 Pumped hydro energy storage system

The pumped hydro energy storage system is widely applied in electrical power system [90]. It utilizes electric motors to convert electrical energy to gravitational potential energy. This ESS pumps water from a low altitude to higher altitude, normally during off-peak hours when the energy demand is low, thus getting 'charged' with energy. When the power system needs energy from this ESS, i.e. during peak hours, the water is released and it flows from the higher altitude downwards, converting the gravitational potential energy to electrical energy. This principle of operation is illustrated in Figure 2-13.This energy storage method has a large energy storage capacity, a long service lifetime and low lifecycle costs.

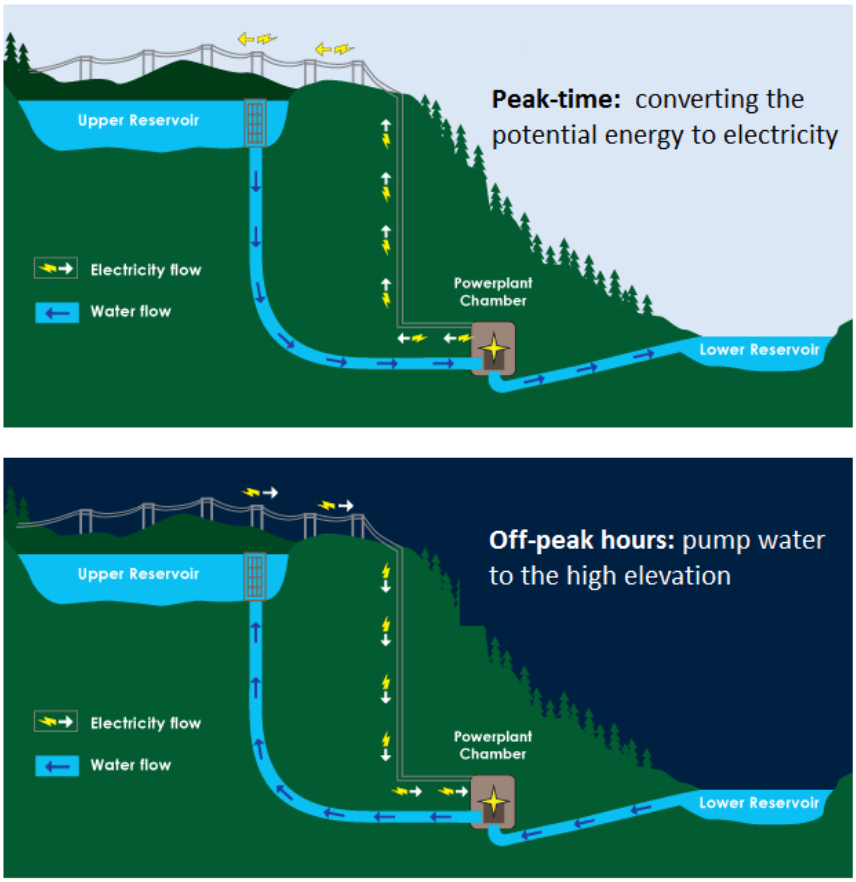

Figure 2-13 A typical pumped hydro storage system [78]

However, this energy storage method has high capital investment, environmental damages and long responding time. Therefore, it can only be used in power grid applications [90].

2.2.3 Flywheel energy storage system

The flywheel energy storage system uses a spinning mass to store energy. When the flywheel ESS is getting charged, the spinning mass is accelerated by the motor. When the system discharges, the spinning mass operates as a generator that generates electrical power from the rotational energy. The flywheel ESS has 90-95% efficiency, long service time and high power density. But it has a high cost and high self-discharge rate which can cause it to be fully discharged in 24 hours [7, 77, 78, 91].

The power capacity of the flywheel ESS depends on the size of the motor and the energy capacity depends on the speed and the size of the rotor. As a result, the power rating of the flywheel can be designed to be relatively high. However, the energy capacity is lower than other long-term energy storage systems such as battery based ESSs [41, 91].

2.2.4 Supercapacitor energy storage system

The supercapacitor is one newly developed energy storage device in recent years. The supercapacitor is made with the porous microstructure such as carbon resulting in large surface area hence higher capacitance can be achieved. The principle of the supercapacitors is more like batteries that are based on electrochemical cells relying on conductor electrodes, electrolytes and porous membrane [92].

The electrons at the cathode can attract positive ions and vacancies of electrons at the anode attract negative ions. Between two electrodes, the electrically insulating separator is placed to allowing ions to go through.

The supercapacitor is working as the same theory as the conventional capacitor. The energy stored in the supercapacitor relate to the supercapacitor's terminal voltage V and its capacity C. The energy stored in the supercapacitor can be represented by Eq. 2-2:

$$\mathrm{E} = \frac{1}{2}\mathrm{CV}^2 \qquad 2\text{-}2$$

The supercapacitor ESS has a high power density and long service lifetime, and such systems can have efficiencies ranging between 85% and 95%, with fast charge/discharge response speed [93, 94, 95]. However, it has low energy capacity per unit and lower efficiency compared with other short-term energy storage devices such as SMES [7, 96, 97].

2.2.5 Superconducting magnetic energy storage system

SMES is another energy storage solution that has been getting more popular in recent years. SMES stores the magnetic energy in the SMES magnet where the magnetic field in the SMES magnet is created by the current flows in the SMES magnet [98, 99, 100]. Figure 2-14 shows a SMES magnet which was used in a cooperative project between the University of Bath and the Electric Power Research Institute in China [101]. The SMES energy capacity is 6 kJ at 69 K, and the designed power capacity is 200 kW.

Figure 2-14 SMES unit above the cryostat [101]

The energy stored in the SMES magnet depended on the self-inductance L and the current in the SMES magnet I. The energy stored in the SMES can be calculated by Eq. 2-3:

$$\mathrm{E} = \frac{1}{2}\mathrm{LI}^2 \qquad 2\text{-}3$$

Pickard et al. [88] research show that magnetic flux density around 10T at 4.2K is able to provide energy densities of 40MJ/m^3, which explains the enormous potential of high energy capacity of the SMES. Moreover, the second generation of high-temperature

superconducting materials has been significantly enhanced, increasing the current density and maximum background magnetic field and thus improving the power and energy densities of the SMES.

2.2.6 Comparison of different energy storage systems

Table 2-1 shows the summary of different energy storage systems listed before. As can be seen from these tables, the SMES has highest power capacity with fast response time. Moreover, the SMES has long service lifetime and highest energy density.

Table 2-1 Comparison of different energy storage systems

Energy storage technology	Pumped hydro energy storage system[102, 103]	Lithium-ion battery[104, 105]	Lead-acid battery[79, 106]	Supercapacitor[93, 107]	SMES[108, 109]
Power capacity cost($/kW)	50-100	400-2500	50-400	300-2000	500-10000
Discharge at rated capacity(hours)	12+	0.017-2+	0.0027-2+	2.7×10^{-7} -1	2.7×10^{-7}-0.0022
Rated power capacity (MW)	100-5000	0-0.1	0-20	0-0.3	0-100
Response time	minutes	milliseconds	milliseconds	milliseconds	milliseconds
Daily parasitic loss	Very small	0.1%-0.4%	0.1%-0.4%	20%-40%	10%-15%
Life (years)	30-40	5-10	5-7	8-10	30
Cycle efficiency	70-80	90-99	63-90	85-95	97+
Cycle life	10000-30000	1000-10000	500-1800	10000+	20000+
Energy density (m^3/kWh)	0.02	0.03	0.058	0.04	6-26

2.3 SMES applications in power systems

Different SMESs have been proposed using different superconducting materials. A MJ level MgB_2 SMES magnet was designed by M Sander et al [110]. Two SMESs using magnets based on a BSCCO-type HTS were developed and tested for use in power systems [111, 112], both of which will be discussed in this section. Most SMES magnet designs now focus on using YBCO-type HTS tapes because of their higher current capacity and better performance under high background magnetic field. The 800 kJ level[113] and 2.5 MJ level[114] YBCO made SMES magnet has been designed. Two applied SMES magnet are shown in the following section.

2.3.1 10 MJ SMES in Kameyama

A 10MJ SMES in Kameyama, Japan [112] is used to stabilise the bus voltage dips to protect industrial facilities such as semiconductor plant. Such voltage dips require huge power outputs and fast responding speed to counteract, making a SMES the optimal choice for this application. Field tests showed that this SMES was successful in counteracting voltage dips and stabilising the grid. The parameters of this10 MJ SMES are shown in Figure 2-15, and a photo of the SMES is shown in Figure 2-16.

Rated capacity and compensation time	10 MVA, 1-s
Rated input-and-output alternating voltage	3φ-6600 V, 60 Hz
Change over time	1/2 cycle + α
Coil configuration	4-pole coil arrangement
Rated current	1400 A
Rated voltage	DC 6.6 kV
Withstanding voltage	DC 13 kV
Inductance	21.1 H
Stored energy	20.7 MJ
Utilized energy	10.0 MJ
Maximum field	4.44 T
Coil dimension (A/B)	
Inner radius	0.346 m/0.410 m
Outer radius	0.404 m/0.468 m
Height	0.194 m/0.495 m
Cooling method	LHe pool boiling

Figure 2-15 10 MJ SMES parameters [112]

Figure 2-16 10 MJ SMES operation site photo [112]

2.3.2 1 MJ SMES built by the Chinese Academy of Sciences

The Chinese Academy of Sciences fabricated a 1MJ SMES magnet winded by BSCCO superconducting tape[111]. The SMES magnet is installed in a 10 kV substation to deal with power quality problems. The designed parameters of the 1 MJ SMES magnet are shown in Figure 2-17.

Parameters	Value
Inner diameter (mm)	400
Outer diameter (mm)	568
Height (mm)	645
Number of double pancakes	44
Number of tapes	82
Total length of used HTS tape (km)	16.4
Inductance (H)	6.28
Operating current (A)	564
Max. (B_r) (T)	2.39
Max. (B) (T)	5.72
Operating temperature (K)	4.2
Stored energy (MJ)	1.0
Withstand voltage (V)	2000

Figure 2-17 1 MJ SMES magnet parameters [111]

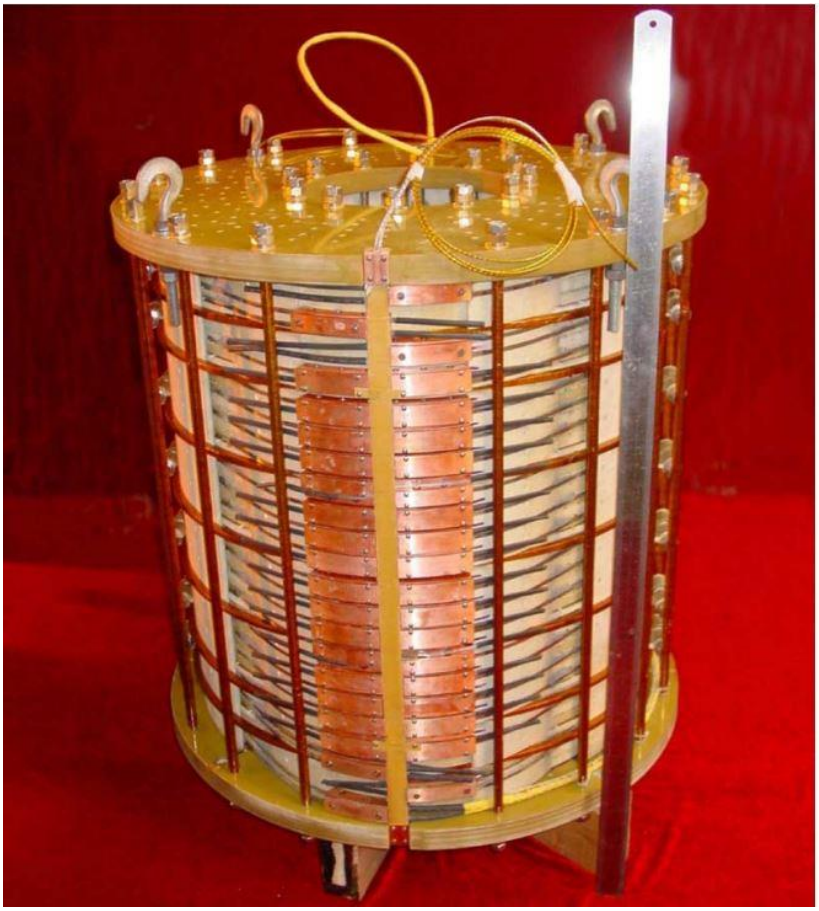

Figure 2-18 View of 1 MJ SMES magnet [111]

2.4 The applications of energy storage systems

The energy storage systems explored in previous sections have been applied in a variety of different applications. In this research, a summary of different energy storage systems used in power system has been done. The overview is shown in Table 2-2 which is based on the review paper [115]

Table 2-2 Energy storage system applications in power system

Applications in power system	The power demand characteristics and requirements	Applicable energy storage systems
Power quality improvement (voltage/frequency compensations) [7, 14, 116, 117]	Demand size is from kW to MW Require few millisecond response time	Flywheel, SMES, supercapacitor, battery
Backup power supply for power system [118, 119, 120]	Demand size up to 1MW, require few millisecond response time and long discharge duration	Batteries, flywheel, battery
Compensate the power output fluctuating from the renewable generations [78, 121, 122, 123]	The power demand for the ESS from kW to MW, request millisecond level responding speed and long discharge duration	Flywheels, supercapacitor, SMES and battery
Power demand peak shaving	Demand size up to MW. Request responding time is about few minutes and few hours discharge time.	Pumped hydro energy storage system, battery
Energy management [124, 125, 126]	Demand size is variable from 1MW. Request long time operation during the day	For large system is pumped hydro energy storage system. The battery can be used for small size system

The response speed and power/energy capacities of different energy storage systems are applied differently to different applications in power systems. Fast responding devices such as flywheels, supercapacitors and SMESs benefit applications which require fast response

times, while battery and pumped hydro-energy storage systems benefit systems which need a large amount of energy. However, the fast-response devices have small energy capacities and thus can only be used for short-term applications, while pumped hydro-energy storage system has the largest energy capacity but requires a long time to deliver electricity. Battery systems offer both high power and high energy capacities, but a highly fluctuating power demand can decrease its service lifetime, thus making it an expensive option.

Therefore, combining fast-response devices with high energy capacity devices has been proposed for this project, providing the hybrid energy storage system (HESS) with both fast response times and a high energy capacity.

2.5 Hybridization of different energy storage systems

2.5.1 Overview of hybrid energy storage system

The combination of different energy storage systems to build a new ESS which has high power density, high energy capacity, long service lifetime and fast responding speed.

The lead-acid battery energy storage system which is characterized by the high energy density and high efficiency can be widely applied in power systems [76]. However, this system also has low power density and offers relatively short service lifetimes. Therefore, the lead-acid battery ESS is proposed for hybridization with another high power density and fast-response energy storage device to build a HESS.

Flywheel and battery HESSs have been proposed to stabilize the power output of renewable energy generation [76, 127, 128]. Flywheels have the advantages of long service lifetimes and high power densities, but they also have high self-discharge rates which limits the application of the flywheel and battery HESS.

Battery and supercapacitor HESSs have also been proposed for power system applications [77, 115, 129, 130, 131, 132]. The supercapacitor and battery HESS has been widely researched

which covering the modelling design, control theory, energy management, sizing design, and HESS topology improvement. Then, it comes to the question that why to study the SMES-battery HESS in this thesis.

2.5.2 Advantages of SMES-battery HESS

The SMES magnet is composed of superconducting coils. The cooling system is used to cool down the magnet's operating temperature to make the superconducting coil achieve its superconductivity state. The external power electronic circuit is connected to the SMES magnet to control the charging/discharging of the SMES. By considering the cooling system consummation, the SMES overall efficiency can reach 95%-98% [78, 133].

With the appropriate power electronic control, the SMES can deal with the power demand in all four quadrants [134], making it a great choice for use in power systems. Moreover, the energy storage medium in the SMES magnet is air which has no operational lifetime limits. The magnetic field is constrained within the cooling system, eliminating concerns of environmental pollution. The SMES service lifetime is about 20 to 40 years.

The SMES can respond to changes in power demand within milliseconds because the conversion of energy within the SMES is an electrical process. Moreover, Sannomiya et al. studied a 1 MW/1 kWh SMES, and found that the SMES takes 20ms to charge 200 kJ [135], showcasing the good performance of high power capacity SMES.

2.5.3 Disadvantages of SMES-battery HESS

Even though the price of superconductors is decreasing, the total cost of the SMES magnet is still very high, which means that the initial investment in this HESS is huge. Moreover, the cooling system design for the SMES magnet is another challenge for HESS applications. However, this will also not be studied in this research.

2.6 Microgrids in power system

The recent trend of making power systems more environmentally sustainable has turned towards onsite power generation, resulting in an increase in the popularity of the microgrid, which was first proposed by Lasseter [136]. The microgrid is normally composed of distributed renewable energy generators (such as solar panels, wind turbines, etc.), energy storage systems and local residential loads.

2.6.1 Microgrid operation modes

The microgrid can operate under two different operation conditions: grid connection mode and islanded mode. The grid connection mode allows the microgrid to function as one distribution network within the power system. The microgrid is working on its islanded mode when the microgrid disconnected from the main grid. The locally distributed power generators and the energy storage systems are used to support the microgrid's power demand. Therefore, a power electronic interface is required to connect and disconnect the microgrid to and from the main grid. Moreover, in the islanded mode, the microgrid becomes very sensitive to load power demand fluctuations and generation power output changes. As such, a reliable power source such as a HESS is required to support the difference between load demand and generation output of the microgrid. The energy storage is used to keep the voltage and the frequency in the microgrid at the required levels. On the other hand, the microgrid has low inertia due to fewer rotating parts within it, making the effective control of the ESS more critical.

Microgrids have been successfully applied in different countries such as Akagi in Japan which integrates solar panels and wind turbines. Another one built by the Consortium for Electric Reliability Technology Solution (CERTS) in the USA integrated heat and power sources in their

microgrid, while other microgrids in Malaga, Spain and Hailuoto, Finland combined diesel generation and wind generation.

2.6.2 Benefits of microgrids

The microgrid has advantages from an economic perspective and enhances power system stability [137, 138, 139]. For the end users in the microgrid, they can get electricity from local renewable energy generators, reducing the energy costs on their end. By using local generators, the utility grid is required to deliver less power to the microgrid, reducing overall transmission losses, in addition to maximizing local utilization of renewable energy [140]. Moreover, the microgrid can maximize local utilization of renewable generations. By integrating energy storage into the microgrid, the power reliability is also increased for the end users [141]. Additionally, microgrids reduce the impact of high penetration of renewables in the power system by isolating the microgrid from the main grid whenever necessary [142].

2.6.3 Challenges of microgrid integration

Due to changes in weather and some unpredictable reasons, the renewable generation power output in the microgrid is highly fluctuating. Moreover, microgrids serve a relatively small portion of end users which makes the microgrid load profile uncertain. These two reasons make balancing power output and demand a critical problem. Even though energy storage systems are applied to microgrids to compensate power imbalances, control algorithms are also a challenge, especially when it comes to switching the microgrid from the grid-connected mode to islanded mode.

When the microgrid is disconnected from the main grid, most of the power demand from the microgrid transfer to the energy storage system in the microgrid. The instantaneous increase in power demand for the ESS can decrease the energy storage system service lifetime. Moreover, the fast power demand increasing requires the ESS to have a high power discharge

rate. If the energy storage device does not have a sufficient discharge rate during the time the microgrid disconnected from the main grid, the HESS cannot sustain the microgrid voltage at the required level, which causes the microgrid unstable.

2.7 HESS energy management methods

The control method of the SMES-battery HESS is the main challenge for HESS applications. Due to the different energy storage systems that have their own unique features, the control method for the HESS is more complicated. The proposed SMES-battery HESS control method should take the advantages of the SMES fast response time [143], high energy capacity [7, 144] and a battery high energy capacity. Moreover, the control method should consider the battery charge/discharge cycle and discharging rate, which relate to the battery service lifetime [145, 146]. There are different control methodologies that have been proposed to deal with fluctuating power demands for HESSs. The filtration method is the most commonly used HESS energy management method which is able to distinguish high fluctuating power demand and slow changing power demand. And let the SMES deal with fast changing power demand and battery handle with the slow changing power demand. The filtration method is able to extend battery service lifetime by decrease battery charge/discharge cycle.

Moreover, a real-time data-driven control method has been proposed by Allègre et al. [147] to control a supercapacitor-battery HESS, to deal with fluctuating power demands. A real-time data-driven control method can highly utilise a supercapacitor by holding back the battery activation until the energy capacity of the fast-response energy storage device reaches a threshold. However, this method may damage the battery when a fast-response device (such as a SMES or supercapacitor) is fully charged. Power grading control is proposed to be applied for electrical vehicles to deal with fluctuating power demands. The power grading control manually classifies different energy storage devices response for different power demands. However, the power grading method is not suited for power system applications due to the fact that the power demands are highly fluctuating and uncontrollable. A model predictive control methodology [148] for the HESS aims to reduce the maximum

power demand from the battery but the fast response energy storage device has low efficiency.

By using the conventional filtration method, the battery power output will follow the trend of the HESS's power demand which means numerous battery charge/discharge cycles. It would be better to develop a new intelligent energy management method that can shift the power demand in short time periods by using more energy from the SMES, and can prevent the SMES from fully charging/discharging through the filtration method.

Fuzzy logic is one intelligent control method which is based on human knowledge with more varying levels than normal methods. By carefully designing the fuzzy logic energy management method to consider the energy remaining in the SMES and the power demand it will be able to shift the power demand between the battery and the SMES, thus reducing the number of battery charge/discharge cycles and extending the battery's service lifetime. Moreover, by considering the SMES's state of charge, the fuzzy logic energy management method will be able to prevent the SMES from fully charging/discharging.

2.8 Conclusions

In this chapter, different superconducting materials have been studied. By considering the performance of the different materials under high background magnetic fields and operating temperatures, the YBCO-type superconductor will be used in further studies. Different types of energy storage systems and their applications were investigated and advantages of SMES-battery HESSs were determined. The challenges of microgrid integration and shortcomings of conventional HESS energy management methods were pointed out and will be investigated in the following studies.

Chapter 3 SMES magnet design for the HESS

In this thesis, as discussed in section 1.5, the research starts with the SMES-battery HESS experimental platform design. The SMES sizing design optimization in the HESS is not considered in this research. Therefore, in this research, the SMES magnet structure design helps to build the SMES magnet used in the HESS. The 2.5 kJ solenoid SMES magnet structure design will be applied to the self-made SMES magnet manufacturing which will be used in the SMES-battery HESS experimental platform described in chapter 7. Moreover, the systematic study of the foundational knowledge of SMES magnets will help inform the SMES magnet control method design. The SMES magnet design study will also support the SMES-battery HESS electrical circuit design. After the simulation of the SMES magnet design, the weak point area in the solenoid SMES magnet will be located, which can help the SMES magnet manufacturer to protect the SMES magnet from quenching in future studies. Moreover, in order to design the SMES used for the HESS, a SMES automatic design process has been developed. The designed program can automatically develop the SMES magnet structure for the requested energy capacity. Moreover, the weak point area in the solenoid SMES can be located. The weak point area location research can help the SMES quench protection and detection for the SMES-battery HESS to improve HESS security. That also helps to improve the reliability for the HESS applied in the microgrid.

3.1 Introduction

Superconductors have zero-ohm losses and a high current capacity which makes them an ideal material to build the magnet. SMES magnets are one kind of magnet which are used for energy storage. The SMES magnet is not used to generate a high magnetic field but needs high magnetic energy stored in the magnet. The amount of magnetic energy in the magnet is related to the SMES magnet's self-inductance and the rated current capacity. Most of all, the SMES rated energy capacity is associated with the working temperature and the SMES structure. Tasaki K et al. proposed the use of a racetrack pancake coil to build SMES magnets [149], and S. Noguchi [52] studied the solenoid SMES magnet with different sizes of superconducting pancake coils stacked together to reduce the winding volume. However, most SMES magnet structures are solenoid and toroid which will be discussed in the following sections. Moreover, different SMES-battery HESS systems need different SMES energy capacities. Therefore, for the HESS applications, the required SMES magnet structure design process to be developed is one which can design the SMES magnet structure with the requested energy capacity.

BSCCO [150, 151, 152], MgB_2 [110, 153, 154] and YBCO [155, 156, 157] are the three most commonly used high temperature superconductors (HTS) in superconductor research. Compared with low temperature superconductors (LTS) such as Nb-Ti [158, 159]and Nb_3Sn [160, 161] which can only work at temperatures around 10 kelvin, the HTS has a much higher working temperature. This means the HTS material has a low requirement for the cooling system and the high temperature is relatively easy to achieve. Compared with the other two commonly used HTS materials, YBCO material has a better performance under high magnetic fields [162, 163], and a higher working temperature [164]. Moreover, the long length YBCO HTS tape that is available for manufacture [165], and its good performance under high mechanical pressure [166] makes YBCO an ideal material to build SMES magnets. In addition, YBCO has a higher current density which is crucial for increasing the SMES magnet's energy capacity [167, 168]. Therefore, YBCO is the proposed material with which to build SMES magnets [101, 169, 170].

3.2 SMES magnet design method

SMES magnet design includes electrical design [171], mechanical stability design [172], and cooling system design [173]. The electrical design is the foundational and crucial design element in the construction of a magnet. The electrical design is used to design the magnet structure. Once the magnet structure has been defined, the critical current and the rated energy capacity for the magnet can be calculated. Electrical design is used to optimise the magnet structure to reach a higher energy capacity with less HTS material usage. In this study, the working temperature for the SMES magnet is 50K as this allows the YBCO HTS to have a higher current capacity and it is relatively easy for the cryocooler to reach a 50K working temperature.

Mechanical stability design needs to be considered after the electrical design. In HTS magnets, the magnetic field in the magnet will be very strong and the current in the magnet is a few hundred amps. Therefore, the Lorentz force on each strand will be very high. Moreover, for a YBCO HTS tape winded magnet structure, mechanical strength will be accumulated. The innermost layer in the SMES magnet will suffer the highest mechanical pressure. As discussed before, the mechanical pressure on the HTS tape cannot exceed 700MPa. If the pressure exceeds this the HTS critical current will be attenuated. Because all HTS tapes are connected in series, the partial low critical current will decrease the working current of the whole magnet and decrease the SMES magnet's energy capacity. Therefore, the mechanical force is analysed after the electrical design decides the initial structure. The cooling design is related to the cooling system and the cooling head locations in the SMES magnet. Therefore, the cooling design will not be discussed in this study.

The SMES magnet electrical design is used to inform the structure of SMES magnets. In this research, the number of double-pancake coils in the SMES magnet and the double-pancake coil's inner radii are alterable. This study changes these two parameters to find out the SMES structure with request energy capacity for the power system usage.

3.2.1 Design process of SMES magnet

The SMES magnet electrical design process is shown in Figure 3-1.

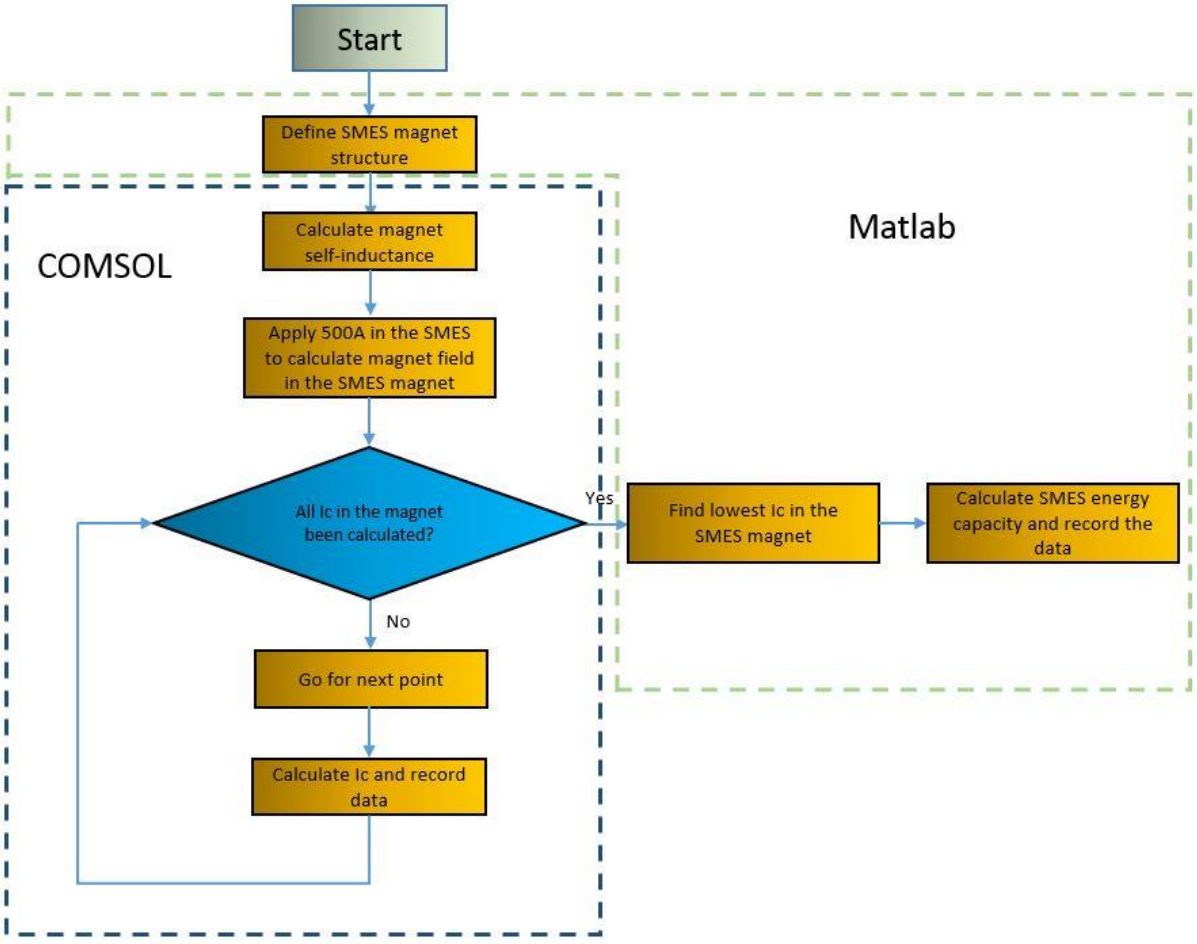

Figure 3-1 SMES magnet electrical design process

The number of double pancake coils and inner radius are defined automatically by MATLAB. Then the SMES structure data is written in COMSOL. The SMES structure is automatically built into the software. COMSOL is the software that uses the Finite Element Method (FEM) to solve problems. Due to the fixed structure fixed, the self-inductance of this structure can be calculated using FEM. The SMES magnet is always placed in an enclosed cooling system [174] which shield the magnetic field from the outside. This ensures the magnet field in the SMES

magnet is generated only by itself and no external magnetic field is applied to the SMES magnet.

3.2.2 SMES magnet critical current calculation

In the SMES magnet electrical design study, the SMES critical current calculation is the most important part of the design process. Because all superconducting SMES coils in the SMES magnet are series connected, the SMES magnet critical current is determined by the lowest superconductor critical current in the SMES. Therefore, it is necessary to calculate the critical current of each point in the SMES magnet to find out the lowest critical current which is also called the critical current of SMES magnet.

In this study, after the magnet been built in COMSOL, a 500 A current is applied to the SMES magnet which is used for further electrical design study. The 500 A current is much higher than the rated current of the SMES magnet working at 50K. The data of the magnetic field and angle in the SMES magnet are recorded. Due to the magnetic field having a linear relationship with the magnetic field and the magnetic field calculation can be calculated by Eq. 3-1:

$$B = K \times L \times I \qquad 3\text{-}1$$

Where B is the magnetic field generated by the SMES magnet, L is the self-inductance of the magnet and K is a constant value, I is the current go through the SMES magnet.

Then the angle dependency on the HTS material needs to be applied. There is no published paper describing the angle dependency of YBCO tape at 50 K. Therefore, for the angle dependency tendency of the YBCO tape at 50 K we will use the same attenuation tendency of the YBCO working at 75 K which is shown in section 2.1.6. The critical current at different angles converts to the percentage of the critical current when the magnetic field is applied

perpendicularly to the YBCO tape. The critical current curve at one example point P under predefined working temperature 50 K can be calculated by Eq. 3-3:

$$\mathrm{I'c}(50\ \mathrm{K}, \theta, \mathrm{B}) = \mathrm{Icb}(50\ \mathrm{K}, 0, \mathrm{B}) \times \mathrm{k}(\theta) \qquad 3\text{-}2$$

Where $\mathrm{Ic}(50\ \mathrm{K}, 0)$ is the YBCO tape critical current under 50 K when the magnetic field is applied perpendicularly to the tape which is shown in Figure 2-8. θ is the angle between the magnetic field and HTS tape surface which can be obtained from the COMSOL simulation. $\mathrm{k}(\theta)$ is the critical current angle dependency factor of the YBCO tape which is shown in Figure 2-10. The variable parameter for the two curves $\mathrm{I'c}(\mathrm{p}, 50\ \mathrm{K}, \theta, \mathrm{B})$ and $\mathrm{Icb}(50\ \mathrm{K}, 0, \mathrm{B})$ is the magnetic field B. In this study, we define the magnetic field on point P with 500 A current going through it as B_1 which can be calculated by COMSOL. Combining Eq. 3-1 and Eq. 3-2, the critical current of point P can be calculated by:

$$\mathrm{I'c}(50\ \mathrm{K}, \theta, \mathrm{B}) = \frac{\mathrm{B}_1}{500} \qquad 3\text{-}3$$

The critical current at one point can be found by Eq. 3-3 which is explained in Figure 3-2 where the blue curve is the relationship of the critical current curve and the different magnetic field strength with angle θ applied to the HTS tape. The green line is the magnetic field at the point P when using the different current in the SMES magnet. The cross point of these two curves is the real critical current at point P.

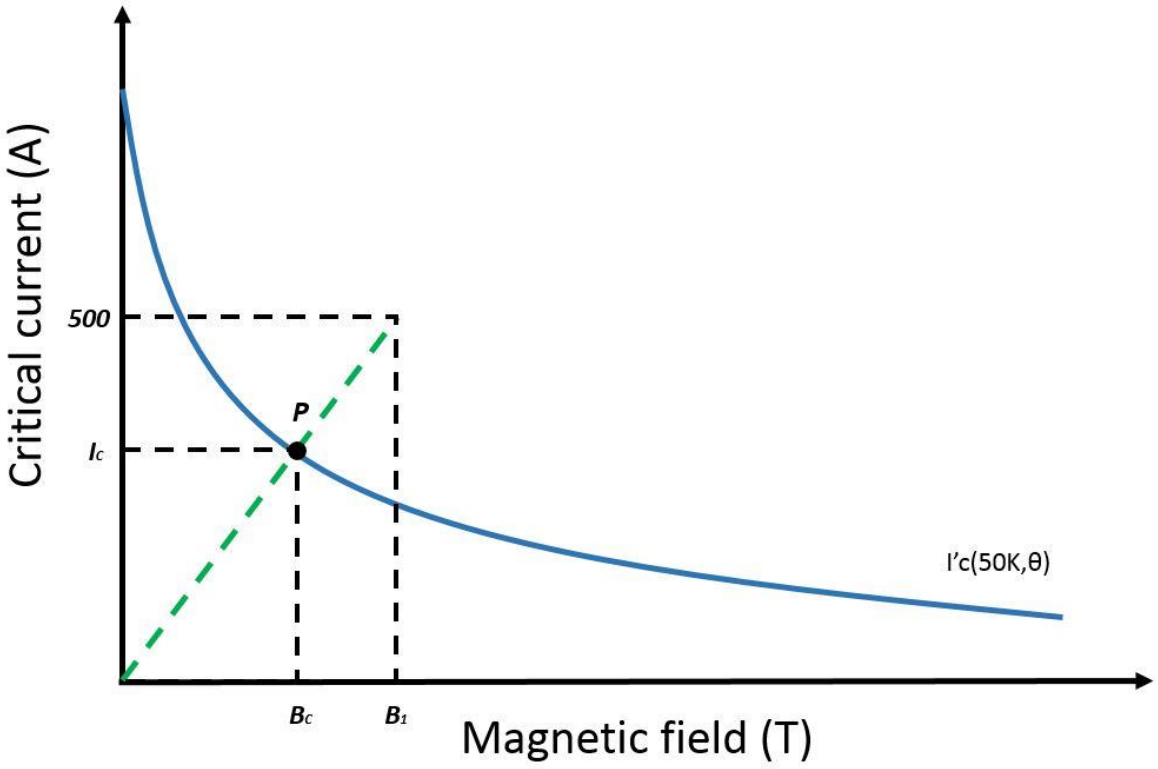

Figure 3-2 Critical current calculation of superconductor in SMES magnet

Theoretically, all points in the SMES magnet need to be calculated. However, to save calculation time, only 4 points at each layer will be calculated. After all layers in each pancake coil has been calculated, the MATLAB software can find the lowest critical current in the SMES magnet which is also the critical current for the whole SMES magnet.

After this process, the critical current of one SMES structure is calculated, by applying Eq. 3-4 to find out the energy capacity of the SMES magnet.

$$E_{SMES} = {}^{1}/_{2}\,LI^{2} \qquad 3\text{-}4$$

3.3 Solenoid SMES magnet design

Solenoid structure [175, 176] and toroid structure [177, 178] are the two main structures used for the SMES magnet design. The solenoid structure magnet is easy to build and has a relatively simple structure. However, the mechanical force and the magnetic field distribution in solenoid winding SMES coils are unequal which means solenoid SMES magnets can be easily damaged under high background magnetic fields. Therefore, a solenoid structure is usually used for smaller SMES magnet design.

In this research, the solenoid structure is used to design the 2.5 kJ SMES magnet for further usage in the SMES-battery HESS experimental platform. The solenoid SMES magnet uses 4 mm wide superconducting tape where the critical current is 1/3 of the 12 mm tape width.

3.3.1 Solenoid SMES magnet structure

YBCO material made SMES magnets are constructed with YBCO pancake/double-pancake coils. For solenoid structure SMES magnets, all the YBCO double-pancake coils are series connected and stack together to build the SMES magnet. The 3D model of the solenoid structure SMES magnet is shown in Figure 3-3.

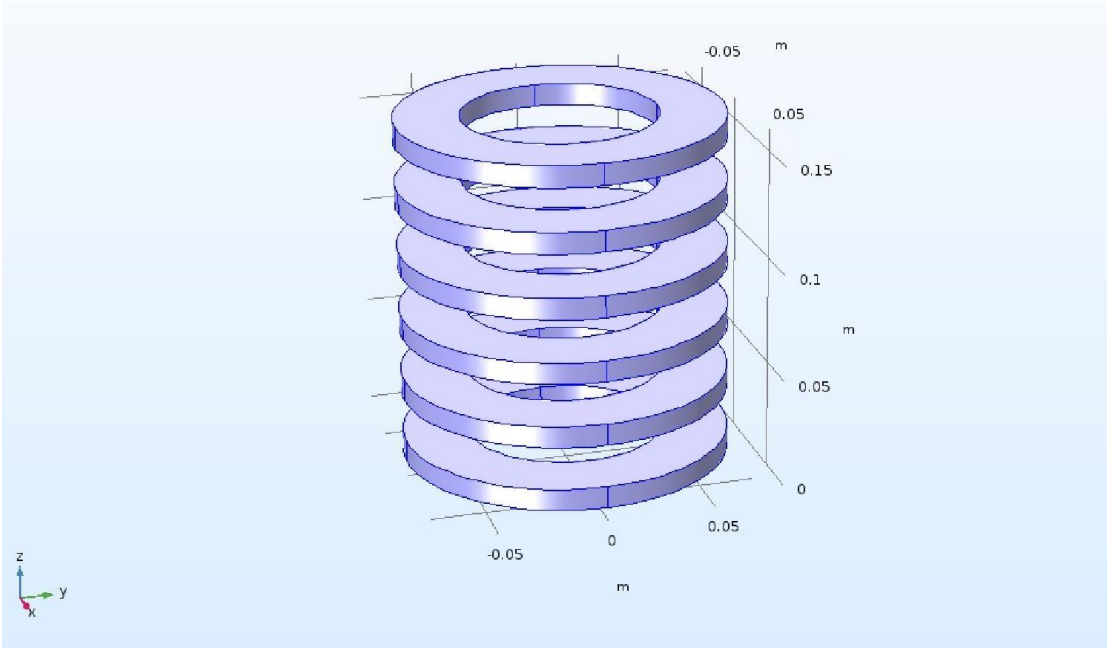

Figure 3-3 3D solenoid SMES structure

3.3.2 Solenoid SMES magnet design

In this research, the author researches the energy capacity of different diameter SMES magnets. The SMES magnet structures and energy capacities is researched in this study. The optimised 2.5 kJ SMES magnet is designed which will be used for the SMES-battery HESS experimental platform.

The solenoid magnet design process is shown in Figure 3-4, MATLAB and COMSOL are used. MATLAB is used to analyse and record the data. Moreover, MATLAB can change the parameters of the SMES magnet structure in COMSOL. COMSOL is used to analyse the magnetic field in the SMES and the self-inductance of the proposed structure. MATLAB changes the coil number of the solenoid structure, inner radius of the magnet and turns of the double-pancake coils in the SMES magnet.

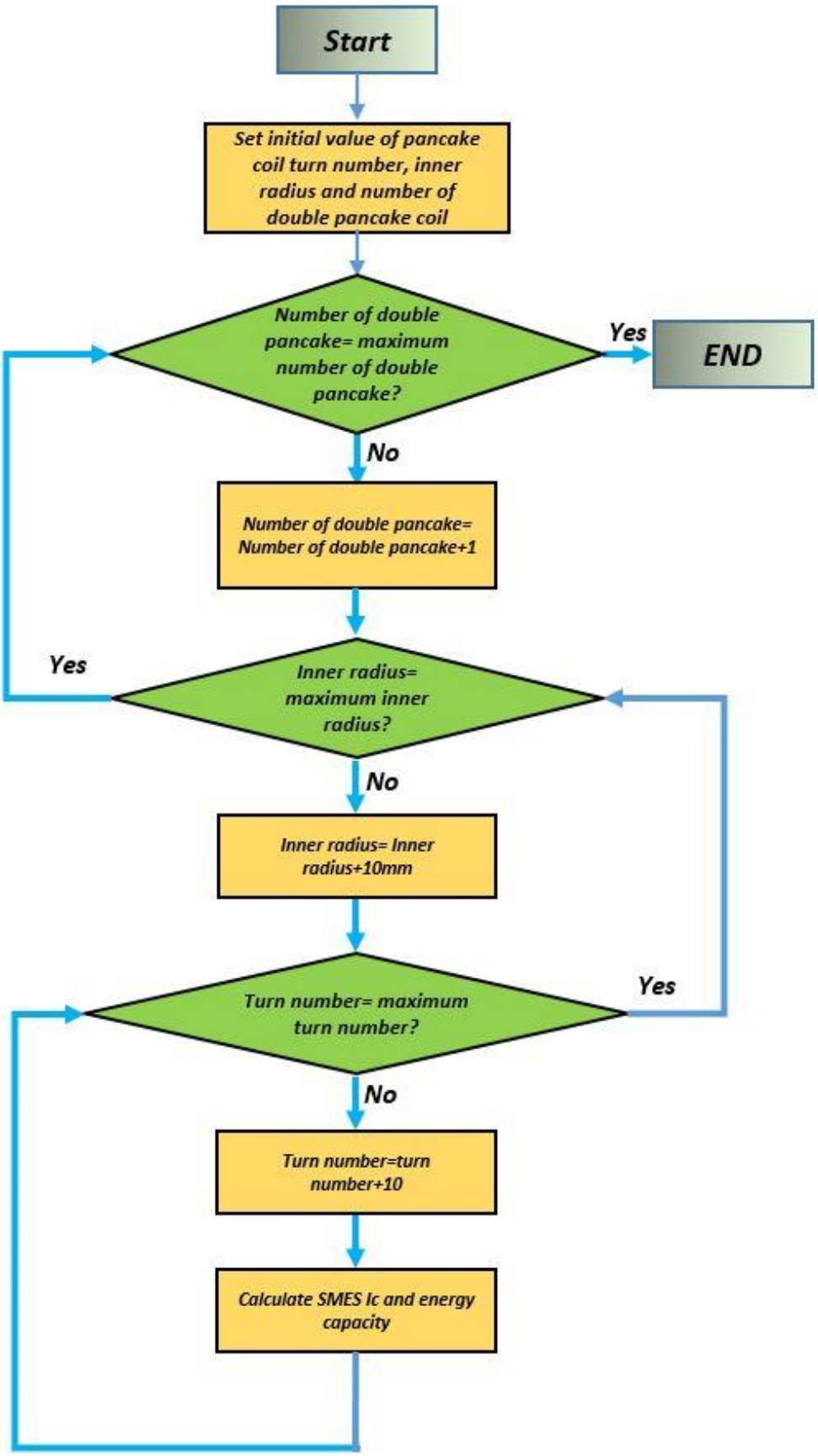

Figure 3-4 Solenoid SMES magnet structure design process

Where the maximum coil number, maximum inner radius and maximum turn number are pre-defined to shorten the calculation time. The SMES critical current is calculated by the process described in section 3.2.2.

3.3.3 Results of the solenoid SMES magnet design

Simulation results of the 2.5 kJ solenoid structure SMES magnet design is shown in Table 3-1. The designed 2.5 kJ solenoid SMES magnet has 6 double pancakes and each pancake coil has 140 turns.

Table 3-1 2.5 kJ SMES design

SMES magnet structure	Solenoid
Working temperature	50 K
Number of double pancake coils	6
SMES inner radius	45 mm
SMES outer radius	73 mm
Number of turns in one pancake coil	140 turns
Rated current	168 A
Self-inductance	0.18 H
Energy capacity	2540 J
YBCO tape width	4 mm
Pancake to pancake distance	3 mm

The mechanical force analysis is calculated by COMSOL. The maximum mechanical strength on the superconductor tape is 1.259 MPa at 47.61° to the YBCO surface. The mechanical stress does not exceed the YBCO maximum mechanical withstand pressure which is 700 MPa. Therefore, the designed solenoid SMES magnet passes the mechanical analyses.

3.4 Toroidal SMES magnet design

Toroidal SMES magnets are mostly applied to high energy capacity SMES magnet design. The toroidal SMES magnet is difficult to build. However, due to the toroidal structure, the background magnetic field applied on each pancake coil is the same, which means the toroidal SMES magnet can store more energy than the solenoid structure. This study calculated for the 900 kJ toroid SMES magnet which will be applied for the SMES-battery HESS in the microgrid.

3.4.1 Toroid SMES magnet structure

Same as solenoid SMES magnets, toroid SMES magnets are also constructed with the HTS pancake/double pancake coils. The construction of the toroid magnet structure is shown in Figure 3-5. Toroid SMES magnets are difficult to manufacture and assemble due to the complex structure of the magnet. However, the magnet field is evenly distributed on each pancake coil which means the toroid SMES magnet can store more magnetic energy.

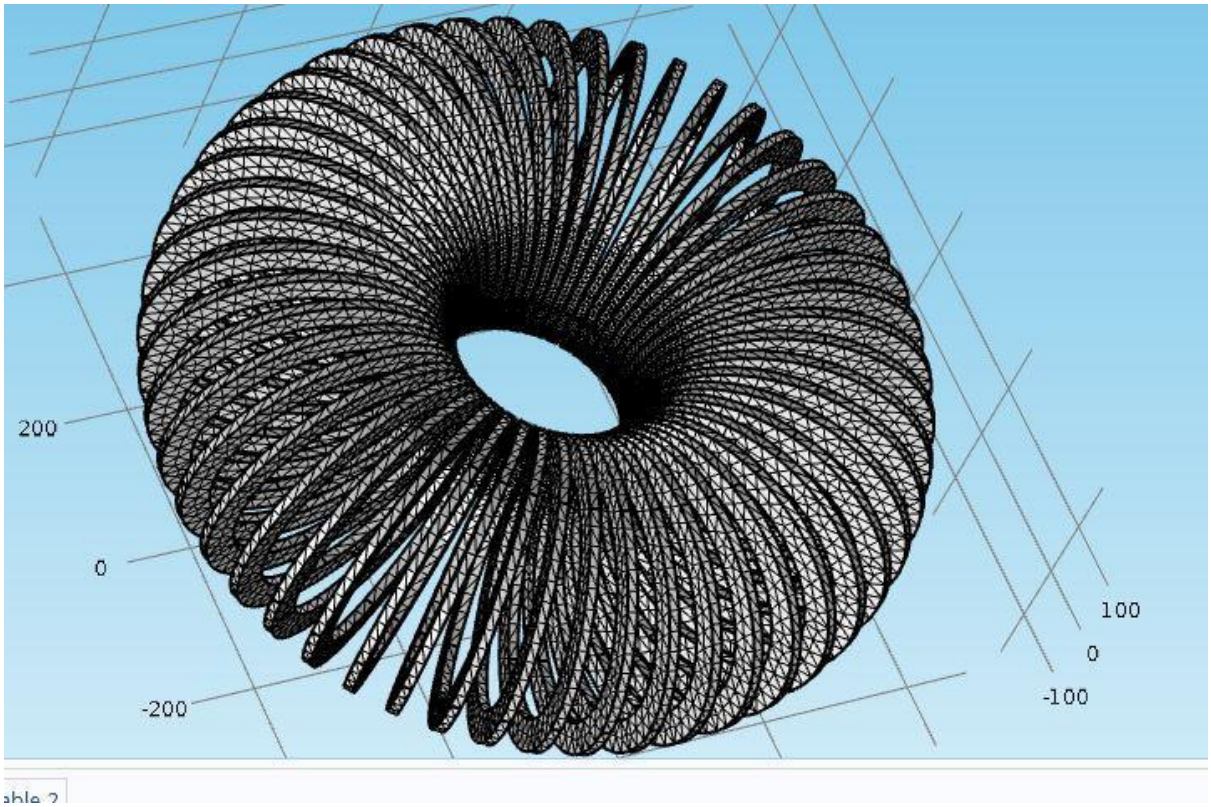

Figure 3-5 Toroid SMES magnet structure

3.4.2 Toroid magnet design

MATLAB and COMSOL are used to design the Toroid SMES magnet. The toroid SMES magnet with 50 pancake coils has been researched. The 0.9 MJ toroid SMES magnet parameters are shown in Table 3-2.

Table 3-2 0.9 MJ SMES magnet design

SMES magnet structure	Toroid
Working temperature	50 K
Number of HTS pancake coils	50
YBCO tape width	12 mm
Pancake coil inner radius	117 mm
SMES outer radius	150 mm
Number of turns in one pancake coil	165 turns
Rated current	936 A
Self-inductance	2.08 H
Energy capacity	914761 J

The maximum mechanical pressure the YBCO superconducting tape can withstand is 700 MPa. The maximum mechanical force on the designed toroid SMES magnet is 29.85 MPa which does not affect the YBCO tape's electrical performance.

3.5 SMES weak point in solenoid SMES magnet

As discussed in the previous section, the SMES magnet's critical current depends on the lowest critical current in the SMES magnet. That point in the SMES magnet is called the weak point. One contribution from this SMES magnet design research is finding out the weak point area in the solenoid SMES magnet.

The solenoid SMES magnet has an unevenly distributed magnetic field distribution which means the top and the bottom pancake coils have the strongest background magnetic field. The magnetic field distribution of the designed 2.5 kJ solenoid SMES magnet is shown in Figure 3-6.

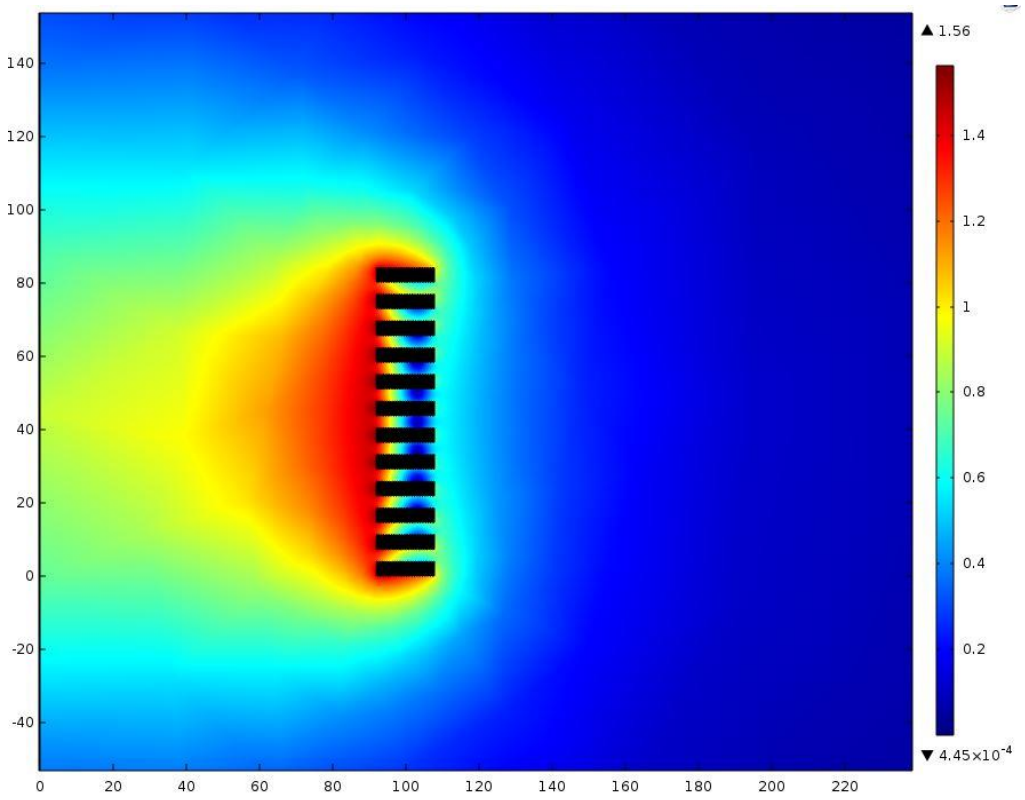

Figure 3-6 Magnetic field distribution on the solenoid SMES magnet

After the simulation of solenoid SMES magnets in section 3.5, it is found that the lowest critical current on the SMES magnet occurs in the range between 1/5 to 1/2 of the total turns from the inner radius. Take the solenoid SMES magnet with 100 turns as an example. The weak point in the solenoid magnet is between 10 turns and 50 turns from the top and bottom coil of the magnet. This statistical result can also be explained by magnetic field distribution in the SMES magnet. The magnet is generated by each coil and accumulates at the top and bottom coil. Moreover, due to the magnetic field diverging it makes the magnetic field have a different angle against the superconductor surface, the first quench point happens at the inner side of the top/bottom SMES coil. As can be seen from the angular dependency of the superconductor, the inner most tape is parallel to the magnetic field which makes the critical current higher. The outer side coil has a low background magnetic field which makes that part difficult to quench.

The magnetic field on the first pancake of the 2.5 kJ solenoid SMES magnet is shown in Figure 3-7

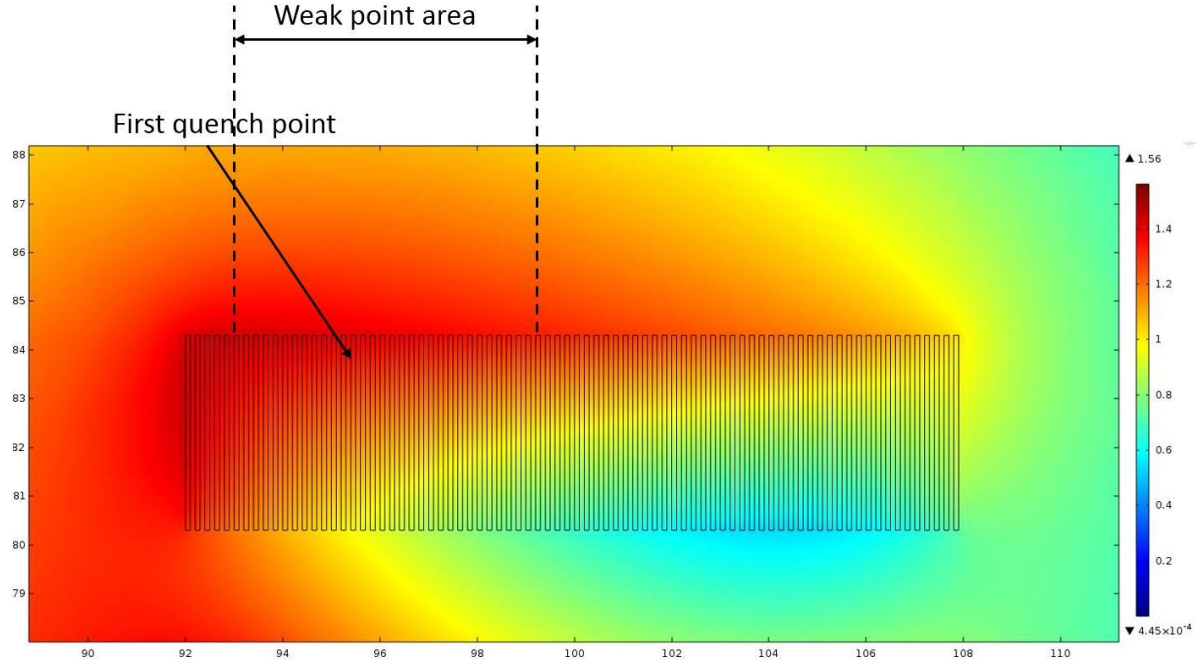

Figure 3-7 Weak point area in 2.5 kJ solenoid SMES magnet

The weak point area and the first quench point in the 2.5 kJ solenoid SMES magnet are as shown above.

In this study, the weak point analysis helps to find out the easiest quench point in the SMES magnet which can improve quench detection and protection for the solenoid magnet. According to the weak point area study, more quench measurement points need to be added on the weak point area to detect the quench. More cooling power needs to be applied to these areas to prevent the SMES magnet from overheating. Moreover, it is necessary to cool down the weak point area rather than the easiest quench point in each SMES design. This can help to prevent the whole SMES magnet quench and enhance the SMES system performance.

3.6 Conclusions

YBCO material performs excellently under high background magnetic fields and at a relatively high working temperature compared to other superconductors, these features mean the

YBCO has an advantage when building SMES magnets. In this chapter, the solenoid SMES magnet and toroid SMES magnet have been studied and the energy capacity was calculated by COMSOL and MATLAB. The designed 2.5 kJ SMES magnet will be used for the SMES-battery HESS experimental platform verification. This numerical study helps to build the self-made SMES magnet which will be used in the SMES-battery hybrid energy storage system. Moreover, one highlight of this study is that the weak point area is located during the magnet design study. In the SMES system, the weak point area in the SMES magnet needs to receive special care. More quench detection points and more cooling power are needed to be added to these areas to prevent SMES quenching during the operation.

However, for HESS applications in the microgrid, the microgrid has a high-power demand fluctuation. Therefore, it is better to use the SMES with a higher power capacity to compensate the power demand fluctuation. In the next section, the feasibility research of using a different winding structure to build the SMES magnet is studied. The designed SMES magnet has the advantage of a high-power capacity when compared with the conventional SMES magnet which is a benefit for the SMES-battery HESS in the microgrid application.

Chapter 4 Feasibility study and evaluation of Roebel cable SMES

Better performance of the SMES can help the HESS performance in microgrid applicants. In this chapter, the author proposes to use a Roebel cable SMES magnet in the HESS to achieve higher power capacity. The Roebel cable has a high current capacity, uniform current sharing and low AC losses, which are all benefits to SMES magnet applications. The low AC losses can reduce the size of the SMES cooling system requirements and increase the SMES's total efficiency. The high current capacity of the Roebel cable can help to increase the SMES power capacity, which is beneficial to HESS applications for microgrids. Chapter 3 analysed how the different diameters of the SMES magnet design can affect the SMES energy capacity. The SMES magnet designs aimed to develop the SMES magnet with a higher energy capacity, more robustness and higher power capacity. In this study, the feasibility of the Roebel cable wound SMES magnet is analysed and evaluated. The advantages of the Roebel cable SMES magnet is analysed. The feasibility study is based on four different aspects of the Roebel cable SMES, which have been evaluated. The Roebel cable critical current measurement experiment has been done to test the Roebel cables working performance. The feasibility of the Roebel cable SMES magnet is concluded at the end of this chapter.

In this study, the Roebel cable SMES magnet is proposed and compared with the conventional YBCO tape SMES magnet. The advantages and the challenges of the Roebel cable SMES have been analysed.

4.1 Introduction

In 2005, assembling coated conductors into the flat Roebel bar was proposed by J Lehtonen et al. [179]. Roebel cable has a complex winding structure, which is used to achieve a high transport current with low AC losses [180, 181, 182]. Because of the advantages of the Roebel cable, the cable has been proposed for use in HTS transformers, high field magnets and electric motors. A Roebel cable HTS transformer has been designed and tested in New Zealand [183, 184, 185]. The transformer used the Roebel cable as a low voltage side winding by utilising the advantage of the high current carrying capacity of the cable. By applying the Roebel cable, the cooling system size can be reduced because of the low AC losses [183, 185]. Also, the transformer size was reduced by using the Roebel cable due to its high current capacity [184]. A Roebel cable accelerator magnet was proposed by CERN [186, 187]. The high current density achieves a fast charge/discharge speed for this magnet application. The rapid discharge speed can protect the HTS magnet from overheating when a quench occurs. The high charging speed can make the magnet reach its required magnetic field in a short time. A Roebel cable motor is now presently being developed by the University of Bath and the University of Strathclyde.

In this study, the author studied the feasibility of using the Roebel cable to build an SMES magnet. Theoretically, the Roebel cable SMES has the advantages of low AC losses and high current capacity. The low AC losses increase the SMES system's efficiency and the high current capacity increases the SMES's power capacity. Therefore, the Roebel cable wound SMES magnet is one promising design for the SMES application.

4.2 Advantages of Roebel cable SMES magnet

The SMES magnet is built using a solenoid or toroid structure. The main differences between the Roebel cable SMES and a conventional tape SMES is caused by the winding structure. For the conventional solenoid structure SMES magnet and Roebel cable solenoid SMES magnet, the main difference is the superconducting coils in the SMES magnet. Therefore, comparing two different winding coil methods under SMES working conditions is the comparison of two different kinds of SMES magnet performances. The same as the toroid SMES magnet, comparing the superconducting coils can help to analyse the differences of the toroid SMES magnet with different winding strategies. Therefore, a comparison between the Roebel cable SMES and a conventional SMES is to compare the Roebel cable pancake and conventional pancake under SMES working conditions.

4.2.1 Roebel cable structure

The Roebel cable is commercially available. General Cable Superconductor Ltd. established a production line for 10/2 and 15/5 Roebel cable [188]. 15/5 Roebel cable means the Roebel cable has 15 strands and the width of each strand is 5 mm. The 10/2 Roebel cable is the superconducting cable with 10 strands and each strand width is 2 mm. A photo of the Roebel cables is shown in Figure 4-1 and the dimensions of the Roebel cables are shown in Figure 4-2 and Table 4-1, respectively.

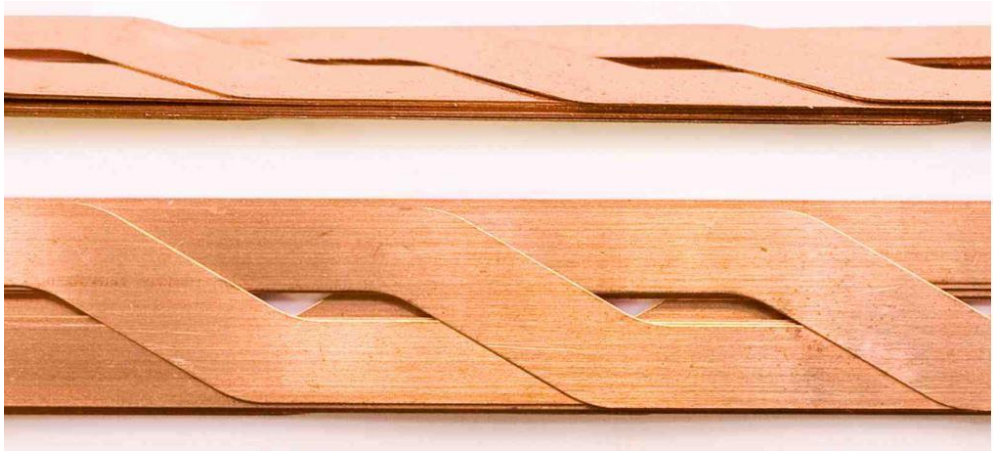

Figure 4-1 Roebel cable photo [189]

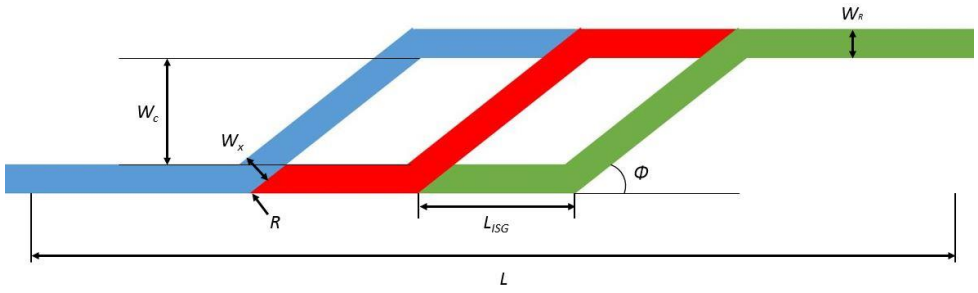

Figure 4-2 Roebel cable structure

Table 4-1 Roebel cable parameters

Parameter	Name	10/2 cable	15/5 cable
$L_{TRANS}(=2L)$	Transposition length	90 mm	300 mm
W_R	Stand width	2 mm	5 mm
W_x	Crossover width	1.76 mm	6.0 mm
W_c	Stand edge clearance	1.0 mm	2.0 mm
Φ	Roebel angle	30°	30°
L_{ISG}	Inter-strand gap	9 mm(10 strand)	20 mm(15 strand)
R	Cut-out fillet radius	0.75 mm	3.0 mm

4.2.2 Current capacity and power density analysis

The Roebel cables have a multi-strand structure, which makes a Roebel cable SMES design have a higher current carrying capacity than a normal superconducting tape wound SMES. Therefore, a Roebel cable SMES magnet has a fast charge/discharge speed, which makes the SMES magnet have a higher power capacity. A high field magnet made using Roebel cable is utilising the advantage of fast charging/discharging [187]. The high power capacity makes the Roebel cable SMES have more potential applications in power systems such as dealing with voltage sag. Moreover, one more bonus is that the fast discharging speed can protect the SMES when a quench occurs. This is because the long period of SMES magnet discharging can cause more joule heat to be generated and overheating occurring in a superconducting tape can permanently damage the superconductor.

A YBCO made SMES magnet is constructed by the stacking of pancake coils. Therefore, a case study of the comparison of a 10/4 Roebel cable pancake coil with a standard 4 mm width HTS tape double pancake coil has been investigated using the Finite Element Method (FEM). To simplify the simulation, the average radius for each pancake was 100 mm. For the same amount of HTS material usage, comparisons of the Roebel cable pancake with a normal HTS tape are shown in

Table ***4-2***. The simulation results show that the energy capacity of the Roebel cable pancake coil and the HTS tape double pancake coil are almost the same.

Table 4-2 Comparison of normal SMES and Roebel cable SMES

	Normal 4mm HTS tape double pancake coil	10/4 Roebel cable pancake
Inner radius	92 mm	96 mm
Outer radius	108 mm	104 mm
Total HTS material usage	100 m	10 meter Roebel cable (Equivalent to 100 m, 4 mm HTS tape (10 m × 10 layer = 100 m))
Self-inductance	8.5 mH	0.096 mH
Rated current(at 50K)	313	3000
Energy capacity	416.4 J	432 J

Compared with conventional YBCO tape, the Roebel cable SMES has no insulation. The none insulation structure makes the Roebel cable SMES achieve a smaller size. Due to the structure changes, the energy capacity and self-inductance for the different winding structures are slightly different. Therefore, it will affect the charge/discharge speed for different winding structures.

When an external power source charges the SMES, the SMES charge state can be represented by applying Kirchhoff's voltage law (KVL) as:

$$U - L\frac{dI(t)}{dt} - I(t)R_l = 0 \qquad 4\text{-}1$$

Where U is the DC bus voltage, L is the inductance of the SMES magnet, R_l is the equivalent self-resistance of the SMES magnet (which is mainly caused by the resistance of the power junctions in the SMES magnet), and $I(t)$ is the current in the SMES magnet at time t.

Assuming that the initial current in the SMES magnet is I_o, the instantaneous current in the SMES magnet can be represented by:

$$I(t) = I_o \exp\left(-\frac{R_l t}{L}\right) + \frac{U}{R_l}\left[1 - \exp\left(-\frac{R_l t}{L}\right)\right] \quad 4\text{-}2$$

In this study, the inner resistance of the SMES magnet is neglected, which means that $R_l \approx 0$. Therefore, Eq. 4-2 can be simplified as:

$$I(t) = \frac{U}{L} t \times D + I_o \quad 4\text{-}3$$

Where D is the duty ratio of the IGBT in the SMES chopper.

The power stored in the SMES can be calculated by:

$$E(t) = \frac{1}{2} L I^2(t) \quad 4\text{-}4$$

For the SMES magnet charged from zero current, which means that $I_o = 0$, the energy in the 4 mm tape made superconductor pancake can be represented by:

$$E(t) = \frac{U^2}{2L} t^2 \times D^2 \quad 4\text{-}5$$

As has been discussed before, the 4 mm HTS tape double pancake coil has a higher self-inductance than the Roebel cable wound SMES. For the same charge duty ratio D, the Roebel cable has a faster charging speed.

However, for the SMES discharged to an external load R, applying KVL to analysis the SMES discharge process yields:

$$-L\frac{dI(t)}{dt} + I(t)R_l + I(t)R = 0 \qquad 4\text{-}6$$

Assuming the initial current in the SMES is I_o, the current in the SMES at time t can be represented by:

$$I(t) = I_0 \exp[-\frac{(R + R_l)t}{L}] \qquad 4\text{-}7$$

Therefore, if the discharge duty ratio is constant D $(0 \leq D \leq 1)$, Eq.8 can be simplified as:

$$I(t) = I_0 \exp -\frac{R \times t \times D}{L} \qquad 4\text{-}8$$

For the 10/4 Roebel cable, $I(t)$ can be calculated as:

$$I(t) = I_0 \exp -\frac{R \times t \times D}{L} \qquad 4\text{-}9$$

$$I(t) = I_0 \exp -\frac{R \times t \times D}{0.000096} \qquad 4\text{-}10$$

For the 4 mm normal HTS double pancake coil, the discharging current can be calculated as:

$$I(t) = I_0 \exp - \frac{R \times t \times D}{0.0085} \qquad 4\text{-}11$$

Therefore, the high current density of the Roebel cable SMES can increase the SMES power density. The power density difference depends on the number of strands in the Roebel cable. Furthermore, the high power density of the Roebel cable SMES can charge and discharge the SMES several times quicker (depending on how many strands are in the Roebel cable) than normal HTS tapes, which is good for SMES applications in power systems.

4.2.3 Uniform current sharing

The unique structure makes sure that no single strand in the Roebel cable remains as the outermost layer or innermost layer. Hence, each strand in the N strands Roebel cable is exposed to the cable surface only for 1/N of each transposition length at the top and bottom cross-over. This particular structure makes the flux evenly penetrate each strand and therefore, each strands impedance is the same.

One advantage of the Roebel cable is that the current sharing of each strand is the same due to its structure. This is significantly important for a superconductor working under a high background magnetic field. Compared with coaxial cable [190] and stacking multiple strands tape [191], the Roebel cable has better current sharing performance [192]. And a stacked-tape has been proposed to build a SMES magnet [193]. Unequal current sharing in a SMES magnet can cause it not to reach its rated energy capacity and can easily create a HTS quench.

Therefore, the Roebel cable SMES has a better current sharing capability than other kinds of HTS parallel connected structures for the SMES design.

4.2.4 Low AC losses

The transport loss and the magnetisation loss are the two main losses in superconducting devices. Due to the SMES charge and discharge cycles, the AC losses in the SMES cannot be neglected. High AC losses in the SMES magnet will generate more joule heating and require more power from the cooling system to cool it down. Therefore, one way to enhance the SMES magnet is to reduce the AC losses generated. According to previous researchers, the Roebel cable can reduce the transport loss and magnetisation loss. Long NG *et al.* [194] compared the transposition loss in a single strand with the transposition loss in a whole Roebel cable. The results showed that the transport loss of the Roebel cable was much less than the sum of each strands standalone transport loss. This result demonstrates the structure of the Roebel cable can reduce the transport loss. The transport loss depends on the shape of the conductor's cross section and for each cable will depend on its detailed architecture. The transposition of the strands within a cable helps equalise the currents and averages the field experienced by each strand. Jiang Z et al. [195] compared the Roebel cable transport loss with stack tape. The results showed that the transport loss in the cable and the stack tape were almost the same at low current. However, the Roebel cable had less transport loss under high operating current.

Magnetisation loss is another kind of AC loss in a superconductor. Y. Yang's study [196] showed the Roebel cable had less magnetic loss under low background magnetic field than the stack of standard superconducting tape. However, when the whole Roebel cable was fully penetrated with magnetic field, the total magnetic loss was the same.

In conclusion, SMES magnets are working under a high background magnetic field during their operation. Moreover, the superconductor in the SMES magnet is not fully penetrated. Therefore, the Roebel cable SMES has lower magnetisation loss and transport loss than a

normal HTS wound SMES magnet. Low AC losses reduce the power demand of the cooling system, which is an important part to enhance the SMES system's efficiency.

4.3 Roebel cable critical current measurement

The Roebel cable critical current measurement experiment has been done in this study to test its performance. During the experimental process, some manufacturing difficulties were encountered, which helped with the feasibility analysis of the Roebel cable SMES.

4.3.1 Experimental setup

4.3.1.1 Roebel cable

In this section, the critical current of the 10/4 Roebel cable was measured. The disassembled Roebel cable is shown in Figure 4-3. The transposition length is 300 mm and the angle is 30°.

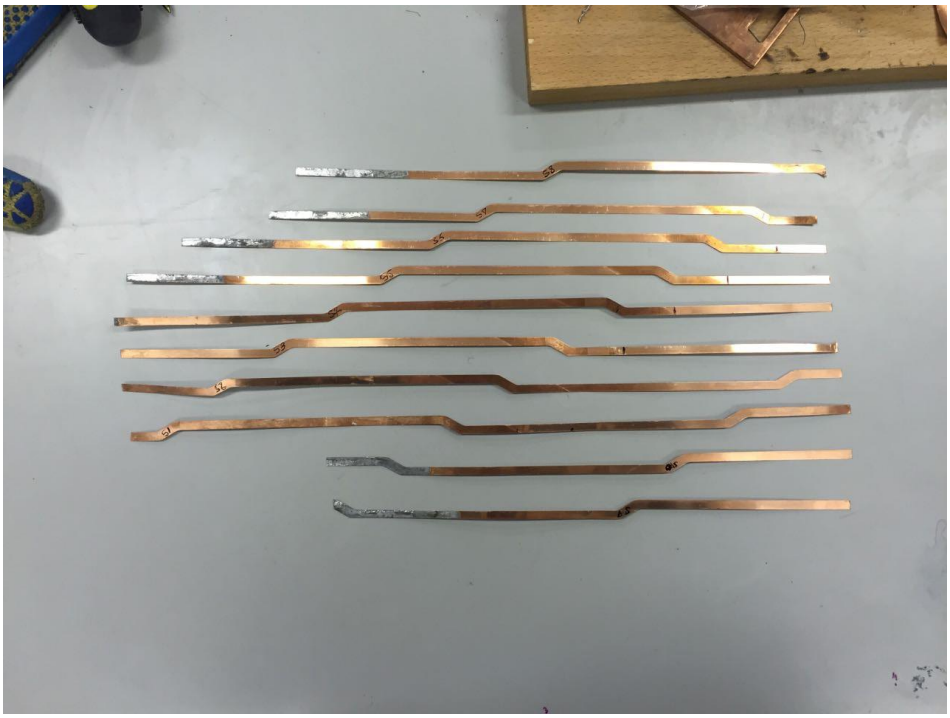

Figure 4-3 10 strands of Roebel cable

4.3.1.2 Critical current measurement platform

A control program based on LabVIEW and a National Instruments (NI) data acquisition card were used. The measurement platform design is shown in Figure 4-4. A DC power supply was controlled by a control program on a PC. A high current shunt was used to measure the current flowing through the Roebel cable. A NI card was used to collect data of the voltage across the current shunt and the voltage on the Roebel cable. The current-voltage relationship on the Roebel cable will be discussed in the following section.

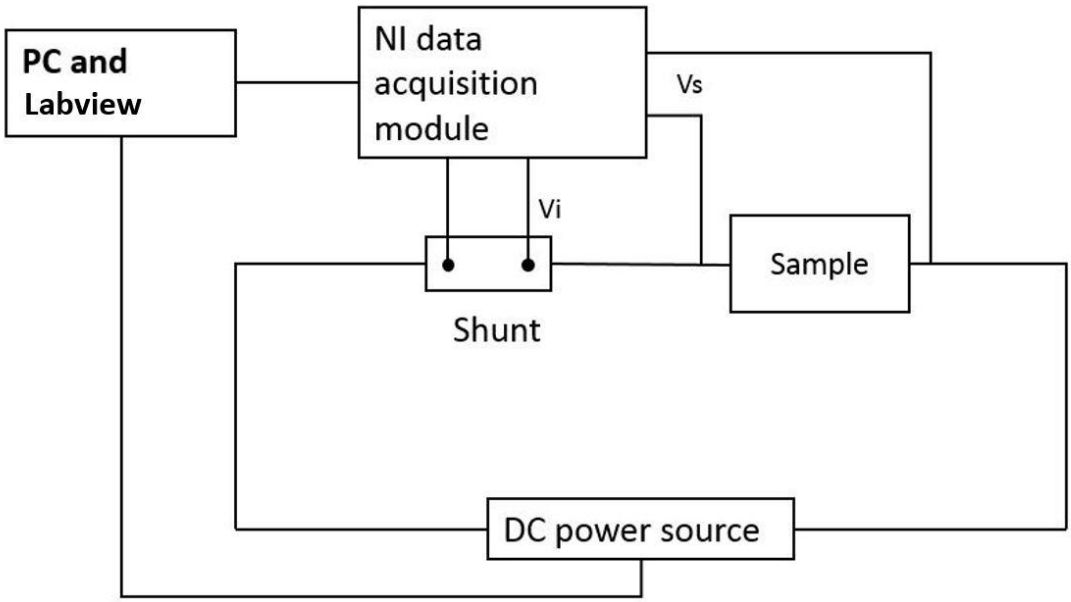

Figure 4-4 Superconductor critical current measurement circuit

The current shunt resistivity is a constant value R_{shunt}. Therefore, the current in the Roebel cable can be calculated by:

$$I_{cable} = V_i / R_{shunt} \qquad 4\text{-}12$$

4.3.1.3 Roebel cable current lead

Superconductor bridges were built between the Roebel cable and copper block as shown in Figure 4-5. Each strand has two 4 mm superconductor bridges on both ends to make sure the bridges can support enough current. Moreover, this method can make sure that the current lead can occupy a short length of the Roebel cable (leave more space for the voltage measurement). In this experiment, the current lead length on one side was approximately 6 cm.

Figure 4-5 Superconductor bridges between the Roebel cable and copper block

4.3.1.4 Voltage measurement points on the Roebel cable

In this experiment, the voltage on the Roebel cable is measured. Two voltage measurement points distance on each strand is 700 mm. Moreover, voltage measurement points have at least 600 mm distance to the current lead to guarantee the accuracy of the experiment.

4.3.1.5 Power supply

Two 10 V-1000 A DC power supplies connected in parallel to support the current for the Roebel cable were used. The experiment platform setup is shown in Figure 4-6.

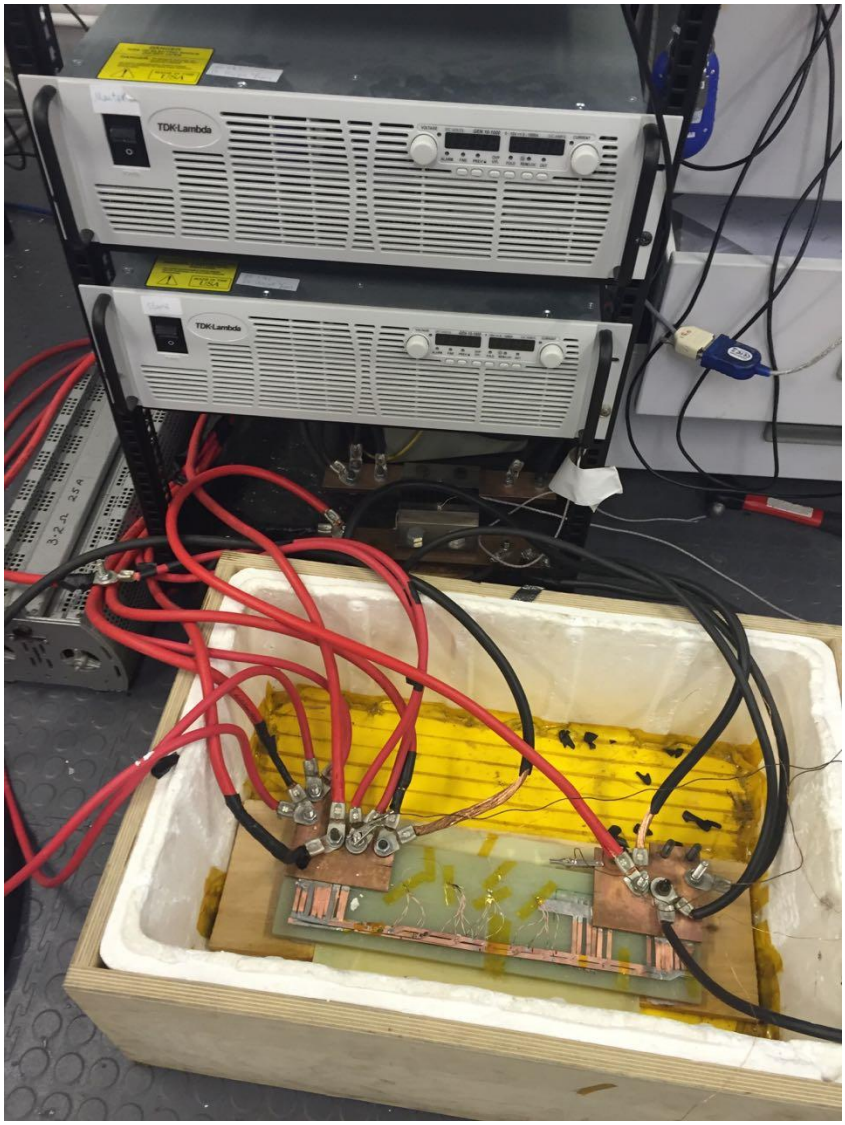

Figure 4-6 Roebel cable critical current measurement experiment setup

4.3.2 Results and discussion

The measurement results are shown in Figure 4-7. The critical current of the superconductor is defined by the voltage across the superconductor, which is 1 μV/cm [197]. The results show that the critical current of this Roebel cable was 987 A at 77 K (liquid nitrogen bathed).

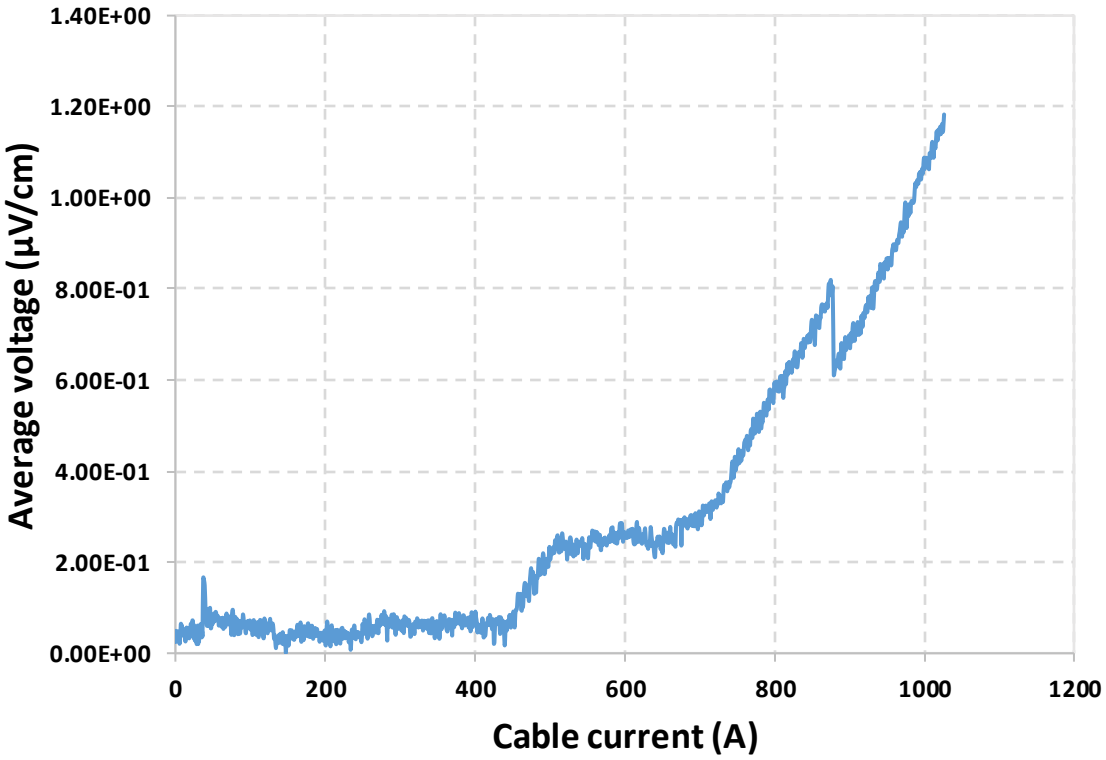

Figure 4-7 Roebel cable critical current measurement result

The average voltage on the Roebel cable was stable when the current increases from 0 A to 440 A. This is because all of the strands of the cable were in a superconducting state. The small fluctuation at 40 A was caused by the slave DC supply turning on. When the current is larger than 440 A, a voltage rise on some of the strands starts to appear. When the superconductor resistivity becomes larger, the current starts to redistribute to other strands. This makes the average voltage on the cable not change between 500 A and 650 A. The voltage drop at 876 A is also caused by current redistribution over different strands in the Roebel cable.

A single strand critical current measurement result is shown in Figure 4-8. The Roebel cable has a lower N value than a single strand, which is caused by the inequivalent impedance of the power joints in each strand.

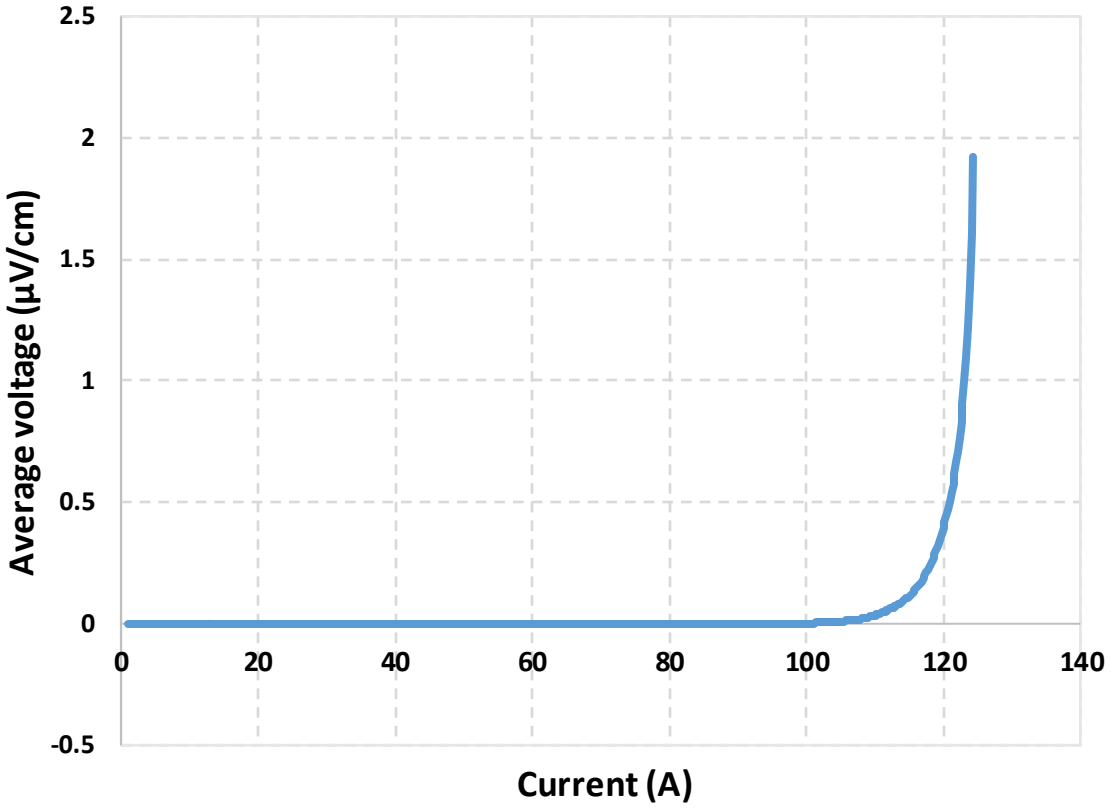

Figure 4-8 Single strand critical current measurement result

Therefore, as can be seen from the results, the power joint soldering is one of the most important parts for an application. The different power joint impedance between the current leads and each strand in the Roebel cable can cause an uneven current distribution. The imbalanced current distribution can cause the Roebel cable to easily quench, which can damage the HTS material.

4.4 Comparison between Roebel cable SMES and conventional YBCO tape SMES

4.4.1 Energy capacity analysis for the Roebel cable SMES

Compared with a standard HTS tape wound SMES magnet, the Roebel cable SMES magnet has lower self-inductance but higher current carrying capacity. The magnetic field stored in the SMES magnet is almost the same as the Roebel cable pancake and standard HTS tape double pancake. The analysis is discussed in section 4.2.2. Therefore, for the same amount of HTS material usage, the Roebel cable SMES has almost the same energy capacity as the normal HTS tape. The energy capacity difference is caused by the insulation (Kapton tape) on the conventional YBCO tape. The Kapton tape affects the SMES magnet structure, which causes the energy capacity to be slightly different.

4.4.2 Charge/discharge delay and joule heat

The Roebel cable does not have any insulation on each strand. Therefore, the current in the HTS tape have turn-to-turn current sharing and therefore, a small amount of current will go through the substrate in the HTS tape to other strands. The substrate is made of copper or silver, which has a relatively high resistance than the superconducting layer. An equivalent electrical circuit for the three strands Roebel cable pancake coil is shown in Figure 4-9.

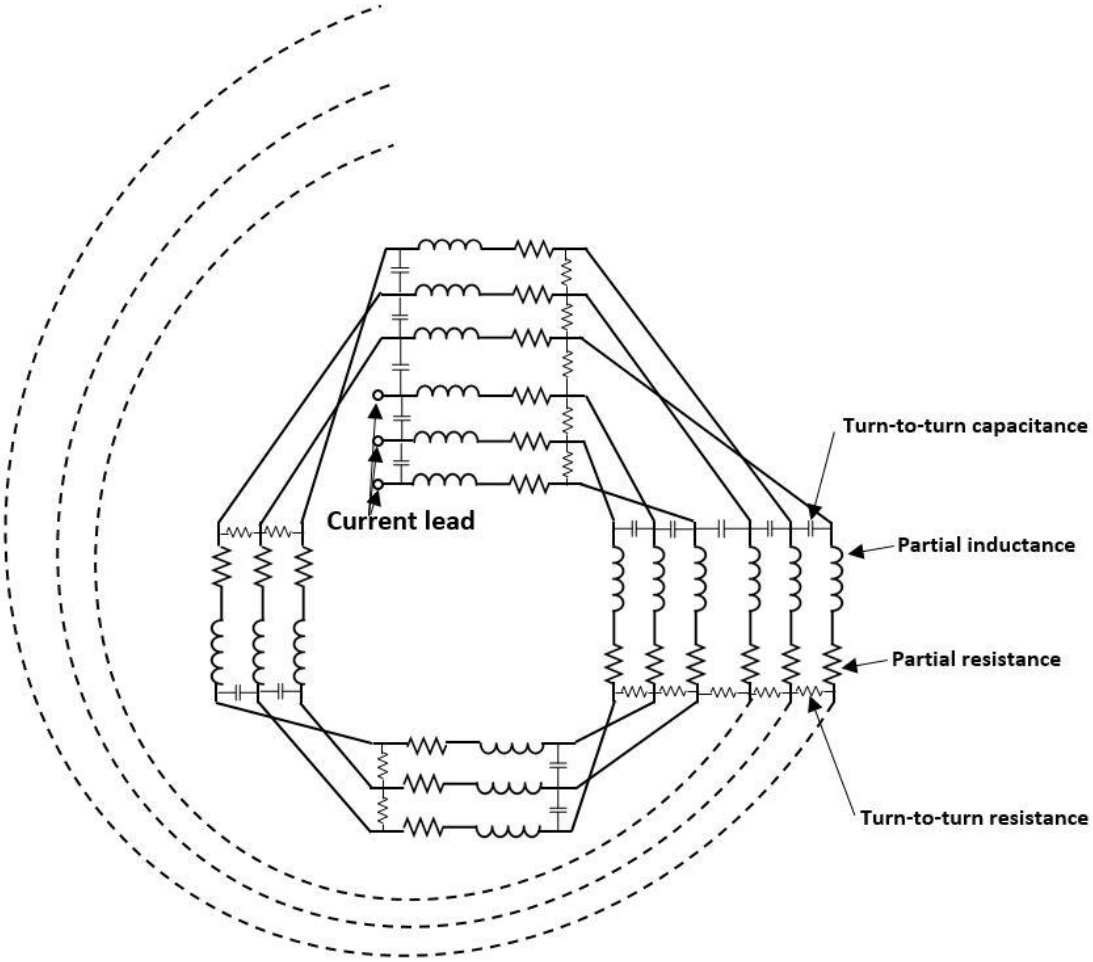

Figure 4-9 Equivalent circuit for Roebel cable pancake

Due to each strand in the Roebel cable not being insulated, there will be a small parallel connected equivalent resistance and equivalent capacitance in the Roebel cable pancake coil, which is caused by the superconductor substrate being next to the other substrate. This makes the electrical circuit in the Roebel cable SMES more complex. For the charge/discharge process, the current will flow to the parallel resistance, which can cause a SMES charge/discharge delay [198]. Moreover, the current flowing in the turn-to-turn resistance can generate joule heating. Previous research has used the Roebel cable to build high field magnets and accelerator magnets [186, 187]. For those two high field magnet applications, the current in the Roebel cable magnet was constant during the operation time. However, for SMES applications, the SMES magnet will be frequently charged and discharged to meet the power demand from the power system. The frequent charge/discharge cycling will cause the HTS equivalent self-inductance to have a high impedance, which results in more current flowing through the turn-to-turn resistances. The current sharing in the HTS substrate will

generate more joule heating in the SMES magnet. The generated joule heat will increase the HTS temperature, which can cause the HTS to quench.

Therefore, for the Roebel cable SMES design, the non-insulated strands in the Roebel cable can cause current sharing, which makes the Roebel cable generate more joule heat. The high joule heat results in a heavy load for the cooling system and it may damage the HTS material when the cooling power cannot eliminate the joule heat generated.

4.4.3 Discussions of mechanical stress for Roebel cable SMES

The Roebel cable has an uneven surface, which makes the mechanical forces unevenly distributed in each strand. Single strand YBCO tape can withstand a compressive stress of approximately 700 MPa [199]. The Roebel cable can only withstand compressive stress of approximately 45 MPa without any significant degradation of the critical current (less than 2%). Roebel cable will be permanently damaged after high transverse stress. M. Park's research [200] shows that the 629 kJ solenoid SMES magnet inner pressure can reach 53.3 MPa, which is higher than the 45 MPa limit of the Roebel cable. Accordingly, the Roebel cable SMES critical current will degrade in this 629 kJ SMES design. The weak mechanical stability of the Roebel cable limits the design and application of large size Roebel cable SMESs due to the large size SMES magnet that has a high background magnetic field and high current capacity, which causes high Lorentz force to be applied on the superconductor surface.

On the other hand, due to Lorentz force, an alternating background magnetic field caused by the SMES charge/discharge cycles will repeatedly exert pressure on the Roebel cable. The Lorentz force will loosen the Roebel cable pancake coils winding in the SMES after a number of charge and discharge cycles.

For now, one solution to enhance the Roebel cable's mechanical stability is to apply an impregnation method to support each strand in the cable to ensure its mechanical integrity. Using Epoxy with fused silica, impregnated Roebel cable can improve the mechanical integrity [201]. For a Roebel cable without impregnation, the critical current will reduce when the pressure is over 45 MPa. The critical current will reduce when the pressure is over 170 MPa

when the Roebel cable is with impregnation. However, the critical current will decrease 20%-25% when adding epoxy to the Roebel cable.

4.4.4 Discussions of manufacturing difficulty for Roebel cable SMES

Regardless of the difficulty of impregnating epoxy into the Roebel cable, another manufacturing difficulty is to build the power junction between the current lead and the Roebel cable in the SMES magnet according to the Roebel cable critical measurement results. There are two commonly used power joint connection methods used by Roebel cable researchers. One method is to use one transposition length of Roebel cable tinned with solder and subsequently soldered to a copper block. This method has a large contact area, which will have a lower contact resistance [181]. Another current lead soldering method is the "Top-only" method. This method uses silver foil at both ends of the Roebel cable, which are then laminated together with solder. Solder joints on the Roebel cable are shown in Figure 4-10, which is because the area is relatively flat [202, 203].

Figure 4-10 Soldering points for the top-only method [50]

The advantages of the top-only method are the current can evenly distribute on each insulated strand and the current on each strand can be measured. However, both of these methods needs at least half the transport length of the Roebel cable to make the power joint. That means the power joint in the Roebel cable SMES magnet will be large, which needs more space in the SMES magnet.

Moreover, due to the multi-strand structure of the Roebel cable, the Roebel cable power joint can be considered as several single HTS tape parallel connections to the current lead. That makes the resistivity of the Roebel cable power joint several times higher than normal HTS tape.

Therefore, for Roebel cable SMES applications, a new Roebel cable connection must be made, which has a shorter length and equivalent current distribution on the Roebel cable.

4.5 Conclusions

The Roebel cable SMES has the advantages on low AC losses and high power density. The high power density makes the Roebel cable SMES have more potential applications in power systems and the low AC losses of the Roebel cable SMES can increase the SMES system's efficiency. However, the Roebel cable withstand stress and strand-to-strand current sharing are two problems that need to be solved. Impregnating epoxy is one solution to increase the maximum withstand stress. Moreover, the epoxy can also increase the strand-to-strand impedance, which is adequate for decreasing the stand-to-strand current sharing. Furthermore, a new power joint connection method needs to be developed for the SMES magnet application, since the power joint needs a shorter length of Roebel cable and lower impedance power joint.

In conclusion, the Roebel cable SMES has high power density and low AC losses, which shows the outstanding potential for applying in power systems that need high power density and fast response speed. But there are still some manufacturing problems that need to be solved such as epoxy impregnation and power joint manufacturing.

Therefore, for the SMES-battery HESS application for microgrids, a conventional YBCO tape SMES magnet is chosen to be applied in the HESS. After the SMES magnet structure is designed, the HESS control method need to be developed. Without a proper control method for the SMES, the SMES magnet has no use in the HESS for microgrid applications.

Chapter 5 Fuzzy logic energy management method for HESS deal with the fluctuation power demand in microgrid

The SMES integrates with batteries to build the SMES-battery HESS for power system applications, which is the primary purpose for the SMES magnet design. The performance of the HESS can be guaranteed by applying a well-designed SMES magnet and appropriate control method. Therefore, after the SMES magnet design has been studied, the energy management control method for the HESS needs to be researched to establish a robust HESS for the microgrid applications.

Power unbalancing is one critical problem during the operation of a microgrid. When a microgrid is disconnected from the main grid, the energy storage system is responsible for compensating for the power differences between the load demand and the distributed generators power output in a microgrid. Both the load demand and the distributed generations' power output have high uncertainty and are highly fluctuating, which makes the power demand from the energy storage system highly fluctuating. One critical problem is to allocate the power demand for different energy storage systems in the HESS.

In this chapter, the fuzzy logic control method is proposed to control the SMES-battery HESS to compensate for the power unbalancing in microgrids, which has the advantages of SMES-battery HESS high power density and fast response speed. The energy management methodology must be designed to take advantage of the characteristics of different energy storage systems, to achieve the effective combination of applying the SMES-battery HESS in microgrid systems. The SMES-battery HESS has the advantages of the SMES high power capacity and fast response speed. Moreover, the battery compensates for the disadvantage of the SMES low energy capacity. The proposed energy management method should be able to prevent the battery suffering from a high fluctuating power demand to extend the battery's lifetime. In this chapter, the fuzzy logic energy management method is proposed to deal with long-term high fluctuating power demands for the SMES-battery HESS.

5.1 Introduction

The microgrid has been proposed in recent years. A microgrid usually consists of a group of distributed renewable generation sources such as PV panels or wind turbines, located in the same area, which are subsequently connected into the utility grid. Moreover, a microgrid is also able to operate independently. Microgrid electric power security becomes more and more important in microgrid applications. For example, renewable generation has fluctuating power output caused by weather changes (wind speed, sun irradiance, etc.), which is uncontrollable. Moreover, the renewable generation highly penetrated power system has low inertia, which increases the risk of power system collapse. The power demand in a microgrid has high uncertainty. Therefore, power unbalancing in a microgrid is one important problem that needs to be solved to guarantee electric power security. Power unbalancing results in a high fluctuating power demand for the energy storage system in a microgrid.

The energy storage system has been proposed to deal with fluctuating power demands in the power system. B. Dunn et al. [104] have proposed to use a battery only system to deal with highly fluctuating power unbalancing in microgrids. However, the highly fluctuating power demand for the battery energy storage system will accelerate the batteries' attenuation.

Therefore, some other kinds of energy storage systems have been proposed to hybridise with batteries to constitute a HESS. The supercapacitor [204, 205] and SMES [7, 206] are two fast response energy storage devices that can be used to hybridise with a battery. Compared with the supercapacitor, the SMES has a longer service lifetime and less environmental pollution [207, 208]. In this study, the SMES and battery HESS will be discussed for microgrid applications.

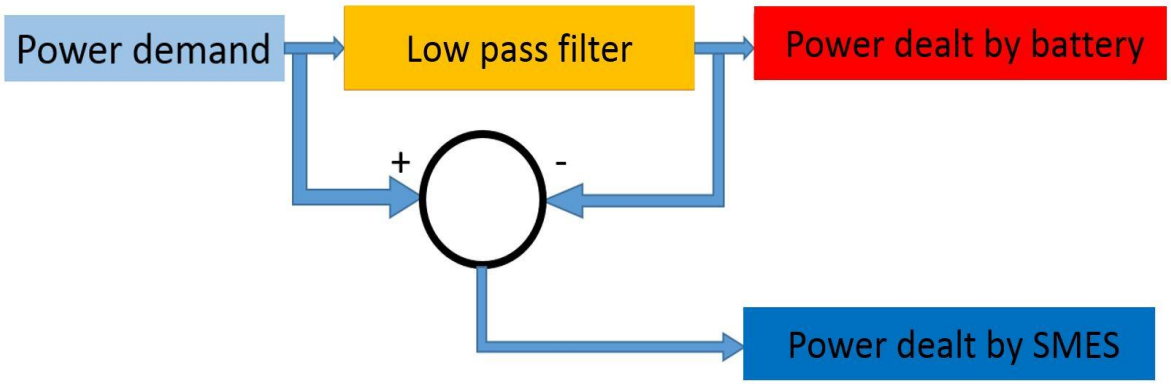

Figure 5-1 Filtration energy management method

The fast response energy storage device deals with the high-frequency power demands and the battery deals with the low-frequency power demands. The filtration method has the advantage of extending battery service lifetime [20, 125, 209]. However, the sizing design and the cut-off frequency design for the filtration method is difficult because it highly depends upon system power demand. If the cut-off frequency is too low or the SMES size is too small, the SMES can be easily fully charged/discharged. If the cut-off frequency is too high or the SMES size is too large, SMES-utilization becomes inefficient.

In this study, the fuzzy logic control method is proposed to apply for the SMES-battery HESS, to deal with fluctuating power demands for the energy storage system. The fuzzy logic control methodology is based on human knowledge and the main purpose of the proposed method is to extend the battery service lifetime. Moreover, the proposed control algorithm considers the state-of-charge (SOC) of the fast response energy storage device. When the SMES is about to be fully charged/discharged, the battery will contribute more towards the power demand. That results in the SMES having less chance of being fully charged/discharged, which prevents

the battery dealing with the fluctuating power demand directly. Battery sizing design is not considered in this research. Previous research shows that reducing the number of battery charge/discharge cycles extends battery service lifetime [145, 146]. Therefore, by reducing the number of battery charge/discharge cycles, the battery service lifetime will be extended.

5.2 Introduction of fuzzy logic controller

The fuzzy logic controller is composed of a fuzzification part, decision making part and a defuzzification part [210]. The input data is processed by the fuzzification part into a suitable linguistic value. The fuzzification part has a different number of fuzzy levels. The large number of fuzzy levels can increase the input resolution, which improves the accuracy of the controller. The decision making part includes the designed rules and database, which is used to generate the fuzzy values. The designed rules and database are based on the designer's knowledge and experience, which makes the fuzzy logic controller more intelligent and easier to achieve a specific design target. The defuzzification part is used to convert the fuzzy value from the decision making part to a real value, which the energy storage system can subsequently use to stabilise the power system. A schematic diagram of the fuzzy logic controller is shown in Figure 5-2.

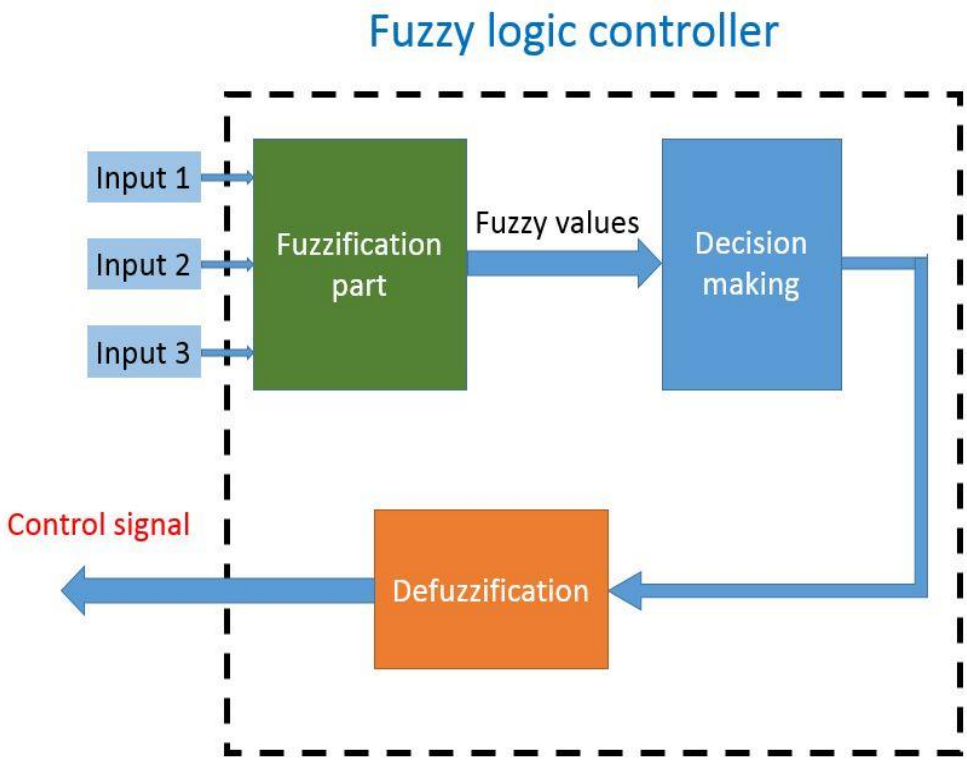

Figure 5-2 Scheme diagram of the fuzzy logic controller.

5.2.1 Fuzzification part in fuzzy logic controller

The fuzzification part uses the collected data from the system to convert the values so that the decision making part can recognize them. The triangular shape fuzzification module is selected in this study. The fuzzification part classifies the input values to some linguistic value such as BIG, SMALL, ZERO, VERY BIG, VERY SMALL. The fuzzy values are generated by the fuzzification part, which is based on the input and fuzzy levels. The example fuzzy levels, shown in Figure 5-3, are five different fuzzy levels: negative big (NB), negative small (NS), zero (ZE), positive small (PS), and positive big (PB). Take input value three for example, the output fuzzy values are $\mu_{1,\mathrm{PS}}$ and $\mu_{1,\mathrm{PB}}$ after the fuzzification part. All the input data need to go through the fuzzification part to convert to fuzzy values for the fuzzy logic decision part.

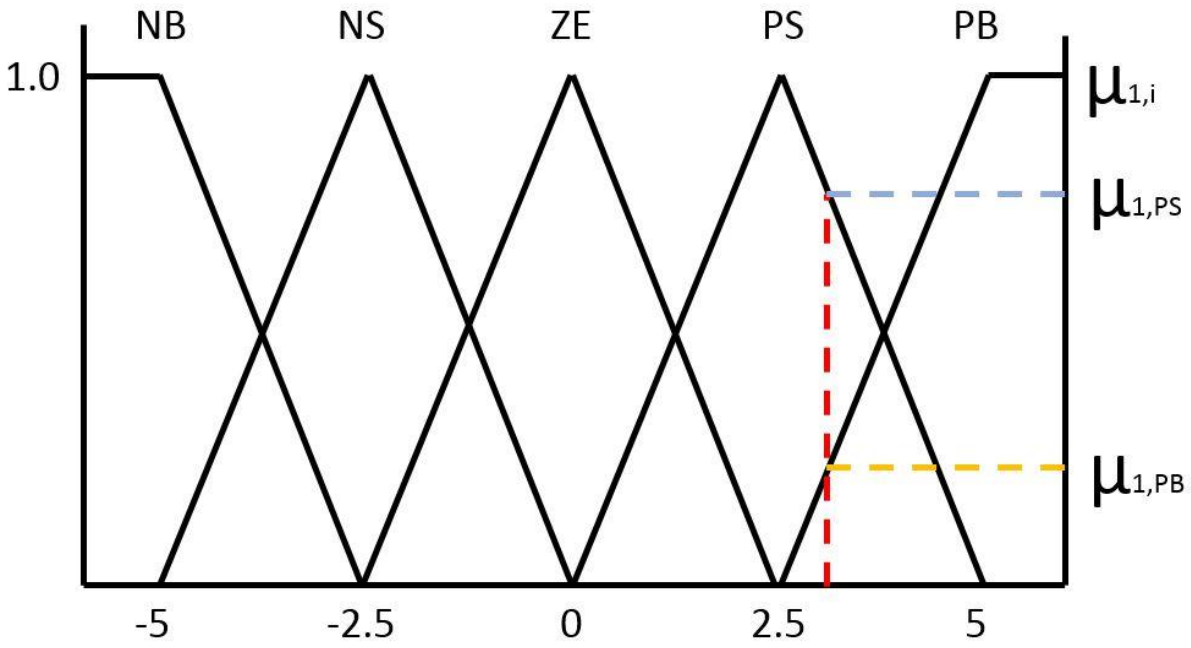

Figure 5-3 Fuzzification part in the fuzzy logic controller

5.2.2 Decision making part in fuzzy logic controller

The decision making part is based on a logic table. The table is built by the designer. The rules are based on the designer's knowledge and experience. The logic table describes the relationship between the logic outputs and fuzzy inputs. The fuzzy logic table is described by linguistic terms.

5.2.3 Defuzzification part in fuzzy logic controller

The defuzzification part is to combine the fuzzy value from the fuzzification part and the design rules. One example defuzzification scheme is shown in Figure 5-4.

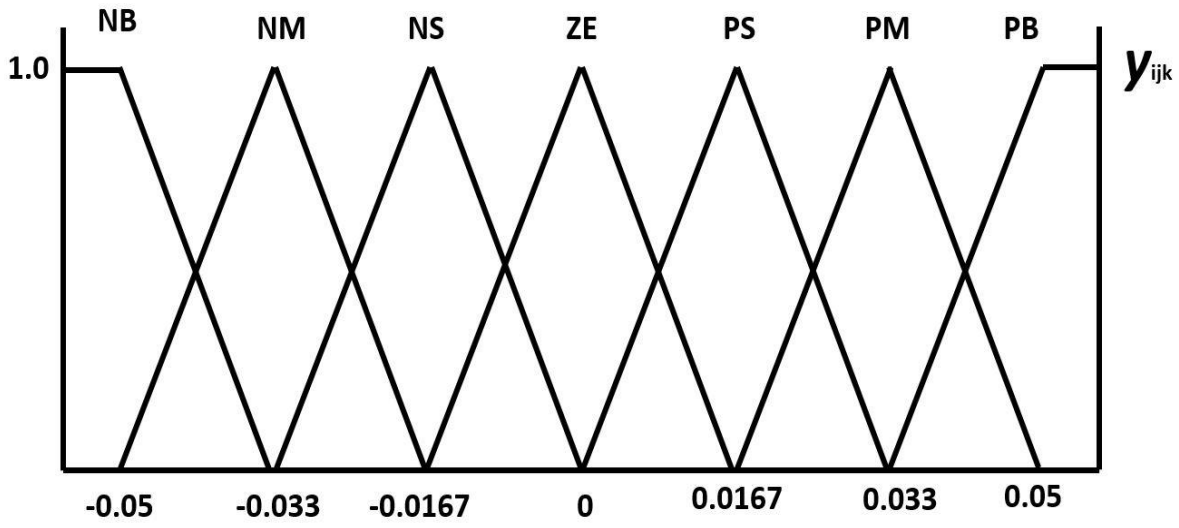

Figure 5-4 Defuzzification part in the fuzzy logic controller

y_{ijk} is the fuzzy output value, which will be used to generate the output values. The output value y_o for three input parameters can be calculated by:

$$y_o = \frac{\sum i \sum j \sum k \min\{\mu_{1i}(x_1) \cdot \mu_{2j}(x_2) \cdot \mu_{3k}(x_3)\} \cdot y_{ijk}}{\sum i \sum j \sum k \min\{\mu_{1i}(x_1) \cdot \mu_{2j}(x_2) \cdot \mu_{3k}(x_3)\}} \quad 5\text{-}1$$

Where $i, j, \text{and } k$ are input parameters.

5.3 System description for SMES-battery HESS in microgrid

The designed system is shown in Figure 5-5. The system contains renewable power generations (PV panels, wind power electric generators), the power grid, residential loads and a SMES-battery HESS. The power demand for the HESS is given by the power difference between the loads and the power generations. For the HESS power system, a three-phase transformer is used to decrease the voltage level of the HESS. The SMES and batteries are connected to a common DC link. A voltage source converter (VSC) is applied between the DC

link and the transformer to achieve the power exchanges between the HESS and the grid. In this study, the distribution network voltage level is 380 V.

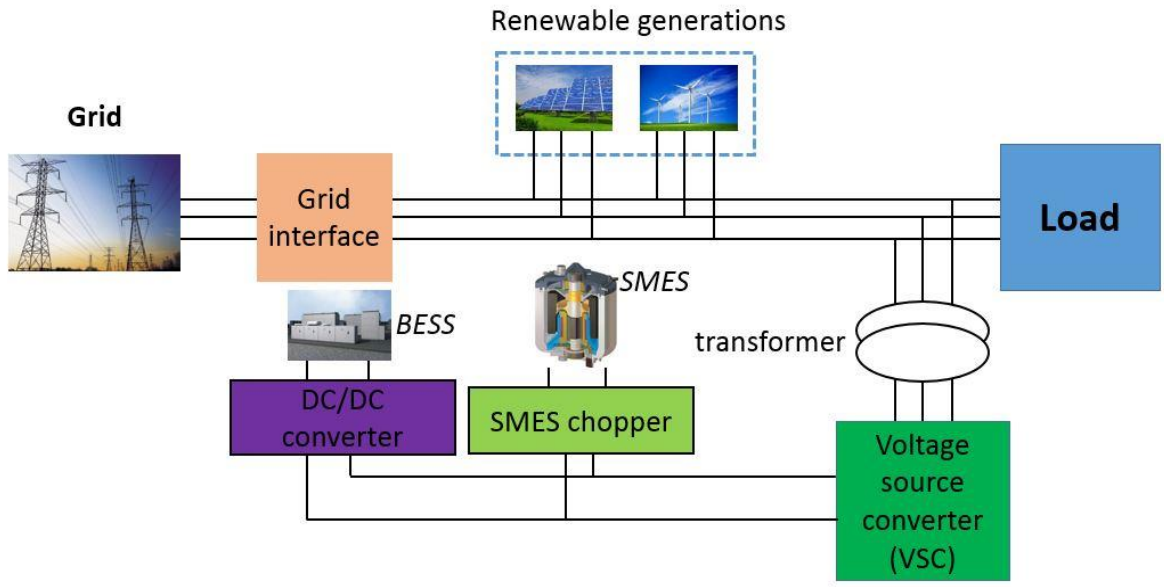

Figure 5-5 System scheme of the SMES-battery HESS in microgrid

5.4 Fuzzy logic controller design for HESS energy management

In this design, the fuzzy logic controller is used to coordinate the SMES and battery power output to compensate for the power demand in the microgrid. Moreover, the new control method needs to extend the battery service lifetime. According to previous battery lifetime research, frequent charge/discharge cycles will accelerate a battery's attenuation [211, 212]. The controller needs to prevent the SMES from being fully charged/discharged. When the SMES is fully discharged, if the system needs power from the HESS, the battery needs to compensate for the high fluctuating output power demand. The same as when the SMES is fully charged, the battery may suffer high fluctuating power demands, which is not good for extending the battery service lifetime. In this research, a new proposed fuzzy logic controller

can shift the power demand for the battery and SMES, to prevent a situation where only the battery energy storage system can deal with fluctuating power demands.

The control rule is based on a 'trial and error' method to control the battery power output [213, 214]. The rest of the power demand is supported by the SMES. Therefore:

$$P_{SMES} = P_{demand} - P_{battery} \quad 5\text{-}2$$

In this control method, the controller is used to control the battery charge/discharge gradient, which can reduce the battery power output fluctuation. The battery power output can be calculated by:

$$P_{b\_change(k)} = P_{b\_change(k-1)} + P_{fuzzy\_out(k)} \quad 5\text{-}3$$

$$P_{b(k)} = P_{b(k-1)} + P_{b\_change(k)} \quad 5\text{-}4$$

Where the battery power output changes at time k is $P_{b\_change(k)}$ and the fuzzy logic controller output is $P_{fuzzy\_out(k)}$ at time k.

The SMES SOC is also considered in the fuzzy logic energy management method as input 2. The third input provides information concerning the previous output power changes of the battery. Input 3 is given as:

$$\text{Input } 3 = (P_{demand(k)} - P_{b(k-1)}) - (P_{demand(k-1)} - P_{b(k-2)}) \quad 5\text{-}5$$

The control configuration of the fuzzy logic controller is shown in Figure 5-6.

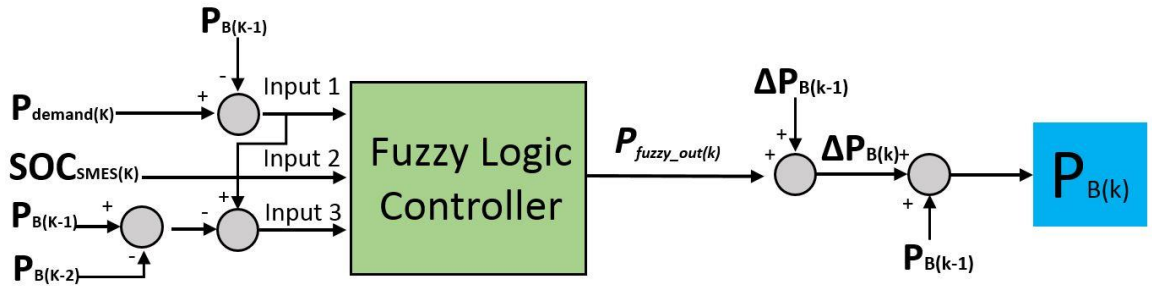

Figure 5-6 Control scheme of the fuzzy logic controller

The three inputs are the power demand from the power system. *ΔP* means the change of battery output power.

The fuzzy logic controller is based on the following logic:

- The sum of SMES and battery power output should meet the power demand of the HESS.
- A situation where only the battery deals with the high fluctuating power demand needs to be prevented. This is because the fluctuating power demand can decrease the battery service lifetime. To prevent this from happening, the energy management method should avoid the SMES from being fully charged or discharged.
- The battery power output relates to the SMES SOC percentage and the power demand from the power system. That is because the rate of the SMES SOC has the advantage on representing the ability of the SMES to deal with the power demand rather than using the amount of energy that remains in the SMES. Moreover, the percentage of SMES can be applied to different sizes of SMES systems.
- To prevent the battery from having a high fluctuating power output/input, the energy management method is to control the battery power output changes rather than directly control the battery power output.
- When the power system requests power from the energy storage system:

1. If the SMES has a low SOC, the batteries need to make more contribution to the power output, to prevent the SMES from being fully discharged.
2. If the SMES has a high SOC, the SMES is requesting to provide a high power output to decrease battery power output, which is to extend battery service lifetime.

- When the power system needs to inject the power to the HESS:
    1. If the SMES has low SOC, the SMES deals with the high amount of power and the battery slowly gets charged. The low power charging helps extend battery service lifetime.
    2. If the SMES has high SOC, the SMES is allocated low charging power, to prevent the SMES from being fully charged, which means the SMES cannot deal with the fluctuating power demand. The battery absorbs the rest of the power from the power system.

Three inputs of the fuzzy logic controller have five fuzzification levels, which are: negative big (NB), negative small (NS), zero (ZE), positive small (PS) and positive big (PB).

When three inputs are NB (as shown in red in Table 5-1), that means the system power demand is less than the battery power output in the last second (input 1: NB); the SMES SOC is at a relatively low level (input 2: NB); if the battery power output changing rate is same as the last second, the battery power output will be higher than the power demand (input 3:NB). Therefore, according to the control logic, the battery discharging rate change should decrease dramatically to let the battery power output meet the power system demand. The SMES is used to deal with the power differences between the power demand and battery power output.

When three inputs are NB,NB,NS (as shown in blue in Table 5-1), that means if the battery power output changing rate is same as last time, the battery output power will be slightly higher than the power demand (input 3: NS). Therefore, the battery will slightly decrease its discharging changing rate and allow the SMES to absorb more energy due to the SMES's low SOC. Therefore, the power shifting can be achieved by using more of the energy in the SMES.

Based on the statements described above, the fuzzy rules are shown in Table 5-1.

Table 5-1 Fuzzy rules in fuzzy logic controller

Input 1	**NB**	**NB**	NB	NB	NB	NB	NB	NB	NB	NB	NB	NB	NB	NB	NB
Input 2	**NB**	**NB**	NB	NB	NB	ZE	ZE	ZE	ZE	ZE	PB	PB	PB	PB	PB
Input 3	**NB**	**NS**	ZE	PS	PB	NB	NS	ZE	PS	PB	NB	NS	ZE	PS	PB
Output	**NB**	**NM**	NS	ZE	PS	NM	NS	ZE	PS	PM	NB	NM	NS	ZE	PS
Input 1	NS	NS	NS	NS	NS	NS	NS	NS	NS	NS	NS	NS	NS	NS	NS
Input 2	NB	NB	NB	NB	NB	ZE	ZE	ZE	ZE	ZE	PB	PB	PB	PB	PB
Input 3	NB	NS	ZE	PS	PB	NB	NS	ZE	PS	PB	NB	NS	ZE	PS	PB
Output	NM	NS	ZE	PS	PM	NS	ZE	ZE	ZE	PS	NM	NS	ZE	ZE	PS
Input 1	ZE	ZE	ZE	ZE	ZE	ZE	ZE	ZE	ZE	ZE	ZE	ZE	ZE	ZE	ZE
Input 2	NB	NB	NB	NB	NB	ZE	ZE	ZE	ZE	ZE	PB	PB	PB	PB	PB
Input 3	NB	NS	ZE	PS	PB	NB	NS	ZE	PS	PB	NB	NS	ZE	PS	PB
Output	NS	ZE	ZE	PS	PM	NS	ZE	ZE	ZE	PS	NM	NS	ZE	ZE	PS
Input 1	PS	PS	PS	PS	PS	PS	PS	PS	PS	PS	PS	PS	PS	PS	PS
Input 2	NB	NB	NB	NB	NB	ZE	ZE	ZE	ZE	ZE	PB	PB	PB	PB	PB
Input 3	NB	NS	ZE	PS	PB	NB	NS	ZE	PS	PB	NB	NS	ZE	PS	PB
Output	NS	ZE	ZE	PS	PM	NS	ZE	ZE	ZE	PS	NM	NS	ZE	PS	PM
Input 1	PB	PB	PB	PB	PB	PB	PB	PB	PB	PB	PB	PB	PB	PB	PB
Input 2	NB	NB	NB	NB	NB	ZE	ZE	ZE	ZE	ZE	PB	PB	PB	PB	PB
Input 3	NB	NS	ZE	PS	PB	NB	NS	ZE	PS	PB	NB	NS	ZE	PS	PB
Output	NS	ZE	PS	PM	PB	NM	NS	ZE	PS	PM	NS	ZE	PS	PM	PB

The control performance will be better if the input parameters are divided into a higher number of levels, but that also increases the energy management method complexity. The fuzzy output has seven different levels, which are: negative big (NB), negative medium (NM), negative small (NS), zero (ZE), positive small (PS), positive medium (PM) and positive big (PB). The NB and PB are the overreaction of the SMES-battery HESS to prevent the SMES from being fully charged/discharged.

The fuzzy level boundaries for the three inputs and one fuzzy output are dependent on the power system size and the HESS power demand ranges. A case study of the proposed method dealing with the fluctuating power demand is described in the following case study.

5.5 Fuzzy logic applied in power system

The novel fuzzy logic energy management method is valued for taking both the power demand and the SMES SOC into consideration to extend battery service lifetime. A case study was conducted to prove the validity of the new energy management methodology.

A numerical model has been built in Matlab/Simulink. To simplify the simulation model, only the power flows in the power system will be considered in this chapter. The simulation uses the proposed fuzzy logic energy management method to allocate the power output for the battery and SMES, to compensate for the power demand in the power system. The HESS is designed to compensate for the power difference of the loads and the power supply. The simulation model is shown in Figure 5-7. In this simulation, a 100 MJ SMES magnet is applied in the SMES-battery HESS. A 1 GJ SMES magnet is been designed by H Hayashi et. al [215]. Therefore, a 100 MJ SMES magnet is achievable. In this research, the SMES size is determined by the author's experience and previous research, and the size of the HESS is not optimized.

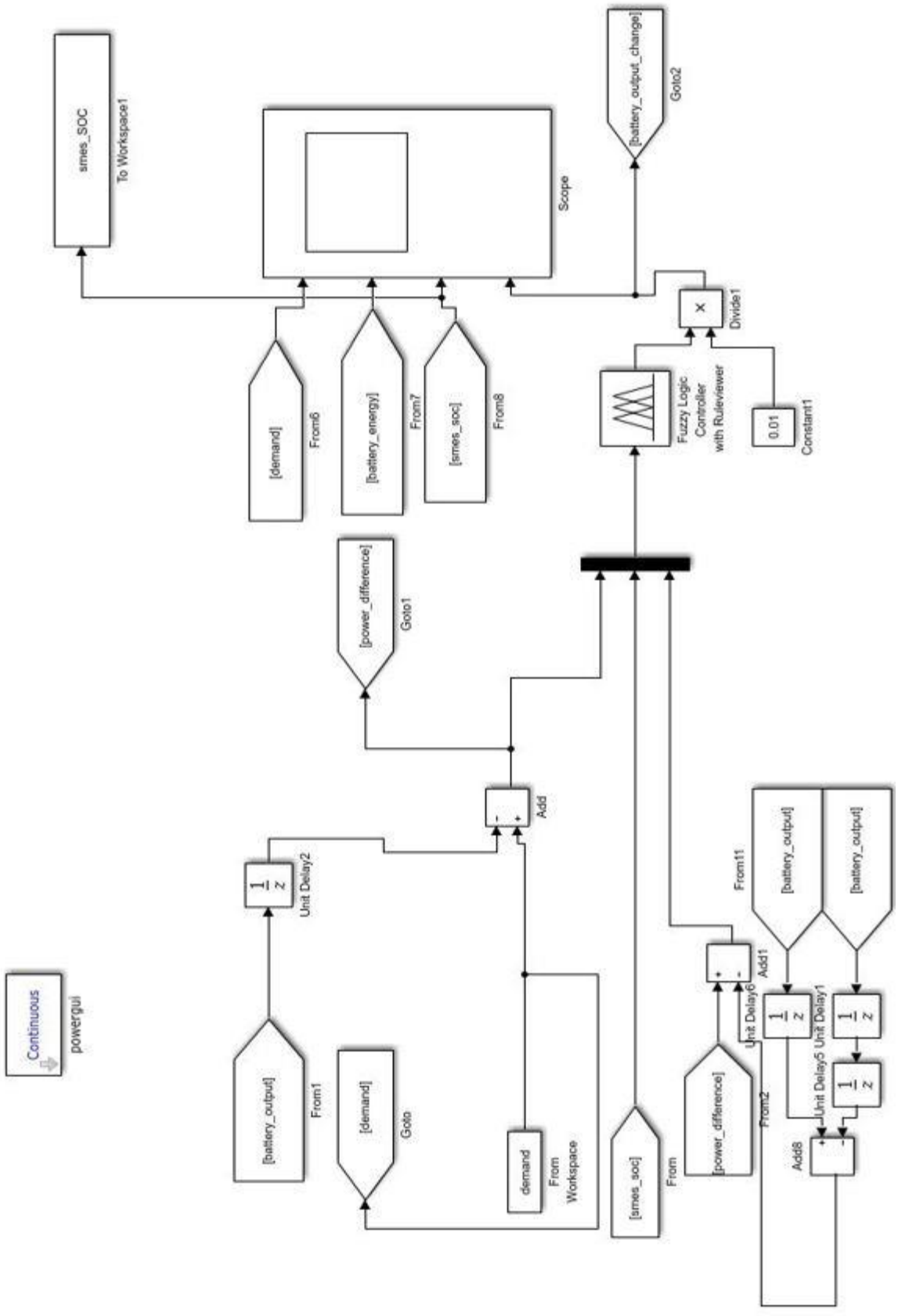

Figure 5-7 Simulation model for fuzzy logic energy management method verification (part 1)

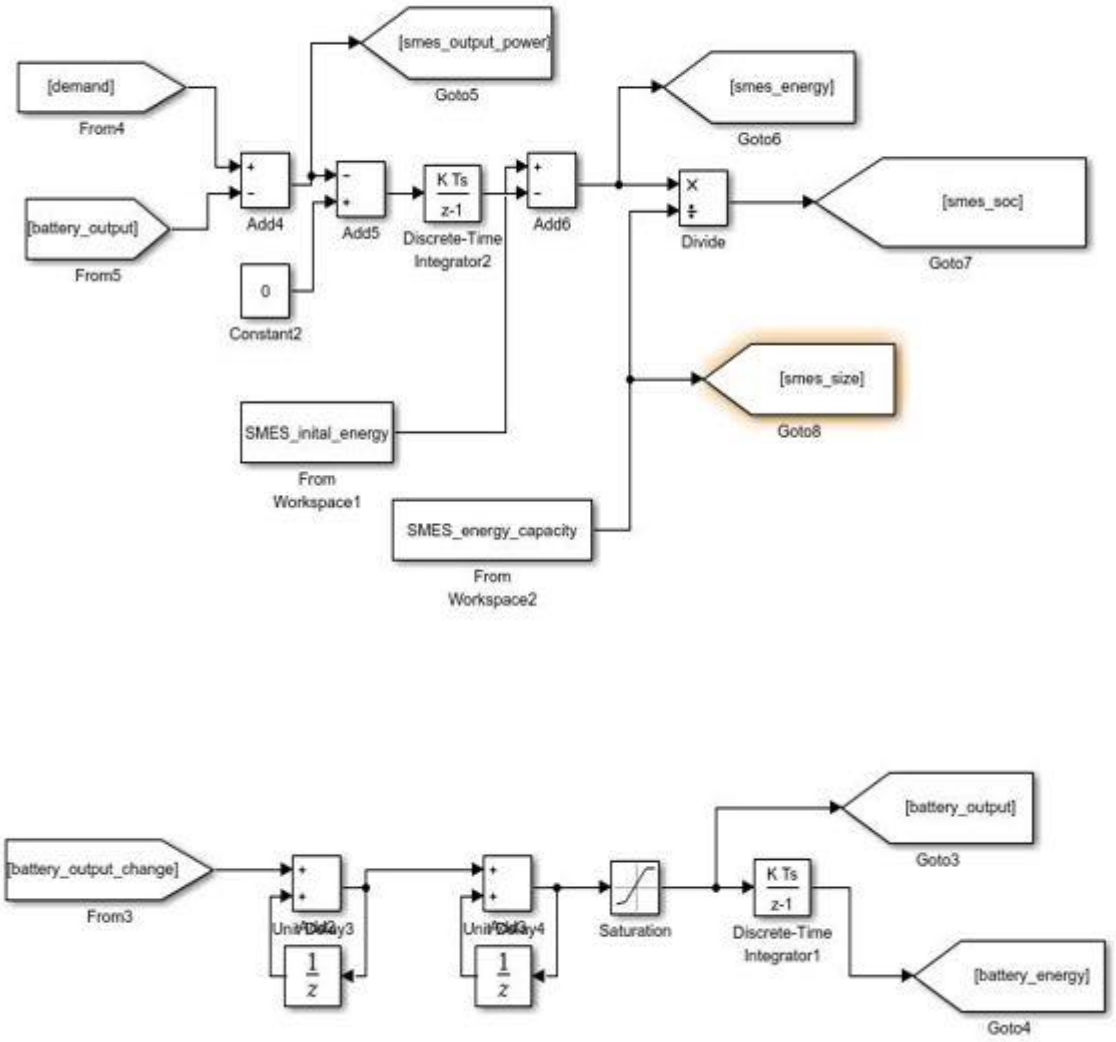

Figure 5-8 Simulation model for fuzzy logic energy management method verification (part 2)

The high fluctuating power demand for the HESS is shown in Figure 5-9 . This data is processed by the wind speed from one wind farm near London to represent the generation part of the system. The power demand in the microgrid is highly fluctuating to represent loads in the microgrid. The Figure 5-9 also means that the amount of unbalanced power in the microgrid.

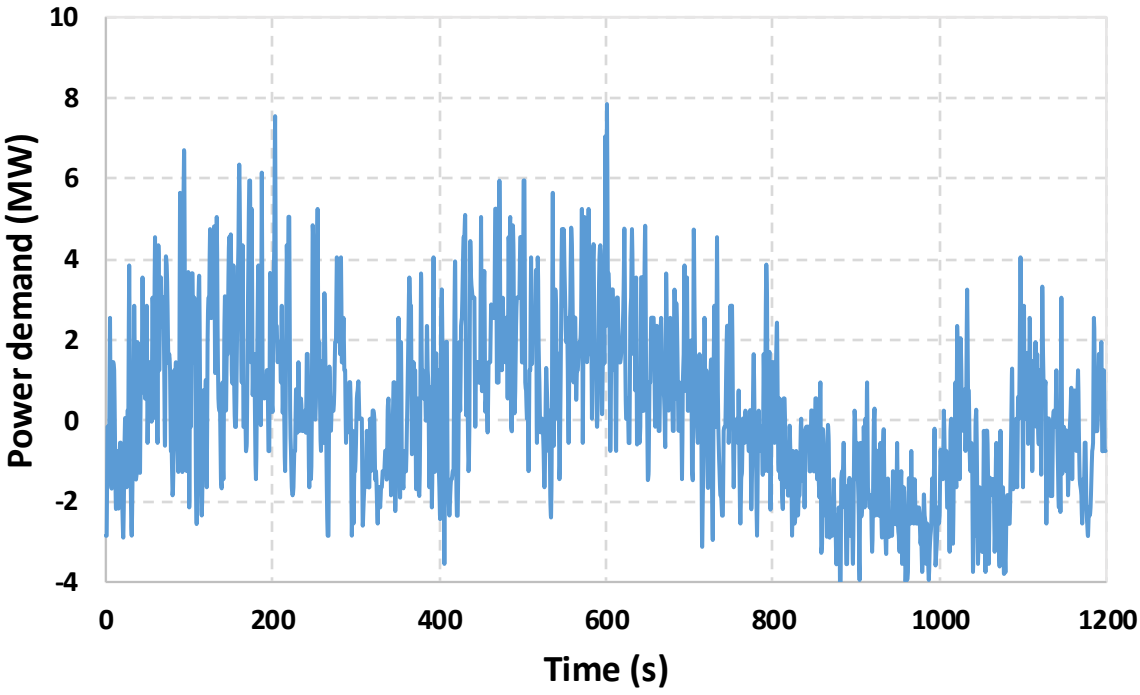

Figure 5-9 Power demand for the SMES-battery HESS

Based on the system size and the power demand ranges, the fuzzy levels for the fuzzification part are shown in Figure 5-10. The defuzzification levels are shown in Figure 5-11.

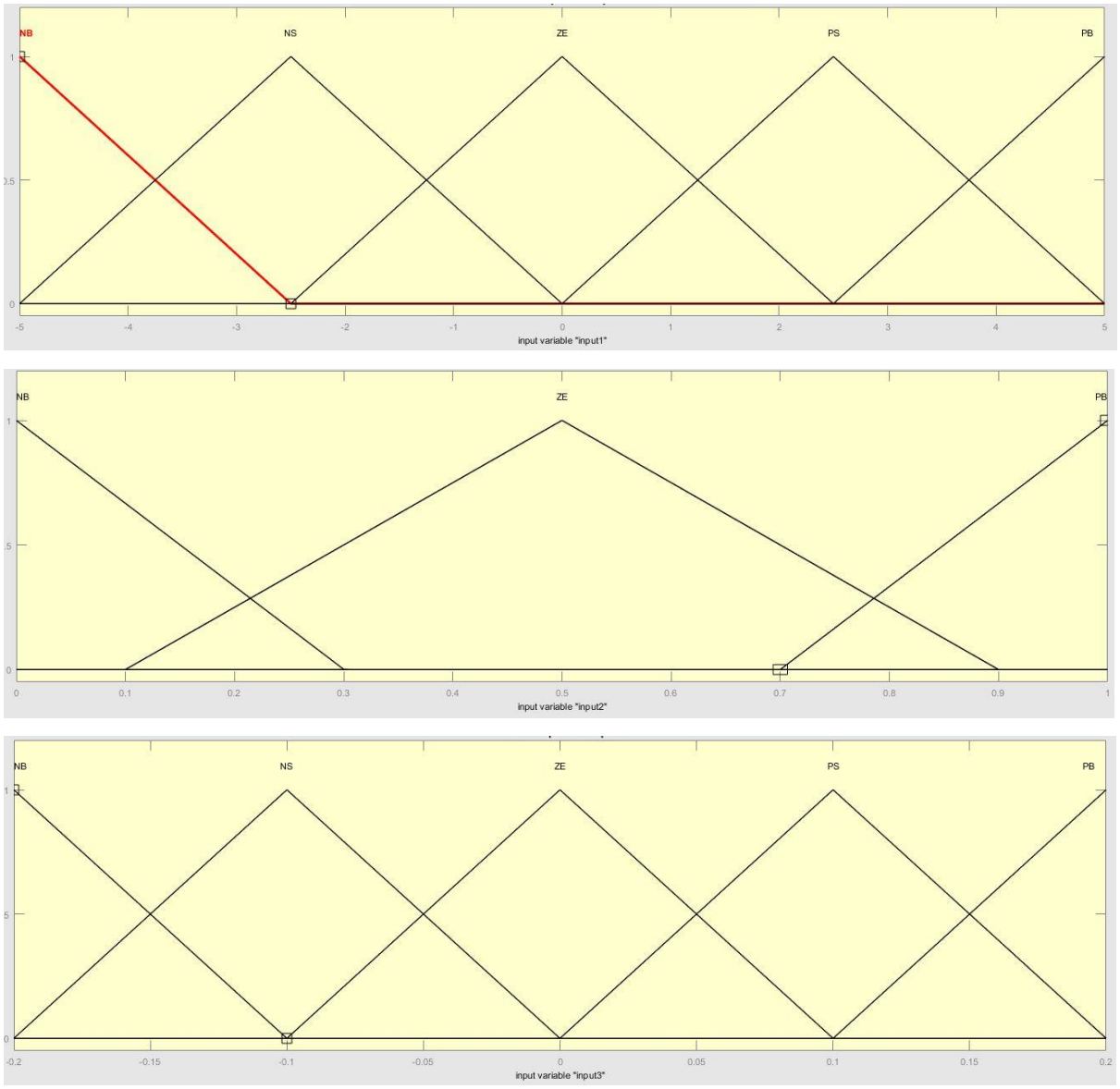

Figure 5-10 Fuzzification levels in the fuzzy logic controller

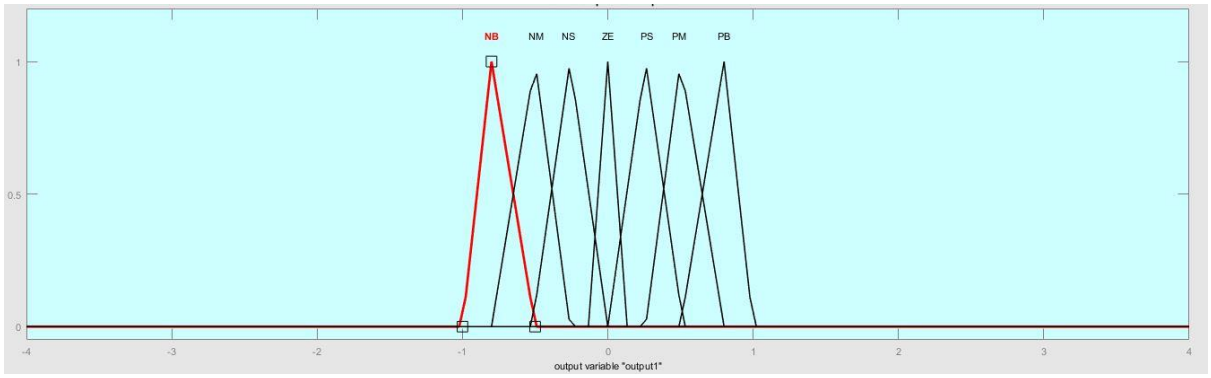

Figure 5-11 Defuzzification levels in the fuzzy logic controller

The fuzzification and defuzzification levels are designed based on the designer's knowledge and experience.

The fuzzy rules 3D output relationship surfaces for the three inputs are shown in Figure 5-12, Figure 5-13 and Figure 5-14.

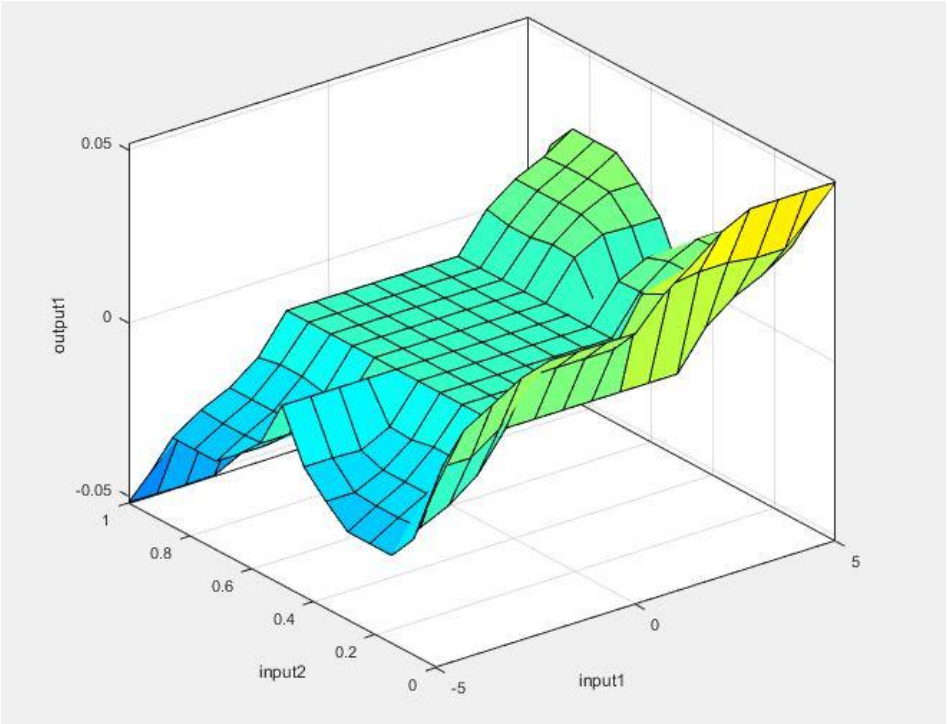

Figure 5-12 3D relationship surface of input 1 and input 2

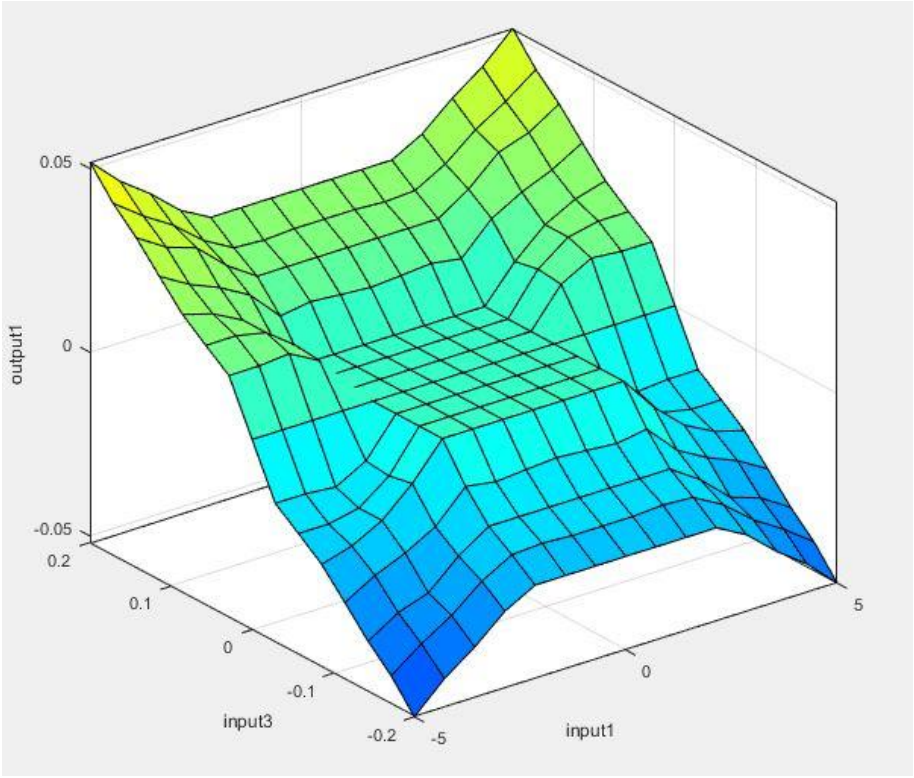

Figure 5-13 3D relationship surface of input 1 and input 3

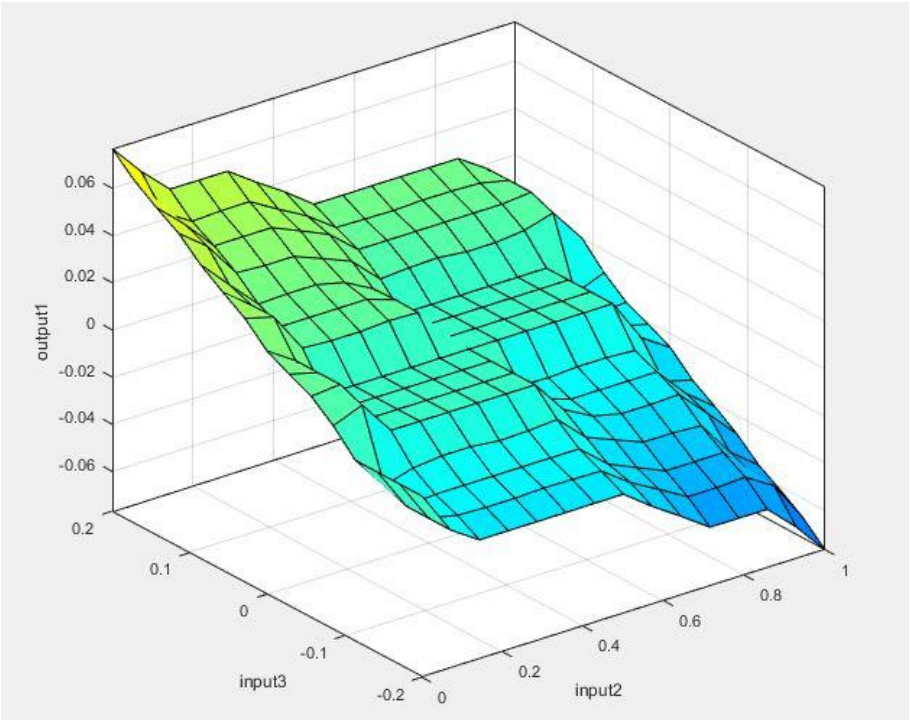

Figure 5-14 3D relationship surface of input 2 and input 3

5.5.1 Fuzzy logic HESS compared with battery only system

Compared with a battery only system in the microgrid, the battery power output is shown in Figure 5-15. Due to the battery being the only energy source to compensate for the power demand, the battery energy storage needs to compensate for all the power demand from the microgrid.

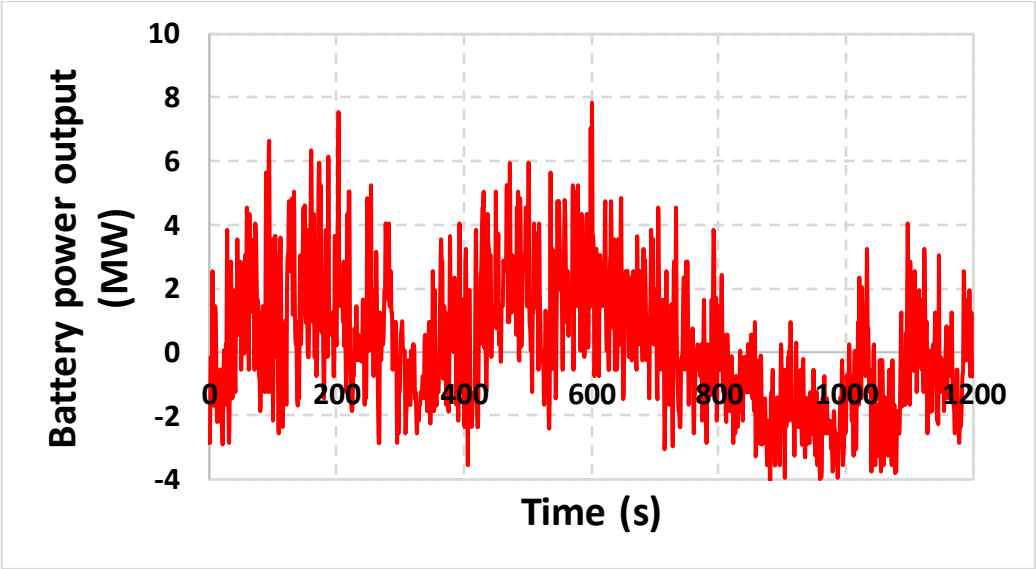

Figure 5-15 Battery power output of the battery only system in microgrid

The charge/discharge cycling is one crucial aspect to evaluate battery service lifetime. The frequent charge and discharge of a battery can accelerate battery attenuation. A battery only system needs 146 charge and discharge cycles to compensate for the highly fluctuating power demand from the microgrid.

5.5.2 Fuzzy logic HESS compared with filtration method HESS

The filtration method is one conventional control method for the hybrid energy storage system. The battery and SMES power output comparison are shown in Figure 5-16 and Figure 5-17.

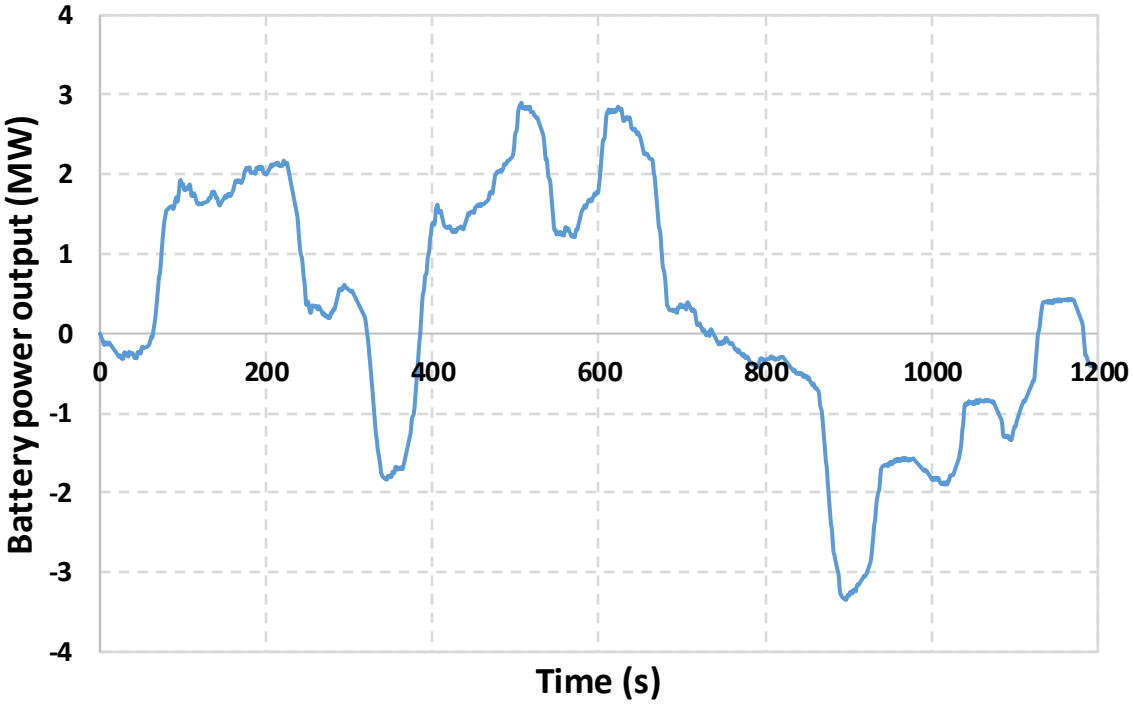

(a)

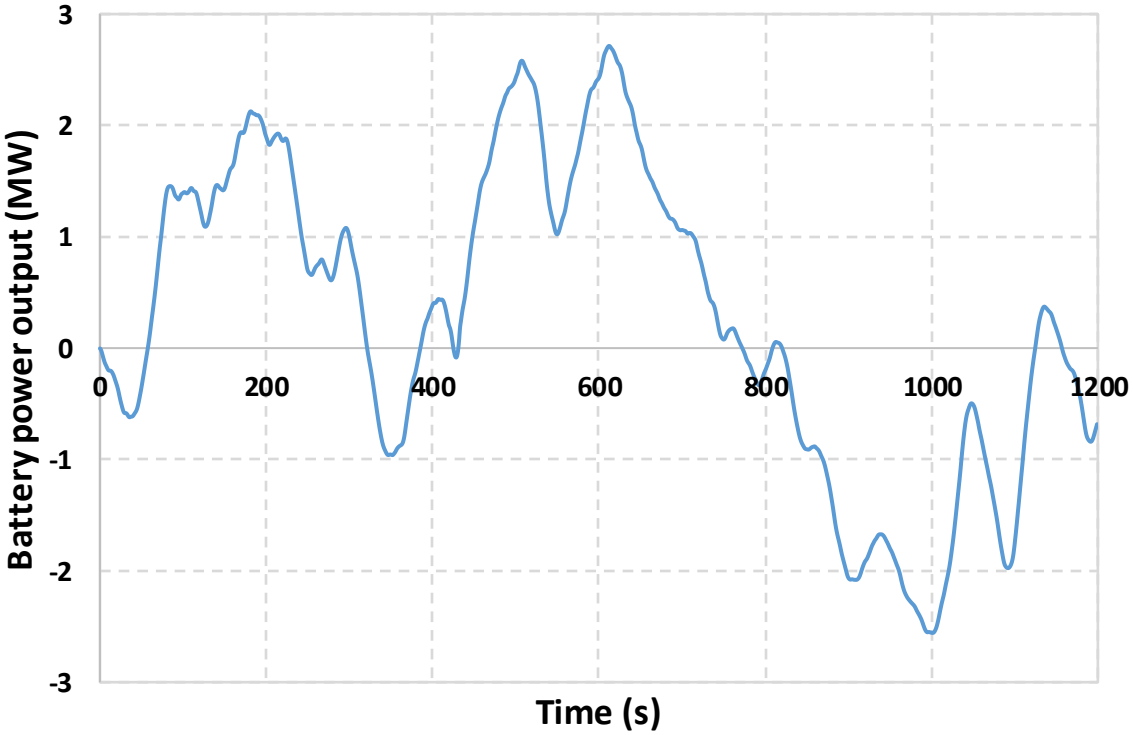

(b)

Figure 5-16 Battery power output (a) fuzzy logic control (b) filtration method

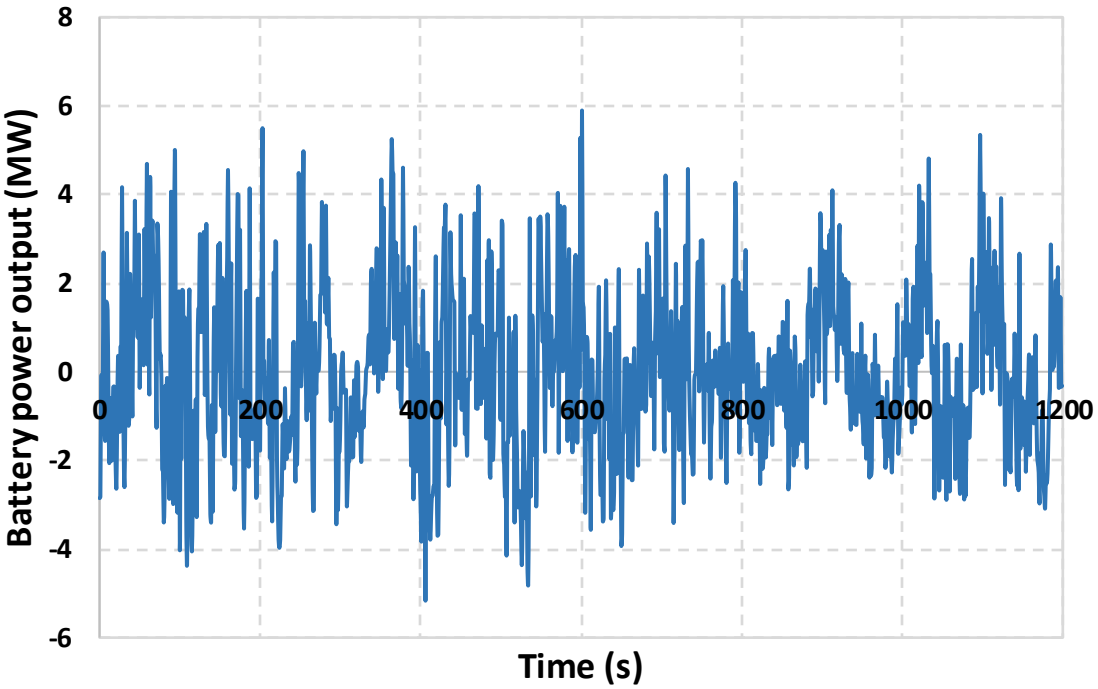

(a)

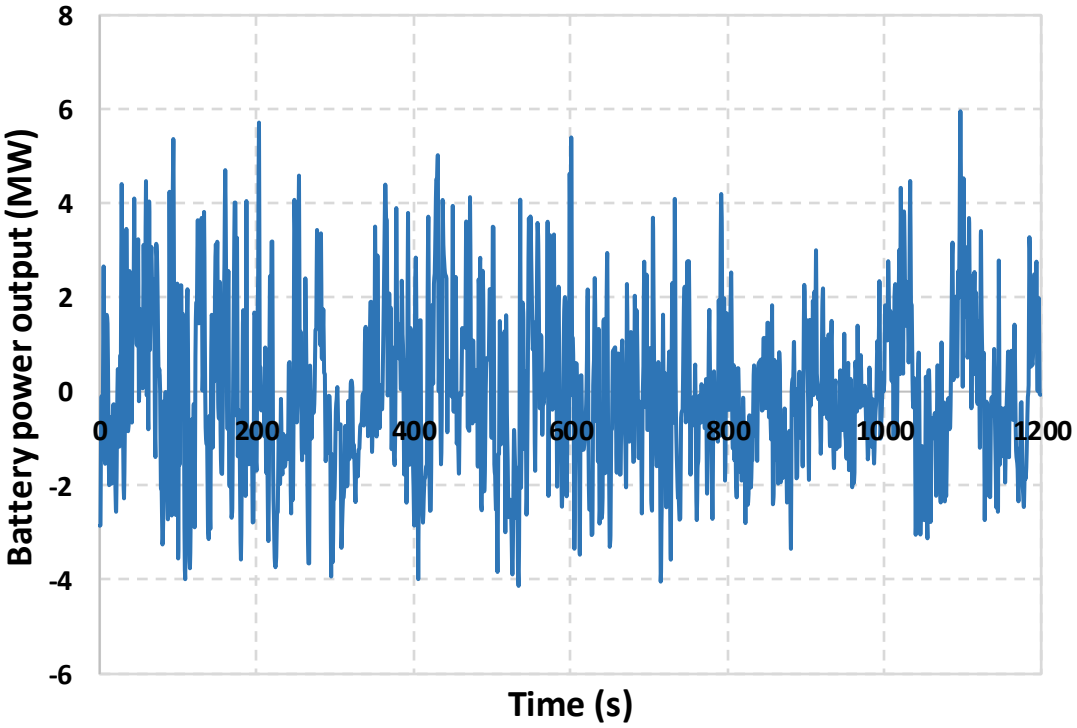

(b)

Figure 5-17 SMES power output (a) fuzzy logic control (b) filtration method

The battery power output performance by using the filtration method from time 400 s to 450 s and from time 800 s to 850 s are shown in Figure 5-18.

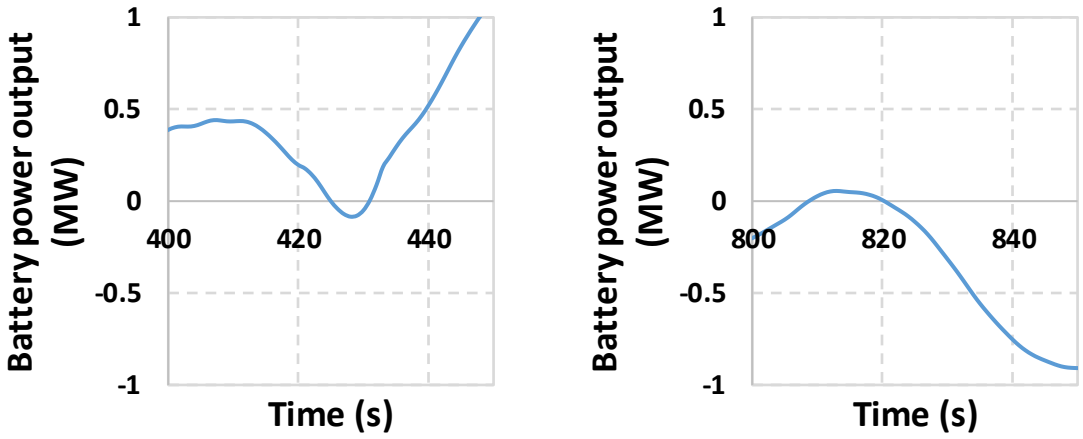

(a) (b)

Figure 5-18 Battery performance by using the filtration method: (a) 400 s to 450 s; (b) 800 s to 850 s

The filtration method has difficulty shifting the power demand. Therefore, at time 420 s to 440 s and time 810 s to 830 s, the battery is required two charge/discharge conversions, which are caused by the variation trend of the microgrid power demand. On the contrary, the fuzzy logic method aims to take more usage of the energy in the SMES. When the SMES has sufficient energy, the power demand is mainly dealt with by the SMES, which results in the battery having less charge/discharge conversions.

A comparison of the charge and discharge cycles for the newly proposed fuzzy logic method, conventional filtration method and battery only system are shown in Figure 5-19:

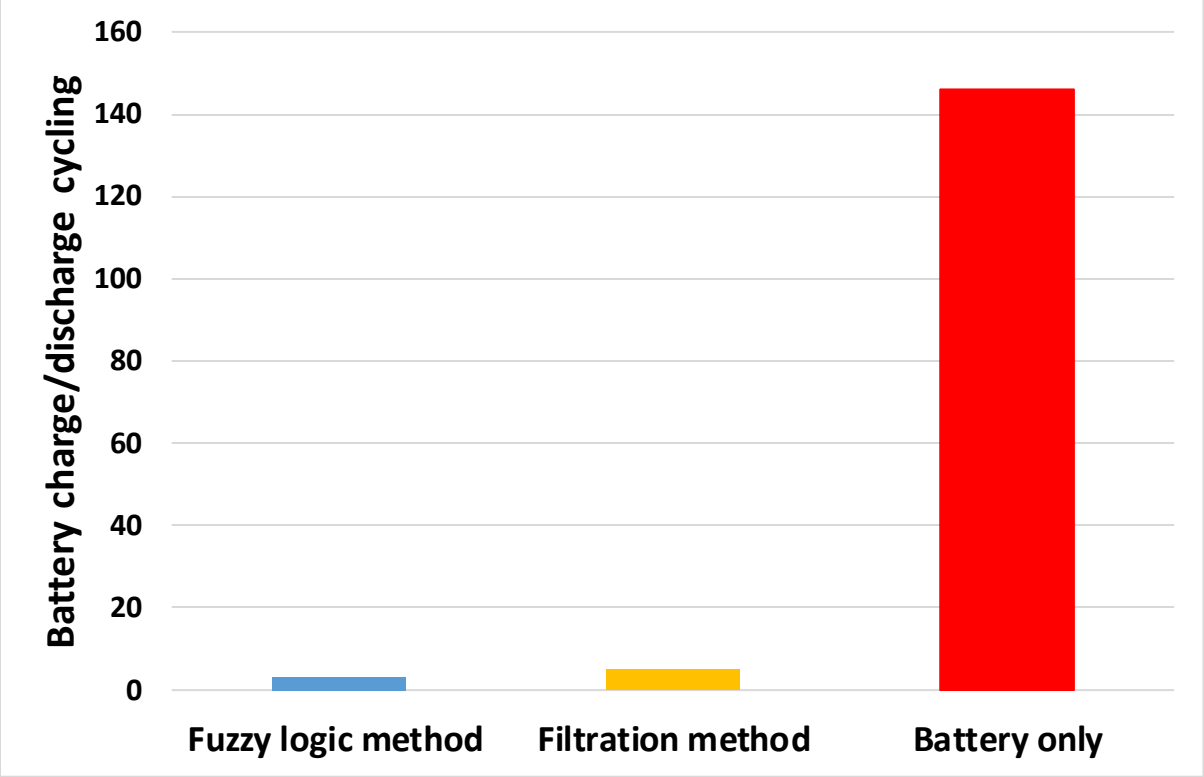

Figure 5-19 Battery charge/discharge cycle analysis

With the new proposed fuzzy logic control method applied in the HESS, the battery only has three charge and discharge cycles. The SMES is a benefit to decrease the battery charge/discharge time, which is a benefit to extend battery service lifetime.

The newly proposed fuzzy logic method has the advantage of saving the power demand by considering the SMES SOC and battery output power. Compared with the conventional filtration method, the fuzzy logic control method reduces the charge/discharge cycle by 40%, which is significantly important on battery service lifetime extension. In microgrid applications, power demand for the energy storage system is always suffering frequent charge and discharge cycles. For the filtration method, the battery will have the same trend on charge and discharge with power demand for the energy storage system. However, with the proposed fuzzy logic control method, the SMES power output can prevent frequent charge and discharge cycles, which can be seen from 750 s to 850 s. The filtration method requests three charge/discharge conversions for the battery. The fuzzy logic method only requires one battery charge/discharge conversion during that time. The changing charge/discharge requirement for the energy storage system is one typical scenario in

microgrid applications. Therefore, the proposed method has the advantage of decreasing battery charge and discharge cycles, which helps battery lifetime extension.

The proposed fuzzy logic control method also has the advantage of stabilizing the battery output power. As can be seen from the battery power output by using the filtration method and the newly proposed fuzzy logic control method, the fuzzy logic has more stable output power than the filtration method from time 10 s to 50 s, 100 s to 230 s and 1000 s to 1180 s, etc. The charge/discharge changing rate is one important factor to evaluate the battery power output changes. The battery power output changing rate comparison is shown in Figure 5-20:

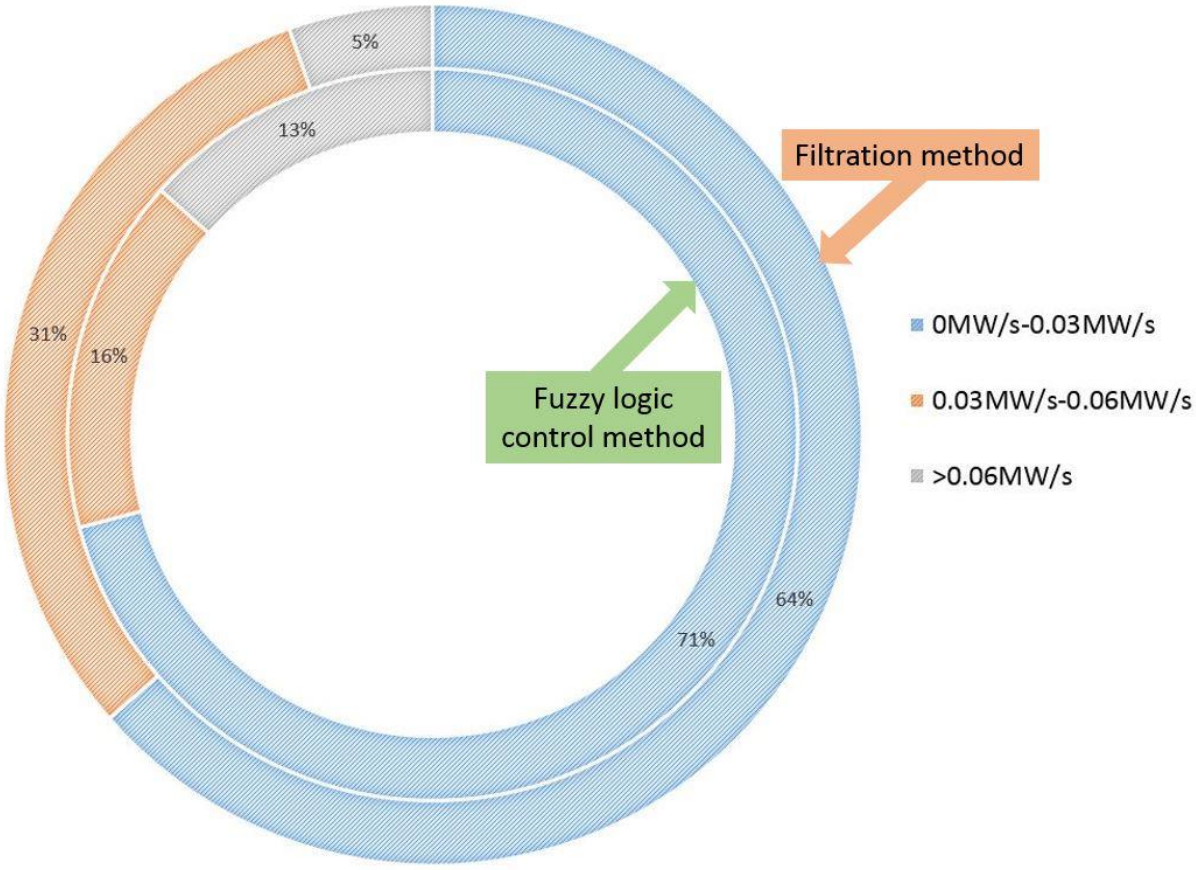

Figure 5-20 Battery power output changing rate comparison

The stable power output can help extend battery service lifetime [132, 216, 217]. By using the newly proposed fuzzy logic method, the battery power output becomes more stable, which because the battery has less than 0.03 MW/s output power changes on 71% of the battery operation time. Therefore, the proposed fuzzy logic control method can also be used to stabilise battery power output under high fluctuating power demands.

In conclusion, the proposed energy management method has the advantage of decreasing the battery output power fluctuation for the SMES-battery HESS to deal with the high fluctuating power demands in microgrids. Moreover, the proposed method can effectivity reduce battery charge and discharge cycles, and save the power demand for the battery by allocating more power output for the SMES. The case study shows that the fuzzy logic method has better performance than the filtration method.

5.6 Conclusions

The improvement of battery service lifetime is one of the key advantages of the proposed SMES-battery HESS. In this study, a new 75 level fuzzy logic energy management method has been proposed to control the HESS to deal with long-term fluctuating power demands. The SOC of the SMES is firstly considered in the control method as one input parameter. The proposed energy management method shows good performance constraining the battery power output than the commonly used filtration method.

This study discussed the HESS energy management method for microgrids to deal with long-term power demand fluctuations. For microgrid applications, a microgrid disconnection from the main grid is another inevitable process for microgrid applications. The next chapter will introduce a new control method to control the short-term performance of the HESS when a microgrid is disconnected from the main grid.

Chapter 6 Two-stage energy management control methodology of the HESS for a microgrid decoupling process from the main grid

The previous chapter introduced a new fuzzy logic control method for the SMES-battery HESS to deal with power unbalancing in microgrids. In this chapter, one new two-stage energy management control method will be developed. The proposed method is used to control the SMES-battery HESS to compensate for the load power demand when a microgrid disconnects from the main power grid. Different from chapter 5, which studied the long-term response of the HESS, the control method proposed in this chapter is used to control the HESS during microgrid decoupling from the main grid. The proposed method has the advantages of the SMES fast response speed and high power density. The new method allows the battery to have a longer response time to increase the power output, which can be used to extend the battery service lifetime. With the combination of fuzzy logic control to deal with power unbalancing in the microgrid and the two-stage method to control the HESS when the microgrid connect/disconnect from the main grid. A comprehensive control algorithm for the SMES-battery HESS for microgrid applications is established.

The newly proposed two-stage control methodology with novel PI-droop control shows good performance stabilising the HESS power output and improves battery output performance. To the author's best knowledge, no published papers have studied the SMES-battery HESS response for a microgrid decoupling scenario. Therefore, the proposed method is important for SMES-battery HESS applications for microgrids.

6.1 Introduction

The microgrid concept is gaining popularity to electrify remote areas and support the energy to islands [218, 219, 220]. The DC microgrid has gained more attention due to the rise of DC power sources and energy storage applied in microgrids, e.g., PV, battery, fuel cells, etc. [221, 222, 223]. DC power systems typically have higher efficiencies than AC power systems [224]. Moreover, compared with an AC network, a DC system does not need to be concerned about system synchronisation, system harmonics and reactive power [225, 226, 227]. In a microgrid system, the energy storage devices are integrated into the system to compensate for the load power demand when disconnected from the main grid. If only a battery energy storage system is applied in a system, when a microgrid is disconnected from the main power grid, the instantly increasing power demand from the battery energy storage system will accelerate the battery lifetime attenuation. Therefore, the SMES is proposed to be integrated into a system to build a SMES-battery HESS due to the benefits that the SMES has a short response time and high power output capacity. Moreover, both the SMES and the battery are DC energy storage devices, which can directly be integrated into a DC power system.

Previous researchers [56] have studied the SMES-battery HESS applied in microgrids to deal with long-term power demand fluctuations. The energy storage system implemented in a microgrid has been studied in previous studies [219, 228, 229], with most of these studies focusing on the energy storage system dealing with long-term fluctuating power demands. To the author's best knowledge, there are no published papers focusing on the short time response process of the HESS when a microgrid disconnects from the main grid. When a microgrid is decoupled, the energy storage devices need to support the load demand in the

microgrid. Therefore, the energy storage system needs to provide instantaneous high power when the main grid is disconnected from the microgrid. As discussed previously, the SMES has the advantage of fast response time and high power density, which are ideal for dealing with fast increasing power demands. However, it is too costly to build high energy capacity SMESs for microgrid applications. Therefore, a battery is applied with the SMES to build a HESS, which has the added benefit of the high energy capacity of a battery.

A proportional-integral controller is composed of a proportional part and an integral part. A PI controller is a control loop feedback mechanism controller, which is commonly used in industrial control systems. PI control is mostly applied to a liner system where the dynamic character does not vary with time. A PI controller to control a system is based on the proportional parameter and integral parameter designed in the PI controller. For the PI controller, the controller collects the data from the system and compares it with the predefined reference values to get the error signal (value) for calculation. The error signal goes through the PI controller to get the output of the system, which aims to reach the reference value of the system. The result of the controller output can be calculated by:

$$\mathrm{Y(t)} = \mathrm{K_p e(t)} + \mathrm{K_i} \int_0^{\mathrm{t}} \mathrm{e(t)dt} \qquad 6\text{-}1$$

Where $\mathrm{K_p}$ is the proportional term, $\mathrm{K_i}$ is the integral term and $\mathrm{e(t)}$ is the difference between the measured value and the reference value at time t. The control scheme is shown in Figure 6-1.

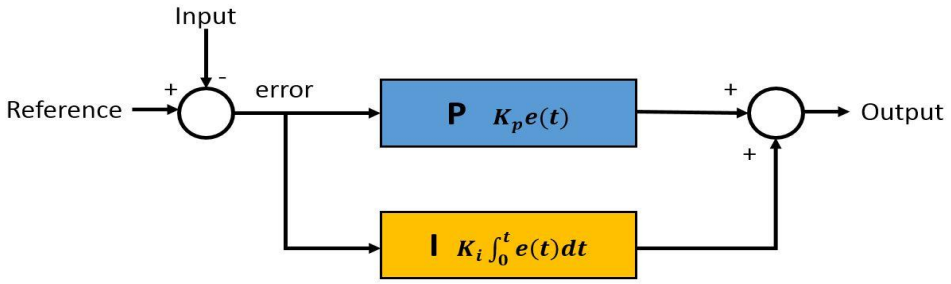

Figure 6-1 PI controller control scheme

Because the PI controller output only depends on the measurement variable, not on the knowledge base, the controller is broadly applicable. By changing Kp and Ki, the controller performance can be changed. Furthermore, the PID controller is easy to design once the designer decides the performance of the controller. However, it has a high requirement of the system and the control parameters can only be designed after the system is decided.

In the new proposed control method, the PI controller is used to control the SMES to stabilise the load voltage. Due to the battery power output continuously changing and the PI controller only considering the difference between the reference value and the input data, PI control is an ideal controller to control the SMES.

Droop controllers are first proposed to control the synchronous generator for the prime mover. In recent years, the droop controller has been introduced to control the energy storage systems in the power system. The droop control can control the energy storage system output without communicating with other devices to stabilize system voltage. Moreover, the droop controller can coordinate different energy storage systems' power output effectively to compensate for the power demand in the microgrid. In this study, the proposed method uses the droop controller to coordinate the SMES and the battery power output. The droop coefficient design is the critical point for the droop controller design. The droop controller input and output relationship can be represented by Figure 6-2.

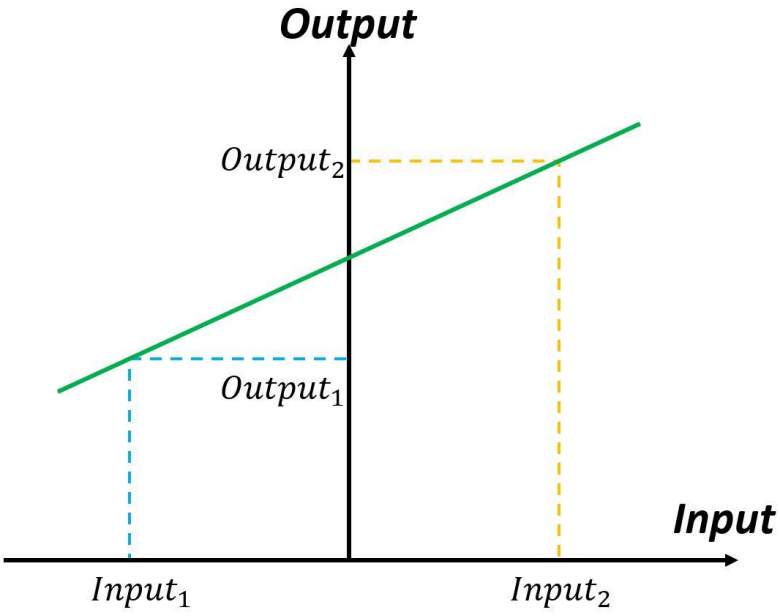

Figure 6-2 Droop controller control scheme

The droop coefficient can be calculated by:

$$K = \frac{\text{Output}_2 - \text{Output}_1}{\text{Input}_2 - \text{Input}_1} \qquad 6\text{-}2$$

A droop controller is easy to design but has a lack of flexibility. A droop controller is a linear controller, which means the controller cannot effectively control a system when the system parameters change.

In the new proposed control method, a droop controller is only used to control the battery power output and the SMES is used to compensate the rest of the power demand for the HESS by using PI controller to stabilize the DC bus voltage in the PI-droop control method. The droop controller makes the overall control strategy easier to design and achieves better battery output performance.

In this study, a novel two-stage energy management method with PI-droop control is designed and tested in Matlab to control the SMES-battery HESS, to compensate for the power demand when a microgrid disconnects from the main grid. The proposed method focuses on controlling the response process of the SMES-battery HESS.

6.2 New proposed two stage energy management method with PI-droop control

Compared with previous researchers, which use the SMES-battery HESS to deal with high fluctuating power demands in the power system [27, 230, 231] (the fluctuating demand is only up to 10% of the system power demand), the SMES-battery HESS is used to compensate for the power demand in isolated grids, which need to support 100% of the power demand in a small system. Therefore, the research in this chapter will be different than other kinds of voltage fault researchers work. The energy management rules for the HESS controller need to consider the characteristics of different energy storage systems. A good energy

management method can not only keep the power system stable but also extend the BESS service lifetime. The new proposed method has the advantages of the SMES fast response speed, long service lifetime and high power density. Moreover, the microgrid load may change, which makes some controllers such as the droop controller not work effectively due to system configuration changes. Therefore, the author proposes a new two-stage energy management method with PI-droop control for the SMES-battery HESS to keep the system stable and extend the battery service lifetime.

The control scheme of the new two-stage energy management method is shown in Figure 6-3.

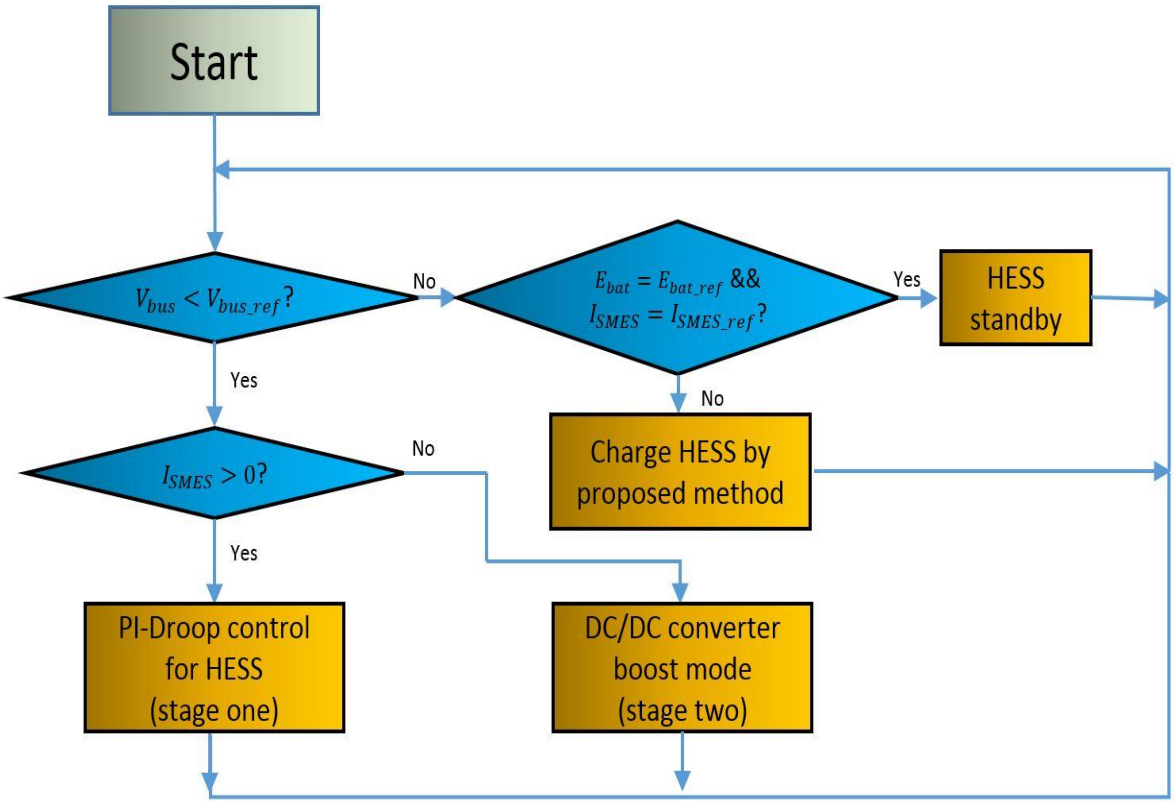

Figure 6-3 Control scheme of the new two-stage energy management method

As shown in Figure 6-3, when the system is connected to the grid, the controller controls the SMES and BESS to charge to their rated energy capacities. After the HESS is at rated energy capacity, the HESS switches to standby mode, which results in no power exchanges between the HESS and the main grid. When a microgrid is decoupled, a voltage drop will appear on the load side. When a voltage drop occurs, stage one works to collaborate the SMES and battery to compensate for the power demand from a microgrid. In stage one, the SMES has a high

power output at the beginning to deal with the instant high power demand from the microgrid. The battery output power slowly increases, which makes the SMES output power decrease. This method is able to reduce the battery discharging rate and allows the BESS to have a longer response time when a voltage drop occurs. If the SMES is fully discharged and the BESS power output cannot sufficiently compensate for the power demand of the microgrid, stage two starts to function. The reason stage one may not work effectively may be caused by load size changes. The HESS charge state and discharge state are discussed in the following sections.

6.2.1 HESS charge state control methodology

In previous SMES-battery HESS research, most of the control methodologies charge the SMES and battery in the HESS with unfixed power such as using PI controller [27], droop controller [56] or filtration method [125]. The unfixed power injected into the HESS can cause the power system be unstable. That is because when the HESS gets charged, the HESS acts like a high power load in the system. The unfixed power input makes the power demand for the power system change too quickly. In this new method, to keep the power system stable and enhance the robustness of the HESS, the power demand for the HESS charging state is designed to be constant.

6.2.2 Two-stage discharge control method

The two-stage discharge control methodology only works when a load side voltage drop occurs. One of the advantages of the proposed method is it reduces the discharging rate for the battery in the SMES-battery HESS. The proposed control method has two stages and each stage has a different purpose for the HESS to compensate for the power demand from a microgrid. Stage one starts to operate when a voltage drop on the load side occurs and the main purpose of stage one is not only to deliver enough power to the loads but also to extend the battery service lifetime by decreasing the battery discharging rate. Stage two only works

when the SMES is fully discharged and the battery power output, by using the stage one control, cannot fully compensate for the load power demand in a microgrid.

6.2.2.1 PI-droop discharge method for the two-stage control methodology

The control of the SMES and battery in the SMES-battery HESS, to compensate for the load demand, is the main issue in this research. Moreover, the control method needs to consider the different characters of different energy storage devices. Based on previous battery lifetime research, a low discharging rate can extend battery service lifetime [232, 233, 234]. In this application, the power demand requires a fast response from the HESS. Therefore, the controller controls the SMES to deal with the fast-changing power demand, which allows the battery to have a longer response time to achieve the requested power demand. In stage one of the two-stage energy management method, the SMES is used to stabilise the load voltage and the battery output power is controlled by the energy remaining in the SMES.

In stage one, the PI controller is used to control the SMES to stabilise the load voltage. The reference parameter for the SMES PI controller, $\mathrm{PI}_{\mathrm{SMES}}$, is the load voltage. The battery output power keeps increasing due to the energy remaining in the SMES decreasing. The SMES compensates for the rest of the power demand apart from the battery power output. This method makes the new control system have the advantage of low complexity and prevents the battery from a surge increasing the discharging rate. For the SMES-battery HESS, either only use the PI control or just use the droop control, which needs a complex calculation to coordinate the controller for the battery and SMES. In this two-stage method, the controller coefficient design is much easier due to the combination of the PI controller with a droop controller. The controller coefficients design is discussed in section 6.5.3. The control scheme of the stage one control methodology is shown in Figure 6-4.

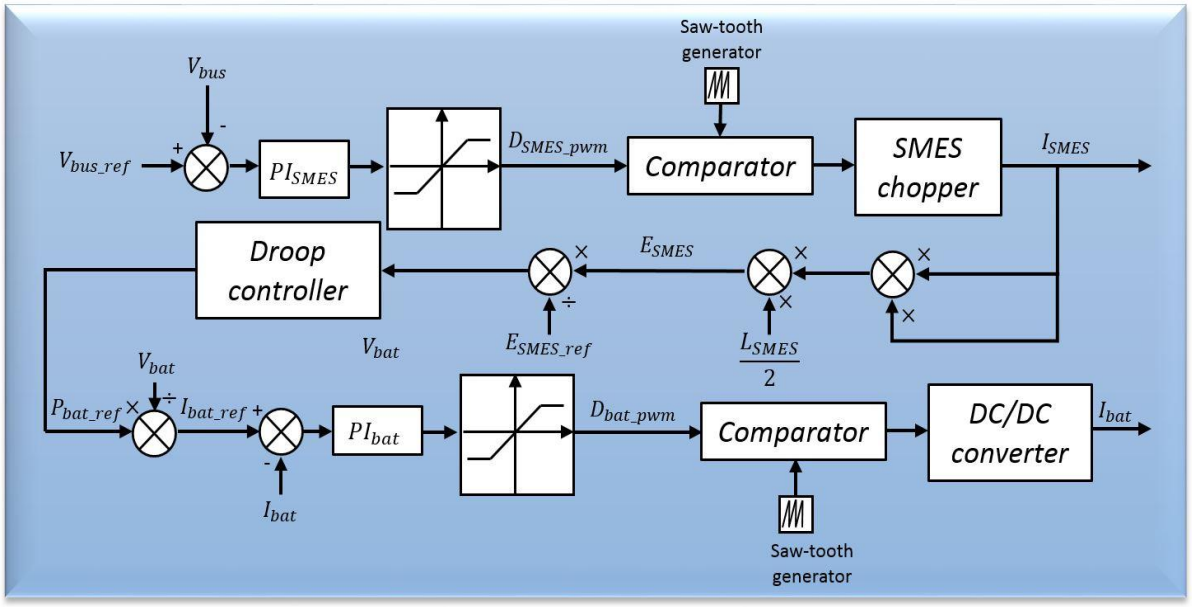

Figure 6-4 Stage one control scheme with PI-droop control

The droop controller control scheme for the battery energy storage system is shown in Figure 6-5. The battery power output can be obtained by:

$$\mathrm{P_{bat\_out}} = \mathrm{P_{load}} \cdot \frac{\mathrm{E_{smes\_max}} - \mathrm{E_{smes}}}{\mathrm{E_{smes\_max}}} \qquad 6\text{-}3$$

Where $\mathrm{E_{smes\_max}}$ is the SMES rated energy capacity, $\mathrm{E_{smes}}$ is the energy remaining in the SMES and $\mathrm{P_{bat\_out}}$ is the battery output power, $\mathrm{P_{load}}$ is the load power demand in the microgrid.

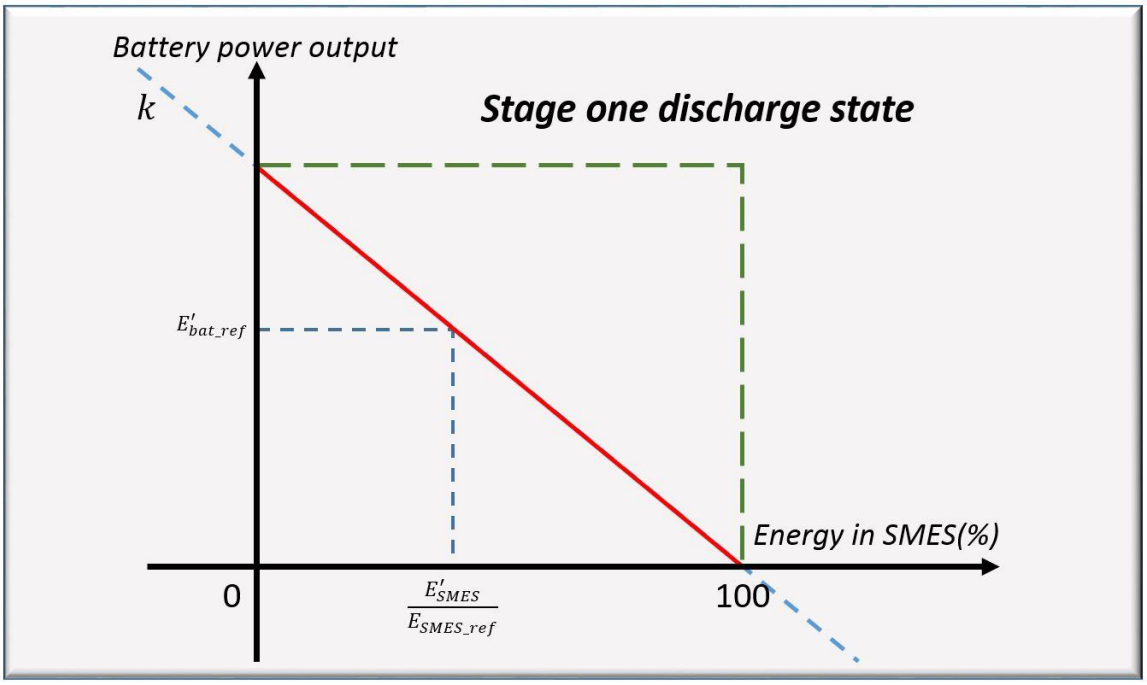

Figure 6-5 Droop controller in the proposed method

The battery output power is determined by the energy remaining in the SMES. To achieve the energy allocation for the HESS, the battery reference output current $\mathrm{I_{bat\_ref}}$ can be calculated by:

$$\mathrm{I_{bat\_ref}} = \frac{\mathrm{E_{bat\_ref}}}{\mathrm{V_{bat}}} \qquad 6\text{-}4$$

Where $\mathrm{E_{bat\_ref}}$ is the allocated battery output power and $\mathrm{V_{bat}}$ is the battery terminal voltage. If the SMES is not fully discharged, the energy management method for the battery energy storage system is droop control. The droop control parameter for the battery droop controller is the ratio of the energy remaining in the SMES, which can be represented by $\mathrm{E_{SMES}}/\mathrm{E_{SMES\_max}}$.

6.2.2.2 Stage two control method for the two-stage energy management method

The stage two control method only starts to operate when the SMES is fully discharged and the battery output power, using the stage one control method, cannot compensate for the power demand. In stage two, only the battery energy storage system is able to deliver the power to the power system. Therefore, the DC/DC converter boost mode is operated. In boost mode [235], the battery power output rating is the maximum battery power output rating. The primary purpose of the stage two control method is to stabilise the load voltage. Therefore, the stage two control method is used to guarantee the HESS robustness when the system size changes.

6.2.3 Droop coefficient design for the PI-droop controller

Battery manufacturers normally provide an optimal discharge rate for their batteries. An over range charge/discharge current rate for a battery can accelerate a battery's degradation. Therefore, for the droop coefficient design, the designed battery maximum output current I_{out_max} for each battery should be smaller than the optimal current discharge limitation I_{out_lim}:

$$I_{out\_max} \leq I_{out\_lim} \tag{6-5}$$

In this study, the BESS in the SMES-battery HESS should be able to provide enough power to a microgrid when disconnected from the main grid. The maximum power consumption of a microgrid P_{load_max} is determined by the system configuration. The BESS maximum power output P_{bat_max} can be represented by:

$$P_{bat\_max} = V_{bat} \cdot I_{out\_max} \geq P_{load\_max} \quad 6\text{-}6$$

Where V_{bat} is the battery sets terminal voltage. The droop controller is a linear controller, which makes the battery power output linearly increase. By considering the energy consumption of the microgrid, the droop coefficient k in the droop controller for the battery output power is designed by:

$$k \geq \frac{P_{load\_max}^2}{2 \cdot E_{smes\_max}} \quad 6\text{-}7$$

Where the load demand P_{load_max} and SMES energy capacity E_{smes_max} are given in the system. Therefore, the droop coefficient can be calculated.

6.3 Sizing design for the SMES and battery in the HESS for the two-stage energy management method

The energy storage system size of both the SMES and the battery are crucial. The designed HESS system should be able to deal with instantaneous high power demand when the system disconnects from the utility grid. Moreover, to support the long-term power demand, the BESS size in the HESS should also be considered. Due to the new proposed control algorithm of the system, the sizing design is different from the previous HESS sizing methodologies [132, 236, 237, 238]. In this study, a new sizing design method has been proposed to fit the newly proposed two-stage energy management method. The new sizing design method has the advantages of less complexity and is also able to guarantee the reliability of the system due to the two-stage energy management method.

The sizing design is one of the most critical parts in this HESS research. The oversizing design of a HESS will increase system costs. Insufficient power or energy capacities of a HESS can

cause a HESS to not be able to meet the system demand. The SMES and battery in a HESS should be able to meet the system power and energy requirements. In conclusion, three specifications for the SMES-battery HESS will be applied in the sizing design:

- The SMES maximum output power P_{smes_max} should larger than the microgrid maximum power demand P_{system_max}:

$$P_{smes\_max} > P_{system\_max} \quad 6\text{-}8$$

- The battery energy capacity should be able to compensate for the long-term power demand of the microgrid.
- The energy capacity of the SMES should be large enough to support the microgrid before the battery output power can adequately compensate for the power demand from the microgrid.

6.3.1 Battery sizing design for the SMES-battery HESS

For the HESS to compensate in microgrid power demand applications, the battery size is designed by the microgrid maximum power demand P_{system} and the designed HESS withstand time T. The withstand time is the time duration for the HESS to compensate for the power demand for the microgrid. The energy capacity of the SMES is much smaller than the BESS. Therefore, for the battery sizing design study, the SMES energy capacity is negligible. The battery energy capacity E_{bat} can be calculated by:

$$E_{bat} \geq P_{system} \times T \quad 6\text{-}9$$

6.3.2 SMES sizing design for the SMES-battery HESS

The proposed PI-droop control methodology can adequately simplify the SMES sizing design process. In the proposed method, the SMES is used to relieve the battery output from instantly increasing the high power demand from the power system.

For the appropriate HESS sizing design, the SMES is able to handle the power demand before the battery energy storage is able to compensate for the microgrid power demand. The SMES size for the proposed control method can be calculated by:

$$E_{smes} \geq \int_{o}^{t} P_{load}(t)dt - \int_{o}^{t} P_{bat}(t)dt \qquad 6\text{-}10$$

The battery discharging rate is designed to be γ [$W \cdot s^{-1}$],which should be smaller than the battery maximum discharging rate. The SMES size can be calculated by:

$$E_{smes} \geq \int_{o}^{t} P_{load}(t)dt - \int_{o}^{t} \gamma t dt \qquad 6\text{-}11$$

The designed discharging rate γ is designed based on the designers experience and the battery characteristics.

6.4 Power system configuration for the two-stage energy management method

The proposed power system configuration is shown in Figure 6-6. The main grid connection to the microgrid is through a grid interface converter. The SMES-battery HESS is connected in parallel to the distribution network. The reasons to use a DC microgrid is that a DC grid does not require synchronisation with the utility grid and also does not have reactive power. Moreover, a DC microgrid is suitable for integrating with the SMES-battery HESS due to the output power of the HESS being DC power. In this study, the DC bus voltage level is 380 V DC.

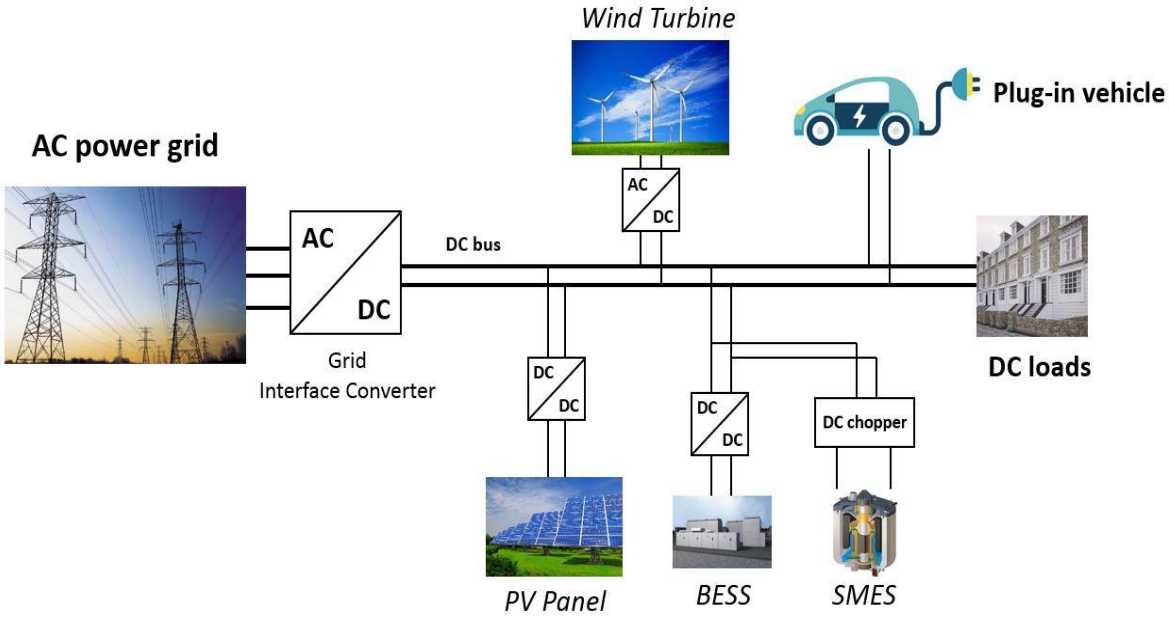

Figure 6-6 System configuration of DC microgrid

6.5 Case studies

In this research, two case studies have been carried out to simulate two operating conditions during microgrid operation. Case one is the normal operating condition of the microgrid and the power demand in the microgrid is the normal operating power demand when the microgrid is decoupled. Case two is used for the microgrid with unexpected load demands added in the microgrid. The proposed method is to control the HESS to keep the bus voltage stable and improve battery performance to improve the battery service lifetime.

6.5.1 Case one: Microgrid with rated power demand

This case study is carried out in this section to test the new proposed energy management method. In this case, the normal operation of the SMES-battery HESS to deal with the microgrid decoupled is researched. The comparison of the proposed method with the commonly used filtration method has been done.

The simulation model is built in Matlab/Simulink to demonstrate the performance of the SMES-battery HESS with the proposed two-stage method. The overall system configuration is discussed in section 6.7. The proposed energy management method controls the SMES chopper and the battery DC/DC converter to achieve the requested power exchange of the energy storage system with the microgrid. In the simulation model, a microgrid with 334 kW power demand is applied. The microgrid bus voltage is 380 V. The designed battery discharging rate is 56 kW/s. According to the sizing design, which is discussed in section 6.6, the SMES size is 0.98 MJ. The power demand of the SMES-battery HESS is shown in Figure 6-7, which shows that the main grid is disconnect from the microgrid at 2 s. Moreover, the microgrid bus voltage is also shown in Figure 6-7, which shows the proposed method can fully compensate for the power demand from the microgrid.

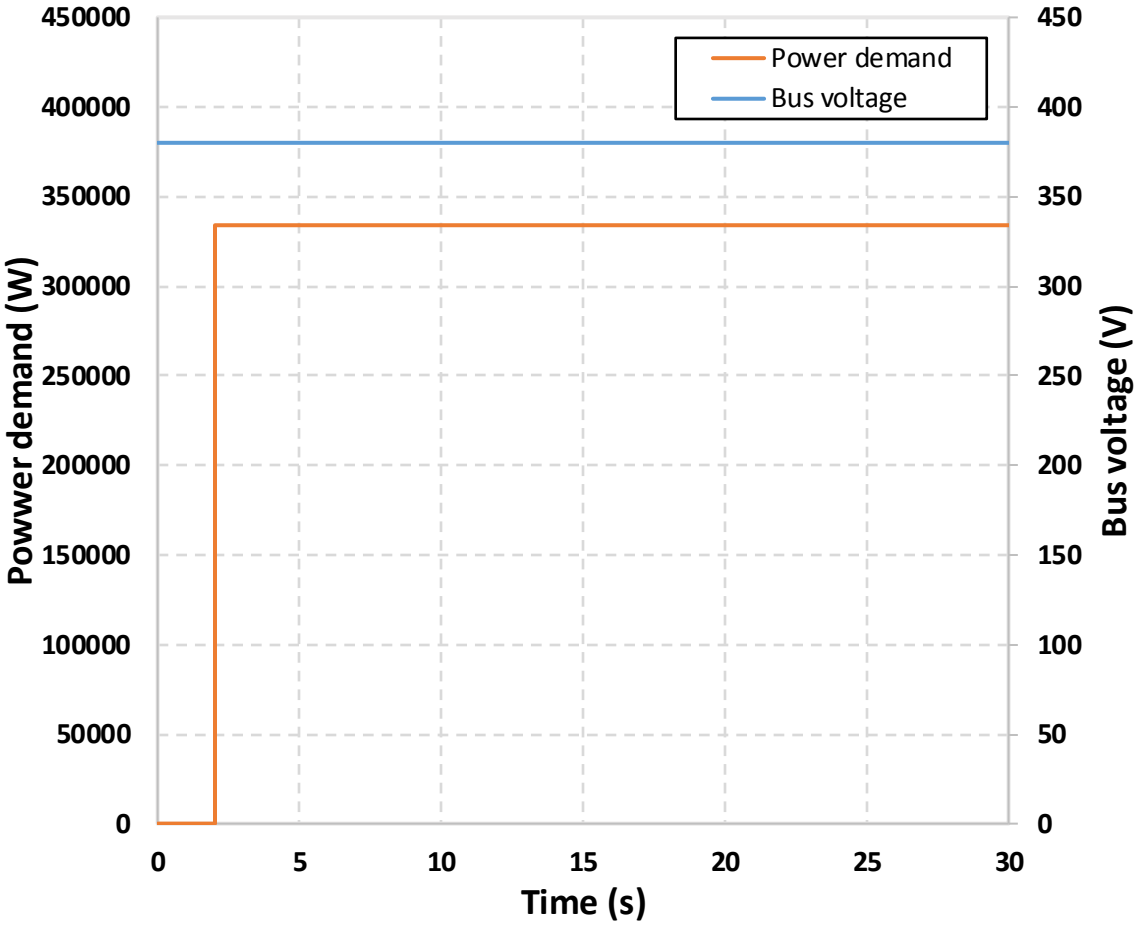

Figure 6-7 Bus voltage and power demand for the HESS

The battery power output and the SMES power output are shown in Figure 6-8. The battery power output steady increases to achieve the 334 kW, which meets the power demand from the microgrid. The fast response energy storage device SMES is used to compensate for the rest of the power demand before the battery fully compensates for the power demand from the microgrid.

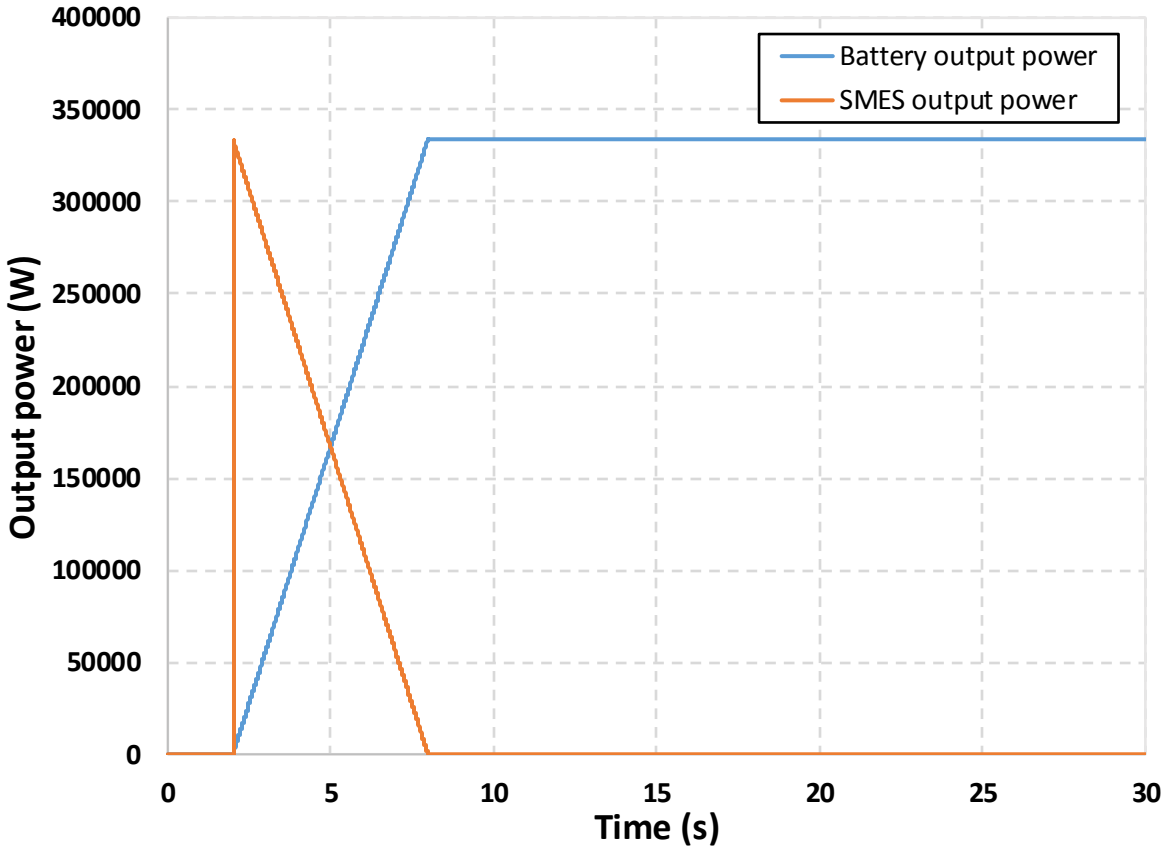

Figure 6-8 Battery power output demand and SMES power output demand

A comparison of the proposed method with the filtration method is shown in Figure 6-9 and Figure 6-10. The battery power output demand for the filtration method and the proposed method are shown in Figure 6-9. The battery power output of the filtration method increases fast when the voltage drop occurs. The highest discharging rate for the filtration method is uncontrollable, which means the filtration method may cause the discharging rate to exceed the battery's maximum discharging rate. Moreover, compared with the proposed method, the filtration method requires higher maximum battery power output, which will accelerate battery attenuation. According to the battery performance results, the battery overcharges the system from 8.6 s to 17.2 s using the filtration method. To keep the microgrid stable when the battery overcharges the system, the SMES requests to absorb the overcharged energy. The overcharge of the battery decreases the efficiency of the HESS and also accelerates battery attenuation. Furthermore, the filtration method requests a longer time for the battery to reach the requested power output. The proposed PI-droop method only needs 5.99 s to stabilise the power output and without the battery being overcharged. By using the filtration method, the battery's maximum power output reaches 348435 W, which is 4.3% higher than

the requested power demand. The proposed PI-droop method does not overcharge the system and can quickly stabilise the battery power output to the requested power from the microgrid.

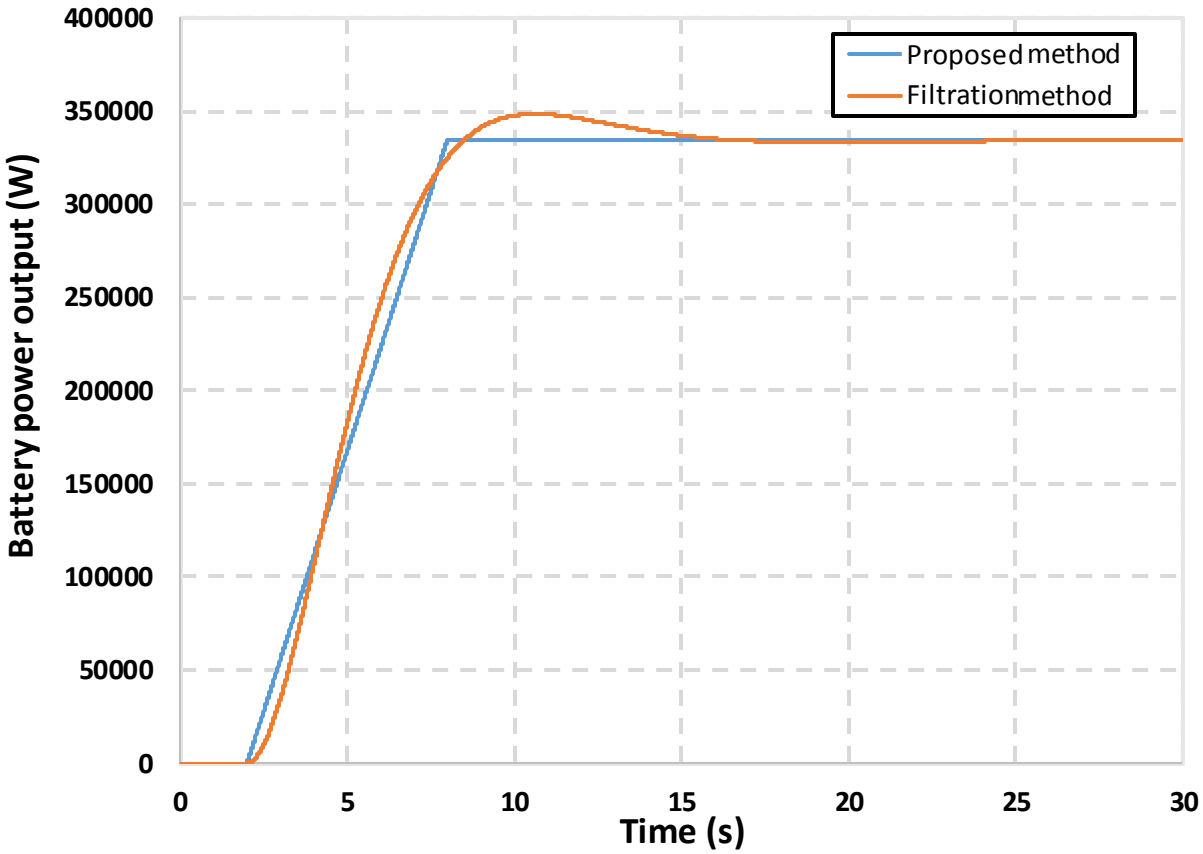

Figure 6-9 Battery power output demand for the filtration method and the proposed method

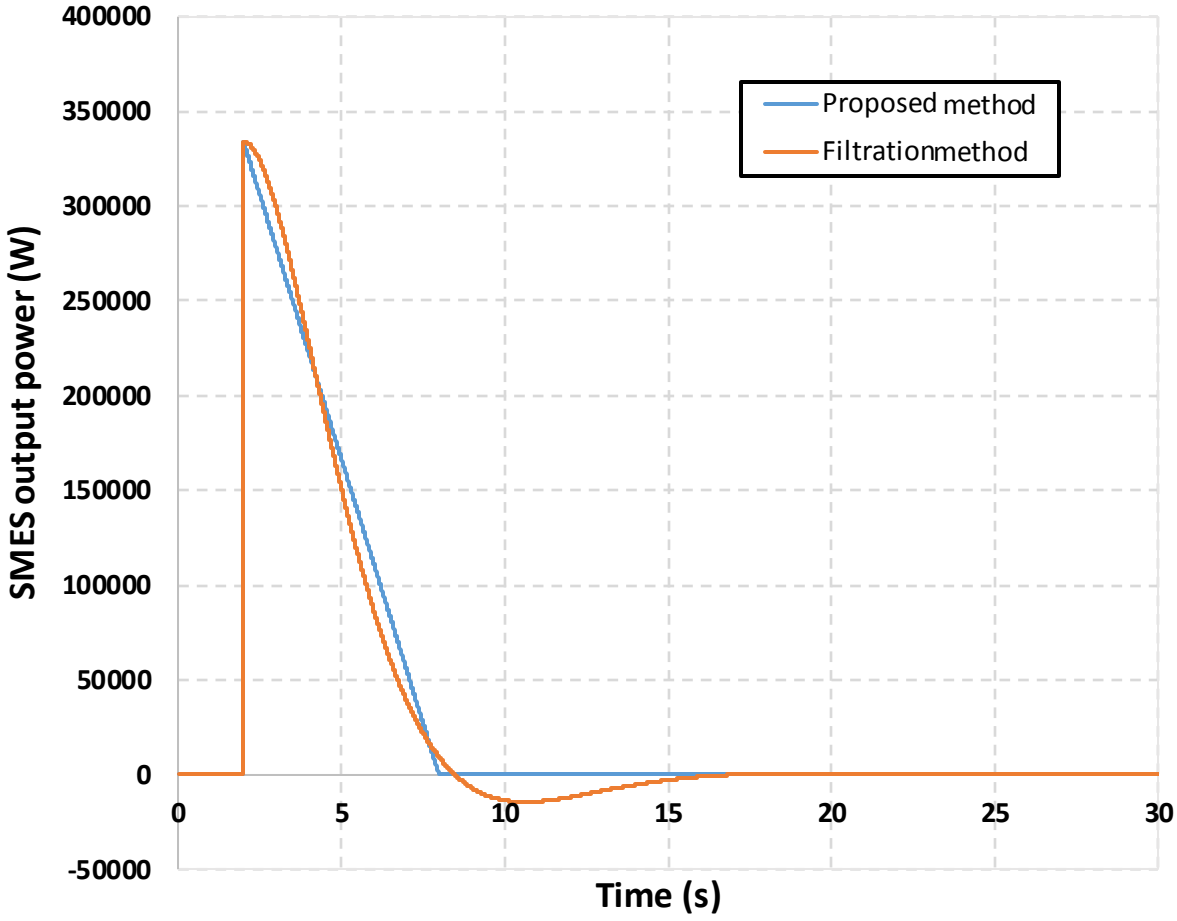

Figure 6-10 SMES power output demand for the filtration method and the proposed method

The discharging rate analysis for the two methods is shown in Figure 6-11. The HESS by using the PI-droop method has a fixed battery discharging rate, which is 55.80 kW/s. However, the filtration method has a variable discharging rate. The highest discharging rate for the filtration method is 78.46 kW/s, which is 141% of the PI-droop method. The higher discharging rate also accelerates battery attenuation. The negative discharging rate shows that the filtration method needs a long time to adjust the battery power output to meet the power demand from the microgrid.

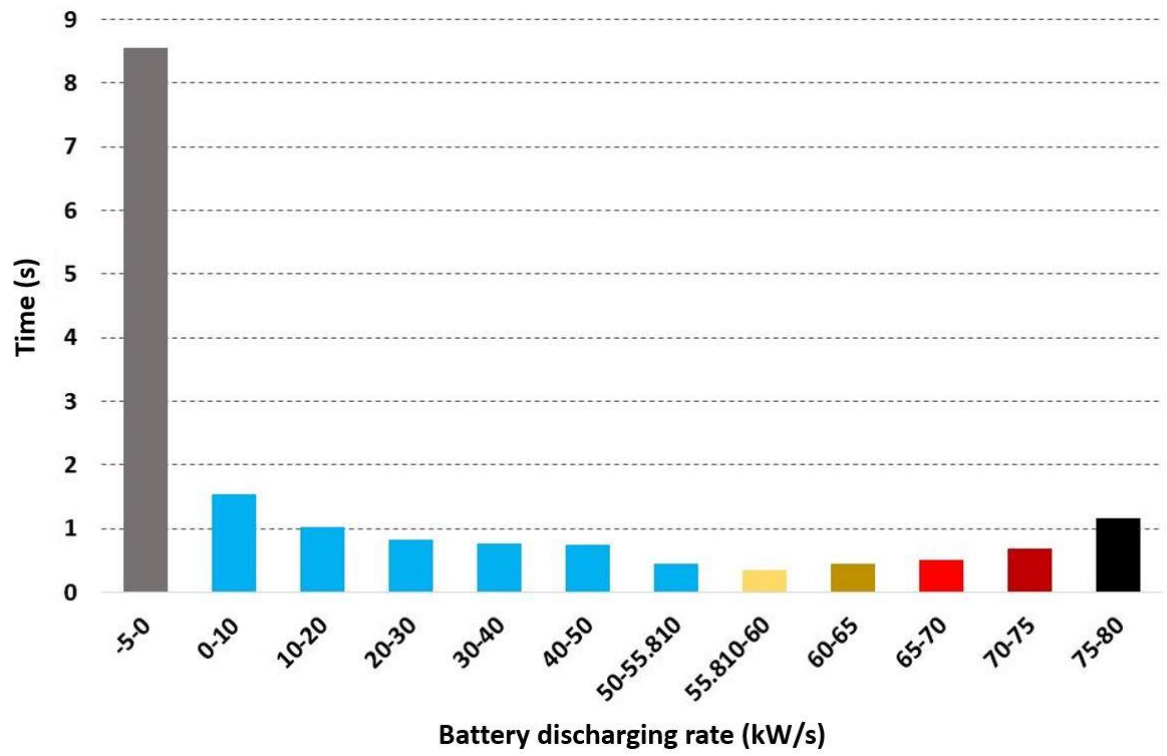

Figure 6-11 Battery discharging rate analysis for the filtration method

Figure 6-12 compares the discharging rates verses time between the filtration method and the new proposed PI-droop method. The filtration method request 17.05 s to adjust the battery power output, while the PI-droop method only needs 5.99 s. By using the two-stage method, the battery output stabilisation time is shorter, which is good for system voltage regulation. After the HESS can compensate for the microgrid power demand, the HESS is able to switch to the mode (such as fuzzy logic method described in chapter 5) to stabilise the fluctuating power demand from the microgrid.

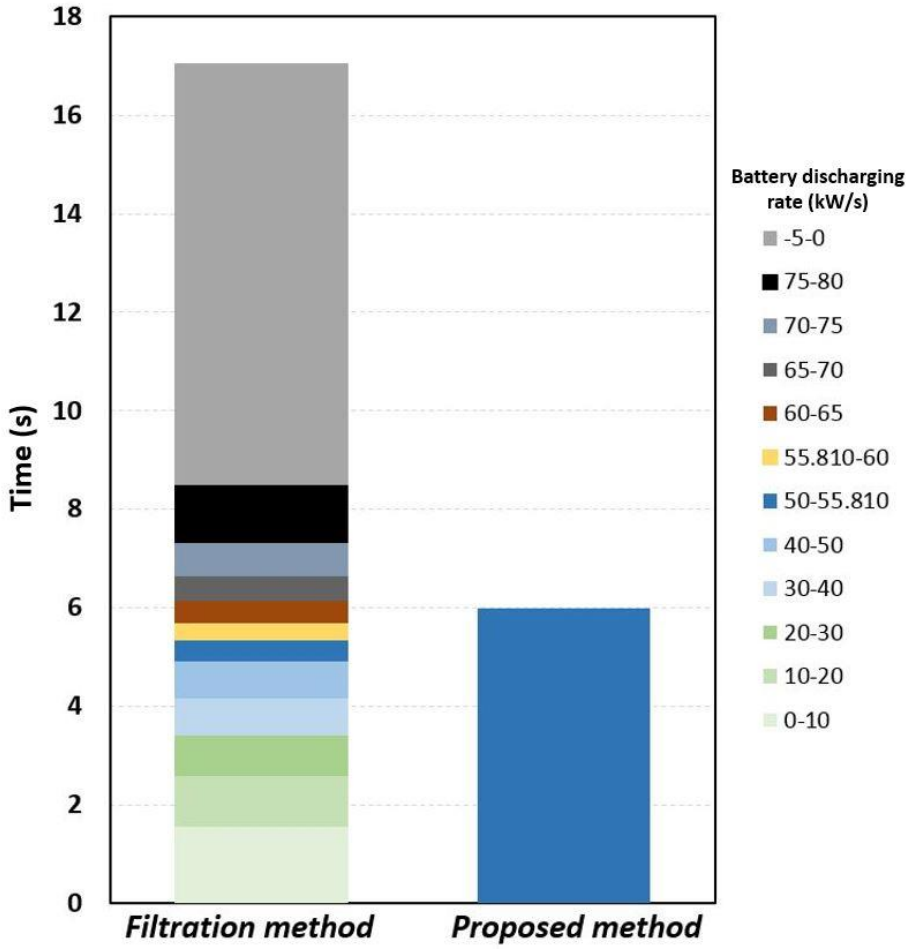

Figure 6-12 Discharging rate analysis of the filtration method and the proposed method

The battery performance by using two different control methods are summarized in Table 6-1.

Table 6-1 Battery performance by using two different control methods

	Two-stage method	Filtration method	Novel two-stage method compared with filtration method
HESS response time until battery reach required power output	5.99 second	17.05 second	Filtration method 185% longer
Battery maximum power output	334 kW	348.435 kW	Filtration method 4.3% higher
Battery maximum discharging changing rate	55.8 kW/s	78.47 kW/s	Filtration method 41% higher

Therefore, according to the study above, the new proposed PI-droop method has the advantages of high system robustness, high reliability and fast response duration. These advantages are beneficial to extend the battery service lifetime and compensate for the power demand from the microgrid. In this case, the PI-droop method decreases the battery power output by 4.3% and shortens the HESS response speed from 17.05 s to 5.99 s. Moreover, the battery maximum discharging rate decreases by 29%. The low discharging rate and low maximum discharge power helps to extend battery service lifetime. Furthermore, the fast response time helps enhance the system security and reliability.

6.5.2 Case two: Microgrid with excessive power demand

Case two researched the SMES-battery HESS performance when some unexpected load was added to the microgrid, which makes the microgrid power demand higher than the designed power. The proposed method not only needs to control the battery performance but also needs to stabilise the bus voltage. In this situation, a 380 kW power demand is applied for the HESS. The battery maximum discharging power rating for the battery energy storage system is 120 kW/s (in real applications, the discharging rate is much higher than 120 kW/s. In this study, however, the low maximum discharging rate can show the performance of the battery response process when working in stage two). The simulation of the battery power output and SMES power output are shown in Figure 6-13.

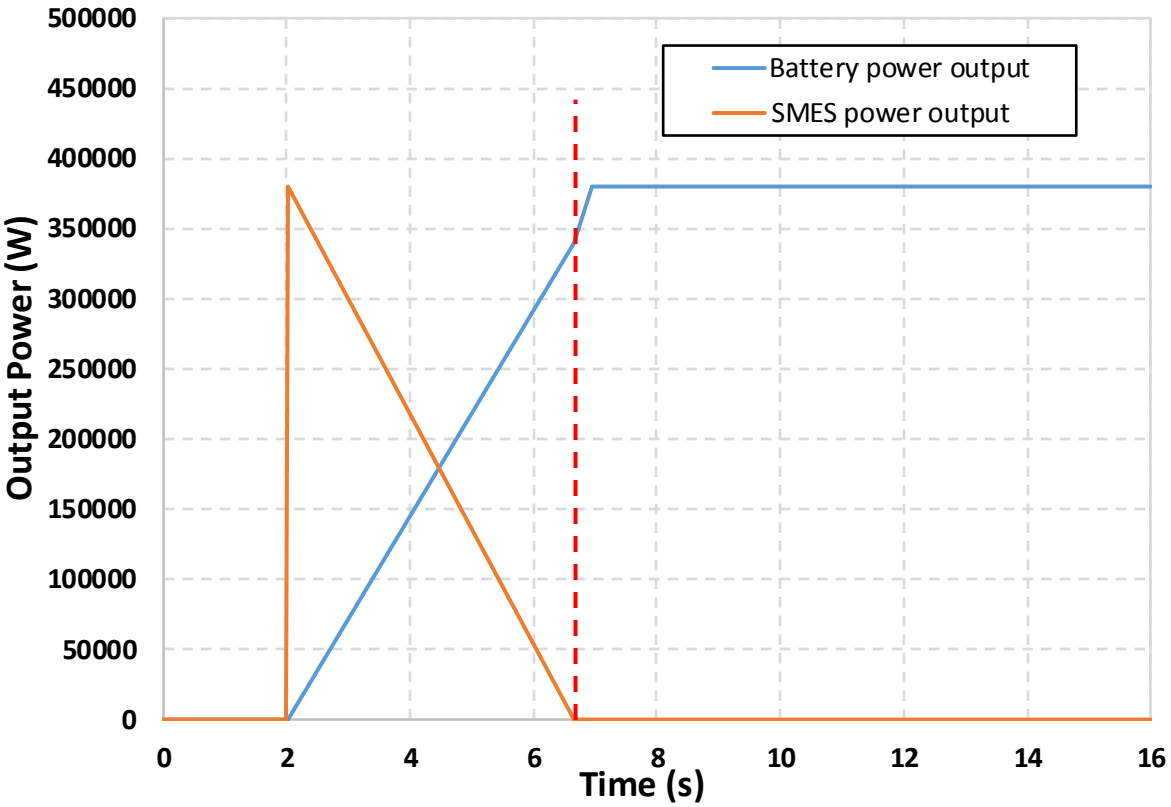

Figure 6-13 HESS power output demand by applying two-stage method for the microgrid with excessive power demand

For case two, when the microgrid switches to isolation mode, stage one starts to operate. The SMES has a high power capacity, which is used to stabilise the power demand to the requested demand. The battery power output is controlled by the stage one control and is working at a 72.85 kW/s discharging rate. At time 6.67 s, the SMES is fully discharged and the battery output power cannot adequately compensate for the power demand from the microgrid. Therefore, stage two starts operating to stabilise the microgrid power demand. From time 6.67 s, the HESS is working in stage two mode, which is the battery DC/DC converter boost mode. The output power is dependent on the battery energy storage system's maximum output power changing rate. The HESS power output reaches 380 kW at 7 s. If the battery energy storage system in the HESS has a higher maximum discharging rate, the battery output power climbing time will become shorter when working with stage two control.

The simulation results of the HESS dealing with an excessive power demand is summarised as Table 6-2.

Table 6-2 Simulation result for the microgrid with excessive power demand

Time working at stage one	4.667 s
Time working at stage two	0.333 s
Stage one discharging rate	72.85 kW/s
Stage two discharging rate	120 kW/s
Microgrid voltage unstable time	0.333 s
Maximum power shortage	39.96 kW

The microgrid voltage becomes unstable, which is caused because the HESS not able to deliver enough power to the microgrid. Because the SMES is fully discharged, the SMES cannot support any power output. The battery power output does not reach the required power demand. Therefore, a voltage dip occurs for a short time (0.33 s in this study) until the battery is able to deliver the required power to the system. During the time the HESS is working in stage two, the battery is operating at its maximum discharging rate and trying to meet the microgrid power demand as fast as it can. The maximum power shortage during the microgrid decoupling is 39.96 kW, which is approximately 10% of the overall power demand from the microgrid.

For the same HESS capacity to deal with the excessive power demand, the SMES and battery power output using the filtration method is shown in Figure 6-14.

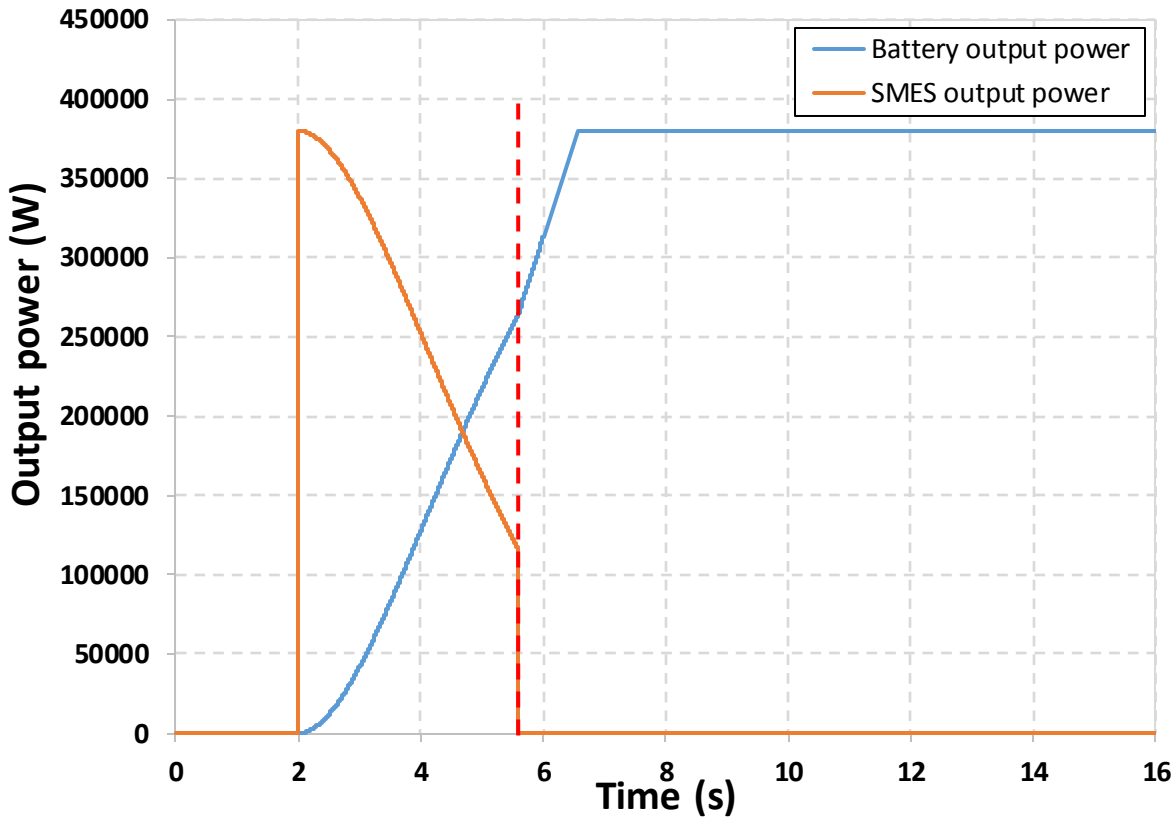

Figure 6-14 HESS power output demand by applying filtration method for the microgrid with excessive power demand

Due to the power demand changes, the filtration method cannot work properly to compensate for the power demand. That is because the cut-off frequency of the filtration control controller is fixed for the normal operating condition and not suitable for different power demands. When the microgrid is disconnected from the main power grid, the HESS, using the filtration method, can keep the voltage stable for the first 3.58 s. However, after the SMES fully discharged, the battery is requested to support most of the power demand from the microgrid, which causes the microgrid bus voltage to be unstable for 2.97 s. In this study, the maximum power shortage is 117.16 kW, which is 31% of the microgrid total power demand.

A comparison of the two-stage method and the filtration method are shown in Table 6-3.

Table 6-3 Comparison of the two-stage method and filtration method

	Two-stage method	Filtration method
Time duration of battery working at maximum power output	0.333 second	2.97 second
Maximum microgrid power shortage	39.96 kW	117.16 kW
Microgrid voltage unstable time	0.333 second	2.97 second

The filtration method cannot compensate for the microgrid power demand for 2.97 s, which is 791% longer than the proposed two-stage method. Moreover, the higher power shortage of the filtration method can cause a more severe voltage drop in the microgrid. Therefore, the proposed two-stage control method is more suitable for microgrid applications to guarantee microgrid voltage level and improve battery performance.

As can be seen from the results, the two stage method can normally operate to support the microgrid. However, the conventionally used filtration method is not capable of supporting the demand, which is because the pre-set value does not match the system demand. When some edge cases happen such as unexpected load added in the system, the conventional method is not able to support the system with stable voltage. Therefore, the two-stage method is suitable for the microgrid coupling/decoupling process.

6.6 Conclusions

The improvement of the battery power output performance is one of the key advantages of the proposed two-stage PI-droop control method. In this study, the PI-droop controller is applied in the two-stage control methodology to control the HESS performance when only the HESS supports the power demand in a microgrid. In this case, the two-stage PI-droop control is able to decrease the battery maximum output power by 4.3% and decrease the battery maximum discharging rate requirement by 29%. Furthermore, the proposed method

can shorten the HESS response process from 17.05 s to 5.99 s. When a microgrid demand unexpectedly increases, the proposed method is able to compensate for the power demand, which the conventional HESS control method is not able to achieve. The new method shows better performance on controlling the battery power output than the commonly used filtration method.

After the control method for the SMES-battery HESS in the microgrid operation has been designed, it is essential to test the system achievability. Therefore, the SMES-battery HESS experimental platform needs to be established to examine the proposed control method and sizing design feasibility. A lab-scale experiment needs to be done before the HESS is applied in the power system.

Chapter 7 Design and test of the SMES-battery HESS experimental platform

The SMES magnet design for the SMES-battery HESS experimental platform was studied in chapters 3 and 4, which informs the HESS experimental platform setup. The HESS control method was investigated in chapters 5 and 6, which will be applied in the microgrid application. In this chapter, the SMES-battery control circuit topology and the experimental platform will be researched. At the end of this chapter, a lab-scale SMES-battery HESS experimental platform, which has been established to represent the SMES-battery HESS in a microgrid application, will be presented. The designed SMES magnet is used in the experimental platform and the proposed two-stage control method, described in chapter 6, will be applied to test the HESS achievability. However, due to the magnet energy capacity of the SMES being too small to deal with a fluctuating power demand, the fuzzy logic control method, described in chapter 5, will not be tested in this research.

7.1 Introduction

As has been previously discussed in chapters 5 and 6, the SMES-battery HESS shows great potential for power system applications, as it can deal with power fluctuations, compensate for voltage drop and provide system frequency regulation, etc. However, no previous research in the literature has built a SMES-battery HESS experimental platform to test its reliability. In this research, one novel point is that the author firstly uses a real SMES system integrated into the SMES-battery HESS to test the system's reliability and achievability. A semi-active control topology [132, 239] and a full-active control topology [240] have been proposed to control the SMES-battery HESS. However, no research has compared the reliability of these two control topologies. Therefore, in this research, the semi-active control topology and the full-active topology have been compared using the experimental platform.

AM Gee et al. [240] have conducted experimental work using a conventional copper inductor with a battery to represent the SMES-battery HESS in an AC system. However, in the experiments, the author found that the copper inductor was incapable of representing the SMES in the HESS system. The copper inductor had a high resistivity and added high noise into the power system. Moreover, the ohmic losses also decreased the energy capacity of the copper inductor. Therefore, a conventional chopper cannot adequately represent the real SMES in the HESS. For this reason, a real SMES integrated into the HESS is crucial for the HESS feasibility verification.

7.2 SMES-battery HESS topology design

The SMES-battery HESS topology design is the foundational part of the HESS application. The semi-active and full-active control topologies have been proposed to control the SMES-battery HESS for power system applications. The semi-active topology for the SMES-battery HESS is shown in Figure 7-1(a). This topology only has a single SMES chopper to control the

SMES magnet charge/discharge cycles and the battery is directly connected to the DC bus. Therefore, the semi-active control topology has the advantage of less use of electrical components. The semi-active circuit structure has been proposed for supercapacitor-battery HESS control [132, 239] and SMES-battery HESS control [126]. However, no previous research has built an experimental setup either for the semi-active or full-active control topologies. The battery is directly connected to the DC bus, which means the DC bus voltage is regulated by the battery terminal voltage. Therefore, in the semi-active control topology, the battery input/output power is uncontrollable.

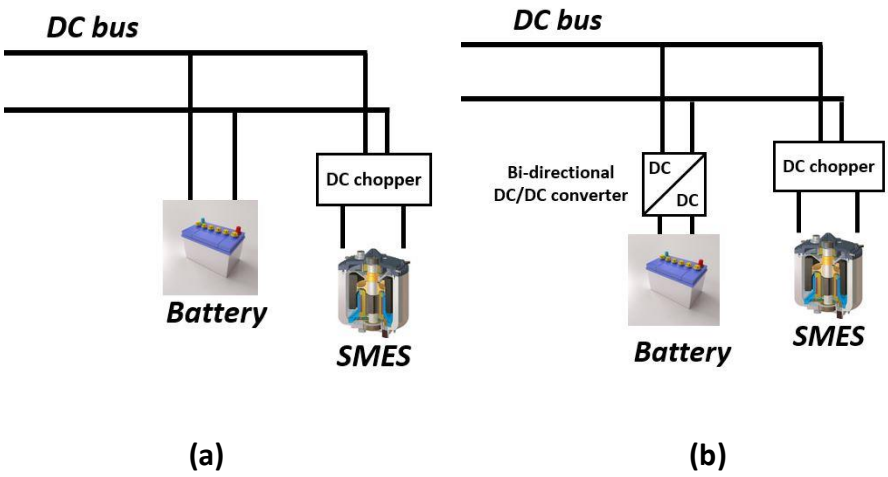

Figure 7-1(a) Semi-active topology and (b) full-active topology

In the experimental test platform, the semi-active control topology cannot effectively control the battery power output and affected the DC bus voltage. This is because the battery terminal voltage will slightly change under different battery states of charge. When the battery is fully charged, the battery terminal voltage is slightly higher than the rated terminal voltage and when the battery is fully discharged, the terminal voltage is much lower than the rated terminal voltage. The battery terminal voltage variation leads to DC bus voltage changes, which is not allowed in the power system.

Therefore, to achieve more advanced control of the hybridised system, the full-active control topology is advised to be used for the SMES-battery HESS. The full-active control topology is shown in Figure 7-1(b). The full-active control topology includes a bi-directional DC/DC converter for the battery to achieve the controllable power exchange between the battery and the power system.

In this study, the full-active control circuit has been built and tested. The semi-active circuit has a difficulty with maintaining the DC bus voltage due to the battery charge/discharge cycles affecting the battery terminal voltage which will not be used in this research [241, 242]. The full-active topology has the advantage of controllable power exchange between the energy storage systems and the power system. Therefore, the full-active control topology is applied to the SMES-battery HESS experimental platform.

7.3 Experimental platform preparation

7.3.1 SMES magnet preparation

In this research, the SMES is designed to be applied in the cryocooler in our lab. However, because of the sealing problem of the container, the cryocooler in our lab is not able to cool down the SMES magnet to 50 K. Therefore, the SMES will work in a liquid nitrogen bathed environment (working temperature approximately 77 K). The self-made SMES magnet is used in the HESS and the SMES magnet parameters are shown in Table 7-1.The measured SMES critical current is 42 A. According to the SMES magnet critical current calculation, described in chapter 3, the calculated SMES critical current at 77 K is 46 A, which is higher than the measured value. The critical current mismatch is caused by the winding process of the SMES coil. In future studies, the rest of the superconducting coils used in the 2.5 kJ SMES magnet will be wound using a winding machine. For safety reasons and also low joule losses in the SMES magnet, the SMES rated current is approximately 80% of the critical current, which is 33 A.

Table 7-1 SMES magnet parameters

Inner radius	45 mm
Outer radius	73 mm
Turn to turn distance	3 mm
Critical current	42 A
Working current	33 A
Inductance	14.65 mH
Number of pancake coils	2

7.3.2 SMES chopper design

The SMES chopper is designed to control the SMES magnet charge and discharge cycles. The SMES magnet needs continuous current flowing in the SMES magnet to store the magnetic energy. Therefore, the SMES chopper needs to build the closed loop for the current flowing in the SMES magnet. The electrical circuit for the SMES chopper is shown in Figure 7-2. Three states of the SMES chopper are described in the following sections.

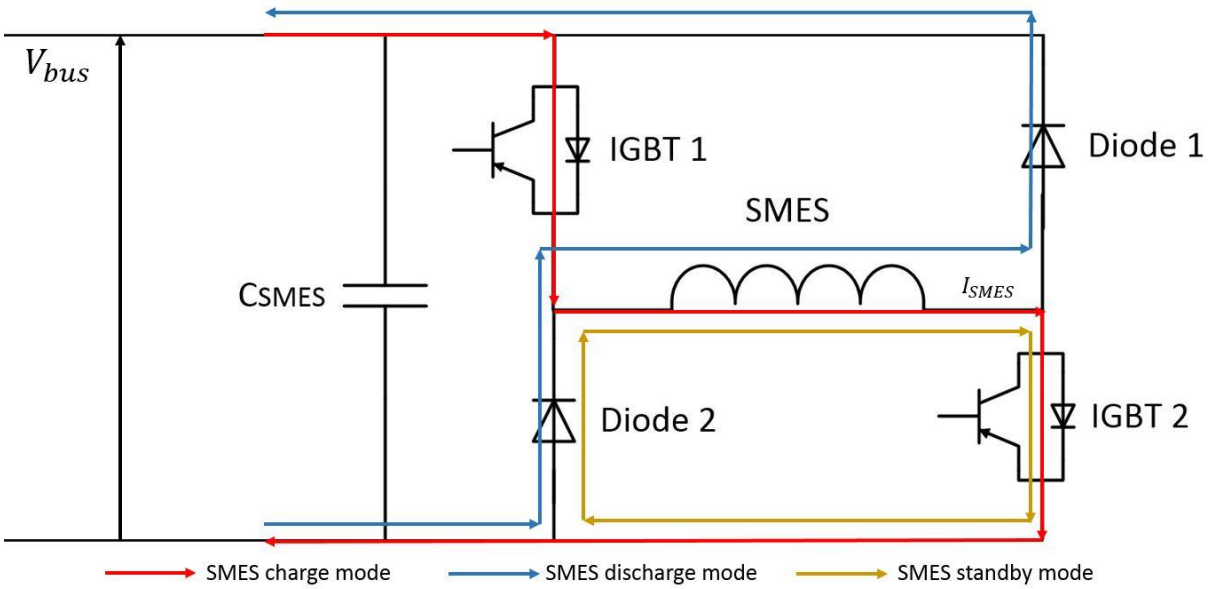

Figure 7-2 SMES chopper charge, discharge and standby

7.3.2.1 Charging mode:

The charging mode only works when the controller requests the SMES to absorb energy. In this situation, the current path in the SMES is shown in Figure 7-2. In this mode, IGBT 1 and IGBT 2 in Figure 7-2 are switched on to charge the SMES from the DC bus.

Applying Kirchhoff's voltage law (KVL), the SMES charge state can be represented by:

$$U - L\frac{dI(t)}{dt} - I(t)R_l = 0 \qquad 7\text{-}1$$

Where U is the DC bus voltage, L is the inductance of the SMES magnet, R_l is the equivalent self-resistance of the SMES magnet (which is mainly caused by the resistance of the power junctions in the SMES magnet), and $I(t)$ is the current in the SMES magnet at time t.

Assuming that the initial current in the SMES magnet is I_o, the instantaneous current in the SMES magnet can be represented by:

$$I(t) = I_o \exp\left(-\frac{R_l t}{L}\right) + \frac{U}{R_l}\left[1 - \exp\left(-\frac{R_l t}{L}\right)\right] \qquad 7\text{-}2$$

In this study, the inner resistance of the SMES magnet is neglected, which means that $R_l \approx 0$. Therefore, Eq. 7-2 can be simplified as:

$$I(t) = \frac{U}{L} t \times D + I_o \qquad 7\text{-}3$$

Where D is the duty ratio of the IGBT 1.

The power stored in the SMES can be calculated by:

$$E(t) = \frac{1}{2} L I^2(t) \qquad 7\text{-}4$$

7.3.2.2 Discharging mode

The current flow for the discharge mode is shown in Figure 7-2. For the discharging mode, IGBT 1 is off and the controller controls the duty cycle of IGBT 2 to achieve the desired output current I_{ref}.

For the discharge process, applying KVL to analyse the SMES discharge process yields:

$$-L\frac{dI(t)}{dt} + I(t)R_l + I(t)R = 0 \qquad 7\text{-}5$$

Assuming the initial current in the SMES is I_o, the current in the SMES at time t can be represented as:

$$I(t) = I_0 \exp[-\frac{(R + R_l)t}{L}] \qquad 7\text{-}6$$

Therefore, when the duty ratio for IGBT 2 is D, Eq. 7-6 can be simplified as:

$$I(t) = I_0 \exp -\frac{R \times t \times D}{L} \qquad 7\text{-}7$$

The SMES power output can be represented as:

$$P_{SMES}(t) = \frac{dE_{SMES}(t)}{dt} = \frac{d0.5 * I^2(t) * L}{dt} \quad 7\text{-}8$$

As can be seen from Eq. 7-8, the relationship between the SMES discharge duty ratio and the SMES output power are not linear. In this research, a PI controller is used to control the IGBTs for SMES discharge.

7.3.2.3 Standby mode

When the SMES does not need to exchange power from the power grid, the chopper needs to operate in standby mode to keep the power stored in the SMES. Due to the feature of the SMES, the chopper needs to frame an electrical closed loop to maintain the current flowing in the SMES magnet. The current path for the standby state is shown in Figure 7-2, which only requires IGBT 1 to be constantly held off and IGBT2 to be constantly held on.

In this study, the SMES chopper design, as shown in Figure 7-2, is used to control the SMES magnet in the lab-scale experimental platform.

7.3.3 Bi-directional DC/DC battery converter

Bi-directional DC/DC converters have the advantages of being able to track battery current capacity, high robustness and high efficiency [236, 243]. The battery DC/DC converter is shown in Figure 7-3.

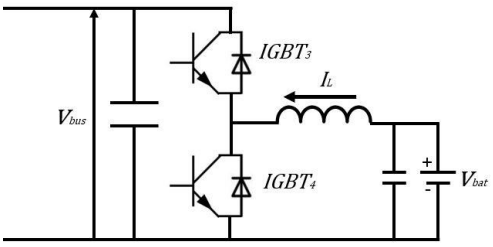

Figure 7-3 Battery DC/DC converter

When the system charges the battery, the $IGBT_4$ constantly off and change the duty cycle of $IGBT_3$ to charge the battery. The $IGBT_3$ Keeps off and change the duty cycle of $IGBT_4$ to discharge the battery.

7.3.4 HESS control loop design

7.3.4.1 Control board design

The control board is an essential component of the experiments. The PCB control board needs to integrate the gate drive module, digital signal processor (DSP), voltage measurement module and current measurement module. A TDK-Lambda KMS40-5 AC/DC converter is used to support the power for the whole PCB board. The AC/DC converter can only support a 5V DC voltage. Therefore, NMK0515SAC, LM3940IMP-3.3 and REF3025 DC/DC converters are used to convert the 5 V to 15 V DC, 3.3 V DC and 2.5 V DC, respectively, to supply the measurement module, DSP, gate drive module and OP-amp on the control board. The block diagram of the PCB design is shown in Figure 7-4.The PCB design is shown in Figure 7-5. The photo of the control board used in the experiment is shown in Figure 7-6.

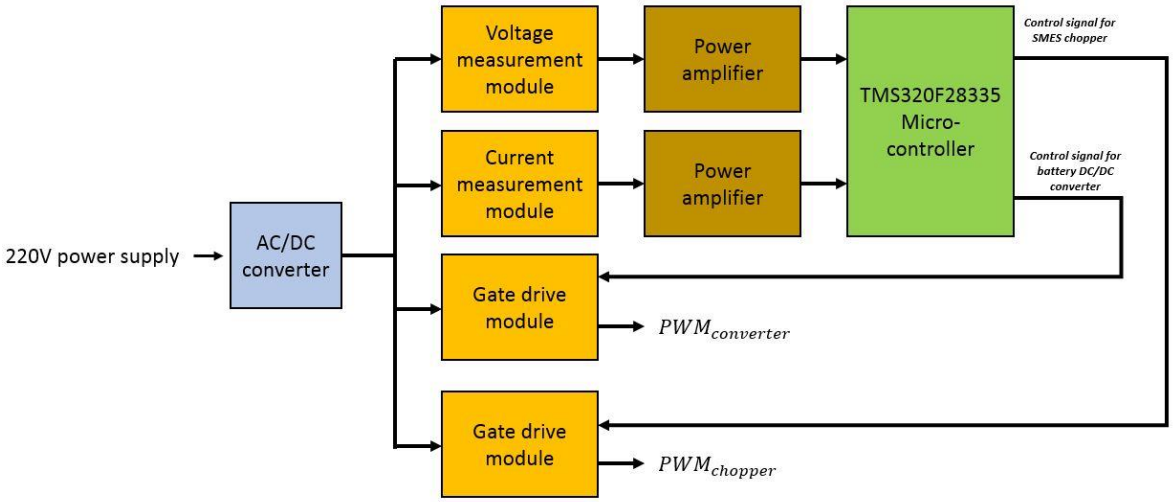

Figure 7-4 Block diagram of control board design

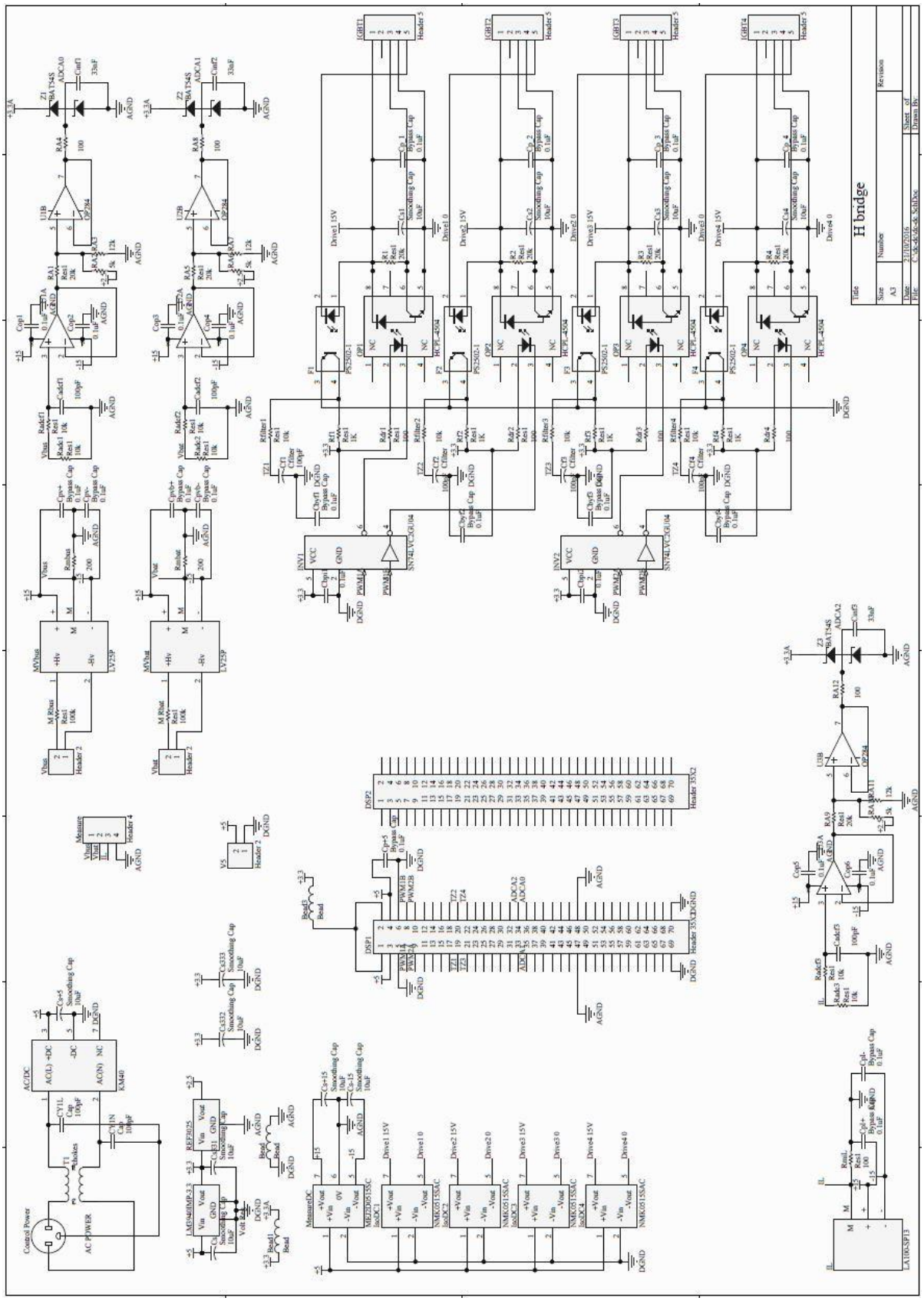

Figure 7-5 Control board PCB design

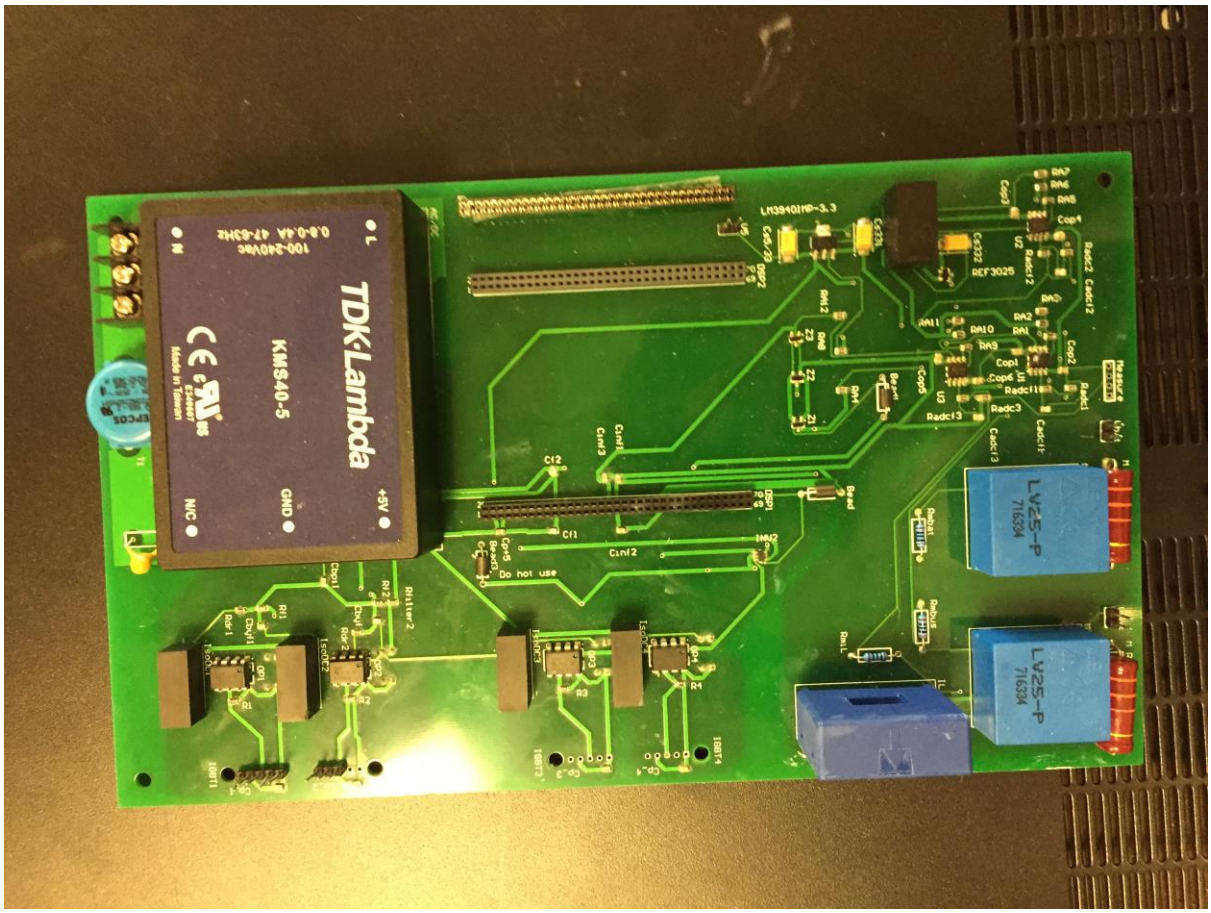

Figure 7-6 Control board in the experiment

7.3.4.2 TSM320F28335 microcontroller

The TSM320F28335 microcontroller, as shown in Figure 7-7, is used to implement the designed control algorithm and generate a physical PWM signal to control the IGBTs in the SMES chopper and battery DC/DC converter. The software is based on C programming language, which is easy to program. In the power application study, only limited modules are used such as the clock module, ADC (analogue-digital converter) module and PWM module.

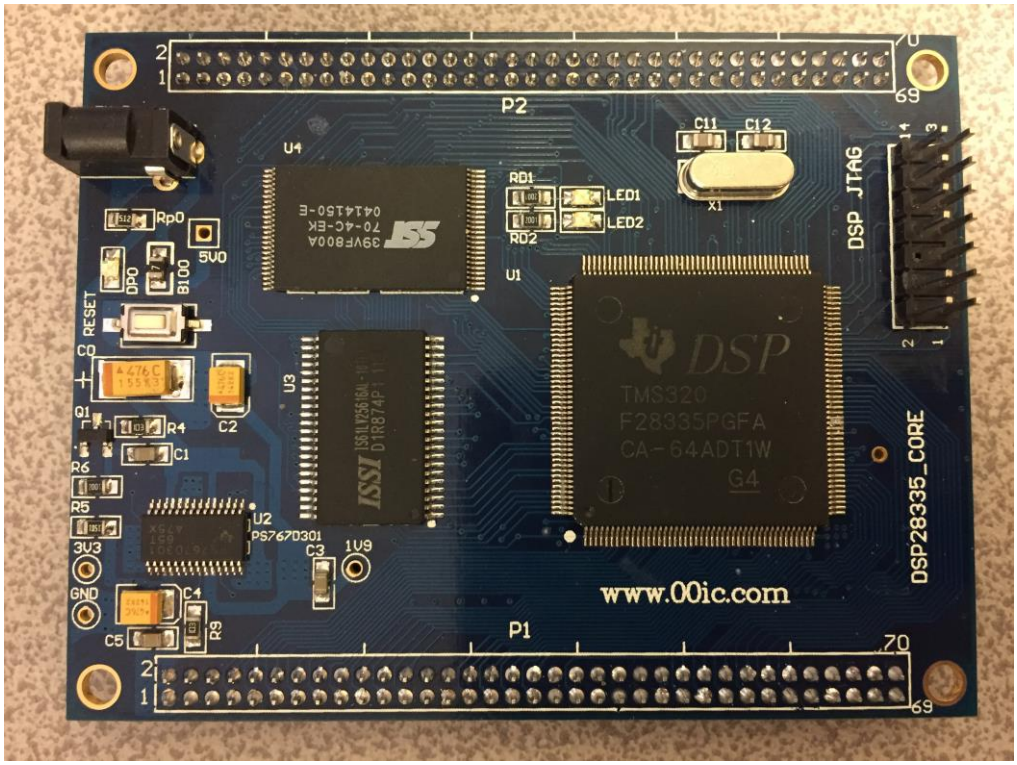

Figure 7-7 TMS320F28335 microcontroller board

7.4 SMES-battery HESS in lab-scale microgrid experimental platform setup

The experiments are a powerful tool for verification of the proposed SMES-battery HESS applied in the power system. In some respects, the simulations are easier to achieve. However, the accuracy of the power module in the numerical simulations needs to be validated. To some extent, the real-time experiments are more convenient than the numerical simulations. Furthermore, some experimental faults cannot be simulated in the numerical model, which makes the experimental study more important to verify the feasibility of the proposed method. However, it is a challenge to build a real domestic power system with a HESS involved in the laboratory environment at the University of Bath. Therefore, a lab scale microgrid with the SMES-battery HESS was built, as shown in Figure 7-8.

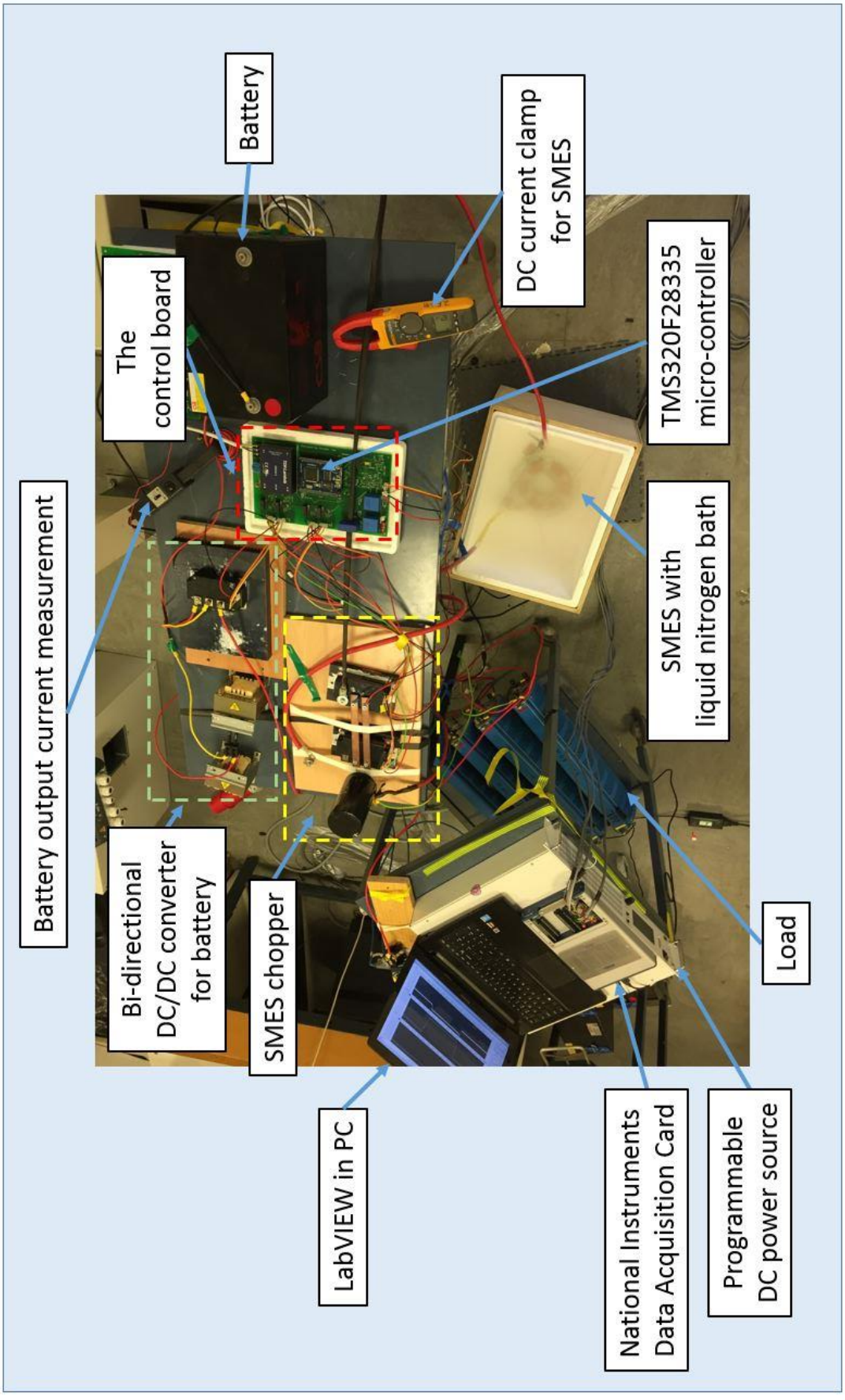

Figure 7-8 Experimental platform of the SMES-battery HESS

In this study, the SMES and battery HESS were built, as discussed previously, by using the full-active control topology. The TSM320F28335 was used in the experimental platform to control the HESS. The effectiveness of the experimental platform was analysed as follows:

- Verify the achievability of the SMES-battery HESS, which builds the foundation of further applications in the power system.
- The programmable microcontroller can program in different control methodologies and test the designed method in the lab.
- The experimental platform is isolated, which does not affect the main grid safety. In the future, the new proposed control method will be applied in this experimental platform first to test its robustness. It can also make sure that the new method is secure when applied in the power system.
- The main contribution of this study is the design of the HESS concept and the power sharing method of the SMES and battery energy storage system. The lab scale experimental platform is the small-scale power system, which also shows the achievability of the SMES and battery hybridisation can be applied in the power system.
- Test the control method of coordinating two different types of energy storage systems. (The SMES is a current source energy storage system and the battery is a voltage type energy storage system.)
- The newly built HESS system is highly modular. By adding different external electrical circuits with the HESS, the experimental platform can create different faults in the microgrid system to test the performance of the HESS under different scenarios.

Therefore, it is essential and reasonable to establish the SMES-battery HESS experimental platform. The platform can be used to study the SMES-battery HESS's ability to deal with different faults. Furthermore, the programmable controller can apply different control algorithms for the HESS to test the different control methods performance.

7.5 SMES-battery HESS in lab scale microgrid application

A two-stage method with PI-droop control is programmed into the TMS320F28335 microcontroller to test the control method described in chapter 6. The control method and research background have been previously discussed in chapter 6.

In this case study, the SMES-battery HESS is applied in the DC microgrid to verify the new proposed two-stage control method for the voltage drop application, as discussed in chapter 6. The external electrical circuit used to create the DC voltage drop is added in the SMES-battery HESS, as discussed in section 7.4. To the author's best knowledge, there has been no published literature on any experimental work related to an SMES-battery HESS experimental platform. The experimental structure for the HESS to deal with voltage drop applications is shown in Figure 7-9. The LAB/SMS5300 programmable DC power source is used to represent the main power grid, and the high power resistive load represents the load in the system. The microgrid disconnection process is created by the programmable DC power source. As discussed previously, the control algorithm is applied in the microcontroller TMS320F28335 to control the SMES chopper and battery DC/DC converter.

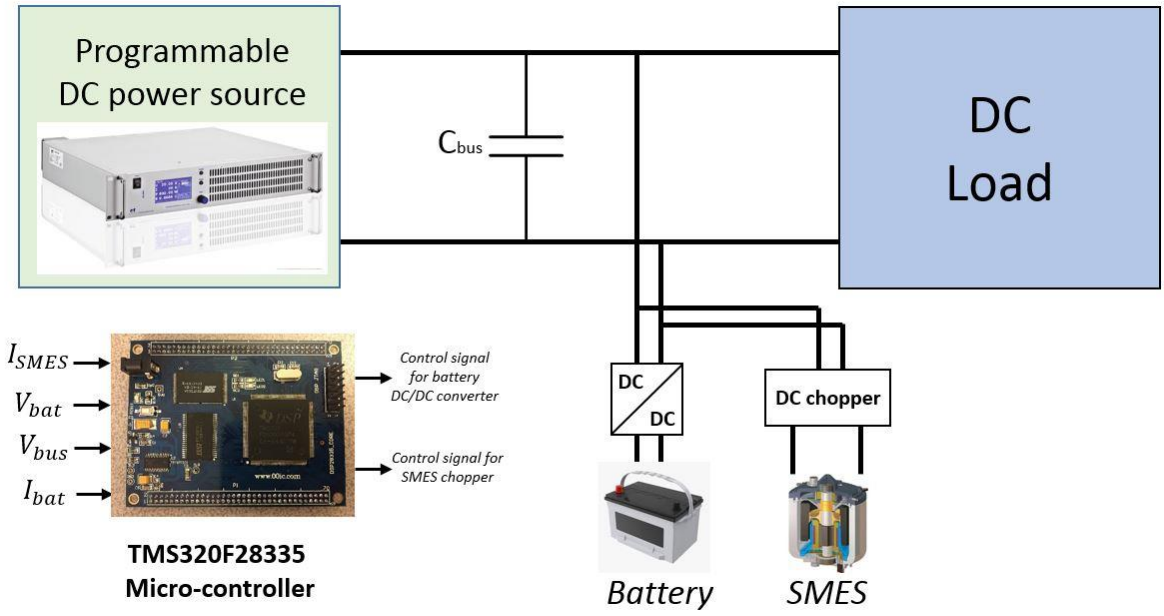

Figure 7-9 Laboratory experimental platform configuration

A National Instruments (NI) data acquisition card is used to collect measurement data of the load voltage, SMES current, battery current output and battery terminal voltage.

In this case study, the SMES initial current is zero and the battery is at its rated energy capacity. The controller starts to charge the SMES when the DC bus is at the rated value. After the HESS is at its rated capacity, the HESS turns into standby mode. When the microgrid is disconnected from the main grid (a voltage drop appears on the load), the two-stage control method is applied for the HESS to charge the DC load and keep the DC bus voltage stable. Moreover, SMES charge mode modification were made for the HESS control during the experimental study.

7.5.1 SMES charge state modification

In the previous SMES-battery HESS investigations in the literature, most of the researchers charged the HESS with unfixed input power such as using PI control [27], droop control [56] and the filtration method [125] to charge the HESS. These methods charge the SMES and battery with unfixed power. However, during the experimental study, it was found that the unfixed power injected into the HESS can cause system bus voltage fluctuation. That is because the HESS is acting as a high-power load when it is charged. The high fluctuating power demand of the energy storage system causes the power system to become unstable.

To make the power system stable and to enhance the power system's robustness, a new HESS charging methodology has been developed. The new control method charges the HESS with a fixed power. Therefore, the HESS is charged by the fixed power and is equivalent to a fixed load in the power system.

In this study, once the SMES magnet get charged from fully discharged mode, the SMES current is charged to slightly higher value than the designed operating current but lower than the SMES magnet critical current. This is used to help the quench detection in the future study. Because resistance will appear on the SMES magnet when the quench happens. The higher current makes the voltage across the quench point has higher voltage which helps the quench detection circuit to detect the quench easily.

The new proposed method is applied in the new proposed two-stage method for the microgrid application. The simulation results and control algorithm have been previously discussed in chapter 6.

7.5.2 Experimental results

7.5.2.1 Case one: SMES-battery HESS response for the microgrid decoupled

The real time operation of the experimental HESS is aiming to test the full-active control topology of the SMES-battery HESS system's performance and the new proposed control algorithm. The experiments can also test the sizing design of the two-stage method for the microgrid disconnection process application.

To test the SMES-battery HESS performance, one whole cycle response of the SMES-battery HESS to deal with microgrid connection and disconnection from the main grid was investigated with the SMES and battery charged by the power system when the system connects to the main grid. When the HESS is at its rated energy capacity, the HESS turns into its standby mode. When the system detects that a voltage drop occurs, which means that the microgrid has disconnect from the main grid, the two-stage method is applied to compensate for the voltage drop. When the microgrid reconnects to the main grid, the SMES and battery get charged by the modified charge control methodology to its rated energy capacity. Moreover, the experimental results can be used to compare the simulation results and test the droop coefficient design. A properly designed droop coefficient value can make sure that the battery power output can adequately compensate for the load demand when the SMES is fully discharged. A short time power source disconnection is created by the programmable DC power source to represent the microgrid disconnection from the main grid. The experimental results are shown in Figure 7-10.

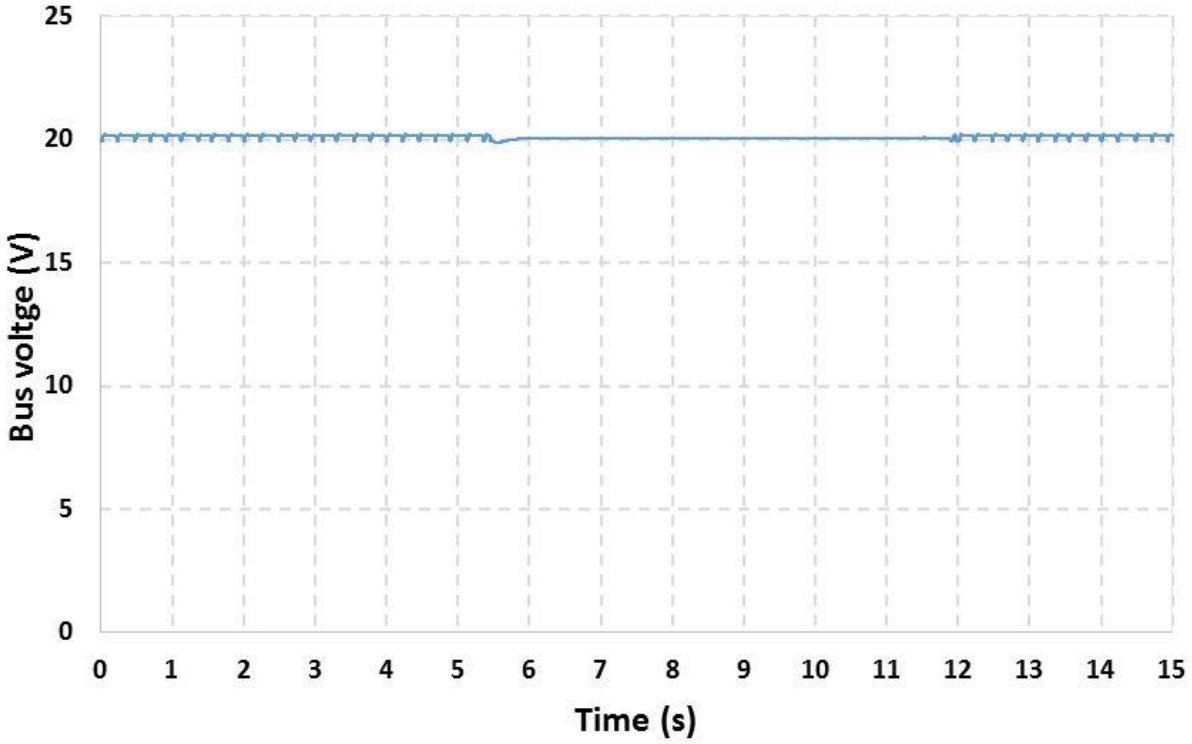
Bus voltge (V)
25
20
15
10
5
0
0 1 2 3 4 5 6 7 8 9 10 11 12 13 14 15
Time (s)

(a)

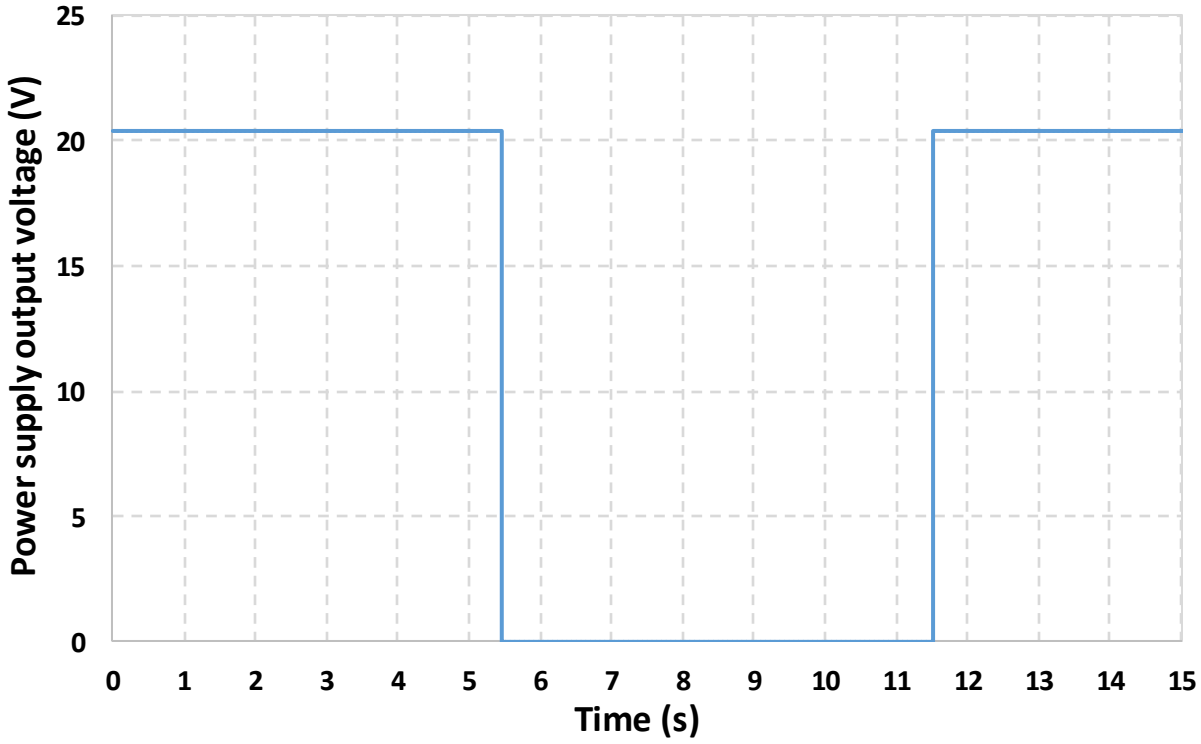
Power supply output voltage (V)
25
20
15
10
5
0
0 1 2 3 4 5 6 7 8 9 10 11 12 13 14 15
Time (s)

(b)

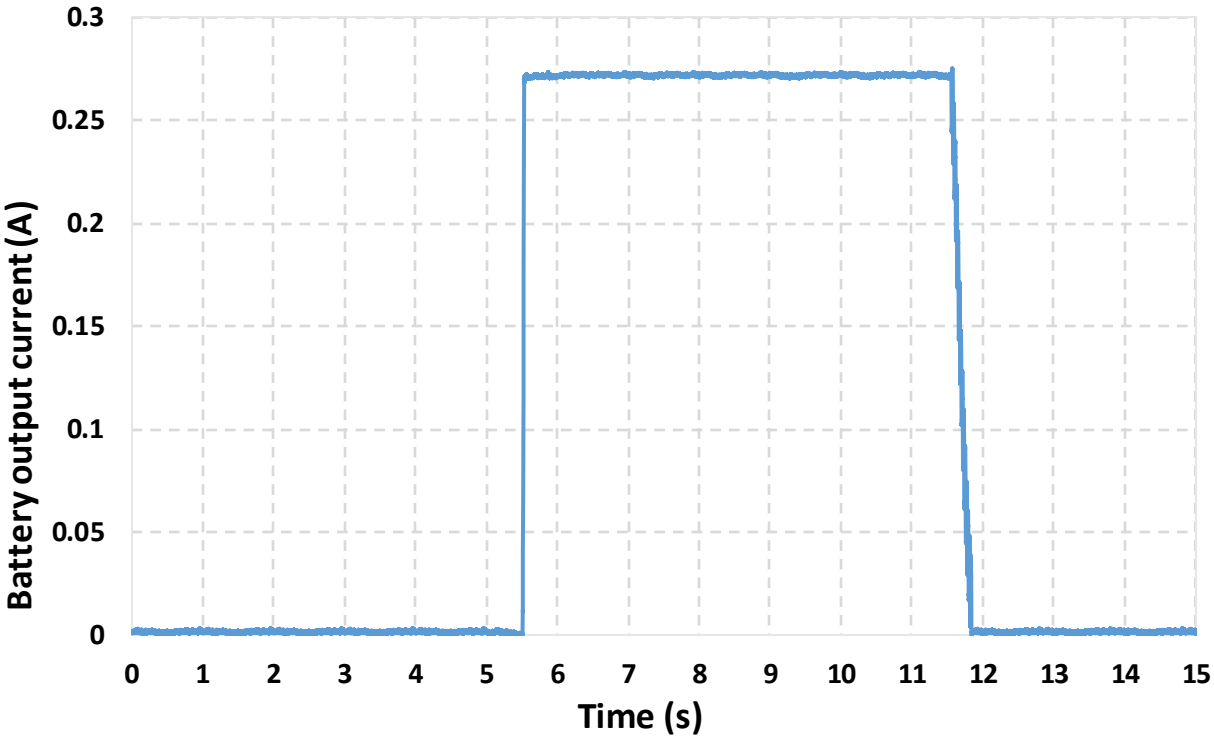

(c)

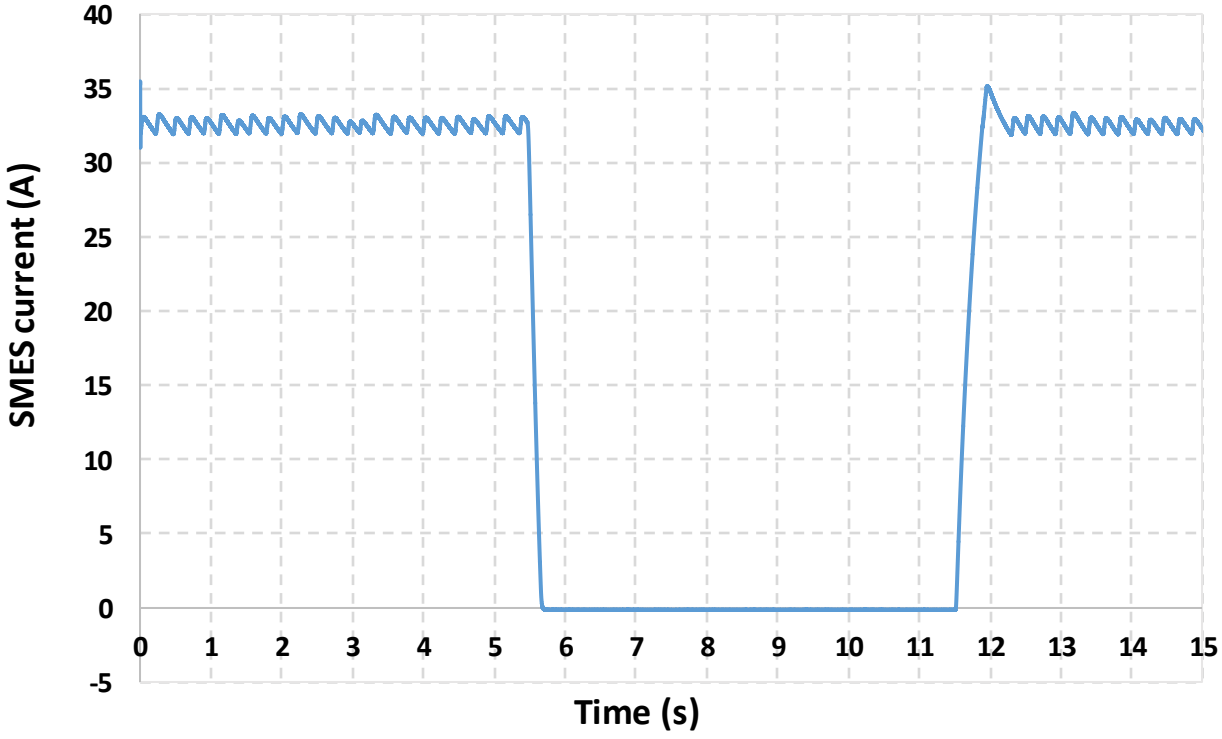

(d)

Figure 7-10 Experimental result for SMES-battery HESS to deal with one microgrid decoupling: (a) microgrid bus voltage (b) main grid support voltage (c) battery output current (d) SMES current

As can be seen from Figure 7-10, the voltage drop occurs at time 5.52 s. According to Figure 7-10(a) and Figure 7-10(b), the HESS is able to compensate for the voltage drop when the voltage drop occurs. The SMES current and the battery output current are shown in Figure 7-10(c) and 7-9(d). The SMES current is 33 A and the battery has no power output when the microgrid connects to the main grid. The SMES operating current is determined by the SMES magnet, which was measured in section 7.3.1. Moreover, the battery output current reaches the required output current to compensate for the power demand when the SMES is fully discharged. This shows that the drop coefficient design is successful, which is because the battery power output is constantly increased when the voltage drop occurs. The constantly increasing battery output current also matches the simulation results previously discussed in chapter 6.

As can be seen from Figure 7-10(a), a small voltage ripple occurs when the HESS is working in its standby state. The small voltage ripple is approximately 0.2 V in this experiment. This is because the eddy current losses of the semiconductors in the SMES chopper decrease the energy stored in the SMES magnet. And the SMES magnet needs a small amount of power to be injected into the SMES, which is equivalent to a small amount of power demand of the power system frequently appears. The voltage ripple will be negligible when the SMES size increases. That is because when the SMES size increases, the eddy current losses consume a smaller percentage of power in the power system.

7.5.2.2 Case two: SMES-battery HESS response for multi-times microgrid decoupled in long time duration

In this study, different time durations of the microgrid disconnection cycle from the utility grid was studied. The experimental results are shown in Figure 7-11. This was to study the proposed HESS control method achievability in long-term operation. The main grid connect/disconnect time is random, which is used to simulate the operation of the microgrid in the power system.

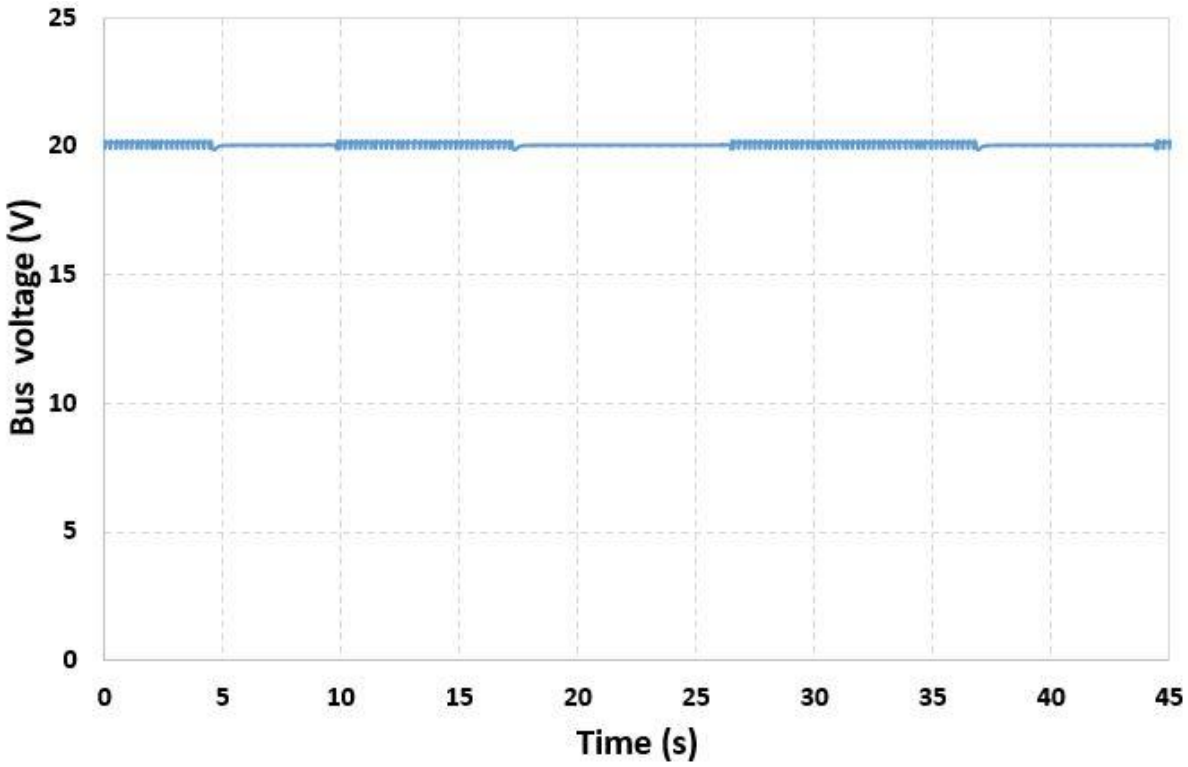
Bus voltage (V)
25
20
15
10
5
0
0
5
10
15
20
25
30
35
40
45
Time (s)

(a)

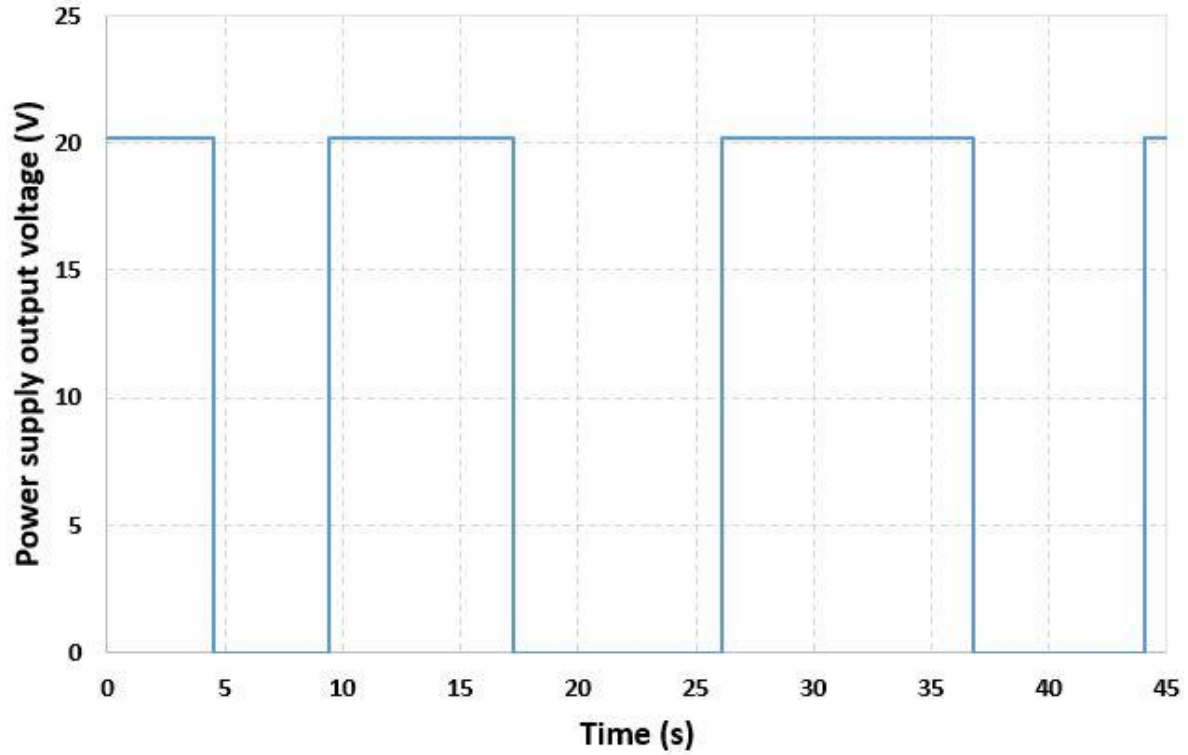
Power supply output voltage (V)
25
20
15
10
5
0
0
5
10
15
20
25
30
35
40
45
Time (s)

(b)

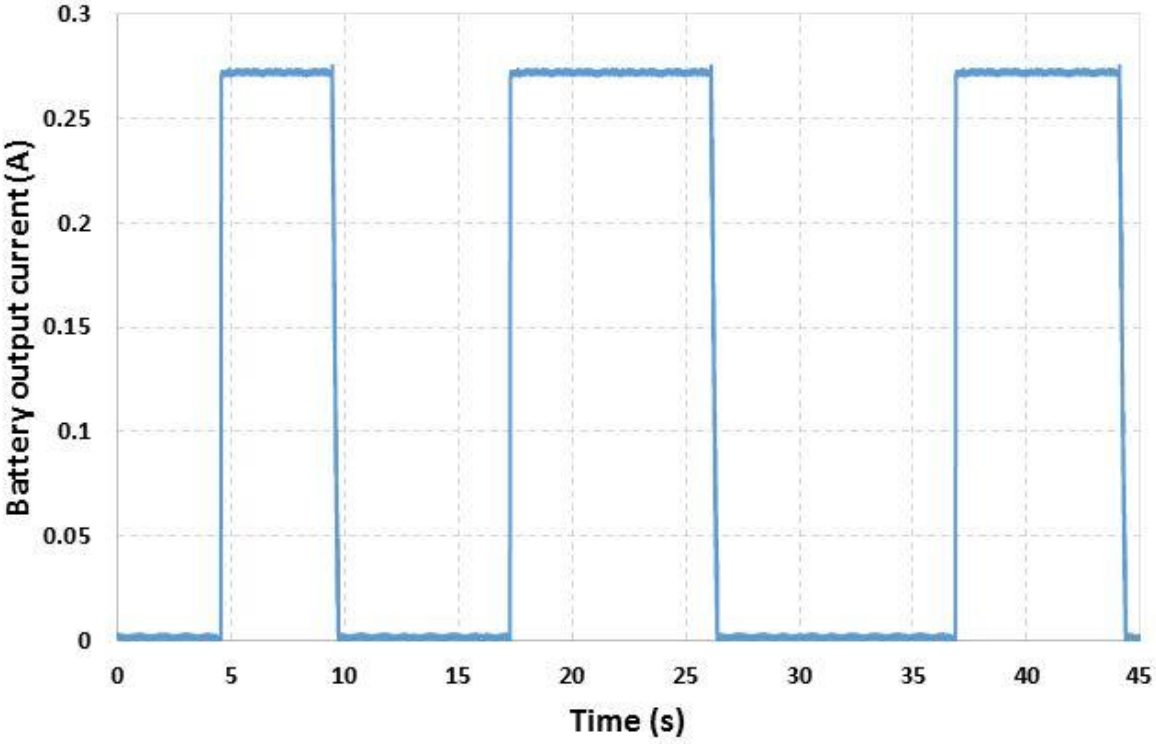

(c)

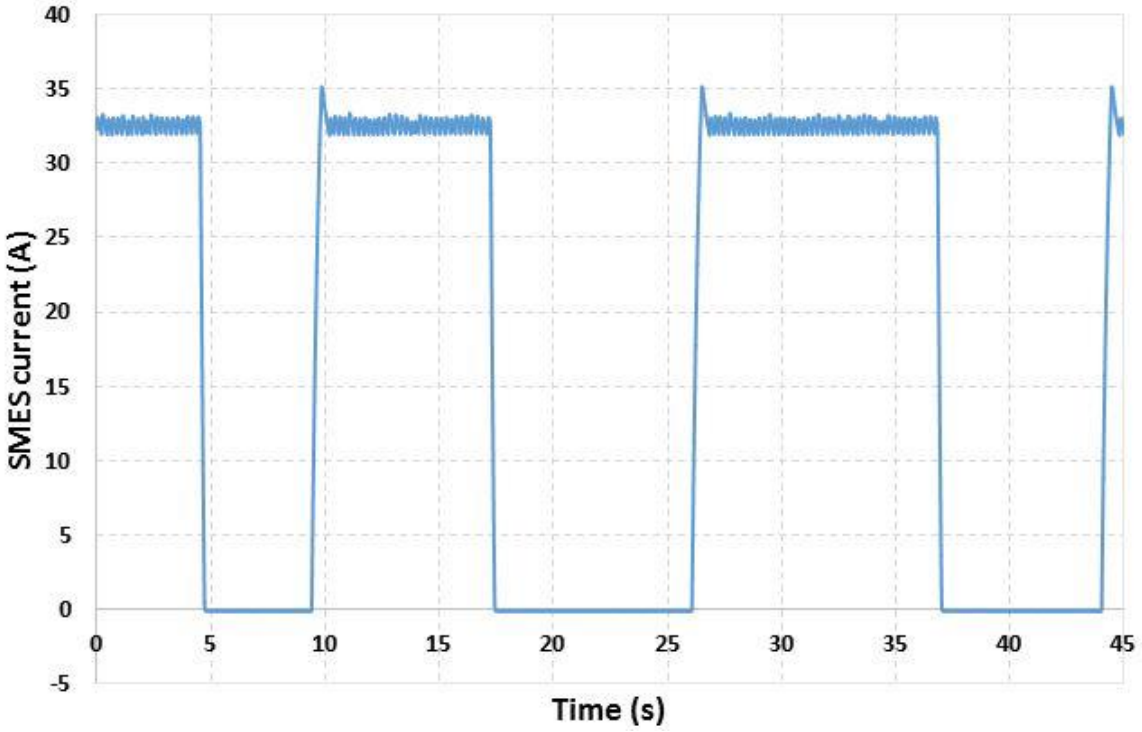

(d)

Figure 7-11 Experimental result for SMES-battery HESS deal with multi-times microgrid decoupling: (a) microgrid bus voltage (b) main grid support voltage (c) battery output current (d) SMES current

As can be seen from experimental results, the SMES-battery HESS used to stabilize the bus voltage during the time the power source connect and disconnect from the microgrid. The microgrid islanded state operating time is randomly selected. From the beginning, the microgrid connect to the main grid and the SMES is fully charged and battery has no power output. When the bus voltage drop occurs, the HESS starts to discharge to keep the bus voltage at the rated value. When the main grid reconnect to the microgrid, the SMES get charged to 100% SOC to prepare for the next operation. At the time 17 second, the microgrid decoupled from the main grid. The HESS is able to support the bus voltage to the rated value. The experiment shows good performance on stabilizing the bus voltage and reliable performance for multi-times of microgrid decoupling process.

In conclusion, this experiment applies three different power support disconnection durations to represent multi-times of microgrid connection/disconnection from the utility grid. The experimental results show that the proposed method is able to compensate for the power demand and stabilise the bus voltage for long term application.

7.5.3 Comparison of the battery with/without SMES integrated for the microgrid decoupling application

An experiment of a battery only system to compensate for the microgrid power demand was also conducted. The same DC voltage drop external circuit was used. The DC/DC converter boost mode control was applied in the microcontroller to control the battery DC/DC converter. The boost mode has the advantage of high robustness and is able to constrain the battery current output.

The battery performance comparison of the HESS and BESS for the microgrid decoupled application is shown in Figure 7-12.

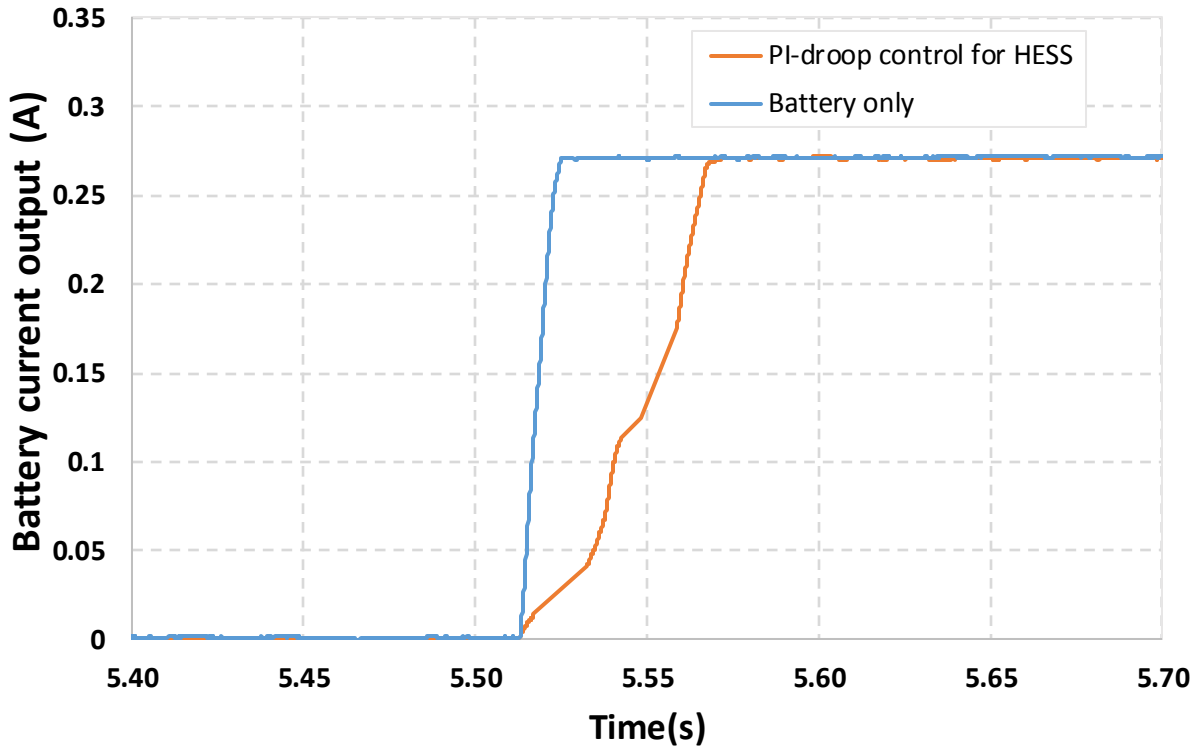

Figure 7-12 Battery current output performance for the HESS and battery only system

According to the experimental results, the HESS with PI-droop control has a lower battery discharging rate compared with the battery only system when dealing with same power demand. Due to the SMES hybridisation, the battery in the HESS has 0.06 seconds more time to reach its rated current output. Moreover, the lower discharging rate also helps to extend battery service lifetime. Both the battery only system and the SMES-battery HESS reach the same power output, which is because the SMES is fully discharged and not able to support any power to the system.

According to the comparison of the HESS and BESS, the HESS with the proposed two-stage control method has the advantage of a lower battery discharging rate, which can be used to extent battery service lifetime and decrease the requirement of the battery maximum discharging rate.

7.5.4 Result analysis

The experimental results show that the SMES-battery HESS has the advantage of extended battery response time compared with the battery only system. Moreover, the battery maximum output power discharging rate also affects the microgrid security. For the battery only system, with a low maximum discharging rate, the battery energy storage system needs time to reach the microgrid power demand. During the time the battery output power is climbing, the energy storage system is not able to compensate for the microgrid power demand, which causes the microgrid voltage to become unstable and even potentially lead to microgrid collapse. For the SMES-battery HESS, the battery discharge current steadily rises to the rated current, which is because the SMES compensates for the power demand when the battery output current is increasing.

The experimental results also show that the full-active topology is suitable for SMES-battery HESS applications. Moreover, the experimental result also show that the control method coded in the DSP is able to control the SMES-battery HESS.

The experiment platform helps to verify the feasibility of the two-stage control method used in the lab-scale microgrid. This also proves the feasibility of the SMES-battery HESS using the microgrid to cope when the microgrid is decoupled. The experimental results show that the two-stage control method is able to stabilise the microgrid voltage and extend battery response time. With the SMES integrated into the microgrid, the SMES can prevent the battery from sudden output current changes and hence, extend the battery discharging response time for 0.06 seconds in the experiments, which is beneficial to extend battery service lifetime. The experiments of multiple microgrid connection/disconnection cycles from the main grid prove the proposed method is able to compensate for the power demand.

Moreover, the experiments also prove the sizing design of the two-stage method is well designed. The experimental results show that the SMES is fully discharged when the battery output is able to compensate for the microgrid power demand.

7.6 Conclusions

In this chapter, the SMES-battery HESS control circuit has been investigated. The SMES-battery HESS working in the DC network system has been built to test its reliability. Moreover, the control method proposed in chapter 6 has been verified on the experimental platform. The sizing design and droop coefficient have also been tested in the experiments. The experimental results show that the proposed method is able to handle the microgrid power demand when disconnected from the main grid and allocate different power demands for the battery and SMES.

Moreover, this chapter also investigated the battery performance for the SMES-battery HESS and battery only systems. The results show that with the SMES hybridised, the battery has a lower discharging rate. The lower discharging rate and longer battery response time results in the battery having a longer service lifetime.

In conclusion, the SMES-battery HESS has the advantage of extended battery service lifetime. The experimental platform built in this study investigated the reliability and controllability of the SMES-battery HESS. The full-active control topology was selected to control the HESS. According to the experimental results, the semi-active control topology was not able to control the SMES-battery topology. In further research, the HESS experimental setup can be applied to different applications by changing the external circuit connected to the HESS for testing the HESS working performance.

Chapter 8 Conclusions

8.1 Summary

This research is about the investigation of the SMES-battery hybrid energy storage system scheme for the SMES design, HESS system establishment, control method, and energy management method improvement for the microgrid application. Both the experimental platform and the numerical model have been built to test the proposed hybrid system with a novel method. The accomplished results are listed below:

- The SMES magnet design is an important step for the SMES-battery hybrid energy storage design and manufacturing. In this study, as shown in chapter 3, an improved SMES magnet structure design process has been developed. The proposed method is able to design the SMES magnet with the required energy capacity for the HESS, demonstrated in case studies of 2.5 kJ and 0.9 MJ SMES magnet structure. The 2.5 kJ SMES magnet is intended to be used in the SMES-battery HESS experimental platform. In the future SMES system experiment, different sizes of SMES magnet structure can

be designed by the developed SMES magnet design method for alternative applications.

- The increasing of the SMES power capacity is one key advantage of the SMES magnet design. In this study, the Roebel cable is considered to wind the SMES magnet to achieve a higher power capacity and a feasibility study of using the Roebel cable to wind the SMES magnet has been done as shown in chapter 4. The results show that even though the Roebel cable has a higher current capacity, the weak mechanical stability affects its application on the SMES magnet. Moreover, the Roebel cable power joint design is another difficulty for the SMES magnet manufacturing. Therefore, according to the feasibility research, the Roebel cable power joint connection and epoxy impregnation of the Roebel cable require further improvement before applying the Roebel cable into SMES magnet.
- In chapter 5, using the fuzzy logic controller to regulate the power sharing between the battery and the SMES in the hybrid energy storage system has been developed in this thesis. The new method considers the power demand, battery output power changes and SMES SOC. The fuzzy logic controller controls the HESS based on the human knowledge and designers' experiences to allocate the power sharing of the battery and the SMES. The proposed method has the advantage of preventing the situation of only the battery dealing with highly fluctuating power demand, spreading the response across the system. Moreover, the proposed method is able to control the battery with a more stable output. The fuzzy logic design rules are described in this thesis. To verify this method, a case study has been done to compare the proposed method with the filtration energy management method. The simulation results show that the proposed method has a better performance in enhancing the battery performance, extending the battery service lifetime.
- In chapter 6, the two-stage energy management method with the new PI-droop controller is developed to control the SMES and battery HESS performance when the microgrid is decoupled. The proposed method has the advantage of improving the HESS performance when the microgrid switches to the islanded mode. The new approach combines the PI controller and droop controller to control the HESS to achieve better performance on stabilizing the load voltage. The simulation results show that the proposed method can control the battery with a lower maximum

discharge power and faster responding speed than the filtration method. This demonstrates that the proposed method has better performance on decreasing the battery attenuation process.

- In chapter 7, the experimental platform of the SMES-battery HESS has been established to test the proposed HESS reliability and achievability. These experimental results show that the full-active topology is more suitable for the HESS control circuit compared with the semi-active control circuit topology. The proposed PI-droop control method is applied in the experimental platform and shows good performance on controlling the HESS. This experimental platform is very meaningful for the battery-SMES hybrid energy storage applications, testing the performance of the designed control method before applying these control method into a real power system.

8.2 Future work

In the numerical simulation, the SMES is represented by the ideal inductance which means it has zero resistance and high inductance. However, this method is not accurate. Therefore, the detail device-level modelling of the SMES magnets needs to be done. The new SMES magnet model must consider the power joint resistance in the SMES magnet. Moreover, due to the current through the HTS, a small resistance appears which the new model must consider in the HTS characteristics. Due to the SMES frequent charging/discharging, the AC losses of the HTS will be generated. Combining the AC losses calculation with the power system application is another topic for the SMES applications.

In the SMES-battery HESS experimental platform, the quench protection is very simple. In further study, a detailed study of the quench detection and quench protection in the HESS experimental platform will be a novel point. The interaction between the quench protection method and HESS control method will generate innovative ideas about the HESS control strategy. Moreover, after the quench protection and detection method have been developed and tested, the SMES can be applied in the cryocooler to make the SMES have a lower working temperature and higher energy capacity.

Moreover, by using the existing SMES-battery HESS experimental platform, more applications and novel proposed control methods can be represented in the lab. For example, the SMES-battery HESS can be combined with a superconducting fault current limiter to cut faults in the DC network. When a fault happens, the SMES can absorb the fault current to make the DC breaker is able to cut off the faulted line.

The HESS sizing optimization needs to be done in future studies. The optimization study needs to decide the best energy capacities of the SMES and the battery for different scales of power demands and system sizes. Moreover, it needs to consider the overall economic costs and battery service lifetimes when sizing the SMES and the battery.

References

[1] A. Vijay and A. Hawkes, "Impact of dynamic aspects on economics of fuel cell based micro co-generation in low carbon futures," *Energy,* vol. 155, pp. 874-886, 2018.

[2] K. Tapia-Ahumada, I. Pérez-Arriaga, and E. J. Moniz, "A methodology for understanding the impacts of large-scale penetration of micro-combined heat and power," *Energy policy,* vol. 61, pp. 496-512, 2013.

[3] S. A. Kalogirou, "Building integration of solar renewable energy systems towards zero or nearly zero energy buildings," *International Journal of Low-Carbon Technologies,* vol. 10, pp. 379-385, 2013.

[4] T. Li, R. Wang, J. K. Kiplagat, and Y. Kang, "Performance analysis of an integrated energy storage and energy upgrade thermochemical solid–gas sorption system for seasonal storage of solar thermal energy," *Energy,* vol. 50, pp. 454-467, 2013.

[5] B. Zakeri and S. Syri, "Electrical energy storage systems: A comparative life cycle cost analysis," *Renewable and Sustainable Energy Reviews,* vol. 42, pp. 569-596, 2015.

[6] P. D. Lund, J. Lindgren, J. Mikkola, and J. Salpakari, "Review of energy system flexibility measures to enable high levels of variable renewable electricity," *Renewable and Sustainable Energy Reviews,* vol. 45, pp. 785-807, 2015.

[7] X. Luo, J. Wang, M. Dooner, and J. Clarke, "Overview of current development in electrical energy storage technologies and the application potential in power system operation," *Applied energy,* vol. 137, pp. 511-536, 2015.

[8] O. Schmidt, A. Hawkes, A. Gambhir, and I. Staffell, "The future cost of electrical energy storage based on experience rates," *Nature Energy,* vol. 2, p. 17110, 2017.

[9] H. Lund and G. Salgi, "The role of compressed air energy storage (CAES) in future sustainable energy systems," *Energy Conversion and Management,* vol. 50, pp. 1172-1179, 2009.

[10] P. Kushwaha and C. Bhende, "Single-phase rooftop photovoltaic based grid-interactive electricity system," in *India Conference (INDICON), 2016 IEEE Annual*, 2016, pp. 1-6.

[11] J. Li, Q. Yang, P. Yao, Q. Sun, Z. Zhang, M. Zhang*, et al.*, "A novel use of the hybrid energy storage system for primary frequency control in a microgrid," *Energy Procedia,* vol. 103, pp. 82-87, 2016.

[12] C. J. Bennett, R. A. Stewart, and J. W. Lu, "Development of a three-phase battery energy storage scheduling and operation system for low voltage distribution networks," *Applied Energy,* vol. 146, pp. 122-134, 2015.

[13] S. Singh, M. Singh, and S. Kaushik, "A review on optimization techniques for sizing of solar-wind hybrid energy systems," *International Journal of Green Energy,* vol. 13, pp. 1564-1578, 2016.

[14] H. Zhao, Q. Wu, S. Hu, H. Xu, and C. N. Rasmussen, "Review of energy storage system for wind power integration support," *Applied Energy,* vol. 137, pp. 545-553, 2015.

[15] M. Aneke and M. Wang, "Energy storage technologies and real life applications–A state of the art review," *Applied Energy,* vol. 179, pp. 350-377, 2016.

[16] S. O. Amrouche, D. Rekioua, T. Rekioua, and S. Bacha, "Overview of energy storage in renewable energy systems," *International Journal of Hydrogen Energy,* vol. 41, pp. 20914-20927, 2016.

[17] S. Few, O. Schmidt, G. J. Offer, N. Brandon, J. Nelson, and A. Gambhir, "Prospective improvements in cost and cycle life of off-grid lithium-ion battery packs: An analysis informed by expert elicitations," *Energy Policy,* vol. 114, pp. 578-590, 2018.

[18] M. Abdel-Monem, O. Hegazy, N. Omar, K. Trad, P. Van den Bossche, and J. Van Mierlo, "Lithium-ion batteries: Comprehensive technical analysis of second-life batteries for smart grid applications," in *Power Electronics and Applications (EPE'17 ECCE Europe), 2017 19th European Conference on*, 2017, pp. P. 1-P. 16.

[19] J. Li, Q. Yang, F. Robinson, F. Liang, M. Zhang, and W. Yuan, "Design and test of a new droop control algorithm for a SMES/battery hybrid energy storage system," *Energy,* vol. 118, pp. 1110-1122, 2017.

[20] L. W. Chong, Y. W. Wong, R. K. Rajkumar, R. K. Rajkumar, and D. Isa, "Hybrid energy storage systems and control strategies for stand-alone renewable energy power systems," *Renewable and sustainable energy reviews,* vol. 66, pp. 174-189, 2016.

[21] W. Jing, C. H. Lai, W. S. Wong, and M. D. Wong, "Dynamic power allocation of battery-supercapacitor hybrid energy storage for standalone PV microgrid applications," *Sustainable Energy Technologies and Assessments,* vol. 22, pp. 55-64, 2017.

[22] W. Jing, C. H. Lai, W. S. Wong, and M. D. Wong, "A comprehensive study of battery-supercapacitor hybrid energy storage system for standalone PV power system in rural electrification," *Applied Energy,* vol. 224, pp. 340-356, 2018.

[23] D. B. W. Abeywardana, B. Hredzak, and V. G. Agelidis, "A fixed-frequency sliding mode controller for a boost-inverter-based battery-supercapacitor hybrid energy storage system," *IEEE Transactions on Power Electronics,* vol. 32, pp. 668-680, 2017.

[24] L. W. Chong, Y. W. Wong, R. K. Rajkumar, and D. Isa, "Modelling and Simulation of Standalone PV Systems with Battery-supercapacitor Hybrid Energy Storage System for a Rural Household," *Energy Procedia,* vol. 107, pp. 232-236, 2017.

[25] Z. Song, J. Hou, H. Hofmann, J. Li, and M. Ouyang, "Sliding-mode and Lyapunov function-based control for battery/supercapacitor hybrid energy storage system used in electric vehicles," *Energy,* vol. 122, pp. 601-612, 2017.

[26] X. Lin and Y. Lei, "Coordinated Control Strategies for SMES-Battery Hybrid Energy Storage Systems," *IEEE Access,* vol. 5, pp. 23452-23465, 2017.

[27] H. Alafnan, M. Zhang, W. Yuan, J. Zhu, J. Li, M. Elshiekh*, et al.*, "Stability Improvement of DC Power Systems in an All-Electric Ship Using Hybrid SMES/Battery," *IEEE Transactions on Applied Superconductivity,* vol. 28, pp. 1-6, 2018.

[28] K. C. Omran and A. Mosallanejad, "SMES/battery hybrid energy storage system based on bidirectional Z-source inverter for electric vehicles," 2018.

[29] A. Malozemoff, S. Fleshler, M. Rupich, C. Thieme, X. Li, W. Zhang*, et al.*, "Progress in high temperature superconductor coated conductors and their applications," *Superconductor Science and Technology,* vol. 21, p. 034005, 2008.

[30] W. Yuan, *Second-generation high-temperature superconducting coils and their applications for energy storage*: Springer Science & Business Media, 2011.

[31] R. Gupta, M. Anerella, P. Joshi, J. Higgins, S. Lalitha, W. Sampson*, et al.*, "Design, construction, and testing of a large-aperture high-field HTS SMES coil," *IEEE Transactions on Applied Superconductivity,* vol. 26, pp. 1-8, 2016.

[32] A. Morandi, M. Fabbri, B. Gholizad, F. Grilli, F. Sirois, and V. M. Zermeño, "Design and comparison of a 1-MW/5-s HTS SMES with toroidal and solenoidal geometry," *IEEE Transactions on Applied Superconductivity,* vol. 26, pp. 1-6, 2016.

[33] X. Zhou, Y. Tang, S. Jing, C. Zhang, K. Gong, L. Zhang*, et al.*, "Cost Estimation Models of MJ Class HTS Superconducting Magnetic Energy Storage Magnets," *IEEE Transactions on Applied Superconductivity,* vol. 28, pp. 1-5, 2018.

[34] G.-D. Nam, H.-J. Sung, B.-S. Go, M. Park, and I.-K. Yu, "Design and Comparative Analysis of MgB2 and YBCO Wire-Based-Superconducting Wind Power Generators," *IEEE Transactions on Applied Superconductivity,* vol. 28, pp. 1-5, 2018.

[35] S. Pfenninger and J. Keirstead, "Renewables, nuclear, or fossil fuels? Scenarios for Great Britain's power system considering costs, emissions and energy security," *Applied Energy,* vol. 152, pp. 83-93, 2015.

[36] J.-J. Andreas, C. Burns, and J. Touza, "Overcoming energy injustice? Bulgaria's renewable energy transition in times of crisis," *Energy Research & Social Science,* vol. 42, pp. 44-52, 2018.

[37] X. Tan, Q. Li, and H. Wang, "Advances and trends of energy storage technology in Microgrid," *International Journal of Electrical Power & Energy Systems,* vol. 44, pp. 179-191, 2013.

[38] D.-J. Lee and L. Wang, "Small-signal stability analysis of an autonomous hybrid renewable energy power generation/energy storage system part I: Time-domain simulations," *IEEE Transactions on Energy Conversion,* vol. 23, pp. 311-320, 2008.

[39] P. F. Ribeiro, B. K. Johnson, M. L. Crow, A. Arsoy, and Y. Liu, "Energy storage systems for advanced power applications," *Proceedings of the IEEE,* vol. 89, pp. 1744-1756, 2001.

[40] P. Mercier, R. Cherkaoui, and A. Oudalov, "Optimizing a battery energy storage system for frequency control application in an isolated power system," *IEEE Transactions on Power Systems,* vol. 24, pp. 1469-1477, 2009.

[41] K. Divya and J. Østergaard, "Battery energy storage technology for power systems—An overview," *Electric Power Systems Research,* vol. 79, pp. 511-520, 2009.

[42] F. Zhang, C. Meng, Y. Yang, C. Sun, C. Ji, Y. Chen*, et al.*, "Advantages and challenges of DC microgrid for commercial building a case study from Xiamen university DC microgrid," in *DC Microgrids (ICDCM), 2015 IEEE First International Conference on*, 2015, pp. 355-358.

[43] H. Talei, B. Zizi, M. R. Abid, M. Essaaidi, D. Benhaddou, and N. Khalil, "Smart campus microgrid: Advantages and the main architectural components," in *Renewable and Sustainable Energy Conference (IRSEC), 2015 3rd International*, 2015, pp. 1-7.

[44] J.-Y. Kim, J.-H. Jeon, S.-K. Kim, C. Cho, J. H. Park, H.-M. Kim*, et al.*, "Cooperative control strategy of energy storage system and microsources for stabilizing the microgrid during islanded operation," *IEEE Transactions on Power Electronics,* vol. 25, pp. 3037-3048, 2010.

[45] H. Kakigano, Y. Miura, T. Ise, and R. Uchida, "DC micro-grid for super high quality distribution-system configuration and control of distributed generations and energy storage devices," in *Proc. IEEE PESC*, 2006, pp. 18-22.

[46] J. Vetter, P. Novak, M. R. Wagner, C. Veit, K.-C. Möller, J. Besenhard*, et al.*, "Ageing mechanisms in lithium-ion batteries," *Journal of power sources,* vol. 147, pp. 269-281, 2005.

[47] A. Barré, B. Deguilhem, S. Grolleau, M. Gérard, F. Suard, and D. Riu, "A review on lithium-ion battery ageing mechanisms and estimations for automotive applications," *Journal of Power Sources,* vol. 241, pp. 680-689, 2013.

[48] D. Uglietti, R. Wesche, and P. Bruzzone, "Design and strand tests of a fusion cable composed of coated conductor tapes," *IEEE transactions on applied superconductivity,* vol. 24, pp. 1-4, 2014.

[49] M. Takayasu, L. Chiesa, P. D. Noyes, and J. V. Minervini, "Investigation of HTS Twisted Stacked-Tape Cable (TSTC) Conductor for High-Field, High-Current Fusion Magnets," *IEEE Transactions on Applied Superconductivity,* vol. 27, pp. 1-5, 2017.

[50] M. Takayasu, L. Chiesa, N. C. Allen, and J. V. Minervini, "Present status and recent developments of Twisted Stacked-Tape Cable (TSTC) conductor," in *IEEE Trans. Appl. Supercond.*, 2016.

[51] K.-M. Kim, A.-R. Kim, H.-Y. Park, J.-G. Kim, M. Park, I.-K. Yu*, et al.*, "Design and mechanical stress analysis of a toroidal-type SMES magnet," *IEEE Transactions on Applied Superconductivity,* vol. 20, pp. 1900-1903, 2010.

[52] S. Noguchi, H. Yamashita, and A. Ishiyama, "An optimization method for design of SMES coils using YBCO tape," *IEEE transactions on applied superconductivity,* vol. 13, pp. 1856-1859, 2003.

[53] W.-S. Kim, S.-Y. Kwak, J.-K. Lee, K.-D. Choi, H.-K. Jung, K.-C. Seong*, et al.*, "Design of HTS magnets for a 600 kJ SMES," *IEEE transactions on applied superconductivity,* vol. 16, pp. 620-623, 2006.

[54] J. Li, M. Zhang, Q. Yang, Z. Zhang, and W. Yuan, "SMES/battery hybrid energy storage system for electric buses," *IEEE Transactions on Applied Superconductivity,* vol. 26, pp. 1-5, 2016.

[55] J. Li, X. Wang, Z. Zhang, S. Le Blond, Q. Yang, M. Zhang, *et al.*, "Analysis of a new design of the hybrid energy storage system used in the residential m-CHP systems," *Applied Energy,* vol. 187, pp. 169-179, 2017.

[56] J. Li, R. Xiong, Q. Yang, F. Liang, M. Zhang, and W. Yuan, "Design/test of a hybrid energy storage system for primary frequency control using a dynamic droop method in an isolated microgrid power system," *Applied Energy,* vol. 201, pp. 257-269, 2017.

[57] M. Wu, J. Ashburn, C. Torng, P. Hor, R. Meng, L. Gao, *et al.*, "Superconductivity at 93 K in a New Mixed-Phase Y-Ba-Cu-O Compound System at Ambient Pressure," in *Ten Years of Superconductivity: 1980–1990*, ed: Springer, 1993, pp. 281-283.

[58] M. Iwakuma, A. Tomioka, M. Konno, Y. Hase, T. Satou, Y. Iijima, *et al.*, "Development of a 15 kW motor with a fixed YBCO superconducting field winding," *IEEE Transactions on Applied Superconductivity,* vol. 17, pp. 1607-1610, 2007.

[59] W.-S. Kim, C. Park, S. H. Park, J. Lee, J.-B. Song, H. Lee, *et al.*, "Magnetic field stability of a small YBCO magnet in persistent current mode," *IEEE Transactions on Applied Superconductivity,* vol. 19, pp. 2194-2197, 2009.

[60] K. Koyanagi, T. Tosaka, K. Tasaki, T. Kurusu, T. Yoshiyuki, N. Amemiya, *et al.*, "Fabrication of YBCO small test coils for accelerator magnet development," *IEEE Transactions on Applied Superconductivity,* vol. 22, pp. 4101904-4101904, 2012.

[61] W. Buckel and R. Kleiner, *Superconductivity: fundamentals and applications*: John Wiley & Sons, 2008.

[62] Z. Hong, A. Campbell, and T. Coombs, "Numerical solution of critical state in superconductivity by finite element software," *Superconductor Science and Technology,* vol. 19, p. 1246, 2006.

[63] L. Prigozhin, "Analysis of critical-state problems in type-II superconductivity," *IEEE Transactions on Applied Superconductivity,* vol. 7, pp. 3866-3873, 1997.

[64] E. J. Kramer, "Scaling laws for flux pinning in hard superconductors," *Journal of Applied Physics,* vol. 44, pp. 1360-1370, 1973.

[65] K. Nakamura, J. Sato, and K. Ogawa, "Formation of thermally stable multilayered BSCCO films with 2223, 2234 and 2245 structures," *Japanese journal of applied physics,* vol. 29, p. L77, 1990.

[66] C. Buzea and T. Yamashita, "Review of the superconducting properties of MgB2," *Superconductor Science and Technology,* vol. 14, p. R115, 2001.

[67] T. Araki and I. Hirabayashi, "Review of a chemical approach to YBa2Cu3O7− x-coated superconductors—metalorganic deposition using trifluoroacetates," *Superconductor Science and Technology,* vol. 16, p. R71, 2003.

[68] A. Solov'ev and V. Dmitriev, "Fluctuation conductivity and pseudogap in YBCO high-temperature superconductors," *Low Temperature Physics,* vol. 35, pp. 169-197, 2009.

[69] Y. Kim, S. Hahn, J. Voccio, J. Song, J. Bascuñán, and Y. Iwasa, "Strain in YBCO double-pancake coil with stainless steel overband under external magnetic field," *IEEE Transactions on Applied Superconductivity,* vol. 25, pp. 1-4, 2015.

[70] P. J. Hall and E. J. Bain, "Energy-storage technologies and electricity generation," *Energy policy,* vol. 36, pp. 4352-4355, 2008.

[71] J. Hernandez-Llambes and D. Hazelton, "Advantages of second-generation high temperature superconductors for pulsed power applications," in *Pulsed Power Conference, 2009. PPC'09. IEEE*, 2009, pp. 221-226.

[72] V. Selvamanickam, Y.-Y. Xie, and J. Reeves, "Progress in scale-up of 2G conductor at SuperPower," *Superconductivity for Electric Systems 2008 DOE Annual Peer Review,* pp. 25-27, 2006.

[73] C. Barth, G. Mondonico, and C. Senatore, "Electro-mechanical properties of REBCO coated conductors from various industrial manufacturers at 77 K, self-field and 4.2 K, 19 T," *Superconductor Science and Technology,* vol. 28, p. 045011, 2015.

[74] H. Ma, H. Liu, F. Liu, H. Zhang, L. Ci, Y. Shi*, et al.*, "Critical current measurements of high-temperature superconducting short samples at a wide range of temperatures and magnetic fields," *Review of Scientific Instruments,* vol. 89, p. 015102, 2018.

[75] B. Ramshaw, B. Vignolle, J. Day, R. Liang, W. Hardy, C. Proust*, et al.*, "Angle dependence of quantum oscillations in YBa 2 Cu 3 O 6.59 shows free-spin behaviour of quasiparticles," *Nature Physics,* vol. 7, p. 234, 2011.

[76] T. Mahlia, T. Saktisahdan, A. Jannifar, M. Hasan, and H. Matseelar, "A review of available methods and development on energy storage; technology update," *Renewable and Sustainable Energy Reviews,* vol. 33, pp. 532-545, 2014.

[77] F. Díaz-González, A. Sumper, O. Gomis-Bellmunt, and R. Villafáfila-Robles, "A review of energy storage technologies for wind power applications," *Renewable and sustainable energy reviews,* vol. 16, pp. 2154-2171, 2012.

[78] H. Chen, T. N. Cong, W. Yang, C. Tan, Y. Li, and Y. Ding, "Progress in electrical energy storage system: A critical review," *Progress in natural science,* vol. 19, pp. 291-312, 2009.

[79] I. Hadjipaschalis, A. Poullikkas, and V. Efthimiou, "Overview of current and future energy storage technologies for electric power applications," *Renewable and sustainable energy reviews,* vol. 13, pp. 1513-1522, 2009.

[80] J. Kaldellis and D. Zafirakis, "Optimum energy storage techniques for the improvement of renewable energy sources-based electricity generation economic efficiency," *Energy,* vol. 32, pp. 2295-2305, 2007.

[81] J. McDowall, "Integrating energy storage with wind power in weak electricity grids," *Journal of Power sources,* vol. 162, pp. 959-964, 2006.

[82] R. Dufo-López, J. M. Lujano-Rojas, and J. L. Bernal-Agustín, "Comparison of different lead–acid battery lifetime prediction models for use in simulation of stand-alone photovoltaic systems," *Applied Energy,* vol. 115, pp. 242-253, 2014.

[83] W. T. Xu, H. J. Peng, J. Q. Huang, C. Z. Zhao, X. B. Cheng, and Q. Zhang, "Towards Stable Lithium – Sulfur Batteries with a Low Self - Discharge Rate: Ion Diffusion Modulation and Anode Protection," *ChemSusChem,* vol. 8, pp. 2892-2901, 2015.

[84] R. M. Dell and D. A. Rand, "Energy storage—a key technology for global energy sustainability," *Journal of power sources,* vol. 100, pp. 2-17, 2001.

[85] L. Lu, X. Han, J. Li, J. Hua, and M. Ouyang, "A review on the key issues for lithium-ion battery management in electric vehicles," *Journal of power sources,* vol. 226, pp. 272-288, 2013.

[86] F. Beck and P. Rüetschi, "Rechargeable batteries with aqueous electrolytes," *Electrochimica Acta,* vol. 45, pp. 2467-2482, 2000.

[87] A. Du Pasquier, I. Plitz, S. Menocal, and G. Amatucci, "A comparative study of Li-ion battery, supercapacitor and nonaqueous asymmetric hybrid devices for automotive applications," *Journal of Power Sources,* vol. 115, pp. 171-178, 2003.

[88] W. F. Pickard, A. Q. Shen, and N. J. Hansing, "Parking the power: Strategies and physical limitations for bulk energy storage in supply–demand matching on a grid whose input power is provided by intermittent sources," *Renewable and Sustainable Energy Reviews,* vol. 13, pp. 1934-1945, 2009.

[89] A. M. Andwari, A. Pesiridis, S. Rajoo, R. Martinez-Botas, and V. Esfahanian, "A review of Battery Electric Vehicle technology and readiness levels," *Renewable and Sustainable Energy Reviews,* vol. 78, pp. 414-430, 2017.

[90] E. Barbour, I. G. Wilson, J. Radcliffe, Y. Ding, and Y. Li, "A review of pumped hydro energy storage development in significant international electricity markets," *Renewable and Sustainable Energy Reviews,* vol. 61, pp. 421-432, 2016.

[91] M. Beaudin, H. Zareipour, A. Schellenberglabe, and W. Rosehart, "Energy storage for mitigating the variability of renewable electricity sources: An updated review," *Energy for sustainable development,* vol. 14, pp. 302-314, 2010.

[92] Z. Yu, L. Tetard, L. Zhai, and J. Thomas, "Supercapacitor electrode materials: nanostructures from 0 to 3 dimensions," *Energy & Environmental Science,* vol. 8, pp. 702-730, 2015.

[93] A. González, E. Goikolea, J. A. Barrena, and R. Mysyk, "Review on supercapacitors: technologies and materials," *Renewable and Sustainable Energy Reviews,* vol. 58, pp. 1189-1206, 2016.

[94] A. Borenstein, O. Hanna, R. Attias, S. Luski, T. Brousse, and D. Aurbach, "Carbon-based composite materials for supercapacitor electrodes: a review," *Journal of Materials Chemistry A,* vol. 5, pp. 12653-12672, 2017.

[95] D. P. Dubal, O. Ayyad, V. Ruiz, and P. Gomez-Romero, "Hybrid energy storage: the merging of battery and supercapacitor chemistries," *Chemical Society Reviews,* vol. 44, pp. 1777-1790, 2015.

[96] S. C. Bhattacharyya, "Review of alternative methodologies for analysing off-grid electricity supply," *Renewable and Sustainable Energy Reviews,* vol. 16, pp. 677-694, 2012.

[97] J. Baker, "New technology and possible advances in energy storage," *Energy Policy,* vol. 36, pp. 4368-4373, 2008.

[98] T. Coombs, "High-temperature superconducting magnetic energy storage (SMES) for power grid applications," in *Superconductors in the Power Grid*, ed: Elsevier, 2015, pp. 345-365.

[99] A. W. Zimmermann and E. A. Young, "Review of the State of the Art Superconducting Magnetic Energy Storage (SMES) in Renewable/Distributed Energy Systems," 2017.

[100] A. S. Yunus and M. Saini, "Overview of SMES units application on smart grid systems," in *Intelligent Technology and Its Applications (ISITIA), 2016 International Seminar on* , 2016, pp. 465-470.

[101] J. Zhu, M. Qiu, B. Wei, H. Zhang, X. Lai, and W. Yuan, "Design, dynamic simulation and construction of a hybrid HTS SMES (high-temperature superconducting magnetic energy storage systems) for Chinese power grid," *Energy,* vol. 51, pp. 184-192, 2013.

[102] P. Denholm and G. L. Kulcinski, "Life cycle energy requirements and greenhouse gas emissions from large scale energy storage systems," *Energy Conversion and Management,* vol. 45, pp. 2153-2172, 2004.

[103] T. Ma, H. Yang, and L. Lu, "Feasibility study and economic analysis of pumped hydro storage and battery storage for a renewable energy powered island," *Energy Conversion and Management,* vol. 79, pp. 387-397, 2014.

[104] B. Dunn, H. Kamath, and J.-M. Tarascon, "Electrical energy storage for the grid: a battery of choices," *Science,* vol. 334, pp. 928-935, 2011.

[105] G. Majeau-Bettez, T. R. Hawkins, and A. H. Strømman, "Life cycle environmental assessment of lithium-ion and nickel metal hydride batteries for plug-in hybrid and battery electric vehicles," *Environmental science & technology,* vol. 45, pp. 4548-4554, 2011.

[106] D. Doerffel and S. A. Sharkh, "A critical review of using the Peukert equation for determining the remaining capacity of lead-acid and lithium-ion batteries," *Journal of power sources,* vol. 155, pp. 395-400, 2006.

[107] G. Wang, L. Zhang, and J. Zhang, "A review of electrode materials for electrochemical supercapacitors," *Chemical Society Reviews,* vol. 41, pp. 797-828, 2012.

[108] X. Xue, K. Cheng, and D. Sutanto, "A study of the status and future of superconducting magnetic energy storage in power systems," *Superconductor Science and Technology,* vol. 19, p. R31, 2006.

[109] D. Sutanto and K. Cheng, "Superconducting magnetic energy storage systems for power system applications," in *Applied Superconductivity and Electromagnetic Devices, 2009. ASEMD 2009. International Conference on*, 2009, pp. 377-380.

[110] N. Atomura, T. Takahashi, H. Amata, T. Iwasaki, K. Son, D. Miyagi*, et al.*, "Conceptual design of MgB2 coil for the 100 MJ SMES of advanced superconducting power conditioning system (ASPCS)," *Physics Procedia,* vol. 27, pp. 400-403, 2012.
[111] L. Xiao, Z. Wang, S. Dai, J. Zhang, D. Zhang, Z. Gao*, et al.*, "Fabrication and tests of a 1 MJ HTS magnet for SMES," *IEEE Transactions on Applied Superconductivity,* vol. 18, pp. 770-773, 2008.
[112] S. Nagaya, N. Hirano, T. Katagiri, T. Tamada, K. Shikimachi, Y. Iwatani*, et al.*, "The state of the art of the development of SMES for bridging instantaneous voltage dips in Japan," *Cryogenics,* vol. 52, pp. 708-712, 2012.
[113] P. Tixador, B. Bellin, M. Deleglise, J. Vallier, C. Bruzek, S. Pavard*, et al.*, "Design of a 800 kJ HTS SMES," *IEEE Transactions on Applied Superconductivity,* vol. 15, pp. 1907-1910, 2005.
[114] S. Kwak, S. Lee, S. Lee, W.-S. Kim, J.-K. Lee, C. Park*, et al.*, "Design of HTS magnets for a 2.5 MJ SMES," *IEEE Transactions on Applied Superconductivity,* vol. 19, pp. 1985-1988, 2009.
[115] R. Hemmati and H. Saboori, "Emergence of hybrid energy storage systems in renewable energy and transport applications–A review," *Renewable and Sustainable Energy Reviews,* vol. 65, pp. 11-23, 2016.
[116] Q. Tabart, I. Vechiu, A. Etxeberria, and S. Bacha, "Hybrid Energy Storage System Microgrids Integration for Power Quality Improvement Using Four-Leg Three-Level NPC Inverter and Second-Order Sliding Mode Control," *IEEE Transactions on Industrial Electronics,* vol. 65, pp. 424-435, 2018.
[117] D. Akinyele and R. Rayudu, "Review of energy storage technologies for sustainable power networks," *Sustainable Energy Technologies and Assessments,* vol. 8, pp. 74-91, 2014.
[118] F. Bonaccorso, L. Colombo, G. Yu, M. Stoller, V. Tozzini, A. C. Ferrari*, et al.*, "Graphene, related two-dimensional crystals, and hybrid systems for energy conversion and storage," *Science,* vol. 347, p. 1246501, 2015.
[119] B. Bolund, H. Bernhoff, and M. Leijon, "Flywheel energy and power storage systems," *Renewable and Sustainable Energy Reviews,* vol. 11, pp. 235-258, 2007.
[120] F. Giraud and Z. M. Salameh, "Steady-state performance of a grid-connected rooftop hybrid wind-photovoltaic power system with battery storage," *IEEE transactions on energy conversion,* vol. 16, pp. 1-7, 2001.
[121] J. P. Barton and D. G. Infield, "Energy storage and its use with intermittent renewable energy," *IEEE transactions on energy conversion,* vol. 19, pp. 441-448, 2004.
[122] M. Black and G. Strbac, "Value of bulk energy storage for managing wind power fluctuations," *IEEE transactions on energy conversion,* vol. 22, pp. 197-205, 2007.
[123] G. Strbac, A. Shakoor, M. Black, D. Pudjianto, and T. Bopp, "Impact of wind generation on the operation and development of the UK electricity systems," *Electric Power Systems Research,* vol. 77, pp. 1214-1227, 2007.
[124] C. Marinescu, "Pumped storage system for wind energy in variable operating conditions," in *Fundamentals of Electrical Engineering (ISFEE), 2014 International Symposium on*, 2014, pp. 1-6.
[125] J. Li, A. M. Gee, M. Zhang, and W. Yuan, "Analysis of battery lifetime extension in a SMES-battery hybrid energy storage system using a novel battery lifetime model," *Energy,* vol. 86, pp. 175-185, 2015.
[126] T. Ise, M. Kita, and A. Taguchi, "A hybrid energy storage with a SMES and secondary battery," *IEEE Transactions on Applied Superconductivity,* vol. 15, pp. 1915-1918, 2005.
[127] T. Bocklisch, "Hybrid energy storage systems for renewable energy applications," *Energy Procedia,* vol. 73, pp. 103-111, 2015.
[128] M. E. Amiryar and K. R. Pullen, "A review of flywheel energy storage system technologies and their applications," *Applied Sciences,* vol. 7, p. 286, 2017.
[129] Y. Cho, J. W. Shim, S.-J. Kim, S. W. Min, and K. Hur, "Enhanced frequency regulation service using hybrid energy storage system against increasing power-load variability," in *Power and Energy Society General Meeting (PES), 2013 IEEE*, 2013, pp. 1-5.

[130] D. B. W. Abeywardana, B. Hredzak, and V. G. Agelidis, "Single-Phase Grid-Connected LiFePO $ _ {\bf 4} $ Battery–Supercapacitor Hybrid Energy Storage System With Interleaved Boost Inverter," *IEEE Transactions on Power Electronics,* vol. 30, pp. 5591-5604, 2015.

[131] S. K. Kollimalla, M. K. Mishra, and N. L. Narasamma, "Design and analysis of novel control strategy for battery and supercapacitor storage system," *IEEE Transactions on Sustainable Energy,* vol. 5, pp. 1137-1144, 2014.

[132] T. Ma, H. Yang, and L. Lu, "Development of hybrid battery–supercapacitor energy storage for remote area renewable energy systems," *Applied Energy,* vol. 153, pp. 56-62, 2015.

[133] S. C. Smith, P. Sen, and B. Kroposki, "Advancement of energy storage devices and applications in electrical power system," in *Power and Energy Society General Meeting-Conversion and Delivery of Electrical Energy in the 21st Century, 2008 IEEE*, 2008, pp. 1-8.

[134] M. H. Ali, B. Wu, and R. A. Dougal, "An overview of SMES applications in power and energy systems," *IEEE Transactions on Sustainable Energy,* vol. 1, pp. 38-47, 2010.

[135] T. Sannomiya, H. Hayashi, T. Ishii, and R. Ikeda, "Test results of compensation for load fluctuation under a fuzzy control by a 1 kWh/1 MW SMES," *IEEE transactions on applied superconductivity,* vol. 11, pp. 1908-1911, 2001.

[136] R. H. Lasseter and P. Paigi, "Microgrid: A conceptual solution," in *Power Electronics Specialists Conference, 2004. PESC 04. 2004 IEEE 35th Annual*, 2004, pp. 4285-4290.

[137] W. Gu, Z. Wu, R. Bo, W. Liu, G. Zhou, W. Chen*, et al.*, "Modeling, planning and optimal energy management of combined cooling, heating and power microgrid: A review," *International Journal of Electrical Power & Energy Systems,* vol. 54, pp. 26-37, 2014.

[138] L. Meng, E. R. Sanseverino, A. Luna, T. Dragicevic, J. C. Vasquez, and J. M. Guerrero, "Microgrid supervisory controllers and energy management systems: A literature review," *Renewable and Sustainable Energy Reviews,* vol. 60, pp. 1263-1273, 2016.

[139] A. Kaur, J. Kaushal, and P. Basak, "A review on microgrid central controller," *Renewable and Sustainable Energy Reviews,* vol. 55, pp. 338-345, 2016.

[140] A. Khodaei, "Provisional microgrid planning," *IEEE Transactions on Smart Grid,* vol. 8, pp. 1096-1104, 2017.

[141] C. Marnay, S. Chatzivasileiadis, C. Abbey, R. Iravani, G. Joos, P. Lombardi*, et al.*, "Microgrid evolution roadmap," in *Smart Electric Distribution Systems and Technologies (EDST), 2015 International Symposium on*, 2015, pp. 139-144.

[142] M. Ross, C. Abbey, F. Bouffard, and G. Jos, "Multiobjective optimization dispatch for microgrids with a high penetration of renewable generation," *IEEE Transactions on Sustainable Energy,* vol. 6, pp. 1306-1314, 2015.

[143] J. Zhu, W. Yuan, M. Qiu, B. Wei, H. Zhang, P. Chen*, et al.*, "Experimental demonstration and application planning of high temperature superconducting energy storage system for renewable power grids," *Applied Energy,* vol. 137, pp. 692-698, 2015.

[144] M. Parchomiuk, R. Strzelecki, K. Zymmer, and A. Domino, "Modular power converter with superconducting magnetic energy storage for electric power distribution system —Analysis and simulation," in *Power Electronics and Applications (EPE'17 ECCE Europe), 2017 19th European Conference on*, 2017, pp. P. 1-P. 6.

[145] Y. Zou, X. Hu, H. Ma, and S. E. Li, "Combined state of charge and state of health estimation over lithium-ion battery cell cycle lifespan for electric vehicles," *Journal of Power Sources,* vol. 273, pp. 793-803, 2015.

[146] B. Qu, C. Ma, G. Ji, C. Xu, J. Xu, Y. S. Meng*, et al.*, "Layered SnS2‐Reduced Graphene Oxide Composite‐A High‐Capacity, High‐Rate, and Long‐Cycle Life Sodium‐Ion Battery Anode Material," *Advanced materials,* vol. 26, pp. 3854-3859, 2014.

[147] A.-L. Allègre, A. Bouscayrol, and R. Trigui, "Flexible real-time control of a hybrid energy storage system for electric vehicles," *IET Electrical Systems in Transportation,* vol. 3, pp. 79-85, 2013.

[148] B. Hredzak, V. G. Agelidis, and M. Jang, "A model predictive control system for a hybrid battery-ultracapacitor power source," *IEEE Transactions on Power Electronics,* vol. 29, pp. 1469-1479, 2014.
[149] K. Tasaki, Y. Sumiyoshi, M. Tezuka, H. Hayashi, K. Tsutsumi, K. Funaki*, et al.*, "Design study of a 3.6 MJ HTS-SMES: Compact magnet design," *Physica C: Superconductivity,* vol. 357, pp. 1332-1335, 2001.
[150] S. Safran, A. Kılıç, and O. Ozturk, "Effect of re-pelletization on structural, mechanical and superconducting properties of BSCCO superconductors," *Journal of Materials Science: Materials in Electronics,* vol. 28, pp. 1799-1803, 2017.
[151] A. H. Aly and D. Mohamed, "BSCCO/SrTiO 3 One Dimensional Superconducting Photonic Crystal for Many Applications," *Journal of Superconductivity and Novel Magnetism,* vol. 28, pp. 1699-1703, 2015.
[152] B. Özçelik, M. Gürsul, A. Sotelo, and M. Madre, "Improvement of superconducting properties in Na-doped BSCCO superconductor," *Journal of Materials Science: Materials in Electronics,* vol. 26, pp. 441-447, 2015.
[153] B. Savaskan, E. T. Koparan, S. Celik, K. Ozturk, and E. Yanmaz, "Investigation on the levitation force behaviour of malic acid added bulk MgB2 superconductors," *Physica C: Superconductivity,* vol. 502, pp. 63-69, 2014.
[154] A. Mamalis, E. Hristoforou, I. Theodorakopoulos, and T. Prikhna, "Critical current density investigations of explosively compacted and extruded powder-in-tube MgB2 superconductors," *Superconductor Science and Technology,* vol. 23, p. 095011, 2010.
[155] J. Smith, M. Cima, and N. Sonnenberg, "High critical current density thick MOD-derived YBCO films," *IEEE transactions on applied superconductivity,* vol. 9, pp. 1531-1534, 1999.
[156] J. Gutierrez, A. Llordes, J. Gazquez, M. Gibert, N. Roma, S. Ricart*, et al.*, "Strong isotropic flux pinning in solution-derived YBa 2 Cu 3 O 7− x nanocomposite superconductor films," *Nature materials,* vol. 6, p. 367, 2007.
[157] S. Hasanain, N. Akhtar, and A. Mumtaz, "Particle size dependence of the superconductivity and ferromagnetism in YBCO nanoparticles," *Journal of Nanoparticle Research,* vol. 13, pp. 1953-1960, 2011.
[158] C. Meingast and D. Larbalestier, "Quantitative description of a very high critical current density Nb - Ti superconductor during its final optimization strain. II. Flux pinning mechanisms," *Journal of applied physics,* vol. 66, pp. 5971-5983, 1989.
[159] M. Deng, C. Yu, G. Huang, M. Larsson, P. Caroff, and H. Xu, "Anomalous zero-bias conductance peak in a Nb–InSb nanowire–Nb hybrid device," *Nano letters,* vol. 12, pp. 6414-6419, 2012.
[160] A. Godeke, "A review of the properties of Nb3Sn and their variation with A15 composition, morphology and strain state," *Superconductor Science and Technology,* vol. 19, p. R68, 2006.
[161] R. Flükiger, D. Uglietti, C. Senatore, and F. Buta, "Microstructure, composition and critical current density of superconducting Nb3Sn wires," *Cryogenics,* vol. 48, pp. 293-307, 2008.
[162] H. Weijers, U. Trociewitz, W. Markiewicz, J. Jiang, D. Myers, E. Hellstrom*, et al.*, "High field magnets with HTS conductors," *IEEE transactions on applied superconductivity,* vol. 20, pp. 576-582, 2010.
[163] A. Ishiyama, M. Yanai, T. Morisaki, H. Ueda, Y. Shiohara, T. Izumi*, et al.*, "Normal transition and propagation characteristics of YBCO tape," *IEEE transactions on applied superconductivity,* vol. 15, pp. 1659-1662, 2005.
[164] Y. Tian, S. Linzen, F. Schmidl, R. Cihar, and P. Seidel, "Large-area YBCO films for device fabrication," *Superconductor Science and Technology,* vol. 11, p. 59, 1998.
[165] A. Usoskin, A. Rutt, J. Knoke, H. Krauth, and T. Arndt, "Long-length YBCO coated stainless steel tapes with high critical currents," *IEEE transactions on applied superconductivity,* vol. 15, pp. 2604-2607, 2005.

[166] A. Leenders, M. Mich, and H. Freyhard, "Influence of thermal cycling on the mechanical properties of VGF melt-textured YBCO," *Physica C: Superconductivity,* vol. 279, pp. 173-180, 1997.

[167] A. Batista-Leyva, R. Cobas, E. Estévez-Rams, M. Orlando, C. Noda, and E. Altshuler, "Hysteresis of the critical current density in YBCO, HBCCO and BSCCO superconducting polycrystals: a comparative study," *Physica C: Superconductivity,* vol. 331, pp. 57-66, 2000.

[168] B. Holzapfel, G. Kreiselmeyer, M. Kraus, S. Bouffard, S. Klaumünzer, L. Schultz*, et al.*, "Angle-resolved critical transport-current density of YBa 2 Cu 3 O 7− δ thin films and YBa 2 Cu 3 O 7− δ/PrBa 2 Cu 3 O 7− δ superlattices containing columnar defects of various orientations," *Physical Review B,* vol. 48, p. 600, 1993.

[169] K. Shikimachi, N. Hirano, S. Nagaya, H. Kawashima, K. Higashikawa, and T. Nakamura, "System coordination of 2 GJ class YBCO SMES for power system control," *IEEE Transactions on Applied Superconductivity,* vol. 19, pp. 2012-2018, 2009.

[170] M. Sugano, T. Nakamura, K. Shikimachi, N. Hirano, and S. Nagaya, "Stress tolerance and fracture mechanism of solder joint of YBCO coated conductors," *IEEE Transactions on Applied Superconductivity,* vol. 17, pp. 3067-3070, 2007.

[171] M. Qiu, S. Rao, J. Zhu, J. Gong, and W. Yuan, "Electromagnetic optimization design of a toroidal HTS-SMES magnet using magneto-circuit coupling analysis method," *Diangong Jishu Xuebao/Transactions of China Electrotechnical Society,* vol. 31, pp. 176-182, 2016.

[172] S. L. Lalitha and R. Gupta, "The mechanical design optimization of a high field HTS solenoid," *IEEE Transactions on Applied Superconductivity,* vol. 25, pp. 1-4, 2015.

[173] Y. Xu, Y. Tang, L. Ren, Q. Dai, C. Xu, Z. Wang*, et al.*, "Numerical simulation and experimental validation of a cooling process in a 150-kJ SMES magnet," *IEEE Trans. Appl. Supercond,* vol. 26, 2016.

[174] P. Tixador, M. Deleglise, A. Badel, K. Berger, B. Bellin, J.-C. Vallier*, et al.*, "First tests of a 800 kJ HTS SMES," *IEEE Transactions on Applied Superconductivity,* vol. 18, pp. 774-778, 2008.

[175] Y. Xu, L. Ren, Y. Tang, C. Xu, Z. Zhang, W. Chen*, et al.*, "A study on the design and comparison of 1–100-MJ-class SMES magnet with different coil configurations," *IEEE Transactions on Applied Superconductivity,* vol. 27, pp. 1-9, 2017.

[176] W. Wei, Y. Luo, and L. Han, "Multi Solenoid Type Magnet for 1 MJ HTS SMES System," *DEStech Transactions on Materials Science and Engineering,* 2015.

[177] M. Qiu, S. Rao, J. Zhu, P. Chen, S. Fu, W. Yuan*, et al.*, "Mechanical Properties of MJ-Class Toroidal Magnet Wound by Composite HTS Conductor," *IEEE Transactions on Applied Superconductivity,* vol. 27, 2017.

[178] M. Qiu, S. Rao, J. Zhu, S. Fu, Z. Li, W. Liu*, et al.*, "Energy Storage Characteristics of MJ-Class Toroidal HTS-SMES Considering Maximum Value of Perpendicular Magnetic Field," *Energy Procedia,* vol. 105, pp. 4179-4184, 2017.

[179] J. Lehtonen, M. Masti, R. Nast, C. Schmidt, W. Goldacker, M. Leghissa*, et al.*, "AC coil, reactor and cable demonstrations of low AC loss elementary and assembled BSCCO conductors," *Superconductor science and technology,* vol. 18, p. 400, 2005.

[180] N. Long, R. Badcock, P. Beck, M. Mulholl, N. Ross, M. Staines*, et al.*, "Narrow strand YBCO Roebel cable for lowered AC loss," in *Journal of Physics: Conference Series*, 2008, p. 012280.

[181] S. Terzieva, M. Vojenčiak, E. Pardo, F. Grilli, A. Drechsler, A. Kling*, et al.*, "Transport and magnetization ac losses of ROEBEL assembled coated conductor cables: measurements and calculations," *Superconductor Science and Technology,* vol. 23, p. 014023, 2009.

[182] E. Pardo and F. Grilli, "Numerical simulations of the angular dependence of magnetization AC losses: coated conductors, Roebel cables and double pancake coils," *Superconductor Science and Technology,* vol. 25, p. 014008, 2011.

[183] N. Glasson, M. Staines, R. Buckley, M. Pannu, and S. Kalsi, "Development of a 1 MVA 3-phase superconducting transformer using YBCO Roebel cable," *IEEE transactions on Applied Superconductivity,* vol. 21, pp. 1393-1396, 2011.

[184] M. Staines, N. Glasson, M. Pannu, K. P. Thakur, R. Badcock, N. Allpress*, et al.*, "The development of a Roebel cable based 1 MVA HTS transformer," *Superconductor Science and Technology,* vol. 25, p. 014002, 2011.

[185] N. D. Glasson, M. P. Staines, Z. Jiang, and N. S. Allpress, "Verification testing for a 1 MVA 3-phase demonstration transformer using 2G-HTS Roebel cable," *IEEE Transactions on Applied Superconductivity,* vol. 23, pp. 5500206-5500206, 2013.

[186] J. Van Nugteren, G. Kirby, G. de Rijk, L. Rossi, H. H. ten Kate, and M. M. Dhalle, "Study of a 5 T research dipole insert-magnet using an anisotropic ReBCO Roebel cable," *IEEE transactions on applied superconductivity,* vol. 25, pp. 1-5, 2015.

[187] G. Kirby, J. van Nugteren, A. Ballarino, L. Bottura, N. Chouika, S. Clement*, et al.*, "Accelerator-quality HTS dipole magnet demonstrator designs for the EuCARD-2 5-T 40-mm clear aperture magnet," *IEEE Transactions on Applied Superconductivity,* vol. 25, pp. 1-5, 2015.

[188] N. Long, "HTS Roebel cables In HTS4Fusion Conductor Workshop," *KIT CN, Karlsruhe,* 2011.

[189] S. Otten, M. Dhallé, P. Gao, W. Wessel, A. Kario, A. Kling*, et al.*, "Enhancement of the transverse stress tolerance of REBCO Roebel cables by epoxy impregnation," *Superconductor science and technology,* vol. 28, p. 065014, 2015.

[190] Z. Zhang, J.-G. Kim, C. H. Kim, S. Pamidi, J. Li, M. Zhang, *et al.*, "Current distribution investigation of a laboratory-scale coaxial two-HTS-layer DC prototype cable," *IEEE Transactions on Applied Superconductivity,* vol. 26, pp. 1-5, 2016.

[191] M. Takayasu, L. Chiesa, N. C. Allen, and J. V. Minervini, "Present status and recent developments of the twisted stacked-tape cable conductor," *IEEE Transactions on Applied Superconductivity,* vol. 26, pp. 25-34, 2016.

[192] W. Goldacker, F. Grilli, E. Pardo, A. Kario, S. I. Schlachter, and M. Vojenčiak, "Roebel cables from REBCO coated conductors: A one-century-old concept for the superconductivity of the future," *Superconductor Science and Technology,* vol. 27, p. 093001, 2014.

[193] H. Liu, G. Song, W. Feng, M. Qiu, J. Zhu, and S. Rao, "Strain Characteristic of a Toroidal HTS-SMES Fabricated by YBCO Stacked-Tape Cables," *IEEE Transactions on Applied Superconductivity,* vol. 27, pp. 1-5, 2017.

[194] N. Long, R. Badcock, K. Hamilton, A. Wright, Z. Jiang, and L. Lakshmi, "Development of YBCO Roebel cables for high current transport and low AC loss applications," in *Journal of Physics: Conference Series*, 2010, p. 022021.

[195] Z. Jiang, K. Thakur, N. Long, R. Badcock, and M. Staines, "Comparison of transport AC losses in an eight-strand YBCO Roebel cable and a four-tape YBCO stack," *Physica C: Superconductivity and its applications,* vol. 471, pp. 999-1002, 2011.

[196] Y. Yang, J. Pelegrin, I. Falorio, E. Young, A. Kario, W. Goldacker*, et al.*, "Magnetization losses of Roebel cable samples with 2G YBCO coated conductor strands," *IEEE Transactions on Applied Superconductivity,* vol. 26, pp. 1-5, 2016.

[197] Z.-m. Bai, X. Wu, C.-l. Wu, and J.-x. Wang, "Quench propagation properties analysis of high-temperature superconductors using finite element method," *Physica C: Superconductivity,* vol. 436, pp. 99-102, 2006.

[198] Y. Wang, H. Song, D. Xu, Z. Li, Z. Jin, and Z. Hong, "An equivalent circuit grid model for no-insulation HTS pancake coils," *Superconductor Science and Technology,* vol. 28, p. 045017, 2015.

[199] X. Chaud, F. Debray, L. Ronayette, E. Mossang, P. Brosse-Maron, A.-J. Vialle*, et al.*, "Characterization of YBCO coated conductors under high magnetic field at LNCMI," *IEEE Transactions on Applied Superconductivity,* vol. 22, pp. 6600704-6600704, 2012.

[200] M.-J. Park, S.-Y. Kwak, W.-S. Kim, S.-W. Lee, S.-Y. Hahn, J.-K. Lee*, et al.*, "Stress analysis of HTS magnet for a 600 kJ SMES," *IEEE Transactions on applied superconductivity,* vol. 17, pp. 1994-1997, 2007.

[201] S. Otten, "Transverse pressure dependence of the critical current in epoxy impregnated REBCO Roebel cables," University of Twente, 2014.

[202] Z. Jiang, M. Staines, R. A. Badcock, N. Long, and N. Amemiya, "Transport AC loss measurement of a five strand YBCO Roebel cable," *Superconductor Science and Technology,* vol. 22, p. 095002, 2009.
[203] Z. Jiang, K. Thakur, M. Staines, R. Badcock, N. Long, R. Buckley*, et al.*, "Transport AC loss characteristics of a five strand YBCO Roebel cable with magnetic substrate," *IEEE Transactions on Applied Superconductivity,* vol. 21, pp. 3289-3292, 2011.
[204] P. Thounthong, S. Rael, and B. Davat, "Energy management of fuel cell/battery/supercapacitor hybrid power source for vehicle applications," *Journal of Power Sources,* vol. 193, pp. 376-385, 2009.
[205] J.-H. Lee, S.-H. Lee, and S.-K. Sul, "Variable-speed engine generator with supercapacitor: Isolated power generation system and fuel efficiency," *IEEE Transactions on Industry Applications,* vol. 45, pp. 2130-2135, 2009.
[206] S. Muyeen, H. M. Hasanien, and A. Al-Durra, "Transient stability enhancement of wind farms connected to a multi-machine power system by using an adaptive ANN-controlled SMES," *Energy Conversion and Management,* vol. 78, pp. 412-420, 2014.
[207] X. Zhou, Y. Tang, and J. Shi, "Enhancing LVRT Capability of DFIG-Based Wind Turbine Systems with SMES Series in the Rotor Side," *International Journal of Rotating Machinery,* vol. 2017, 2017.
[208] A. Cansiz, C. Faydaci, M. T. Qureshi, O. Usta, and D. T. McGuiness, "Integration of a SMES–battery-based hybrid energy storage system into microgrids," *Journal of Superconductivity and Novel Magnetism,* vol. 31, pp. 1449-1457, 2018.
[209] N. Mendis, K. M. Muttaqi, and S. Perera, "Management of battery-supercapacitor hybrid energy storage and synchronous condenser for isolated operation of PMSG based variable-speed wind turbine generating systems," *IEEE Transactions on smart grid,* vol. 5, pp. 944-953, 2014.
[210] C.-C. Lee, "Fuzzy logic in control systems: fuzzy logic controller. I," *IEEE Transactions on systems, man, and cybernetics,* vol. 20, pp. 404-418, 1990.
[211] M. Uno and K. Tanaka, "Influence of high-frequency charge–discharge cycling induced by cell voltage equalizers on the life performance of lithium-ion cells," *IEEE Transactions on vehicular technology,* vol. 60, pp. 1505-1515, 2011.
[212] K. Uddin, A. D. Moore, A. Barai, and J. Marco, "The effects of high frequency current ripple on electric vehicle battery performance," *Applied Energy,* vol. 178, pp. 142-154, 2016.
[213] S. Subiyanto, A. Mohamed, and M. Hannan, "Intelligent maximum power point tracking for PV system using Hopfield neural network optimized fuzzy logic controller," *Energy and Buildings,* vol. 51, pp. 29-38, 2012.
[214] A. Messai, A. Mellit, A. Guessoum, and S. Kalogirou, "Maximum power point tracking using a GA optimized fuzzy logic controller and its FPGA implementation," *Solar energy,* vol. 85, pp. 265-277, 2011.
[215] H. Hayashi, K. Tsutsumi, K. Funaki, M. Iwakuma, K. Tasaki, Y. Sumiyoshi*, et al.*, "Design study of a 1 GJ class HTS-SMES (1): Conceptual design of a magnet system," *Physica C: Superconductivity,* vol. 357, pp. 1327-1331, 2001.
[216] G. He, Q. Chen, C. Kang, P. Pinson, and Q. Xia, "Optimal bidding strategy of battery storage in power markets considering performance-based regulation and battery cycle life," *IEEE Transactions on Smart Grid,* vol. 7, pp. 2359-2367, 2016.
[217] C. Hu, G. Jain, P. Tamirisa, and T. Gorka, "Method for estimating capacity and predicting remaining useful life of lithium-ion battery," in *Prognostics and Health Management (PHM), 2014 IEEE Conference on*, 2014, pp. 1-8.
[218] J. M. Guerrero, J. C. Vasquez, J. Matas, L. G. De Vicuña, and M. Castilla, "Hierarchical control of droop-controlled AC and DC microgrids—A general approach toward standardization," *IEEE Transactions on industrial electronics,* vol. 58, pp. 158-172, 2011.

[219] H. Zhou, T. Bhattacharya, D. Tran, T. S. T. Siew, and A. M. Khambadkone, "Composite energy storage system involving battery and ultracapacitor with dynamic energy management in microgrid applications," *IEEE transactions on power electronics,* vol. 26, pp. 923-930, 2011.

[220] C. A. Cortes, S. F. Contreras, and M. Shahidehpour, "Microgrid Topology Planning for Enhancing the Reliability of Active Distribution Networks," *IEEE Transactions on Smart Grid,* 2017.

[221] C.-S. Karavas, K. G. Arvanitis, G. Kyriakarakos, D. D. Piromalis, and G. Papadakis, "A novel autonomous PV powered desalination system based on a DC microgrid concept incorporating short-term energy storage," *Solar Energy,* vol. 159, pp. 947-961, 2018.

[222] M. Patterson, N. F. Macia, and A. M. Kannan, "Hybrid microgrid model based on solar photovoltaic battery fuel cell system for intermittent load applications," *IEEE Transactions on Energy Conversion,* vol. 30, pp. 359-366, 2015.

[223] P. Arul, V. K. Ramachandaramurthy, and R. Rajkumar, "Control strategies for a hybrid renewable energy system: A review," *Renewable and Sustainable Energy Reviews,* vol. 42, pp. 597-608, 2015.

[224] H. Kakigano, M. Nomura, and T. Ise, "Loss evaluation of DC distribution for residential houses compared with AC system," in *Power Electronics Conference (IPEC), 2010 International*, 2010, pp. 480-486.

[225] E. Planas, J. Andreu, J. I. Gárate, I. M. de Alegría, and E. Ibarra, "AC and DC technology in microgrids: A review," *Renewable and Sustainable Energy Reviews,* vol. 43, pp. 726-749, 2015.

[226] T. Dragičević, X. Lu, J. C. Vasquez, and J. M. Guerrero, "DC microgrids—Part II: A review of power architectures, applications, and standardization issues," *IEEE transactions on power electronics,* vol. 31, pp. 3528-3549, 2016.

[227] Y. Han, H. Li, P. Shen, E. A. A. Coelho, and J. M. Guerrero, "Review of active and reactive power sharing strategies in hierarchical controlled microgrids," *IEEE Transactions on Power Electronics,* vol. 32, pp. 2427-2451, 2017.

[228] H. Kanchev, D. Lu, F. Colas, V. Lazarov, and B. Francois, "Energy management and operational planning of a microgrid with a PV-based active generator for smart grid applications," *IEEE transactions on industrial electronics,* vol. 58, pp. 4583-4592, 2011.

[229] R. Palma-Behnke, C. Benavides, F. Lanas, B. Severino, L. Reyes, J. Llanos*, et al.*, "A microgrid energy management system based on the rolling horizon strategy," *IEEE Transactions on Smart Grid,* vol. 4, pp. 996-1006, 2013.

[230] Q. Sun, D. Xing, Q. Yang, H. Zhang, and J. Patel, "A New Design of Fuzzy Logic Control for SMES and Battery Hybrid Storage System," *Energy Procedia,* vol. 105, pp. 4575-4580, 2017.

[231] L. Chen, H. Chen, Y. Li, G. Li, J. Yang, X. Liu*, et al.*, "SMES-Battery Energy Storage System for the Stabilization of a Photovoltaic-Based Microgrid," *IEEE Transactions on Applied Superconductivity,* vol. 28, pp. 1-7, 2018.

[232] N. Omar, M. A. Monem, Y. Firouz, J. Salminen, J. Smekens, O. Hegazy*, et al.*, "Lithium iron phosphate based battery–assessment of the aging parameters and development of cycle life model," *Applied Energy,* vol. 113, pp. 1575-1585, 2014.

[233] K. Uddin, T. Jackson, W. D. Widanage, G. Chouchelamane, P. A. Jennings, and J. Marco, "On the possibility of extending the lifetime of lithium-ion batteries through optimal V2G facilitated by an integrated vehicle and smart-grid system," *Energy,* vol. 133, pp. 710-722, 2017.

[234] A. Kushima, T. Koido, Y. Fujiwara, N. Kuriyama, N. Kusumi, and J. Li, "Charging/discharging nanomorphology asymmetry and rate-dependent capacity degradation in Li–oxygen battery," *Nano letters,* vol. 15, pp. 8260-8265, 2015.

[235] H.-J. Chiu and L.-W. Lin, "A bidirectional DC–DC converter for fuel cell electric vehicle driving system," *IEEE Transactions on Power Electronics,* vol. 21, pp. 950-958, 2006.

[236] C. Wang, R. Xiong, H. He, X. Ding, and W. Shen, "Efficiency analysis of a bidirectional DC/DC converter in a hybrid energy storage system for plug-in hybrid electric vehicles," *Applied energy,* vol. 183, pp. 612-622, 2016.

[237] Z. Song, H. Hofmann, J. Li, X. Han, and M. Ouyang, "Optimization for a hybrid energy s torage system in electric vehicles using dynamic programing approach," *Applied Energy,* vol. 139, pp. 151-162, 2015.

[238] J. Shen, S. Dusmez, and A. Khaligh, "Optimization of sizing and battery cycle life in battery/ultracapacitor hybrid energy storage systems for electric vehicle applications," *IEEE Transactions on industrial informatics,* vol. 10, pp. 2112-2121, 2014.

[239] Z. Song, J. Li, X. Han, L. Xu, L. Lu, M. Ouyang*, et al.*, "Multi-objective optimization of a semi-active battery/supercapacitor energy storage system for electric vehicles," *Applied Energy,* vol. 135, pp. 212-224, 2014.

[240] A. M. Gee, F. Robinson, and W. Yuan, "A superconducting magnetic energy storage-emulator/battery supported dynamic voltage restorer," *IEEE Transactions on Energy Conversion,* vol. 32, pp. 55-64, 2017.

[241] M. Coleman, C. K. Lee, C. Zhu, and W. G. Hurley, "State-of-charge determination from EMF voltage estimation: Using impedance, terminal voltage, and current for lead-acid and lithium-ion batteries," *IEEE Transactions on industrial electronics,* vol. 54, pp. 2550-2557, 2007.

[242] S. Sato and A. Kawamura, "A new estimation method of state of charge using terminal voltage and internal resistance for lead acid battery," in *Power Conversion Conference, 2002. PCC-Osaka 2002. Proceedings of the*, 2002, pp. 565-570.

[243] S. Naderi, E. Pouresmaeil, and W. D. Gao, "The frequency-independent control method for distributed generation systems," *Applied energy,* vol. 96, pp. 272-280, 2012.